Department of Electrical and Computer Engineering

Analysis and Control of Offshore Wind Power Collection Systems

Yuanyuan Fan

This thesis is presented for the Degree of
Doctor of Philosophy
of
Curtin University

September 2016

Declaration

To the best of my knowledge and belief this thesis contains no material previously published by any other person except where due acknowledgment has been made.

This thesis contains no material which has been accepted for the award of any other degree or diploma in any university.

Date: 21/09/2016

ABSTRACT

The utilization of offshore wind energy in power systems generally includes power generation, power collection and power transmission. The power generation is realized by a Wind Energy Conversion System (WECS) consisting of a wind turbine, a generator and a power converter. The Permanent Magnetic Synchronous Generator (PMSG) based WECS employing the three-leg Voltage Source Converter (VSC) is used in this thesis. The Maximum Power Point Tracking (MPPT) is achieved through the Wind Side Converter (WSC).

Three types of DC collection systems are discussed for offshore wind farms. These are the parallel DC collection system, the series DC collection system and the series-parallel DC collection system. Suitable for large-capacity and long-distance power transmission, the High Direct Voltage Current (HVDC) technique is chosen for offshore wind power delivery. To reach the transmission voltage level, the terminal voltage of a parallel DC collection system must be boosted. The Single Active Bridge (SAB) converter is used as the boost converter. For series and series-parallel DC collection systems, the terminal voltages are stepped up by series connection of the WSCs.

In normal operation, the parallel DC collection system is not sensitive to wind speed variations. However, the series and series-parallel DC collection systems require voltage restriction strategies when the wind speed is uneven within an offshore wind farm. The voltage limitation is achieved through wind power control. Two power balancing strategies are proposed, i.e., Small Sized Battery Application (SSBA) and WSC Power Reference Modification (PRM). The excess wind power resulting from PRM is balanced by modifying the pitch control or employing chopping resistors.

The failure of wind turbines is considered as the fault condition in the thesis. The stable operation of a parallel DC collection system is not influenced by fault. However, overvoltage tends to occur in series and series-parallel DC collection systems upon fault. To prevent overvoltage, a variable HVDC transmission voltage is allowed in a series DC collection system. The transmission voltage can be adjusted by either modifying the Grid Side Converter (GSC) voltage references or using

multiple small sized GSCs. For the series-parallel DC collection system, the transmission voltage is maintained constant. The overvoltage occurrence is achieved by installing power switches for topology reconfiguration or by employing DC/DC converters for independent branch control.

To integrate the power from several offshore wind farms with a grid, the multi-terminal HVDC system is applied. The integration rule is identified and integration points are selected considering the economic factor. The Integration Point (I-point) voltage stabilization is studied using different DC collection topologies in a 3-terminal HVDC system. When only series DC collection systems are employed, the line resistances need to be changed by using variable resistors. When parallel DC collection is involved, the I-point voltage is stabilized through the DC/DC converter in the parallel collection system.

All the proposed topologies and strategies are verified through extensive digital computer simulation using EMTDC/PSCAD software.

ACKNOWLEDGEMENT

For starters, I would like to express my deep gratitude to my principal supervisor Arindam Ghosh for his continuous encouragement, inspiration, and guidance. Professor Ghosh helped me in so many ways with his great patience and profound knowledge. Without his support, the research work for this thesis would not have been accomplished. Through the last three years, I have gained a strong ability in doing research under his supervision. I feel very lucky to have him as my supervisor.

I also thank my co-supervisor Dr. Sumedha Rajakaruna for his help. My chairperson Dr. Yee-Hong Leung provided kind support as well. My colleagues and friends Megha, Andi, Mehdi, Ehsan, Amit all helped me in different ways during my PhD study. I would like to express my sincere gratitude to all of them.

Last but not least, I thank my family, especially my husband, for their great support. My husband Puneet has been encouraging me in every stage of my PhD study. He supported me with his big patience and dedication to our family. His continuous encouragement made this thesis conducted smoothly.

CONTENTS

LIST OF FIGURES

LIST OF TABLES

KEYWORDS

Array Efficiency

Fault Operation

Grid Side Converter (GSC)

High Voltage Direct Current (HVDC)

Maximum Power Point Tracking (MPPT)

Multi-terminal

Normal Operation

Overvoltage

Parallel DC Collection System

Permanent Magnetic Synchronous Generator (PMSG)

Pitch Control

Series DC Collection System

Single Active Bridge

Voltage Control

Voltage Source Converter (VSC)

Wind Energy Conversion System

Wind Power Branch

Wind Power Collection System

Wind Power Unit

Wind Side Converter (WSC)

ABBREVIATIONS

BTB	Back-to-back
DG	Distributed generator
GA	GSC adaption
GR	GSC reconfiguration
GSC	Grid side converter
HVDC	High voltage direct current
IBC	Independent branch control
IPOS	Input parallel output series
IVRM	Input voltage reference modification
MG	Microgrid
MPPT	Maximum power point tracking
OLTC	On load tap changing
OPC	Optimal power control
OTC	Optimal torque control
PMSG	Permanent magnetic synchronous generator
PRM	Power reference modification
PWM	Pulse Width Modulation
RCL	Relative cable length
SAB	Single active bridge
SC	Switch combination
SSBA	Small sized battery application
TSR	Tip speed ratio
UIR	Unit independence rule
USPR	Upstream switch preference rule
VDP	Voltage distribution principle
VSC	Voltage source converter
WECS	Wind energy conversion system

WSC	Wind side converter

LIST OF SYMBOLS

I_d, I_{dc}	Measured DC current
I_d^*, I_{dcref}	DC current reference
V_d, V_{dc}, V_{dci}	Actual DC voltage of a WSC/ WSC-*i*
V_d^*, V_{dc}^*, V_{dcl}^*	DC voltage reference
P_d, P_W	Measured wind power
P_d^*, P_{ref}, P^*	power reference
m, m_1, m_2	Droop coefficient
P_M, P_m	Mechanical power of a wind turbine
ρ	Air density
v_w, v_{wi}	Wind speed of a wind turbine/ turbine-*i*
C_p, C_{pi}	Rotor efficiency a wind turbine/ turbine-*i*
β	Pitch angle (rad)
λ	Tip speed ratio
T	Mechanical torque
ω	Rotating speed (rad/s)
ω^*	Rated rotating speed (rad/s)
f^*	Rated frequency
δ_w	Wind side angle deviation (rad)
δ_g	Grid side angle deviation (rad)
P, P_i	WECS power output a WSC/ WSC-*i*
L_f, L, L_σ	Inductance
ω_M	Turbine blade rotating speed (rad/s)
r_b	Turbine blade radius
g, g_1, g_2	Gate firing signal
V_{dcl}	Input voltage of a DC boost converter

V_{dch}, V_{dchi}	Boosted voltage by a converter/ converter-i
D, α	Duty ratio
u_d, u_{d0}, u_{dp}	PWM control signal
f_{MG}	Actual microgrid frequency
P_{DG}^{*}	DG rating
P_{DG}	DG power output
i_p, i_l, i_{li}	Input current of a SAB/ SAB-i
i_s, i_h	Output current of a SAB
v_{abp}	Primary side voltage of a SAB transformer
v_{abs}	Secondary side voltage of a SAB transformer
i_{ab}	Current of a SAB transformer
f	Switching frequency
V_{TN}	Rated transmission voltage
V_N	Rated wind power unit voltage
V_T	Actual transmission voltage
m_a	Modulation index
V_{lw}	Lower voltage limit
V_{up}	Upper voltage limit
P_{outi}	Power output of PMSG-i
V_i	DC voltage of WSC-i
P_{bi}	Power exchange with battery in WECS-i
U_{av}	Average DC voltage of WSCs
P_{av}	Average power outputs of WSCs
P_{min}/ P_{max}	Minimum/ maximum power limit
P_{minr}/ P_{maxr}	Minimum/ maximum power limit with PRM
P_{iref}	MPPT power reference of WSC-i
P_{irm}	PRM power reference of WSC-i

P_{md}	Biggest PRM power reference
P_{Ri}	Chopping resistor power of WECS-*i*
V_{LL}	AC line-to-line RMS voltage of a VSC
$V_i^{'}$	DC voltage of WSC-*i* after fault
$V_i^{''}$	DC voltage of WSC-*i* with IVRM
$V_T^{''}$	Transmission voltage with IVRM
V_w/ V_g	Rated AC voltage of a WSC/ GSC
$V_g^{''}$	Reset AC voltage of a GSC
V_{g1}/ V_{g2}	Voltage before/ after an OLTC transformer
$V_{T\min}^{''}$	Lowest transmission voltage with an OLTC
V_{ST1N}/ V_{ST2N}	Rated DC voltage of a small/ big sized GSC
V_{STi}	Measured DC voltage of a small GSC-*i*
V_{pi}	The DC voltage of unit type-*i*
K_{BE}	Branch efficiency
V_{piu}/ V_{pid}	voltage by operating up/downstream switches
V_{li}	DC voltage of wind power branch-*i*
V_{li}^{*}	DC voltage reference of wind power branch-*i*
l_d, l_I, l_G, l_i	Relative cable length (of cable-*i*)
V_I	Integration point voltage
V_G	DC voltage at the grid terminal
P_{wi}	Power output of a wind farm-*i*
I_i	DC current through cable-*i*
V_{li}	Distributed voltage on cable-*i*
k_i	Voltage drop slope on cable-*i*
P_{ri}	Rated power output of wind farm-*i*
R_B	reference cable resistance of per unit length
R_i	Resistance HVDC cable-*i*

R_{avi}	Resistance of variable resistor-*i*
$P_{\min i}$	Minimum power output of wind farm-*i*
R_{vi}	Minimum resistance of variable resistor-*i*
V_{Ti}	Actual voltage of HVDC terminal-*i*

CHAPTER 1

INTRODUCTION

As one of the most valuable resources of nature, wind energy has been harnessed since ancient times. This energy is essentially a form of solar energy. Depending on the earth surface environments (land or water) and the time duration (day or night), the heating from the sun is uneven. The exchange of hot air and cold air results in wind [1]. A very important wind pattern is the "trade wind," which mainly blows from the east to the equator continuously [2]. Fig. 1.1 shows the flow directions of trade winds.

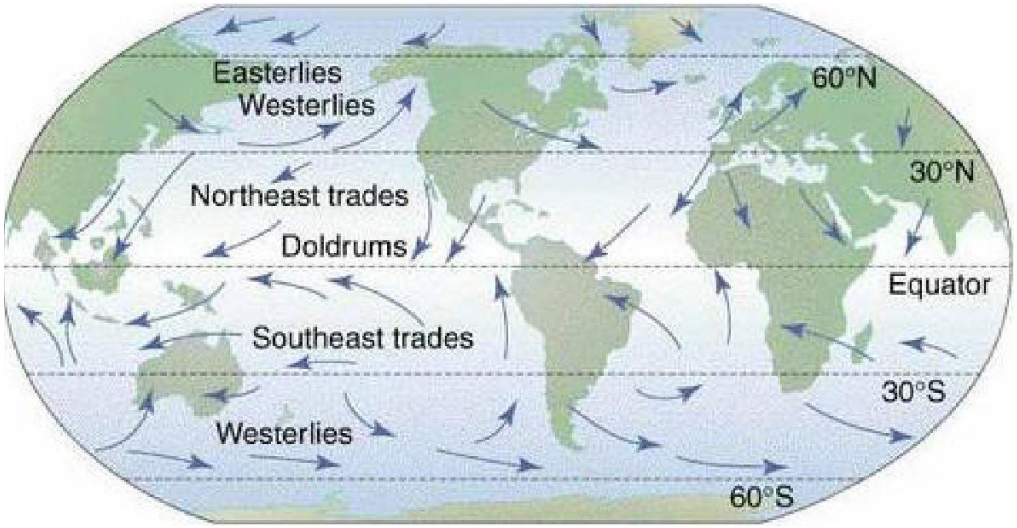

Fig. 1.1. Flowing of trade winds [3].

It is believed that wind power was used as far back as 5000 B.C. to propel boats along Nile River [4]. The trade winds have especially played significant roles in the sailing of ships for generations. Over millennia, wind energy has been used for various purposes (e.g., water pumping, grain grinding, irrigation and electricity generation) after windmills were invented [5-6]. In recent years, using the lessons learned from windmills, wind turbines are employed for electric power supply.

The history and critical developments of wind energy application in power generation are listed in Table 1.1 [7-10]. At first, wind energy was harvested in small capacities in rural areas that were not connected to electricity grids. However, as electricity networks expanded in several parts of the world, the necessity of such

small-capacity turbines diminished and they were shut down. Furthermore, due to the cheap prices of fossil fuels and the abundance of nuclear energy, no further development in wind energy took place for almost 30 years. Later, due to the increasing environmental concerns and the rise in fuel prices, the redevelopment of wind power started between the 1980s to the 1990s. The first offshore wind farm built in 1991 in Denmark marks the beginning of massive offshore wind energy utilization. Afterwards, the worldwide offshore wind power capacity has been increasing dramatically year by year and big strides have been made in wind power technology. Fig 1.2 shows the total and offshore worldwide wind power capacities from 2011 to 2015 provided by Global Wind Energy Council (GWEC) [11-12].

Table 1.1: Wind power history and development.

Time	Development
1887	First windmill for electricity generation being built
1927	First factory to produce wind turbines being opened
1931	First commercial power plant that employed wind turbines to produce electricity being constructed
1941	First megawatt-size turbine being built
1980	First wind farm of 20 turbines being built
1991	First offshore wind farm being installed in Denmark
2009	First operational deep-water large capacity floating wind turbine being installed in the North Sea off Norway

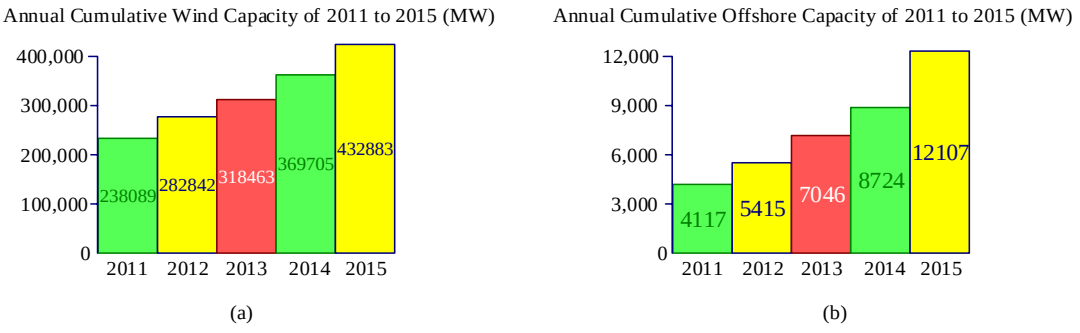

Fig. 1.2. Installed wind power capacity from 2011 to 2015: (a) total capacity and (b) offshore capacity.

The latest Global Wind Report from GWEC shows that the totally installed offshore wind capacity has exceeded 12 GW by 2015, of which more than 91% is in Europe with UK being the leading market. Apart from the numerous developments off the European coast, offshore wind power is blooming in other countries such as

China, Japan, South Korea, US and India. The worldwide popularity of offshore wind energy compared to other renewable resources results from its unlimited availability, short distances to most large cities and avoidance of construction over land properties [13].

In the traditional electricity supply industry, traditional fossil fuels are utilized. This however, is becoming an increasingly serious problem due to its negative impact on the environment. Air pollution in some developing nations and/or cities has already affected people's health directly. Carbon emission which causes global warming is another problem that cannot be ignored. Because of these deleterious effects of fossil fuels vis-à-vis environment and health, the exploitation of renewable energy is developing.

One way of alleviating this problem is to use renewable energy sources, like wind, which is in abundance in offshore areas. Wind power from offshore wind farms are usually evacuated to the onshore electricity grids through subsea HVDC cables. In this regard, the power from a number of wind turbines or even wind farms are collected together before being dispatched through HVDC lines. Unfortunately however, there is no standard collection topology for this purpose. In this thesis, various collection topologies are studied and the merits and demerits of these topologies are pointed out.

1.1. WIND GENERATOR TYPES AND MPPT CONTROL

The first step in wind energy utilization is to convert wind kinetic energy to mechanical energy. This is achieved by wind turbines, which are essentially modern forms of windmills. Second, the mechanical energy is passed to a wind generator to generate electricity, which is usually sent to a power grid. Wind turbines are classified by the axis that the turbine blades spin around. Hence the two types of turbines are Horizontal Axis Wind Turbines (HAWTs) and Vertical Axis Wind Turbines (VAWTs). Modern wind farms favor HAWTs, whose rotors can have 2 or 3 blades [14-15].

1.1.1. TYPES OF WIND GENERATORS

The wind power generators are classified into five types by IEEE, which are discussed below [16-19].

Type-1: Fixed Speed Wind Generators

This type of wind generator is basically a Squirrel Cage Induction Generator (SCIG), which operates within a small range above the synchronous speed. The active power is controlled by a stall control instead of a pitch control. Reactive power is required for a SCIG and shunt capacitors are installed for this purpose. As there is no power converter between a type-1 generator and the grid, the fluctuations in the output voltage and power are inevitable with varied wind speed.

Type-2: Limited Variable Speed Wind Generators

Wound Rotor Induction Generator (WRIG) is referred to as the Type-2 wind generator. It can operate up to 10% above the synchronous speed due to the use of variable rotor resistance. The active power is controlled by a blade pitch control. Similar to a SCIG, a WRIG requires reactive power supply and shunt capacitor banks are installed. However, the output voltage and power fluctuations are less pronounced than those of a Type-1 generator.

Type-3: Variable Speed with Partial Power Electronic Conversion

This type can either be a Doubly Fed Induction Generator (DFIG) or a WRIG. A back-to-back (BTB) voltage source converter, which has control on both active and reactive power, is employed between the generator rotor and the gird. As a result, the operating speed range can be ±25%-35% of the synchronous speed. A blade pitch control is employed for the active power control, but no reactive power compensation is needed. The employment of a Type-3 wind generator reduces voltage and power fluctuations but requires more maintenance work.

Type-4: Variable Speed with Full Power Electronic Conversion

This type of wind generators can be a SCIG, a Wound Rotor Synchronous Generator (WRSG) or a Permanent Magnetic Synchronous Generator (PMSG). A fully rated BTB voltage source converter is employed between the generator and the

gird, which completely decouples the wind side and the grid side. As a result, the operating speed can be between 0 and the synchronous speed. Similar to a Type-3 wind generator, reactive power compensation is not required. Furthermore, the grid side does not get influenced by wind speed fluctuations. The only disadvantage of Type-4 wind generators is their high installation costs.

Type-5: Fixed Speed with Speed/ Torque Conversion

A Type-5 wind generator is actually a synchronous generator, which is connected with the wind turbine through a torque/ speed converter. This converter accommodates the variable rotor speed and the constant generator speed. This type of generators is connected to the grid directly.

Generally speaking, wind generators tend to get more advanced from Type-1 to Type-5. Nowadays, Type-1 and Type-2 wind generators are not installed any more, but they are still operating in some old wind farms. Type-3 wind generators are most widely used, but Type-4 wind generators, especially PMSGs, are gaining popularity worldwide. The Type-5 wind generator is promising, but has not found practical application yet. A comparison of the first four types of wind generators is listed in Table 1.2 (Type-5 is not shown due to the lack of practical data).

Table 1.2: Wind generator comparisons.

Wind Generator	**Speed**	**BTB Converter**	**Maximum Rating**	**Energy Conversion Efficiency**	**Costs**	**Power Losses**
Type-1	Fixed	No	Around 2 MW	Low	Low	Low
Type-2	Semi-variable	No	Around 2 MW	Low	Low	Low
Type-3	Variable	Partial	6 MW or more	High	High	High
Type-4	Variable	Full	6 MW or more	High	High	High

The main focus of this thesis is on DC power collection systems for offshore wind farms, which require connections of large sized wind generators on the DC side. Therefore, the wind generator with a DC link is preferred. Besides, to make the most utilization of wind energy, a variable-speed wind generator is advantageous compared to a fixed-speed one. The other factors that need to be considered for generator selection are the investment costs and power losses.

It can be seen from Table 1.2 that a Type-4 wind generator is the most suitable choice for this thesis. The relatively high power losses and investment costs of Type-4 wind generators are mainly due to the use of full-rated power converters. These economic gaps will be gradually filled with the development of semiconductor techniques. Furthermore, this thesis will make cost-effective wind power collection proposals such that the use of power converters can be reduced.

As been stated previously, a Type-4 wind generator can be an SCIG, a WRSG or a PMSG. For this research, the PMSG is employed as the wind generator of the Wind Energy Conversion System (WECS). The preference of the PMSG to the SCIG or WRSG are based on two reasons [20]. First, compared to induction generators, synchronous generators are better suited for direct-drive or gearless wind turbines, which are more economical. Second, the permanent magnet generators have higher efficiency and power density than wound rotor generators. The only restriction that currently holds back the application of PMSGs results from the high prices of magnets.

1.1.2. MPPT CONTROL

To extract and convert wind energy as much as possible, Maximum Power Point Tracking (MPPT) is employed for a variable-speed WECS. The MPPT control aims to optimize the generator speed in order to maximize the output power from the wind turbine. Generally speaking, the control tasks of the BTB converter in a PMSG based WECS are assigned as: (1) the Wind Side Converter (WSC) controls the active wind power flow through a MPPT algorithm, and (2) the Grid Side Converter (GSC) maintains the DC voltage and reactive power balance.

Regarding MPPT control, various methods have been proposed by researchers and comparisons have been conducted from different aspects [21-25]. The typical MPPT algorithms are summarized as:

- Turbine Power Profile (TPP): the generator power follows the power reference that is obtained through the maximum power to wind speed profile;
- Optimal Tip Speed Ratio (TSR): the tip speed ratio of the wind turbine is kept at its optimal value;

- Optimal Torque Control (OTC): the generator mechanical torque follows the torque reference calculated from the generator speed;
- Perturbation and Observation Control (P&O): observe the power output after the generator speed is perturbed and adjust the direction of the perturbation, if necessary.

The four methods listed above require different information. TPP needs a power versus wind speed curve and a wind speed sensor must be fitted to the system. TSR requires turbine parameters and a wind speed sensor. OTC is a sensorless algorithm, which only needs turbine parameters and air density values. P&O is also senseless and only needs to measure the power output.

It is obvious that the sensorless MPPT methods (OTC and P&O) can save the investment costs, but their performances may not be as good as the methods with speed sensors (TPP and TSR). Favoring the high efficiency of TSR, reference [23] proposes an improved MPPT method, where the TSR control provides fast dynamic characteristics, and the added hysteresis controller corrects the MPP error at the steady state. To achieve a better performance with the sensorless MPPT algorithms, studies have been conducted on their improvements. For the P&O method, the value of the step size has opposite influences on its efficiency and convergence speed. To solve this tradeoff, the step size is scaled by the slope of the power with respect to the perturbation variable in [24] to enhance the tracking capabilities of the MPPT algorithm. With the development in computer science engineering, intelligent heuristic mathematical algorithms such as fuzzy logic control and neutral network are applied in MPPT control methods for performance improvements. Reference [25] also proposed the modified versions of P&O.

This thesis studies offshore wind power, to which the investment costs are a big restriction. Therefore, a sensorless MPPT method is preferred. Furthermore, the operation of a DC power collection system, which will be studied in this research, might be highly sensitive to the outputs of each wind turbine [26]. This implies that a MPPT method with fast response to wind speed variations is favored. According to [25], both the conventional and modified P&O have relatively lower convergence speeds compared to OTC. However, OTC has the problem that it maximizes the

mechanical wind power instead of the output electrical power, which indicates a minor lack of accuracy. A modified version of OTC is proposed in this thesis.

1.2. WIND POWER COLLECTION SYSTEMS

The power output of a wind generator is AC power. However, to facilitate wind power utilization, this AC power is usually converted to a constant frequency AC or DC through power converters. Therefore, distant offshore wind power can be collected through either AC or DC systems. When an AC collection system is employed, transformers are required for the AC voltage regulation of the wind power. For a DC collection system, the voltage regulation is achieved by DC/DC converters.

1.2.1. AC COLLECTION SYSTEMS

Generally speaking, AC collection systems are more commonly used topologies compared to DC systems [27-28]. Reference [27] listed three AC collection topologies, which are AC radial systems, AC radio-loop systems and AC star systems. They all need transformers for voltage boosting before being connected to the onshore grid. AC radial collection systems are divided into the small and the large AC wind farms in [28-29]. The main difference between these two sized systems is that the offshore platform with a transformer can be omitted in a small AC wind farm.

The AC collection systems above are all based on AC transmission. However, with the increasing penetration of wind power into grids, the High Voltage Direct Current (HVDC) transmission is more favoured than an AC transmission system [30]. To apply DC transmission, the power output of each generator is passed through a BTB converter and collected through AC cables. A transformer is used to boost the AC voltage afterwards and the wind power is then delivered to an onshore grid by HVDC [28-29]. A real offshore wind project using such AC/DC hybrid power collection system is discussed in [31].

Another type of hybrid collection systems applies a transformer at the output of each wind generator. The generated power from the entire wind farm is processed by a single power converter and sent out by HVDC [32-33]. An obvious advantage of

this collection system is that the investment costs are significantly reduced due to the use of only one power converter. However, apparently the MPPT control cannot be applied to each individual wind turbine and the maximum power extraction thus cannot be fully achieved. The comparisons of wind power collection systems using multiple and single power converters are conducted in [33].

For a tradeoff between investment costs and wind power extraction, wind turbines within an offshore wind farm are grouped into clusters and each cluster is connected to a common AC/DC converter [34]. In this way, several wind turbines share a power converter, which indicates relatively cheap costs. On the other hand, wind turbines within a cluster receive almost the same wind speed. This implies the MPPT control can be accomplished for almost every wind turbine.

Fig. 1.3 shows the topologies of the typical AC collection systems [28-29, 34]. In this, the AC radial system is illustrated in Fig. 1.3 (a) and the AC/DC hybrid collection system with multiple power converters is demonstrated in Fig. 1.3 (b). It can be seen that both collection systems are based on parallel connection.

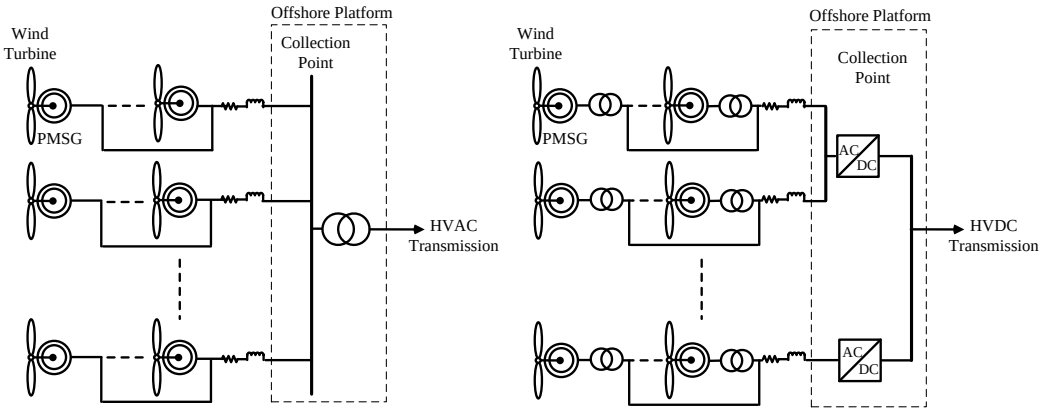

(a) (b)

Fig. 1.3. Typical AC collection systems: (a) AC radial and (b) AC system with HVDC transmission.

1.2.2. DC COLLECTION SYSTEMS

Another type of wind power collection systems only employs DC connection, which has lower costs and losses than when AC connection is involved, especially for large offshore wind farms [27, 35-37]. This type of collection systems requires DC/DC converters for voltage step-up. The most popular DC collection system uses parallel connection to collect DC power from each wind turbine and delivers the

collected power by HVDC after voltage boosting [38-40]. This is the so-called parallel DC collection system. New DC collection topologies for offshore wind farms are proposed involving series connection. These mainly include the series-parallel [41-42] and series DC collection systems [37, 43]. The three wind power DC collection systems described above are shown in Fig. 1.4. It can be seen that DC/DC converters are not required as long as there is series connection.

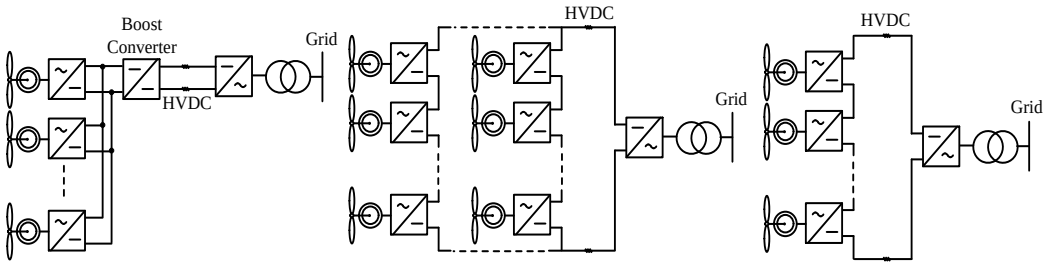

Fig. 1.4. Typical DC collection systems: (a) parallel (b) series-parallel and (c) series collection.

1.3. MULTI-TERMINAL HVDC FOR WIND POWER DELIVERY

As wind power is non-dispatchable, the MPPT output of a wind farm might be excess or inadequate for its connected onshore grid at different instants, depending on wind speeds. Based on this fact, power sharing among wind farms and AC grids is beneficial. This power sharing is realized through the proper interconnection of relevant power systems. Besides, considering the commonly long distances among different systems, high voltage transmission is preferred to minimize power losses. Therefore, the candidate topologies for wind power sharing should be multi-terminal and high voltage transmission. A high voltage transmission system can be HVAC or HVDC. Generally speaking, HVDC is better than HVAC regarding large-capacity power transmission for long distances. Detailed comparisons of HVDC versus HVAC for large offshore wind farms have been conducted in [44-45].

1.3.1. TYPES OF MULTI-TERMINAL HVDC SYSTEMS

Multi-terminal HVDC transmission systems are characterized by having more than two converter stations interconnected on the DC side of the transmission system. The multi-terminal HVDC system has been considered and discussed since 1960s [46]. According to the network structures, six topologies including point to

point, general ring, star, star with a central switching ring, wind farms ring, and substation ring are discussed in [46]. In general, multi-terminal DC (MTDC) configurations are classified into parallel MTDC and series MTDC. Usually, parallel MTDC employs the Voltage Source Converter (VSC) and series MTDC uses the Current Source Converter (CSC). The traditional thyristor based Line Commutated Converter (LCC) has also been used for parallel MTDC systems.

The parallel connection of LCCs has been shown applicable on land, but is not suitable for offshore wind farms [44-45]. There are several advantages of VSC over LCC in MTDC transmission, such as: (1) VSC has independent active and reactive power control, (2) VSC has the capability of feeding island and passive networks, (3) VSC has much smaller size and faster control than LCC, (4) there is no commutation failure problem with VSC, and (5) it is relatively easy to extend to MTDC using VSC [47-51]. However on the downside, a VSC has higher power losses and is more expensive compared to an LCC station.

As for connection types, only the parallel configuration has been proved practical [52]. The series connection may not be the best choice for large MTDC networks considering fault condition [53-54]. However, a CSC based MT-HVDC in series interconnection system is proposed in [55], where the technical obstacles have been ignored. The hybrid MTDC, in which CSC-MTDC and VSC-MTDC are used together, is also discussed [53]. Overall, the VSC based MT-HVDC in parallel connection shows more advantages and is the most promising multi-terminal configuration for offshore wind farms. A schematic diagram of an MT-HVDC system (four-terminal) of this type is shown in Fig. 1.5 [56]. It can be seen that a DC bus to interconnect the multi-terminals may or may not be employed, depending on the connection locations of the terminals.

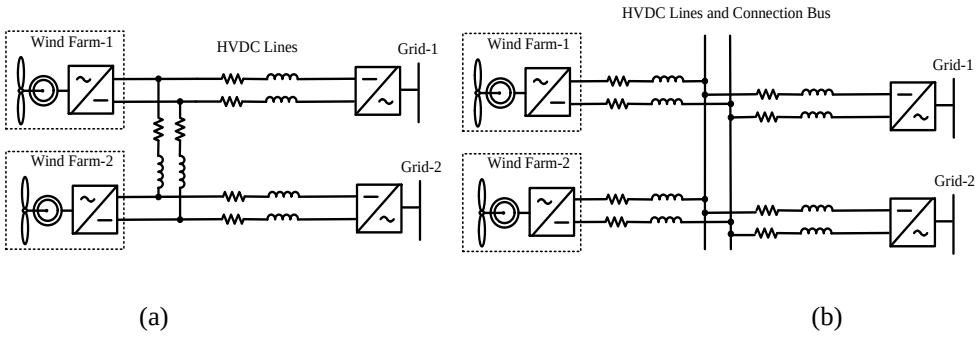

Fig. 1.5. Parallel multi-terminal HVDC for offshore wind farms: (a) without and (b) with a bus.

1.3.2. CONTROL OF VSC BASED MULTI-TERMINAL HVDC SYSTEMS

Numerous control strategies have been proposed for multi-terminal HVDC systems using VSCs. The general way is to control the DC voltage of the transmission system by one or more of the VSCs and the rest of the VSCs control their respective power flow. The entire control system can be divided into four levels, which are current control, primary control, secondary control and tertiary control [57-59]. The referred active power control and DC voltage control belong to the primary control level. Regarding the control schemes of multi-terminal HVDC systems, most studies focus on the primary control. This is because the primary control level aims at achieving a suitable power sharing, while the other control levels generally facilitate a more efficient system operation [58].

The strategies on the primary control level are largely divided into two types, depending on whether a communication system is required [46]. The typical power sharing strategies with and without communication are respectively master-slave control and droop control. There are various derivatives of these two typical power sharing schemes, of which the popular ones include margin voltage control [60-64], ratio control [65], priority control [66], etc. The principles of each control method are described and comparisons are conducted among them from different aspects [53, 58, 67].

Compared to other power sharing strategies, droop control attracts more attention, especially when wind farms are involved [58]. The basic droop control can be the relationship between the DC voltage (V_d) and DC current (I_d) or the DC voltage and active power (P_d), which are respectively written as

$$I_d - I_d^* = m_1 \times (V_d - V_d^*) \tag{1.1}$$

and

$$P_d - P_d^* = m_2 \times (V_d - V_d^*) \tag{1.2}$$

where I_d^*, P_d^*, V_d^* are the DC current, active power, DC voltage references and m_1, m_2 are the droop gains. The current and power based droop control schemes described by (1.1) and (1.2) are illustrated in Figs. 1.6 (a) and 1.6 (b) respectively, where PI stands for proportional-plus-integral controller.

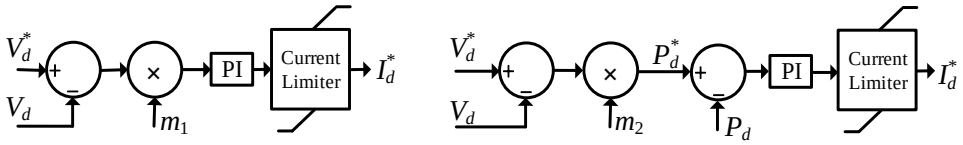

(a) (b)

Fig. 1.6. Schematic diagrams of the droop control: (a) current based and (b) power based.

The control requirements of a multi-terminal HVDC system have some unique features when offshore wind farms are incorporated. First, the power flowing direction is always from the wind farm side to the grid side. Therefore, the terminals connected to the wind farms (wind-terminals) operate as rectifiers, while the terminals connected to the grids (grid-terminals) operate as inverters [56]. Second, as wind power is non-dispatchable, the wind terminals are usually under power control to deliver all the generated power. The DC voltage of the transmission system is usually maintained by the grid terminals [58]. According to the recommendations established by the Great Britain Security and Quality of Supply Standard (GB SQSS) Expert Group, the criteria for a multi-terminal HVDC with offshore wind power system include: (1) controlling DC voltage in both normal and fault operation, (2) providing support to the grid in the event of a gird fault, and (3) ensuring sufficient power flow to the main AC grid under a terminal failure [46].

Multi-terminal HVDC transmission system cases with offshore wind power delivery are studied in [68-70]. In [68], droop control is employed to integrate the optimal offshore wind power flow dispatch in the North Seas. In [56], [69] and [70], a four-terminal HVDC system comprising two offshore wind farms and two girds is studied. Both the wind and grid terminals apply droop control in [56], while [69] only employs droop control for power sharing between the grid-terminals. An improved adaptive droop control method is proposed and applied on the grid side in [70]. All the proposed offshore wind power sharing and voltage control strategies for multi-terminal HVDC systems allow for terminal voltage variations to some extent.

1.4. OBJECTIVES OF THE THESIS AND SPECIFIC CONTRIBUTIONS

Based on the literature review presented in the previous sections, the gaps on wind energy utilization are identified. These gaps involve the generation, collection and transmission of offshore wind power. To improve the operation efficiency of

offshore wind power systems, the objectives of the thesis are established based on these gaps.

1.4.1. OBJECTIVES OF THE THESIS

- Improvement of the parallel DC collection system for offshore wind farms.
- Development of voltage balancing strategies for the series DC collection system under both nominal and faulted conditions.
- Design of overvoltage prevention schemes for the series-parallel DC collection system upon wind turbine failures.
- Design of voltage control strategies for the multi-terminal HVDC integration of offshore wind farms using different power collection systems.

1.4.2. SPECIFIC CONTRIBUTIONS OF THE THESIS

Based on the above objectives, the specific contributions of this thesis are

1. The system topology options for parallel DC collection employed by offshore wind farms are investigated. The favoured topologies include: (1) parallel connected VSC WSCs with an isolated boost converter and (2) several VSC WSCs connected in parallel with a number of Input Parallel Output Series (IPOS) interfaced boost converters. The Single Active Bridge (SAB) DC/DC converter is shown to be advantageous for the voltage boosting of unidirectional wind power. Therefore, both topologies mentioned above employ SAB converters for HVDC offshore wind power transmission.
2. Different offshore wind power collection systems are discussed and the advantages of series DC collection are presented. As the operation of a series DC collection system is sensitive to the wind turbine outputs, voltage balancing strategies might be required considering uneven wind speed within an offshore wind farm. Two such balancing strategies are proposed, which employ (1) small sized batteries and (2) modified pitch control or chopping resistors.
3. The fault condition of wind turbine failures is studied for the series DC collection system. To deal with the overvoltage problem under fault, the input DC and output AC voltage references of the GSC are modified according to needs. A second overvoltage prevention strategy is proposed using multiple grid side converters. An analysis is presented for the best possible choice.

4. For the series-parallel DC collection system, the previously proposed voltage control strategies are proved to be effective under normal operation, but do not apply to the fault operation unconditionally. Therefore, voltage control strategies exclusively for series-parallel DC collection are proposed, which use: (1) power switches for topology reconfiguration and (2) DC/DC converters for partly independent voltage regulation of wind turbine clusters.
5. Offshore wind power integration through multi-terminal HVDC transmission is studied considering different power collection systems. The integration point of each wind farm is selected from both the theoretical and economic point of view. The terminal voltage of a parallel DC collection system is adjustable, while that of a series DC collection system is strictly fixed to the reference value. Based on this, the voltage control of each terminal (wind side or grid side) is achieved either through DC/DC converters in parallel DC collection or by employing semi-conductor controlled variable resistors.

1.5. THESIS ORGANIZATION

The thesis is organized in eight chapters. The organization of the rest of the chapters are presented below.

In **Chapter 2**, the preliminary study of wind energy conversion systems is conducted. First, the wind turbine and generator control (mainly pitch control and MPPT control) are discussed. Then the operation principles of the VSC and diode based WECSs are presented. For the VSC based system, two structures are considered, i.e., VSC realized by three H-bridges and three-leg VSC with PWM control. The power loss of a WECS connected to an infinite bus is simulated in PSCAD with both 3 H-bridge and PWM controlled converters and the latter shows less loss. Finally, the proposed WECS model and its control schemes are verified by an integration example with a frequency droop controlled microgrid.

The parallel DC collection system for offshore wind farms is discussed in **Chapter 3**, where both the diode and the 3-leg VSC based WECSs are considered. Three collection topologies are presented. First, the parallel DC collection of wind power drawn by diode rectifiers with 2-channel boost converters is studied. Since the non-linear nature of the diode rectifier causes stator current harmonics, the three-leg VSC is employed. The control and operation of the WECS with VSC WSC and the

two-channel boost converter are demonstrated. However, the parallel connection of this scheme is not studied because of its distinctive drawbacks.

The second parallel DC collection topology employs VSC based WECSs and an isolated DC/DC boost converter. The SAB is chosen for the voltage boosting of massive offshore wind power due to its advantages. The third type of parallel DC collection system is proposed for the current ripple limitation of SABs. In this topology, the parallel output of the VSC WSCs is connected to a SAB cluster. This cluster is formed by several SABs connected in parallel at the input and series at the output. The third topology is also advantageous when the rating of the high frequency transformer in the SAB is insufficient. Besides, the current harmonic limitation effect of the smoothing reactors installed on HVDC transmission lines is shown as well. Finally, the fault condition of wind turbine failures is simulated for the second and third parallel DC collection systems.

A series DC collection system is proposed in **Chapter 4**. The advantages of this proposed topology are demonstrated through the discussions on different offshore wind power collection topologies. The DC voltage limitations are defined based on device tolerance and the control technique. The operation of series DC collection is shown to be sensitive to the power outputs of the wind turbines. Therefore, the outputs of WSCs need to be balanced to prevent out-of-range voltages caused by uneven wind speed in an offshore wind farm. Based on this, two strategies are proposed. First, a small sized battery is applied between each wind generator and its WSC to absorb or provide power as required. Second, the power references for some WSCs are reduced from the previous references obtained by MPPT and the excess power from wind generators is dissipated by chopping resistors. Besides, the wind turbines can be controlled to convert less wind energy by modifying the pitch control system if chopping resistors are not applied.

Chapter 5 considers the safe operation of the series DC collection system upon wind turbine failures. First, the demand for fault voltage control of series DC collection is demonstrated. During a serious fault condition in the collection system, the transmission voltage reference is reduced upon fault by modifying the input voltage reference of the GSC. Accordingly, the AC side voltage of the GSC is reduced if required. This can be achieved either through low initial AC voltage

selection or by employing an On Load Tap Changing (OLTC) transformer. The two voltage control strategies proposed in Chapter 4 are compared to and combined with this fault voltage control strategy. Another overvoltage prevention strategy is based on modifying the original series DC collection system for fault conditions. In this strategy, the GSC is replaced by several inverters with smaller capacities. One small sized GSC with the same rating of a WSC is bypassed upon each fault.

The series-parallel DC collection topology for offshore wind farms is discussed in **Chapter 6**. The voltage control strategies for normal operation proposed in Chapter 4 are proved to be effective for series-parallel DC collection. However, the GSC voltage reference modification upon fault proposed in Chapter 5 is only conditionally effective for the series-parallel DC collection system. To deal with this fault control limitation, two generic fault voltage control strategies are discussed. First, power switches are applied between adjacent parallel wind turbine branches for topology reconfiguration upon fault. Different switch operations are compared and switching principles are identified. Second, a DC/DC converter is connected at the output of each wind turbine branch for voltage accommodation. In this way, the branches without fault are not influenced by wind turbine failures.

The multi-terminal HVDC transmission system for offshore wind power integration is discussed in **Chapter 7**. This chapter focuses on a 3-terminal system with two wind farms and one main AC network. Firstly, the integration rule for determining the interconnection locations of the terminals is identified and the integration points are located subsequently. The rest of this chapter studies the terminal voltage control strategies when different DC collection systems are employed by offshore wind farms. If at least one wind farm uses parallel DC collection, the terminal voltages can be stabilized through the DC/DC converter(s) incorporated in the collection system(s). If power from both wind farms are collected through the series DC collection system, the HVDC line resistances must be adjusted. This is achieved through the proper control of semiconductor based variable resistors, which are connected in series with HVDC lines.

Chapter 8 summarizes the general conclusions of the thesis and briefly outlines the scope of any future work.

CHAPTER 2

TOPOLOGY AND CONTROL OF PMSG BASED WECSS

Wind power is generated through Wind Energy Conversion Systems (WECSs). Generally speaking, a WECS consists of a wind turbine and a generator, and may also contain a power converter. In this chapter, the operation principle of each WECS element is discussed and respective control strategies are proposed. A PI controller based pitch control is applied to the wind turbine. A direct-drive PMSG is employed as the wind generator. The optimal power control based MPPT method is developed for PMSG based WECSs.

The common control scheme of wind power converters is to control power by a Wind Side Converter (WSC) and the DC voltage is maintained by a Grid Side Converter (GSC). It is noted that the WSC in this thesis incorporates all the power converters between the wind generator and the DC transmission cables. Two VSC topologies with their control are presented. The conversion efficiency of the WECS with these two VSC topologies is compared vis-à-vis their power loss components.

Another type of conversion system is also studied, which contains a diode based uncontrolled rectifier with a DC/DC boost converter. An MPPT control is realized by adjusting the duty cycle of the boost converter. An integration example of wind power with a microgrid is studied to verify the designed PMSG based WECS.

2.1. WIND TURBINE AND GENERATOR CONTROL

Wind energy is captured by the blades of a wind turbine and converted into mechanical power (P_M), which is calculated by

$$P_M = \frac{1}{2}\rho A v_w^3 C_p \tag{2.1}$$

where ρ is the air density, A is the cross-sectional area through which the wind passes, v_w is the wind speed and C_p is the rotor efficiency of the blade. C_p is calculated from [71]

$$C_p = 0.5176 \times (\frac{116}{\lambda_i} - 0.4\beta - 5) e^{\frac{-21}{\lambda_i}} + 0.0068\lambda \tag{2.2}$$

where β is the pitch angle, λ is the tip speed ratio, and λ_i is given by

$$\frac{1}{\lambda_i} = \frac{1}{\lambda + 0.08\beta} - \frac{0.035}{\beta^3 + 1} \tag{2.3}$$

The wind turbine operates at the generator control mode when the wind speed is below the rated wind speed, and works under the pitch control when the wind speed exceeds the rated value. A PI controller is employed in this research for the pitch angle control, which is shown in Fig. 2.1 [72]. The input is the error of the measured wind turbine output power P_m and the reference power P_{ref}. The rate limiter and the hard limiter are to limit the rate of change and the boundary values of the pitch angle.

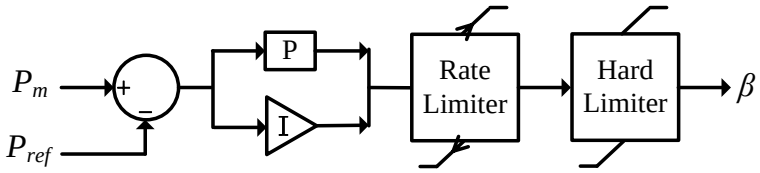

Fig. 2.1. Schematic diagram of the employed pitch control.

According to the pitch control loop, when P_m is equal to or smaller than P_{ref}, their error is negative and β can be kept at its optimal value to capture the maximum power available from the wind. If P_m is bigger than P_{ref}, their error is positive and β will regulate to limit the power output of the wind turbine to prevent the power from exceeding the designed capability. If the wind speed is so high that it is over the designed cut-out speed, β will change to pitch out of the blade and the wind turbine will be shut down.

To extract the maximum power from the wind energy, turbine blades should change their speed as the wind speed changes. Maximum Power Point Tracking (MPPT) controls the Tip Speed Ratio (TSR) at its optimal value for maximum power generation. The TSR is defined as the speed at which the outer tip of the blade is moving divided by the wind speed [14]. Modern wind turbines operate best when their TSR is around 4 to 6. The existing MPPT control methods include [20-21], [73-74]:

- with turbine power profile,
- with optimal TSR,
- with optimal torque control (OTC),
- power signal feedback (PSF) control,
- perturbation and observation (P&O) control,
- Wind Speed Estimation (WSE)-based control,
- fuzzy logic control.

In the last 5 methods mentioned above, wind speed sensors are not required. A method similar to OTC [20], which is named as the Optimal Power Control (OPC), is proposed in this research [75].

2.1.1. OPTIMAL POWER CONTROL (OPC)

The principle of OTC is that the wind turbine mechanical torque T and the turbine speed ω have the following relationship for MPPT control

$$T \propto \omega^2 \tag{2.4}$$

The generator speed is equal to ω considering that the PMSG is direct drive. Besides, the generator mechanical torque is equal to its electromagnetic torque in the steady state. Therefore, the generator power and speed under MPPT control can be written as

$$P \propto \omega^3 \tag{2.5}$$

Equation (2.5) is the basis of Optimal Power Control (OPC). Suppose

$$P = K_{opt} \times \omega^3 \tag{2.6}$$

where K_{opt} is calculated from (2.7) according to the generator rated parameters

$$\begin{cases} K_{opt} = \dfrac{P_r}{\omega^{*3}} \\ \omega^* = 2\pi \times \dfrac{f^*}{p} \end{cases} \tag{2.7}$$

In (2.7), P_r, ω^*, f^* and p are the rated power, rated speed, rated frequency and pole pairs of the generator.

2.2. VSC BASED WIND ENERGY CONVERSION SYSTEM

In this section, VSC based wind energy conversion systems used in this thesis are discussed. First the system structure and its control are presented. This is followed by the discussion on two different types of VSCs used and a comparison of their conversion efficiency.

2.2.1. SYSTEM STRUCTURE AND CONTROL

The schematic diagram of the PMSG with voltage source converters is shown in Fig. 2.2. The wind kinetic energy is converted to mechanical energy by the wind turbine and then transmitted to the generator through the drive train. The PMSG is connected to the WSC directly without a gearbox. The DC power after the WSC is converted to AC power by the GSC and then connected to the AC grid through a transformer.

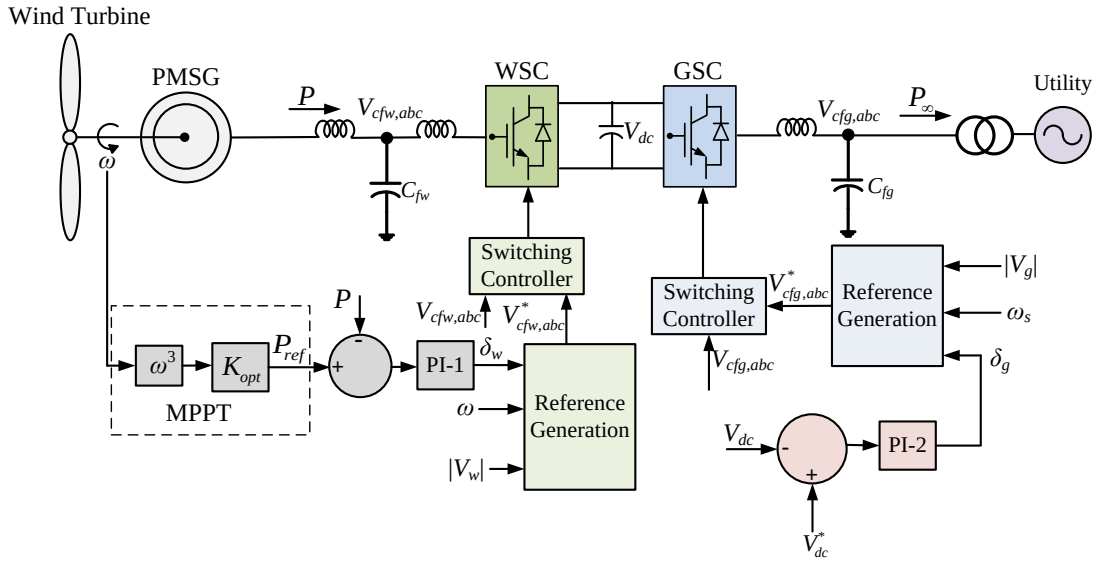

Fig. 2.2. Schematic diagram of a PMSG with back-to-back (BTB) converter [76].

In general, for a PMSG based WECS, the WSC controls the active power through MPPT, while the GSC maintains the DC voltage [20]. The same control methodology is applied in this research. As can be seen in Fig. 2.2, the power reference for the WSC control is obtained through the OPC based MPPT method

(discussed in the previous section), while the DC voltage reference for the GSC control is set according to the WECS demand.

To control MPPT wind power flow to the grid, WSC generates the voltage across the filter capacitor (C_{fw}) with an angle deviation from the PMSG output voltage. This voltage is assumed to have a magnitude of $|V_w|$, while its angle δ_w should be such that a power equal to P_{ref} is extracted from the wind turbine. To accomplish this, a PI controller (PI-1) is designed, which is given by

$$\begin{cases} e_w = P_{ref} - P \\ \delta_w = K_{Pw} e_w + K_{Iw} \int e_w dt \end{cases} \tag{2.8}$$

where P is the actual power from the PMSG.

The purpose of the GSC is to hold the voltage (V_{dc}) across the DC link capacitor constant. Note that V_{dc} will remain constant only when this capacitor neither supplies nor absorbs any real power. Therefore, the power obtained from the WECS should ideally appear at the grid side. However, this is not practical since the converter losses must also be supplied from the generated power. Therefore holding the capacitor voltage is tantamount to extracting the maximum possible power from the wind turbine after supplying the converter losses. For the DC voltage control, another PI controller (PI-2) is designed, which is given by

$$\begin{cases} e_g = V_{dc}^* - V_{dc} \\ \delta_g = K_{Pg} e_g + K_{Ig} \int e_g dt \end{cases} \tag{2.9}$$

where V_{dc}^* is the reference DC capacitor voltage and V_{dc} is the actual DC capacitor voltage. With this angle, the reference voltage across the filter C_{fg} is obtained as

$$\begin{cases} V_{cfga}^* = |V_g| \sin(\omega_s t + \delta_g) \\ V_{cfgb}^* = |V_g| \sin(\omega_s t + \delta_g - 120°) \\ V_{cfga}^* = |V_g| \sin(\omega_s t + \delta_g + 120°) \end{cases} \tag{2.10}$$

where $|V_g|$ is a pre-specified chosen magnitude of the grid side voltage and ω_s is the system frequency, which is usually 100π rad/s (50 Hz). The purpose of the converter switching control is to synthesize the reference voltages across the filter capacitors

(C_{fw} and C_{fg}). Two different VSC structures and their associated control strategies are employed. These are discussed next.

2.2.2. VSC REALIZED BY THREE H-BRIDGES

This converter structure is shown in Fig. 2.3, which contains three H-bridges [77-78]. Here, each switch represents an IGBT and an anti-parallel diode combination. The outputs of the H-bridges are connected to three single-phase transformers that are connected in wye for required isolation and voltage boosting. The resistance R_f represents the switching and transformer losses. Here, an LC filter is chosen to suppress the switching harmonics. For each phase, this filter constitutes of the leakage reactance of the transformers (L_f) and a filter capacitor C_f that is connected to the output of the transformers. The DC side of the converter is supplied by a capacitor C_{dc}, the DC voltage of which is regulated by the GSC as mentioned in the previous subsection.

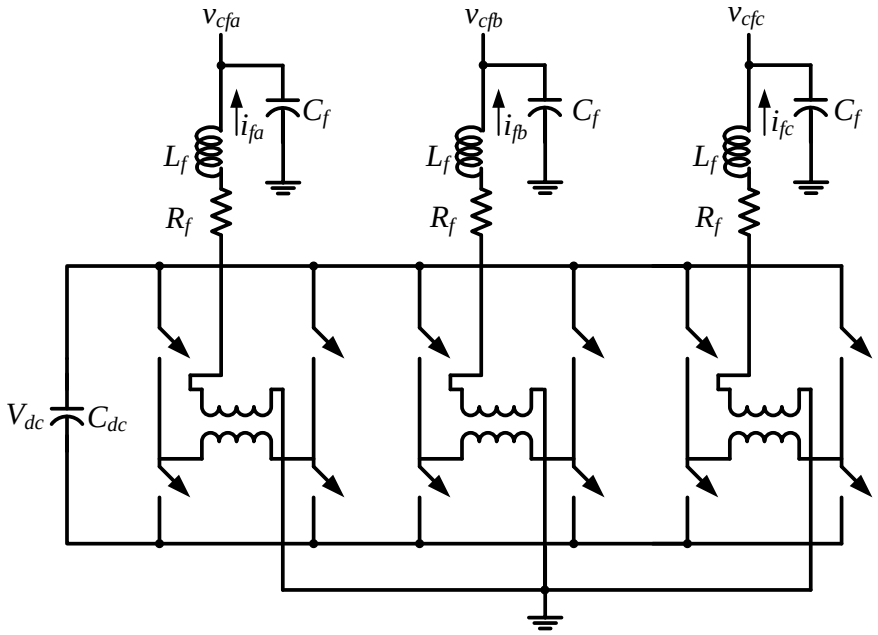

Fig. 2.3. Equivalent circuit of the converter structure realized by three H-bridges.

Each of the three phases is controlled independently, following the same control algorithm, which is presented in a generic form as follows. From the circuit of Fig. 2.3, defining a state vector of $x = [v_{cf} \quad i_f]^T$ for each phase, the state space description of the system can be written as

$$\dot{x} = Ax + Bu_c \tag{2.11}$$

where u_c is the continuous time control input, based on which the switching function u is determined. The discrete-time equivalent of (2.11) is

$$\begin{aligned} x(k+1) &= Fx(k) + Gu_c(k) \\ v_{cf}(k) &= Cx(k) \end{aligned} \tag{2.12}$$

Let the output of the system given in (2.12) be v_{cf}. The reference (v_{cf}^*) for this voltage is obtained as discussed in the previous subsection. The input-output relationship of the system in (2.12) can be written as

$$\frac{v_{cf}(z^{-1})}{u_c(z^{-1})} = \frac{M(z^{-1})}{N(z^{-1})} = C(zI - F)^{-1}G \tag{2.13}$$

The control is computed from [78]

$$u_c(z) = \frac{S(z^{-1})}{R(z^{-1})}\{v_{cf}^*(z) - v_{cf}(z)\} \tag{2.14}$$

Then the closed-loop transfer function of the system is given by

$$\frac{v_{cf}(z)}{v_{cf}^*(z)} = \frac{M(z^{-1})S(z^{-1})}{N(z^{-1})R(z^{-1}) + M(z^{-1})S(z^{-1})} \tag{2.15}$$

The coefficients of the polynomials S and R can be chosen based on a pole placement strategy [78]. Once u_c is computed from (2.14), the switching function u can be generated as

$$\begin{aligned} &\text{If } u_c > h \text{ then } u = +1 \\ &\text{elseif } u_c < -h \text{ then } u = -1 \end{aligned} \tag{2.16}$$

where h is a small number.

2.2.3. THREE-LEG VSC WITH PWM CONTROL

The schematic diagram of the VSC is shown in Fig. 2.4. Note that a transformer can be connected at the output of the VSC as well. In that case, L_f represents the leakage reactance of the transformer. Otherwise, an inductor needs to be added.

Like in the previous subsection, defining a state vector of $x = [v_{cf} \;\; i_f]^T$ from Fig. 2.4, the discrete-time state space description of the system can be written as in (2.12). A discrete time linear quadratic regulator (DLQR) based state feedback control is adopted for the switching control. This is given by

$$u_c(k) = -K\left[x(k) - x^*(k)\right] \tag{2.17}$$

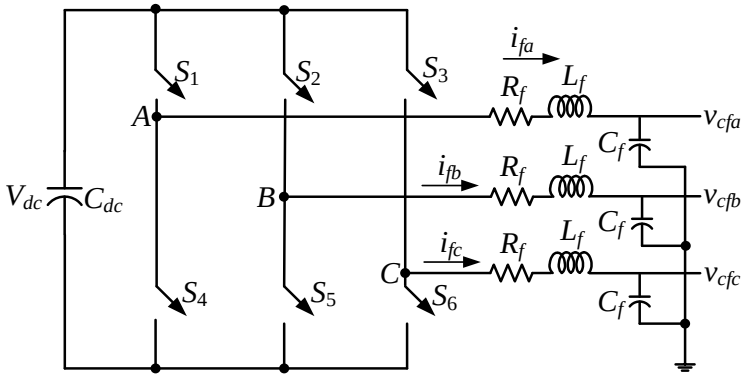

Fig. 2.4. Equivalent circuit structure of the three-leg VSC.

where $K = [k_1 \;\; k_2]$ is the feedback gain matrix. This control requires the availability of the references of all the state variables. Of the two state variables, v_{cf}^* is available as mentioned before. However it is rather difficult to form the reference i_f^*. It is to be noted that the current i_f should only contain low frequency components – its high frequency components should be zero. Therefore, if this current is passed through a high-pass filter (HPF), the output (i_{fHPF}) of the filter can be equated to zero [79]. The HPF structure is given by

$$\frac{i_{fHPF}}{i_f} = \frac{s}{s+\alpha} \tag{2.18}$$

where α determines the cutoff frequency of the filter. The modified control law is shown in Fig. 2.5.

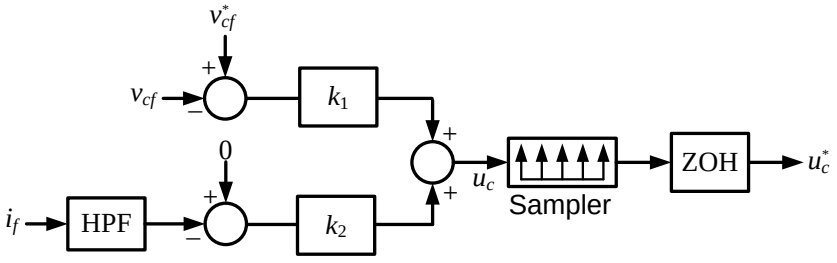

Fig. 2.5. Block diagram of control output computation.

The VSC switching control scheme [79-80] is shown in Fig. 2.6. This consists of a triangular carrier waveform (v_{tri}) that varies from –1 to +1 with a duty ratio of 0.5. The control output u_c is sampled twice in each cycle, once at the negative peak of the carrier waveform and once at the positive peak. Assuming an impulse modulated sampling, the output of the sampler is held by a zero-order hold (ZOH) circuit to obtain u_c^*. This is then compared with a triangular carrier waveform (v_{tri}). The switching signals are generated from the comparison of the carrier waveform and the sampled output. Note that the switches S_1 and S_4 are complimentary – when one is ON the other is OFF and vice versa. The switching law for phase-*a* is given by

$$\begin{aligned}
&\text{If } u_c^* > v_{tri} \text{ then } S_1 \text{ is ON} \\
&\text{elseif } u_c^* < v_{tri} \text{ then } S_1 \text{ is OFF} \\
&\text{If } u_c^* < v_{tri} \text{ then } S_4 \text{ is ON} \\
&\text{elseif } u_c^* > v_{tri} \text{ then } S_4 \text{ is OFF}
\end{aligned} \tag{2.19}$$

Note that the switch pairs S_2 and S_5 and S_3 and S_6 are also complimentary and they are respectively connected to phases *b* and *c*. Their control logic is the same as that given in (2.17).

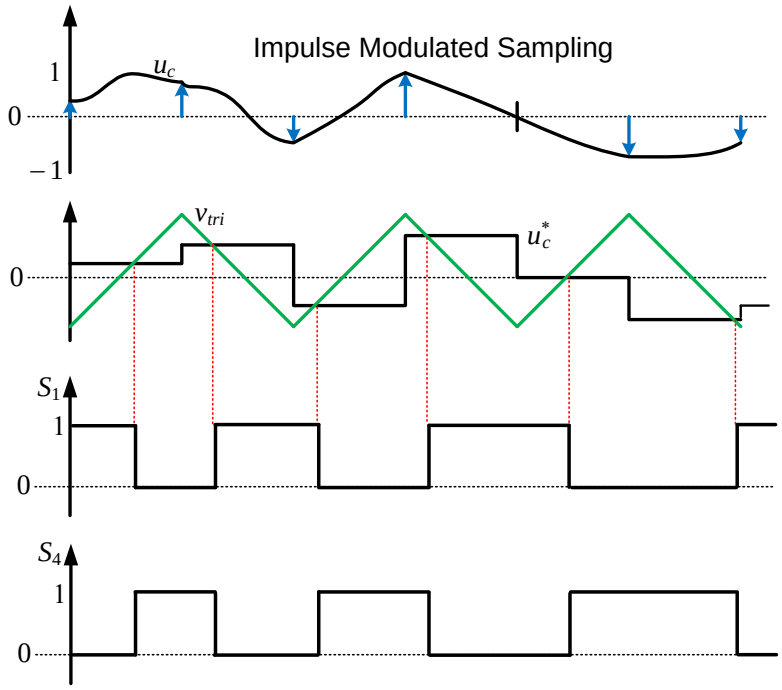

Fig. 2.6. VSC firing pulse generation scheme.

2.2.4. COMPARISON BETWEEN THE TWO VSC STRUCTURES

The power loss of a WECS connected to an infinite bus is simulated in PSCAD with 3 H-bridge and Pulse Width Modulation (PWM) controlled converters respectively. The PMSG used in this research is the model package available in PSCAD [81]. It is a non-salient pole synchronous generator. There is no gearbox between the wind turbine and the generator. Relevant parameters of the wind turbine with its pitch control and wind generator are listed in Table 2.1.

Table 2.1: WECS and pitch controller parameters.

System and Control	Parameters Names	Parameter Values
Parameters of Wind Turbine, PMSG and WSC	Rotor radius	58 cm
	Air density	1.225 kg/m^3
	Rated wind speed	12 m/s
	Rated apparent power	2.5 MVA
	Rated line-to-line voltage	4 kV
	Rated DC link voltage	7.5 kV
	Rated frequency	10 Hz
	Number of pole pairs	49
Pitch Control	Proportional gain	100
	Integral time constant	0.001 s
	Maximum increase/decrease rate	1000/s
	Upper limit	60°
	Lower limit	0
Line Parameters	Inductance	0.002 H
	Resistance	0.05 Ω

Varied wind speed of the same pattern is applied for the two VSC structures discussed above. This is plotted in Fig. 2.7 (a), which shows that the wind speed ramps up from 10 m/s at 8 s and reaches 12 m/s at 8.5 s. It starts to decrease at 14 s and settles at the speed of 11 m/s at 14.5 s. The three steady wind speeds are thus 10 m/s, 12 m/s and 11 m/s. The simulation in both cases has a cold start. The initial dynamic response is not shown here. Fig. 2.7 (b) shows the DC voltages with both converters. The reference value of this voltage is chosen as 7.5 kV. It can be seen that the DC voltage settles to the steady state value after each change in the wind speed. However the excursion in this voltage with the 3-leg converter is higher than that with

the 3 H-bridge converter. The percentage power loss for the two cases is shown in Fig. 2.7 (c). The percentage here is calculated as

$$\text{Power Loss} = \frac{P - P_{\infty}}{P} \times 100\% \tag{2.20}$$

where P is the output power from the PMSG and P_{∞} is the power at the infinite bus. The power loss values in the three steady states are listed in Table 2.2 for the two converter connections. It can be seen that the PWM controlled 3-leg power converter has significantly lower power losses in the steady state compared to the converter realized through 3 H-bridges. This implies the former has a much better conversion efficiency and thus is the chosen converter for this research. However, as in the case of the DC voltage, the power loss excursion of the 3-leg VSC is higher when the wind speed changes.

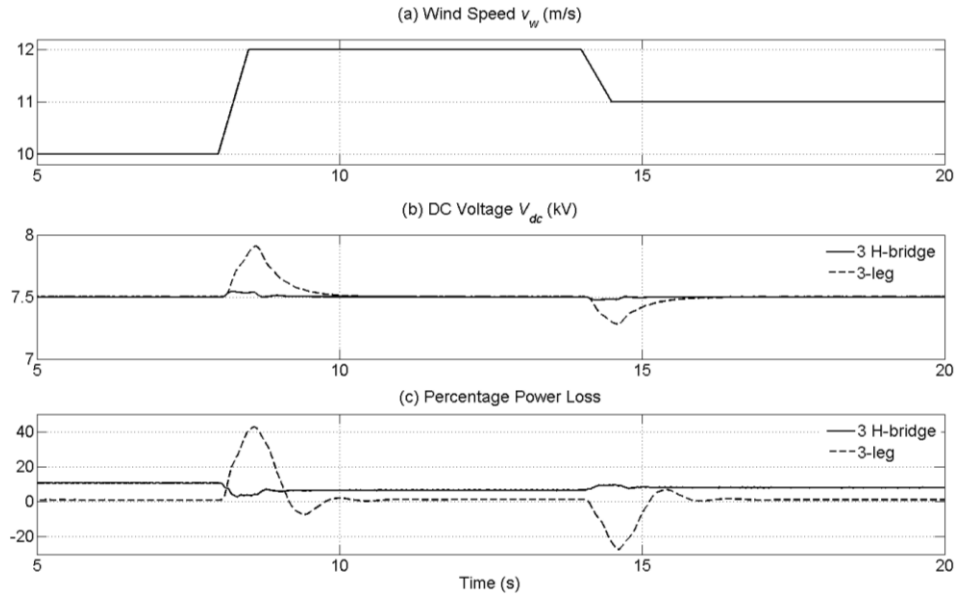

Fig. 2.7. Performance comparison between the two converters.

Table 2.2: Power loss comparison.

	10 m/s	**12 m/s**	**11m/s**
3-leg	1.02%	1.26%	1.11%
3 H-bridge	10.7%	6.56%	8.17%

Tip speed ratio (TSR) is defined as the ratio of the blade tip speed to the wind speed. This is given by [20]

$$\text{TSR} = \frac{\omega_M \times r_b}{v_w} \tag{2.21}$$

where ω_M is the rotating speed of the blade and r_b is radius of the rotor blades. The optimal TSR is constant for a given blade. Also from (2.1), we find that the mechanical power is directly proportional to C_p. The relation between TSR and rotor efficiency is typically shown by the so called 'C_p-λ' curve. When a WECS operates at MPPT, the TSR remains constant and as a result of which, the maximum rotor efficiency that is obtained also remains constant. In general, the Betz limit defines the maximum rotor efficiency as 59.3%. However modern turbines can reach about 80% of Betz's limit under the best operating conditions [14].

When the WECS is operating under pitch control due to the wind speed being higher than the rated speed, the rotating speed of the blade (ω_M) will remain constant. In this case, the TSR will drop as per (2.21) and the wind power output will not follow the wind speed. Therefore the rotor efficiency will also drop. Note that the wind turbine will be shut down when the wind speed is above the cut-out speed. Fig. 2.8 shows the TSR and percentage rotor efficiency with the wind speed variation of Fig. 2.7 when the WECS is connected to a 3-leg converter. It can be seen that these two remain constant (with values of 6.2 and 46.64% respectively) barring some transients during the changes in the wind speed. This indicates the effectiveness of the applied MPPT control.

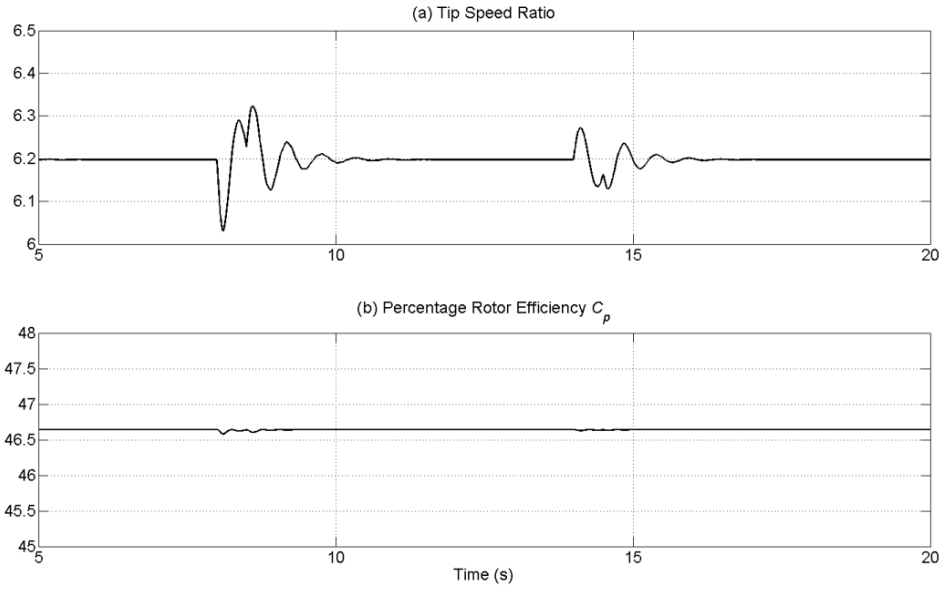

Fig. 2.8. Waveforms of tip speed ratio and rotor efficiency with 3-leg VSC.

2.3. DIODE-BRIDGE BASED WIND ENERGY CONVERSION SYSTEM

The DC/DC boost converter interfaced PMSG topology is another wind energy conversion system considered in this research due to its low cost. The schematic diagram of the PMSG with diode rectifier and a single channel boost converter [20, 41] is shown in Fig. 2.9. The inductance *L*, the diode *D*, the switch IGBT and the capacitor C_2 together form the DC/DC boost converter and *g* is the gate signal controlled by the switch control system. The structure of the 2-channel boost converter is depicted in a dashed frame. It is formed by two single channels connected in parallel and sharing a common capacitor. The two gate signals of the 2-channel boost converter are phase shifted by 180° to create an interleaved operation mode. The advantages of the two-channel boost converter include reduced load power for each channel, smaller input current ripple and higher equivalent switching frequency.

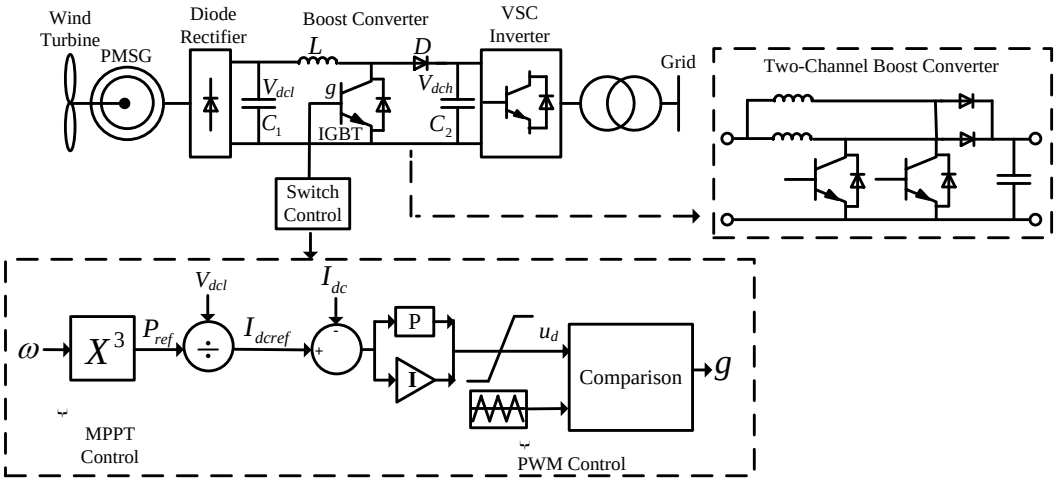

Fig. 2.9. Electrical diagram of a PMSG with the boost converter.

The MPPT generator control is realized by adjusting the duty cycle of the boost converter through a PI controller. Using the DC/DC boost converter, the maximum power can be completely extracted from the wind energy with a much simpler control compared to the voltage source rectifier. Suppose the input and output voltages of the DC/DC boost converter are V_{dcl} and V_{dch} respectively. The boosting relationship is given by

$$\frac{V_{dch}}{V_{dcl}} = \frac{1}{1-D} \tag{2.22}$$

where D is the duty cycle of the DC/DC converter. Since V_{dcl} will change when the wind speed changes, in order to get a constant DC voltage output V_{dch}, the duty cycle of the converter should vary with the wind speed. Therefore, the duty cycle control is applied to extract the maximum power from the PMSG employing MPPT. As shown in Fig. 2.9, the OPC based MPPT method is used to get the power reference P_{ref}. I_{dcref} and I_{dc} are respectively the reference and measured DC currents. The switch signal g is obtained by comparing the firing angle control waveform u_d with a triangular wave, in essentially a PWM control.

Considering the megawatt level rating of the employed PMSG, a multi-channel boost converter is preferred compared to a single channel one. A simulation study is conducted for a diode rectifier with two-channel boost converters. All the parameters are set the same for the two channels and given in Table 2.3. The simulation results are shown in Fig. 2.10, where the wind speed ramps up from 10 m/s to 12 m/s between 7 s and 8 s (Fig. 2.10 (a)). The power reference P_{ref} and the PMSG output power P are shown in Fig. 2.10 (b). It can be seen that the power reference changes according to the wind speed and the power output closely follows the reference. The control signal (u_d) is shown in Fig. 2.10 (c). It changes with the wind speed. The DC voltages are shown in Fig. 2.10 (d). The boosting nature is obvious from this figure.

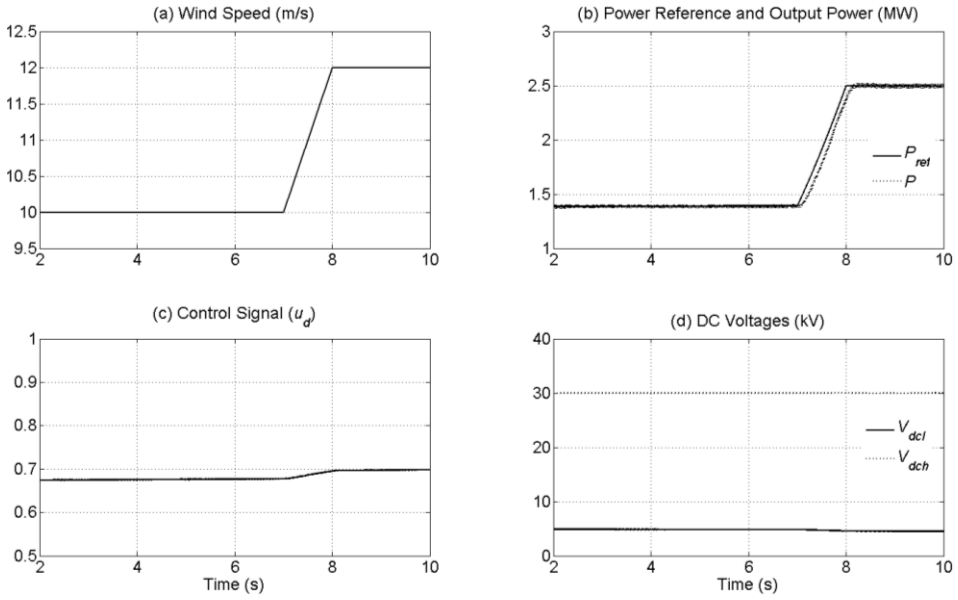

Fig. 2.10. System response with a diode-bridge rectifier and 2-channel boost converter.

Table 2.3: Parameters of the boost converter and its switch controller.

Converter and Control	Parameters Names	Parameter Values
Boost Converter	Inductor	0.01 H
	Capacitor	12000 μF
	Rated voltage after boosting	30 kV
Switch Controller	Proportional gain	0.01
	Integral time constant	1.0 s
	Upper limit	1.0
	Lower limit	0
	Triangular frequency	6500 Hz
	Triangular mimimum output level	0
	Triangular maximum output level	1.0

2.4. MICROGRID CONNECTION EXAMPLE

In this section, a simple wind energy integration example with a microgrid is discussed. Detailed study of various integration methods of WECS with a microgrid are presented in [75-76, 82].

2.4.1. SYSTEM CONFIGURATION AND DROOP CONTROL

A connection example of a PMSG based WECS with a microgrid and its local load is proposed. The simplified system structure is shown in Fig. 2.11, where the PMSG is connected through a 3-leg back-to-back VSC (WSC and GSC) for its integration with the microgrid. As described previously, the WSC controls the wind power under MPPT control, while the GSC holds the DC capacitor voltage V_{dc} constant. It is noted that only real power is shown in Fig. 2.11 as the reactive power is controlled by the microgrid.

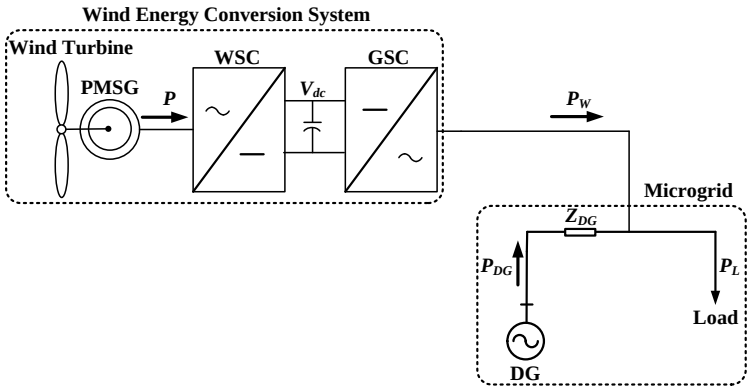

Fig. 2.11. Configuration of a WECS with microgrid connection.

For simplicity, the microgrid (MG) contains a single distributed generator (DG) and an *RL* load. The DG in the MG is operated in a frequency droop control, given by

$$f_{MG} = f_s + m \times (0.5 \times P_{DG}^* - P_{DG}) \tag{2.23}$$

where m is the droop gain, f_s is the reference frequency (50 Hz), f_{MG} is the actual microgrid frequency, P_{DG}^* is the DG rating and P_{DG} is the power supplied by the DG. The droop gain m is chosen such that the maximum frequency deviation is limited within ±0.5 Hz from the reference frequency. The schematic diagram of the frequency droop control is shown in Fig. 2.12. Note that no reactive power vs voltage magnitude droop is included here and the DG is assumed to be supplying voltage at the rated magnitude, with a frequency f_{MG} obtained from the droop equation of (2.23). The system parameters used in this study are listed in Table 2.4.

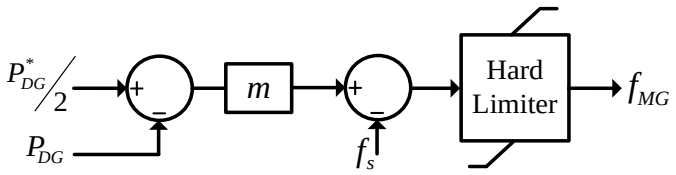

Fig. 2.12. Block diagram of the frequency droop control.

Table 2.4: System parameters for the microgrid example.

System Quantities	Values
DG rating	5 MW, 50 Hz, 4 kV (L-L, rms)
MG feeder impedance	0.1 Ω resistance and 5 mH inductance
MG load	Balanced with per phase values of 2.7 Ω resistance and 5 mH inductance
Droop gain (m)	0.2 Hz/MW
WECS rating	2.5 MW at the rated wind speed of 12 m/s
DC link voltage	7.5 kV

As the microgrid operates in the droop control of (2.23); its frequency will vary with the power demand. Therefore, the GSC in Fig. 2.11 must operate at this frequency. To achieve this, the droop frequency is measured and has been given as the frequency input to the GSC.

2.4.2. SIMULATION STUDIES

Simulation studies are carried out in PSCAD/EMTDC, in which a varied wind speed is considered. The results are discussed here. The wind speed is plotted in Fig. 2.13 (a), where it ramps up from 10 m/s to 12 m/s between 15 s and 15.5 s. Fig. 2.13 (b) shows the power from the DG (P_{DG}), PMSG output power (P) and the power output from the WECS (P_W). It is evident from this figure that the PMSG power output increases as a result of the increase in the wind speed. Since both the WECS and the DG are supplying power to the load, the power output from the DG decreases at 15.5 s following the rising of P_W. Fig. 2.13 (b) also shows that the wind generator power output and the power to the microgrid is almost equal, which signifies a small power loss. This is in accordance with the conclusion previously mentioned that the 3-leg VSC converter has low power loss.

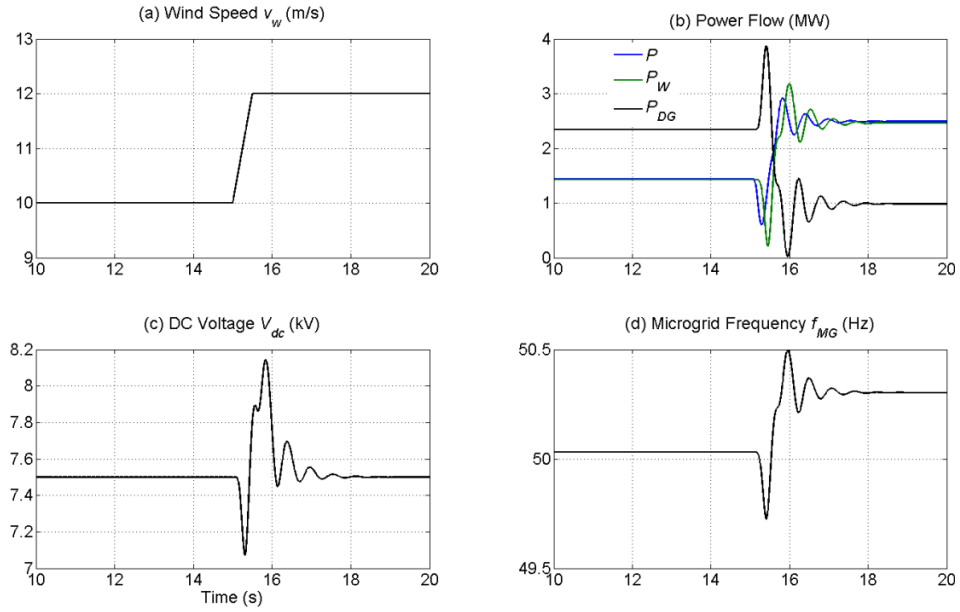

Fig. 2.13. System response for microgrid integration.

The DC voltage is shown in Fig. 2.13 (c), from which it is clear that the GSC maintains the DC link voltage of the BTB converter at the constant value of 7.5 kV with fluctuations during the change in the wind speed. Fig. 2.13 (d) shows the microgrid frequency. It can be seen that this frequency rises as the wind power increases. During this time, the DG supplies less power and hence the frequency increases as per (2.23). However, the frequency still remains below the upper limit of 50.5 Hz.

Some other important control parameters are shown in Fig. 2.14. It can be seen in Fig. 2.14 (a) that, due to the MPPT control, the generator speed ramps up following the wind speed change. It is also noted that the generator speed is 1 pu at the rated wind speed of 12 m/s. The tip speed ratio shown in Fig. 2.14 (b) is kept constant at its optimal value for different wind speeds. The rotor efficiency is also maintained at its maximum value with the optimal TSR, as can be seen from Fig. 2.14 (c). However, both the tip speed ratio and the rotor efficiency experience fluctuations during the change in the wind speed. Fig. 2.14 (d) illustrates the effect of the angle control of (2.8). Once the wind speed and the generator output power increase, the angle becomes more negative to accommodate this change. As a result, the deviation between the angles of the generated voltage and the WSC voltage is bigger. The detailed analysis of the simulation results in this example strongly validates the topology design and control scheme of the proposed WECS.

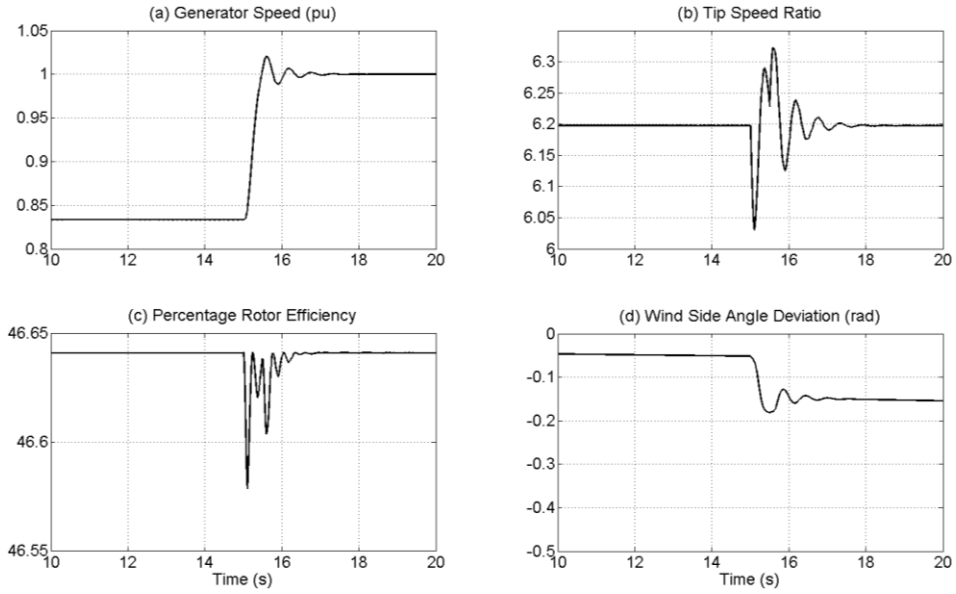

Fig. 2.14. Control effects for microgrid integration.

2.5. CONCLUSIONS

The topology and control of PMSG based WECSs are discussed in this chapter. Pitch control is applied to the wind turbine and a MPPT method is developed for a direct-drive wind generator. The maximum wind power is drawn through the wind side converter control and the grid side converter holds the DC link voltage constant. The WECS with PWM controlled 3-leg voltage source converter is proved to be more

advantageous than the 3 H-bridge converter since the former requires less number of switches and also has less power loss.

As a more economic wind side converter, the uncontrolled diode rectifier with a boost converter is also studied. The MPPT is achieved by adjusting the duty ratio of the boost converter. The proposed 3-leg VSC based WECS model and its control schemes are verified by an integration example with a frequency droop controlled microgrid. The microgrid integration shows the effectiveness of the system proposals. In the following chapters, the effectiveness of WECS integration with an HVDC system will be studied and microgrids will not be discussed in the remainder of the thesis.

CHAPTER 3

PARALLEL DC COLLECTION SYSTEMS FOR OFFSHORE WIND FARMS

The power generated by wind turbines within each offshore wind farm must be collected together to integrate with a grid. This power collection system can be in either AC or DC form. The DC collection system is favored compared to the traditional AC system with regard to massive power delivery through submarine cables [45]. Therefore, this thesis focuses on the study of offshore wind power with DC collection and HVDC transmission systems. The DC output voltage after a wind side converter is usually at several kilovolts, while the voltage level for HVDC ranges from tens to hundreds of kilovolts, depending on the size of the offshore wind farm and the distance to the onshore grid [83]. Therefore, if the WSCs of each wind turbine are connected in parallel, the DC voltage at the collecting point must be stepped up in a certain way to reach the HVDC transmission level. As the parallel DC collection system allows for flexible and independent control of each wind turbine, it is currently the most popular offshore wind power collection topology [38-40].

As mentioned above, the main advantage of this collection topology is on its flexible control. As each wind generator is connected to a power converter, the MPPT control is realized for each of them. If one or more wind turbines are offline, the rest of the wind turbines still operate as usual since the output DC voltage remains unaffected. However, the DC voltage at the collection point of a parallel collection system is far from comparable to HVDC transmission levels [83]. To boost the voltage level, there are two options possible:

1. To have a high power DC/AC converter connected at the DC collection bus and then boost the voltage through a high power transformer. This voltage can then be converted back into DC through an AC/DC converter for HVDC transmission. This is an impractical solution for offshore wind farms as the cost of setting up a converter-transformer-converter stage will be prohibitive, especially over water. This will not be discussed in this thesis.

2. Alternatively, DC boost converters can be used in parallel DC collection systems. In some cases, more than one boosting stage is needed. Most of the boost converters employed are single active or double active bridge converters, which are basically one inverter and one rectifier with a high frequency transformer incorporated. Given that semiconductor devices are the main components to implement power conversion, the employment of large numbers of boost converters obviously increases the investment costs of an offshore wind farm. Despite the high cost of establishing a parallel DC collection system, this collection topology is currently the most popular choice since it is easy to operate.

In this chapter, both the diode and VSC based WECSs are used for the study of parallel collection systems. As has been discussed in Chapter 2, a VSC based WECS contains two converters – one GSC and another WSC. Traditionally in a DC collection system, the HVDC transmission line connects these two converters. For a diode based WECS, a single or two-channel DC/DC connected to an uncontrolled rectifier is considered to be the WSC. This is then connected to the GSC through the HVDC cables.

In this chapter, three types of parallel DC collection topologies for offshore wind farms are discussed. These are:

3. Each PMSG is connected with a diode bridge rectifier and a 2-channel DC/DC boost converter. The boost converters are then connected in parallel for HVDC transmission.

4. Each PMSG is connected with a VSC AC/DC converter. The DC sides of the VSCs are connected in parallel. The resulting DC voltage is boosted through a single active bridge boost converter for HVDC transmission.

5. This scheme is somewhat similar to that of scheme-2, in which the DC sides of the WSCs are connected in parallel. However, several single active bridge converters are used, which are parallel connected at the input and series connected at the output.

These topologies are discussed in detail, and the simulation results for each of the collection topologies are presented. Comparisons among the collection topologies are also conducted.

3.1. PARALLEL COLLECTION OF DIODE BASED WECSS

The parallel DC collection topology of wind power drawn by diode rectifiers with 2-channel boost converters is studied in this section. The diode based WECS has already been discussed in Chapter 2, where both single and two-channel boost converters are considered.

3.1.1. PARALLEL COLLECTION TOPOLOGY OF DIODE BASED WECSS

The diode based WSCs can be connected in parallel after the voltage boosting for wind power from each turbine. This is shown in Fig. 3.1, where P_{out1}, P_{out2}, …, P_{outn} represent the power outputs from PMSG-1, PMSG-2, …, PMSG-*n*, and the DC voltages before boost converters are denoted by V_{dc1},V_{dc2}, …, V_{dcn}. It is to be noted that the power output of a WECS is denoted by P_i (i = 1, 2, …) in this thesis, which is equal to P_{outi} here considering negligible power loss. The boosted DC voltage, which is also the nominal voltage of HVDC transmission, is controlled by the GSC and represented by V_{dc}. Therefore, the boost converters have no control over their output voltages. However, the input voltages of the boost converters can be different as all of them individually depend on their respective wind speeds. With proper duty cycle adjustment, each boost converter draws the maximum available power from each wind turbine, while its output voltage remains constant. This has already been discussed in Chapter 2.

It should be noted that the DC voltage of wind power in a parallel collection system may still not be able to reach the expected level after the voltage boosting stage. The main reason for this can be the boost converter rating limitation or the high voltage requirement of HVDC transmission. To deal with this situation, bridge converters with high frequency transformer isolation are employed in VSC based WECSs, which is discussed in a later section.

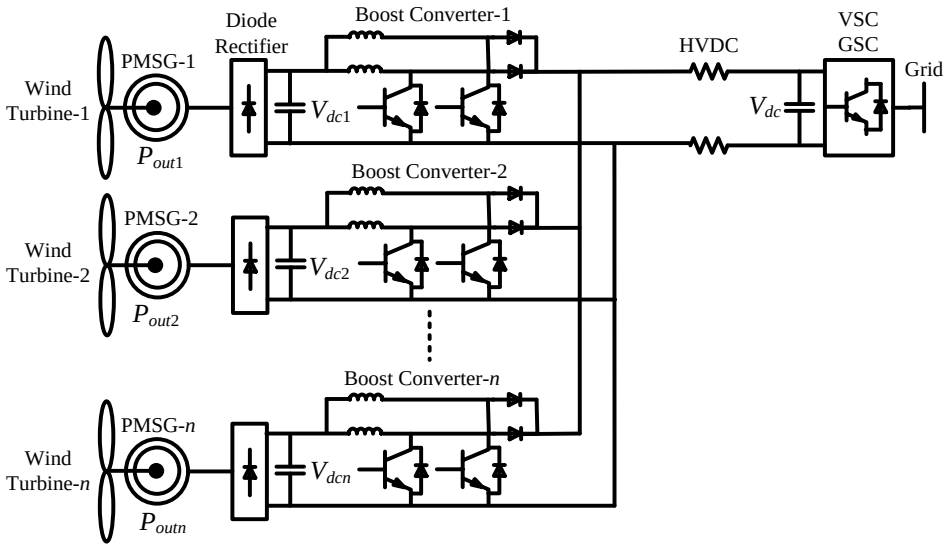

Fig. 3.1. Parallel collection topology of diode based WECSs.

3.1.2. SIMULATION STUDIES

The simulation results of a DC parallel collection system with 4 wind turbines are shown in Fig. 3.2. The parameters of the wind turbines and PMSGs are the same as those listed in Chapter 2 (Table 2.1). These parameters are used for the rest of the thesis as well. The reference DC voltage of the GSC is set as 15 kV. The wind speed pattern of each turbine is shown in Fig. 3.2 (a). It can be seen that all the four wind turbines operate with the rated wind speed of 12 m/s in the initial stage. The wind speeds for turbines 1 to 3 ramp up, while that of turbine-4 ramps down. The changes in wind speeds are:

- Turbine-1: from 12 m/s to 14 m/s from 7 s to 9 s;
- Turbine-2: from 12 m/s to 13.5 m/s from 8 s to 9 s;
- Turbine-3: from 12 m/s to 16 m/s from 9 s to 11 s;
- Turbine-4: from 12 m/s to 11 m/s from 9 s to 10 s.

When the wind speeds exceed 12 m/s, the power outputs of each WECS do not increase as this is the rated speed. Fig 3.2 (b) shows the wind power outputs, where that of turbine-4 decreases.

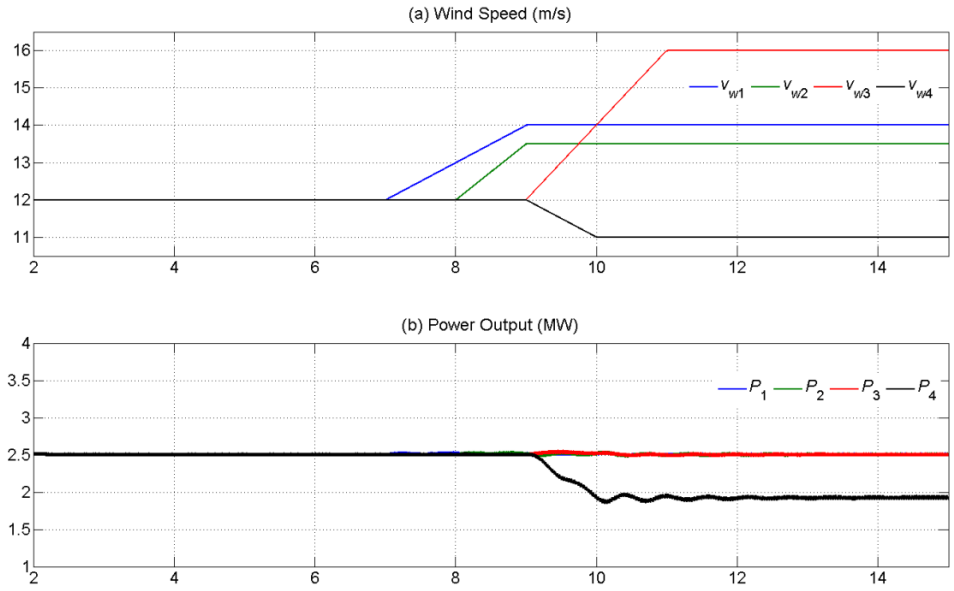

Fig. 3.2. Simulation results of a parallel DC collection system with four diode rectifiers and boost converters.

3.2. VSC WSC WITH A TWO-CHANNEL BOOST CONVERTER

A simple 2-channel boost converter is presented in Chapter 2 and applied in the former section with diode rectifier in parallel connection. However, the stator current has significant harmonic content due to the non-linear nature of the diode rectifier. Therefore, the generator torque waveform contains ripples, which may cause additional mechanical vibrations and torsional resonances in large WECSs [20]. As offshore wind farms can have large capacities, the diode bridge is replaced with the 3-leg bridge VSC in this section to overcome the drawback of the uncontrolled rectifiers.

3.2.1. CONFIGURATION AND CONTROL OF A VSC WITH A TWO-CHANNEL BOOST CONVERTER

The configuration of a 3-leg VSC with a two-channel boost converter based WECS is shown in Fig. 3.3, where V_{dcl} and V_{dch} are respectively the input and output DC voltages of the boost converter, and g_1 and g_2 are the firing pulses applied to the IGBT gate terminals of the two channels. In this topology, the WSC and the GSC control the wind power flow and the DC link voltage respectively in the same manner as discussed in Chapter 2. As the MPPT is controlled by the WSC, the boost converter here is only used for voltage boosting. The switch control strategy is shown in Fig.

3.3, in a framed (dashed) box. The error between the DC voltage reference of the WSC (V_{dcl}^{*}) and the measured V_{dcl} is given to a PI controller and a hard limiter. The obtained control signal u_d is compared with a triangular carrier wave and an IGBT gate firing pulse is generated by the PWM control. It is to be noted that two triangular carrier waves are required for the generation of g_1 and g_2. These are phase shifted by 180° to create an interleaved operation mode, which is stated in Chapter 2.

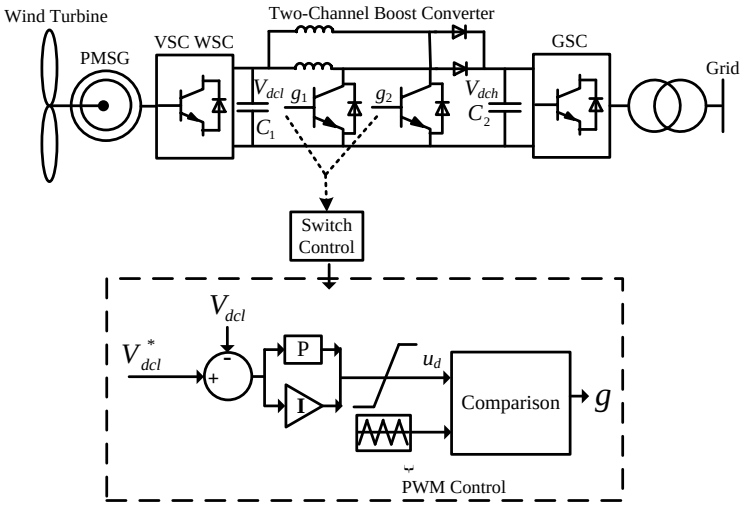

Fig. 3.3. Configuration and control of a VSC and two-channel boost converter based WECS.

A simulation study of a WECS with a 3-leg VSC as the WSC and a two-channel boost converter is conducted in PSCAD. The two channels of the boost converter have the same system and control parameters, which are given in Table 3.1. Fig. 3.4 shows the simulation results, where the wind speed ramps up from 28 s to 28.5 s and decreases between 34 s and 34.5 s. Therefore, the turbine operates with three steady wind speeds of 10 m/s, 12 m/s and 11 m/s, as shown in Fig. 3.4 (a). It can be seen from Fig. 3.4 (b) that the wind power output follows the wind speed changes as a result of the MPPT control.

Fig. 3.4 (c) shows that the input and output DC voltages of the boost converter are kept at their constant reference values of 7.5 kV and 15 kV, irrespective of the changes in the wind speed. The PWM control signal, which is essentially the duty cycle here, stays constant at 0.5, indicating an output voltage boosting at twice the input voltage level, as per (2.22). This duty cycle value is in accordance with the DC voltage values shown in Fig. 3.4 (c). The tip speed ratio plotted in Fig. 3.4 (e) is kept at its optimal value at steady wind speeds under MPPT control, and the rotor

efficiency remains constant accordingly (Fig. 3.4 (f)). Some acceptable small fluctuations occur in all the parameters during the changes in the wind speed.

Table 3.1: Parameters of the two-channel boost converter and its switch controller.

Converter and Control	Parameters Names	Parameter Values
Boost Converter	Inductor	0.01 H
	Capacitor	12000 µF
	Rated voltage after boosting	15 kV
	Rated voltage before boosting	7.5 kV
Switch Controller	Proportional gain	0.1
	Integral time constant	2.0 s
	Upper limit	1.0
	Lower limit	0
	Triangular frequency	6500 Hz
	Triangular mimimum output level	0
	Triangular maximum output level	1.0

The disadvantages of the WECS with a VSC WSC and a two-channel boost converter are: (1) the higher cost compared to a diode based WECS described in Section 3.1 and (2) the lower rating compared to when a bridge boost converter is employed as studied below. Therefore, the parallel connection of this scheme has not been considered further.

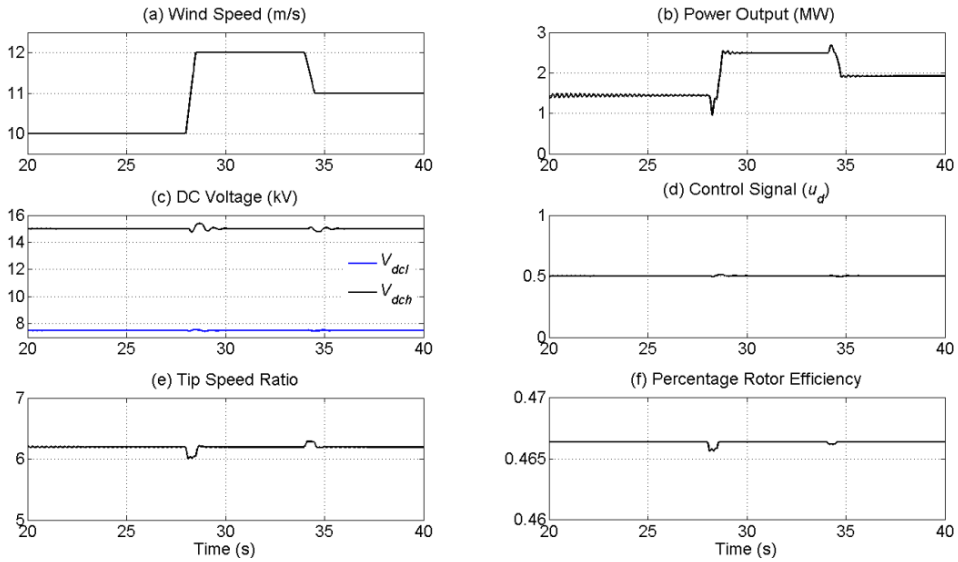

Fig. 3.4. Simulation results of a WECS with a VSC WSC and a two-channel boost converter.

3.3. PARALLEL DC COLLECTION OF VSC BASED WECSS

A parallel DC collection system might need DC/DC converters of different ratings, depending on the processed wind power level. Similar to the function of transformers in AC systems, the different voltage levels in a DC system require DC/DC converters for DC voltage regulation. A high frequency transformer is usually incorporated to a DC/DC converter for galvanic isolation in the case of big power capacities. This kind of converters are termed as bridge DC/DC converters in this research.

3.3.1. TOPOLOGY DETERMINATION OF A BRIDGE BOOSTING CONVERTER

Generally speaking, a bridge DC/DC converter consists of an inverter, a coupling transformer and a rectifier. The inverter is at the primary side of the high frequency transformer to convert DC power to AC. This high frequency AC voltage is stepped up by the transformer and then rectified by the full wave rectifier connected on the secondary side of the transformer. The simplest topology is a Full Bridge (FB) converter, which requires large filter inductance at its output. A Single Active Bridge (SAB) converter is formed when the filter inductance is moved to the primary side of the transformer. Compared to FB, SAB features much smaller filter inductances if needed [83-84].

A modification of SAB is a Dual Active Bridge (DAB) converter, where the rectifier is active like the inverter. A DAB converter allows for bidirectional power flow but are not as simple and compact as a SAB converter. As wind turbines only have a small power demand during standby, no bidirectional power flow is needed for offshore wind power delivery. Besides, for HVDC wind power transmission, the DC/DC converter is used as a boost converter with a high output voltage. Based on these considerations, a SAB converter is more advantageous compared to DAB and is thus employed as the boost converter here.

The schematic diagrams of a single-phase and a three-phase SAB boost converters are shown in Fig. 3.5, where L_f and L_σ are the filter inductance and transformer leakage inductance respectively. It is noted that L_f is optional depending on the size of the leakage inductance L_σ, and is not required if L_σ is big enough. The

turns-ratio of the high frequency transformers is denoted by 1:*k*. Each switch in the full bridge inverter consists of an IGBT and an anti-parallel diode.

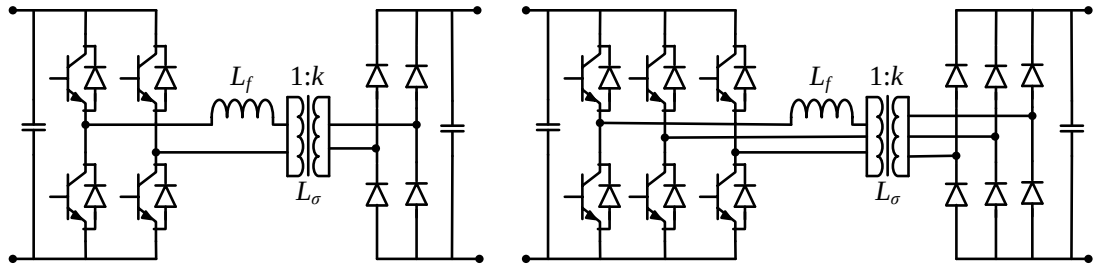

Fig. 3.5. Schematic diagram of (a) single-phase SAB and (b) three-phase SAB.

The galvanic isolation provided by high frequency transformers in Fig. 3.5 is essential due to safety reasons. A high frequency transformer features smaller size, higher power density and lower core loss compared to a 50/60 Hz transformer. These advantages are especially important for an offshore wind farm, where the size and weight of the devices are highly related to the investment costs in terms of substructure requirements, shipping and installation [84-85]. From the technical point of view, a high frequency transformer facilitates the voltage boosting function of a DC/DC converter through its turns-ratio. This means better converter optimization or higher efficiency. High frequency transformers can be single- or three-phase [86-89]. SAB with both types of transformers are considered in this research.

3.3.2. OPERATION OF SINGLE ACTIVE BRIDGE CONVERTER

By referring all the parameters to the primary side of the transformer in Fig. 3.5, the equivalent circuit of a single-phase SAB converter is shown in Fig. 3.6 (a), where $L = L_f + L_\sigma$. The input and output currents of the SAB are represented by i_p and i_s respectively and the current through the filter inductance is denoted by i_{ab} after the connection nodes *a* and *b*. The voltage reference node is *o*, based on which the voltages of node *a*, node *b*, transformer primary side and secondary side are defined as v_a, v_b, v_{abp} and v_{abs} respectively. The input and output DC voltages are denoted by V_{dcl} and V_{dch} respectively. A further equivalent model of SAB in half bridge is drawn in Fig. 3.6 (b). It can be seen from Fig. 3.6 (b) that an SAB is essentially a buck converter if the turns-ratio of the high frequency transformer is given as 1:1.

Therefore, the boost characteristic of a SAB is essentially realized by the high frequency transformer with $k > 1$.

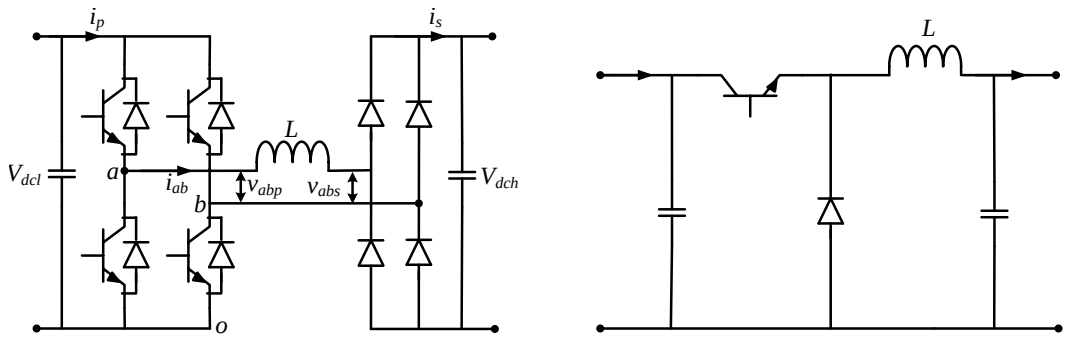

(a) (b)

Fig. 3.6. Equivalent circuit of (a) single-phase full-bridge SAB and (b) single-phase half-bridge SAB.

A simple example of a single-phase SAB is simulated in PSCAD. Related parameters are listed in Table 3.2. Fig. 3.7 illustrates the voltage and current waveforms from the simulation results. It can be seen from Fig. 3.7 (a) that v_{abs} has a phase shift from v_{abp} and does not have frequent level changes as v_{abp}. These changes are related to the value of the transformer leakage reactance [90-91]. The output current (i_s) waveform in Fig. 3.7 (b) implies that the SAB is operating in a border mode (between discontinuous and continuous modes). The operation mode of a SAB can be adjusted by applying filter inductors at the output.

Table 3.2: Parameters of the single-phase SAB.

Parameters Names	**Parameter Values**
Input DC voltage (V_{dcl})	7.5 kV
Capacitors	12000 µF
Output load	10 Ω
Transformer turns-ratio/ frequency	1:1/ 6500 Hz
Transformer leakege reactance	0.4 mH
Duty ratio	0.5
Phase shift between two legs	90°

An SAB operates in a discontinuous mode under most conditions. The output current in this mode is shown in Fig. 3.8. It has three stages in each cycle. Suppose the output current in a certain cycle starts to rise at t_1, reaches its peak value (i_m) at t_2, and decreases to 0 at t_3 (see Fig. 3.8). Then as the current waveform is almost linear, we get

$$\frac{V_{dcl} - V_{dch}^{'}}{L} \times (t_2 - t_1) = i_m \tag{3.1}$$

$$\frac{V_{dch}^{'}}{L} \times (t_3 - t_2) = i_m \tag{3.2}$$

where $V_{dch}^{'}$ is the output voltage of the SAB, when referred to the primary side. It is noted that in (3.1) and (3.2), V_{dcl} is known, all the other values are unknown and are obtained as below. For simplicity, it is assumed that $t_1 = 0$. Since the frequency of the output current is twice the switching frequency, we can write

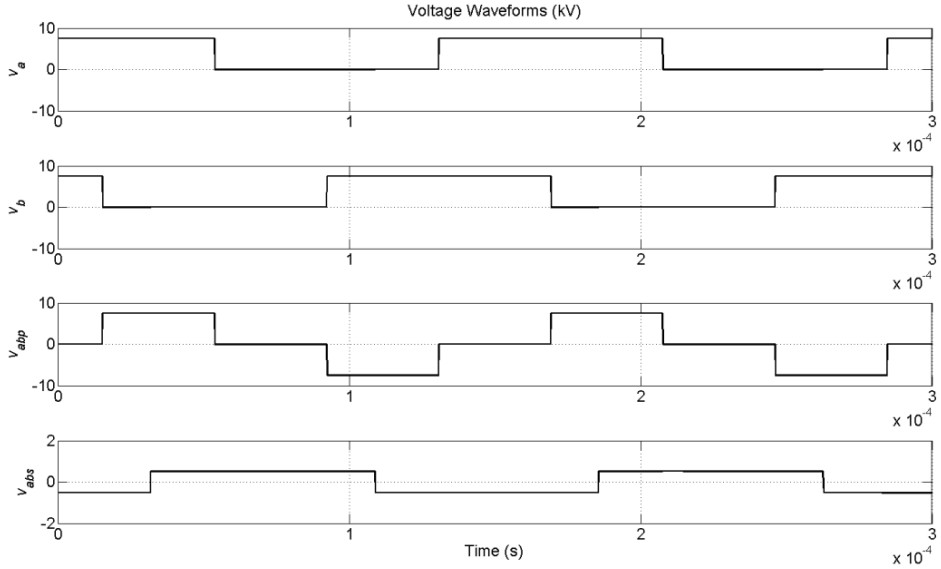

(a)

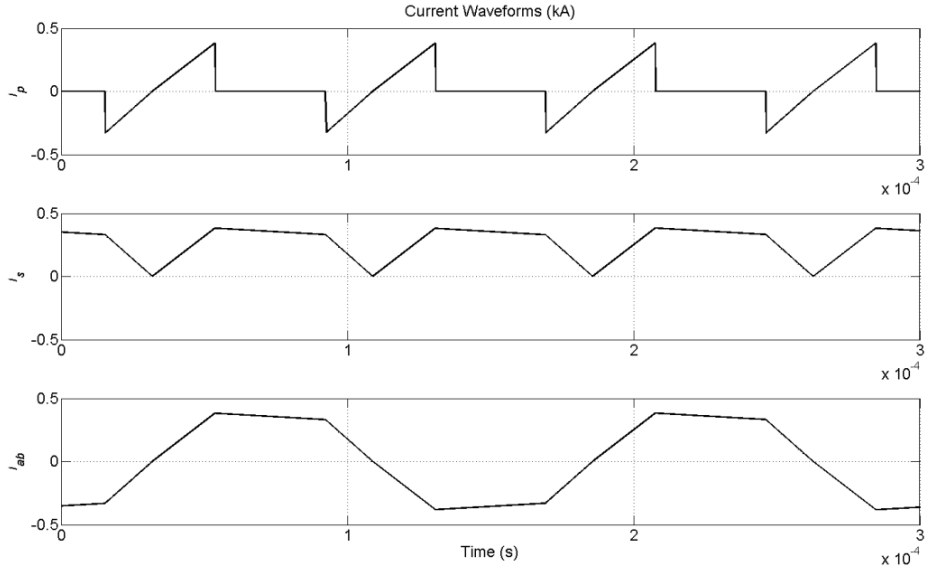

(b)

Fig. 3.7. (a) Voltage waveforms and (b) current waveforms in continuous mode.

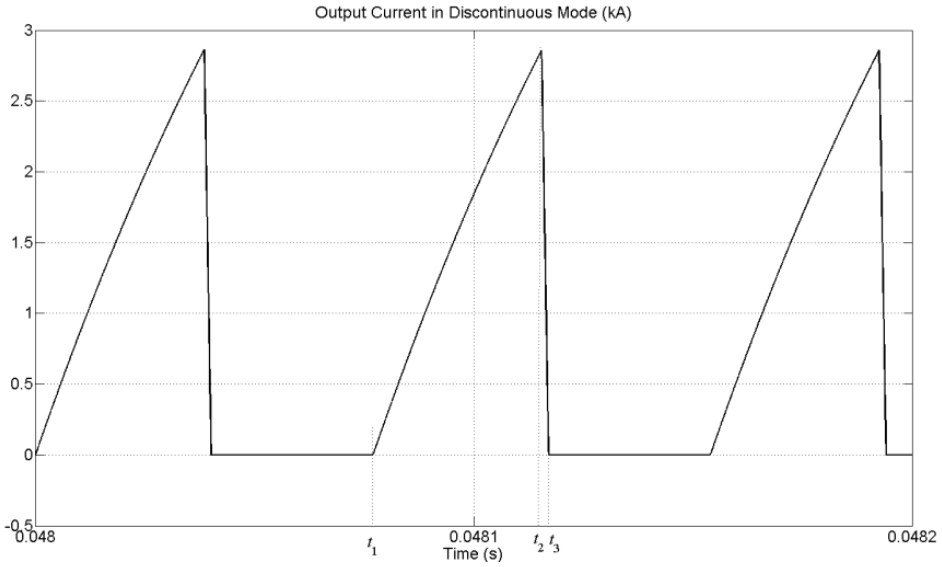

Fig. 3.8. Current waveform in discontinuous mode.

$$t_2 = \frac{\alpha}{2f} \tag{3.3}$$

where α is the duty ratio and f is the switching frequency. Then the following equation is obtained by substituting (3.3) in (3.1)

$$i_m = \frac{V_{dcl} - V_{dch}^{'}}{L} \times \frac{\alpha}{2f} \tag{3.4}$$

Substituting (3.3) and (3.4) in (3.2), the value of t_3 is obtained as

$$t_3 = \frac{V_{dcl}}{V_{dch}^{'}} \times \frac{\alpha}{2f} \tag{3.5}$$

Therefore, the output current referred to the primary side ($i_s^{'}$) is

$$i_s^{'} = \frac{1}{2} \times i_m \times \alpha + \frac{1}{2} \times i_m \times (t_3 \times 2f - \alpha) \tag{3.6}$$

By solving (3.1), (3.3), (3.4) and (3.6), the primary referred output voltage of the SAB converter is given as

$$V_{dch}^{'} = \frac{\alpha^2 \times V_{dcl}^2}{4 \times f \times L \times i_s^{'} + \alpha^2 \times V_{dcl}} \tag{3.7}$$

The transformer is assumed to have a turns-ratio of 1:*k*. Therefore,

$$\begin{cases} V_{dch}^{'} = \dfrac{V_{dch}}{k} \\ i_s^{'} = i_s \times k \end{cases} \tag{3.8}$$

Then the output voltage of the SAB is given by combining (3.7) and (3.8) as

$$V_{dch} = \frac{\alpha^2 \times V_{dcl}^2 \times k}{4 \times f \times L \times i_s \times k + \alpha^2 \times V_{dcl}} \tag{3.9}$$

It can be seen from (3.9) that the output voltage of SAB does not have a linear relationship with its input voltage. Besides, the conversion ratio of a SAB converter is dependent on its output current. This conclusion applies to the other two operation modes, i.e., continuous and border modes [84, 92-93].

3.3.3. PARALLEL COLLECTION OF WSCS WITH SAB BOOST CONVERTERS

Depending on the installation locations of boost converters, a parallel DC collection system for wind power has different topologies. Reference [39] lists three parallel connection based configurations, where a boost converter is employed either for each wind turbine or for an entire wind farm. The three topologies are compared from both the power loss and investment points of view [39]. Actually, apart from these, several wind turbines can share one boost converter, while extra voltage boosting stages can be employed, if necessary.

A general parallel DC collection topology for PMSG based WECSs is shown in Fig. 3.9. Three potential locations for installing boost converters are marked in yellow, green and red. Each boost converter in yellow areas has the same capacity of one wind generator. The rating of a green area converter is in accordance with the total power capacity of its connected cluster (shown in a dashed frame). The boost converter in the red area has a power level of the entire offshore wind farm. The voltage levels of the boost converters in the three areas increase from yellow to green to red. The DC voltage after the red area boost converter must reach the HVDC transmission level. It is mentioned that not all boost converters in the three areas are necessary. However, for each wind generator, at least one boosting stage is needed. The selection of boost converters and their installation locations are influenced by various factors. The main considerations are usually related to power losses and

investment costs. Based on the conclusion in [39], only one big boost converter is applied for one whole offshore wind farm in this research.

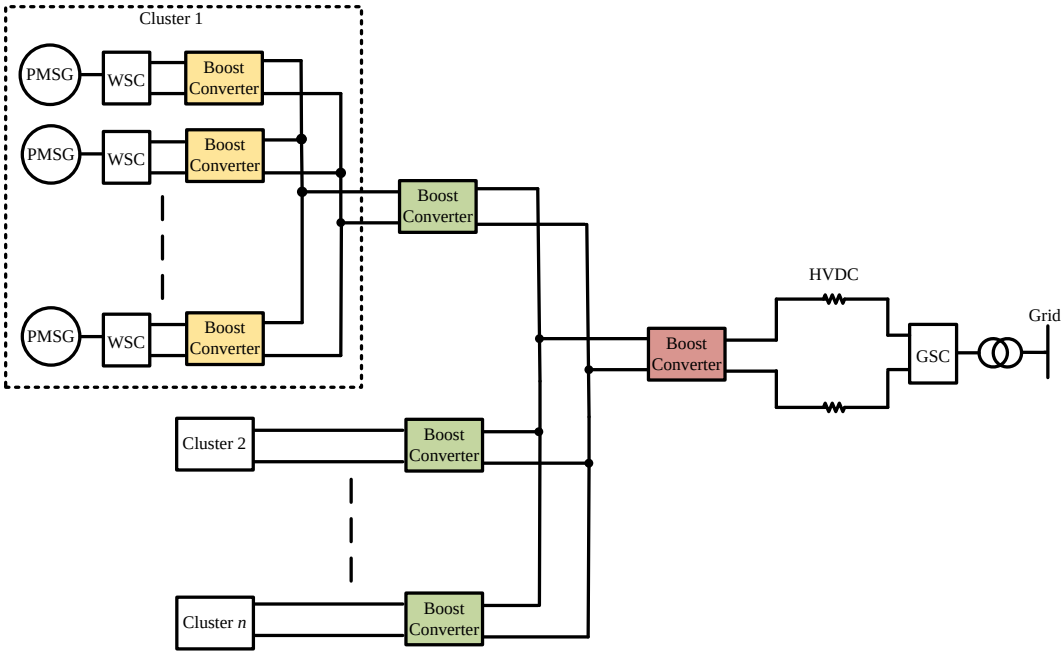

Fig. 3.9. General configuration of parallel offshore wind power DC collection systems.

The configuration of PMSG based WECSs connected in parallel with a SAB boost converter is shown in Fig. 3.10. A single-phase AC connection of the boost converter is depicted as an example. In Fig. 3.10, each wind turbine with a PMSG and WSC is termed as a "wind power unit" and simplified as "unit" for convenience. The power from each unit is collected through the parallel connection on the DC side of each WSC. The DC voltage at the connecting point is stepped up to the HVDC transmission level by the boost converter. The transmission voltage is still controlled by the GSC and the MPPT for each wind generator is realized by their respectively connected WSCs.

The dotted frame in Fig. 3.10 shows the switch control of the IGBTs, which applies the same control scheme as in Fig. 3.3. However, for the bridge inverter of SAB, the IGBT firing pulses follow a different pattern. First, the two IGBTs on each leg conduct in a complementary manner. Second, the switching angles of the IGBTs in different legs are phase shifted. This phase shift value is selected as 180° for a SAB with a single-phase transformer as per the previous analysis, and 120° among the three legs of a three-phase SAB for balancing consideration.

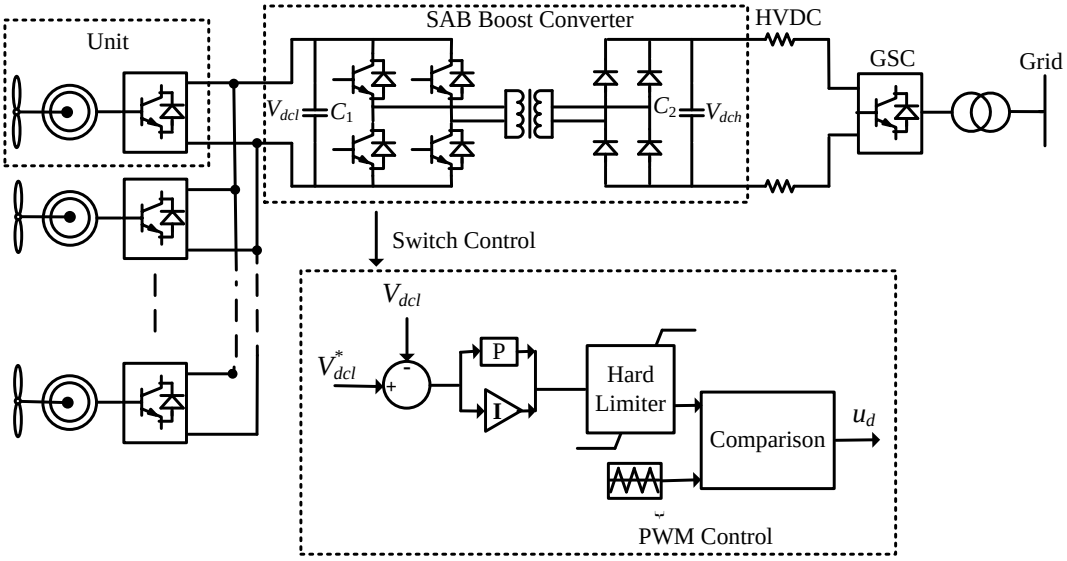

Fig. 3.10. Schematic diagram of a parallel DC collection topology with a SAB converter.

A parallel DC collection system with four wind power units (unit-1 to unit-4) is studied in PSCAD. Two conditions of the SAB with single-phase and three-phase high frequency transformers are simulated and termed as single-phase condition and three-phase condition respectively. The wind turbine, generator and 3-leg VSC models employed in Section 2.2 are considered. The parameters related to the SAB converter are listed in Table 3.3. Figs. 3.11 and 3.12 illustrate the simulation results for the single-phase and three-phase conditions respectively. The wind speed patterns for the 4 turbines in both conditions are the same, which is shown in both Figs. 3.11 (a) and 3.12 (a). It can be seen that all the four wind speeds are 11 m/s at the initial stage and ramp up at different time durations to 13 m/s (v_{w1}), 12 m/s (v_{w2}), 12 m/s (v_{w3}) and 13 m/s (v_{w4}) individually.

Fig. 3.11 (b) shows that the output power of each wind turbine ramps up following their respective wind speed curves. The input and output voltages of the boost converter are both maintained at their respective reference values as plotted in Fig. 3.11 (c). The control signal shown in Fig. 3.11 (d) reduces during the changes in the wind speeds to accommodate the DC voltages before and after boosting. It settles at a lower value than previous. This change of the control signal is explained by rewriting (3.9) as

$$i_h = \frac{\alpha^2 \times (V_{dcl}^2 \times k - V_{dcl} \times V_{dch})}{4 \times f \times L \times k \times V_{dch}} \tag{3.10}$$

It can be seen from (3.10) that the duty cycle α has the same increase/decrease trend with the SAB output current i_h when other parameters remain unchanged as in this simulation. With a bigger power output after a rise in the wind speed, the output current becomes bigger as the output voltage V_{dch} is controlled constant. Therefore, the duty ratio increases following the output current, indicating a drop in the PWM control signal.

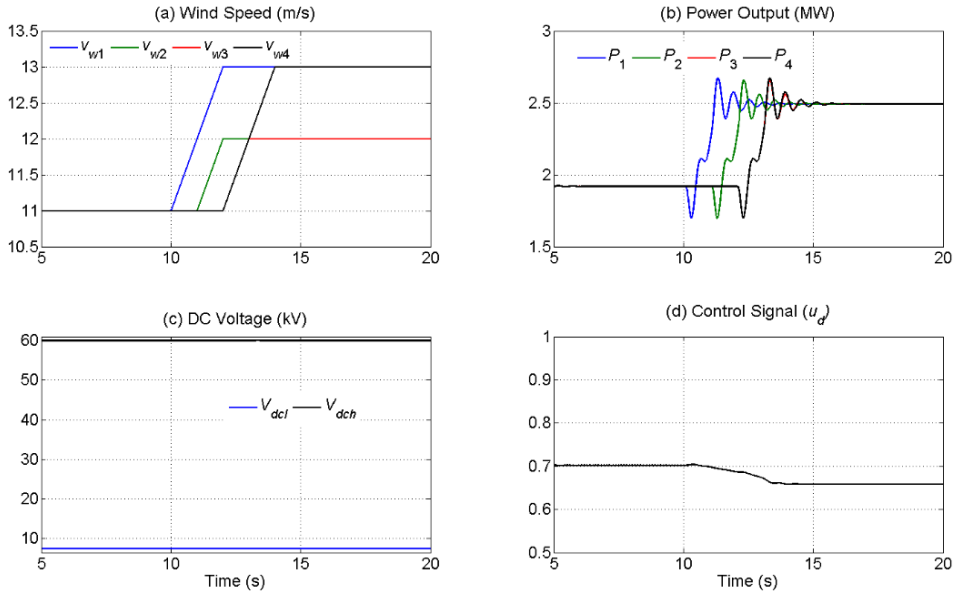

Fig. 3.11. Simulation results of a parallel DC collection system with a single-phase boost converter.

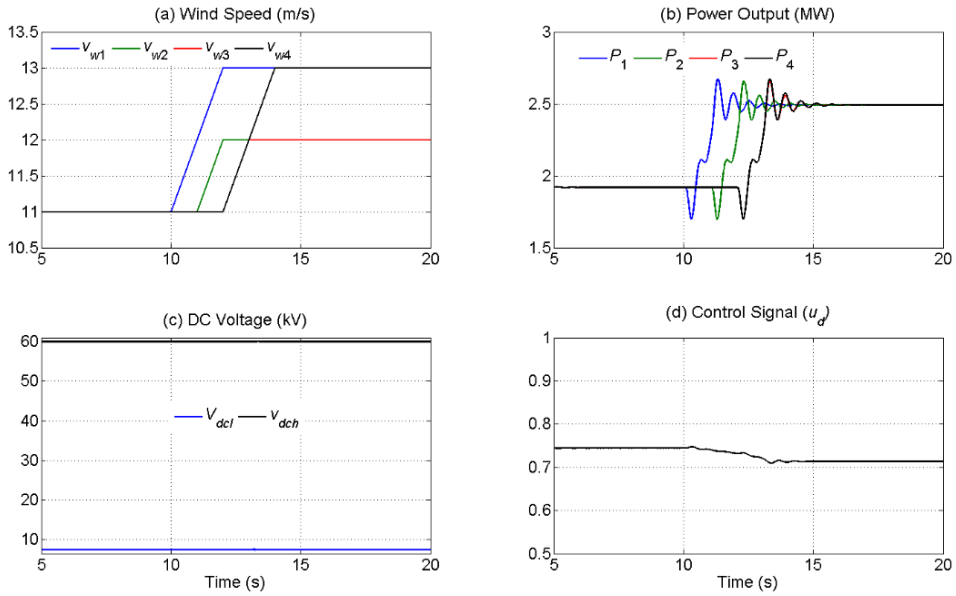

Fig. 3.12. Simulation results of a parallel DC collection system with a 3-phase boost converter.

It can be seen from Fig. 3.12 that the system response with the three-phase condition is similar to that of the single-phase condition. The only difference is that

the control signal is relatively bigger for the three-phase condition, which implies a smaller duty cycle. This is because the power loss is higher for the three-phase condition compared to the single-phase condition with the same parameters applied in these two conditions. Therefore, the difference between the two control signals for the two conditions of this simulation study case can be explained in a similar way according to (3.10).

Table 3.3: Parameters of the SAB and its switch controller (equal for single- and three-phase conditions).

Converter and Control	Parameters Names	Parameter Values
Boost Converter	Transformer capacity	12 MVA
	Transformer turns ratio	1:8.57
	Transformer leakage inductance	0.13 mH
	Transformer base frequency	6500 Hz
	Capacitor (C_1 and C_2)	12000 µF
	Rated voltage after boosting	60 kV
	Rated voltage before boosting	7.5 kV
Switch Controller	Proportional gain	0.001
	Integral time constant	1.0 s
	Upper limit	1.0
	Lower limit	0
	Triangular frequency	6500 Hz
	Triangular mimimum output level	0
	Triangular maximum output level	1.0

Fig. 3.13 shows exactly the same tip speed ratio and rotor efficiency waveforms for both these conditions. Take the single-phase condition as an example. It is shown in Fig. 3.13 (a) that the tip speed ratios for the wind turbines of unit-2 and unit-3 (TSR_2 and TSR_3) are kept at the optimal value at steady states without getting influenced from their wind speed rise. However, the tip speed ratios for the wind turbines of unit-1 and unit-4 (TSR_1 and TSR_4) drop to a same steady value after their wind speeds (v_{w1} and v_{w4}) exceed the rated value of 12 m/s. The decrease of TSR_1 and TSR_4 means that with the wind speeds (v_{w1} and v_{w4}) becoming bigger than 12 m/s, their wind generator speeds stop increasing and remain at the rated value. The rotor efficiency waveforms for wind turbines in each unit (Figs. 3.13 (b) and (d)) thus change in the same manner as their tip speed ratio curves (Figs. 3.13 (a) and (c)). The

response of the tip speed ratios and rotor efficiencies on both conditions demonstrates the effectiveness of the MPPT control.

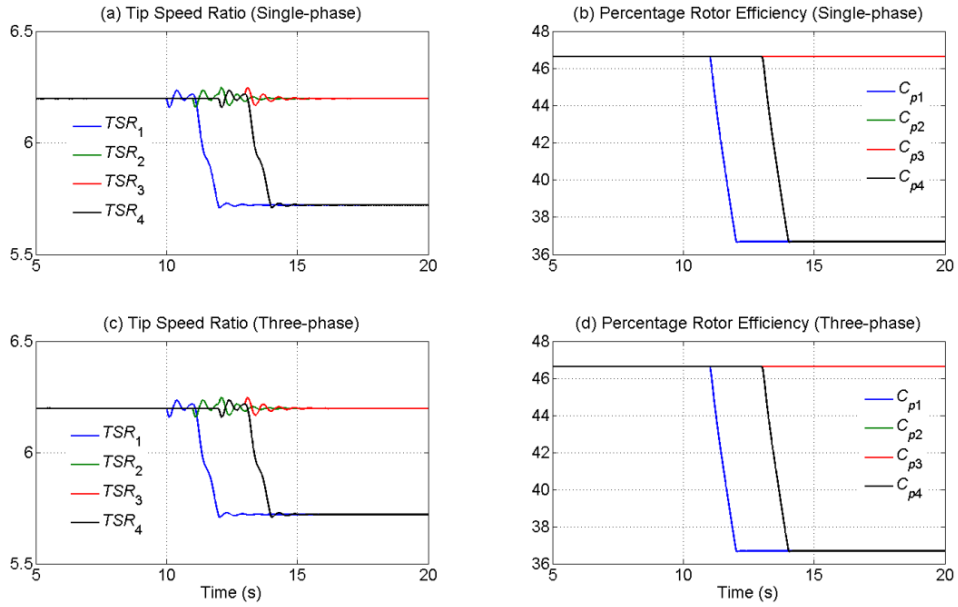

Fig. 3.13. Tip speed ratios and rotor efficiencies of WSCs in parallel with single- and 3-phase boost converters.

3.4. Current Ripple Limitation of SAB Converters Applied in WECSs

Although SAB boost converters are advantageous in many ways, their input and output currents have large ripples [84]. A reduction in these current ripples will reduce the power losses and device stresses. In this section, the limitation of current waveform fluctuations by using existing devices is studied first. After that, a connection pattern of several SAB converters is proposed. The aims of this proposed topology are to reduce the current ripples and to increase the rating of the boosting stage.

3.4.1. Connection of a WECS with a SAB Boost Converter

To reduce the DC current ripples of a SAB boost converter, the most direct way is to install more filters. In fact, HVDC transmission lines/ submarine cables usually employ smoothing reactors. This can reduce the harmonic currents in the DC system, reduce the rate of the current increase during fault conditions and improve the dynamic stability of the HVDC system. Therefore, the output current ripples of a SAB

might be reduced to an acceptable level by smoothing reactors without installing additional filters. To show the effectiveness of the smoothing reactors in limiting current fluctuations, a system with a wind power unit, a SAB boost converter, HVDC submarine cables, a GSC and a grid is studied as shown in Fig. 3.14. The smoothing reactors (represented by two inductors) are connected in series with the HVDC cables.

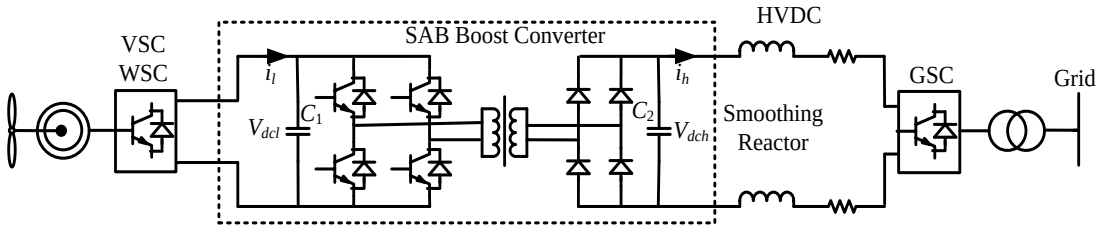

Fig. 3.14. Configuration of a WECS with SAB and HVDC system.

Simulation studies are conducted in PSCAD both with and without smoothing reactors. The system and control parameters are the same as those listed in Tables 2.1 and 3.3, except that the rating of the high frequency transformer used here is 3 MVA. The smoothing reactors are modelled as ideal inductors of 2 mH each. The focus is on DC current in this study, and therefore, the constant rated wind speed of 12 m/s is used as the turbine input. Since the waveforms of wind power outputs, DC voltages and other parameters have been shown previously (Figs. 3.11 to 3.13) to validate the system with its control, only relevant current waveforms are illustrated in this section. The simulated input and output DC currents of the SAB boost converter are shown in Fig 3.15, where the currents for the system with and without smoothing reactors are plotted in the same figures for the convenience of comparison. It can be seen from Fig. 3.15 (a) that the peak value of the input current is reduced from 3.0 kA to 0.7 kA with the smoothing reactor, which is around 76.7% smaller. Fig 3.15 (b) shows a significant decrease in the output current ripples when smoothing reactors are used. Also note that the input and output currents are in the discontinuous mode of operation without the smoothing reactors, and they are in continuous mode with these reactors. This result is in accordance with the conclusion in the previous section.

It is calculated from Table 3.3 that the DC voltage at the unit connecting point is boosted by 8 times after SAB (60 kV / 7.5 kV). Therefore, the average value of the input current should be 8 times of the average output current. This is the reason for that the ripples of the output current are much smaller than that of the input current, either with or without smoothing reactors (shown in Fig. 3.15). For the WECS

connected to HVDC cables, the high voltage at the output of the SAB boost converter greatly reduces the output current ripples. This significant difference of the SAB input and output current magnitudes indicates that, for a wind power collection system, the output current might be up to the standard only with the use of smoothing reactors. To deal with the input current ripples, a wind power collection topology with interconnected SAB boost converters is proposed in the next subsection.

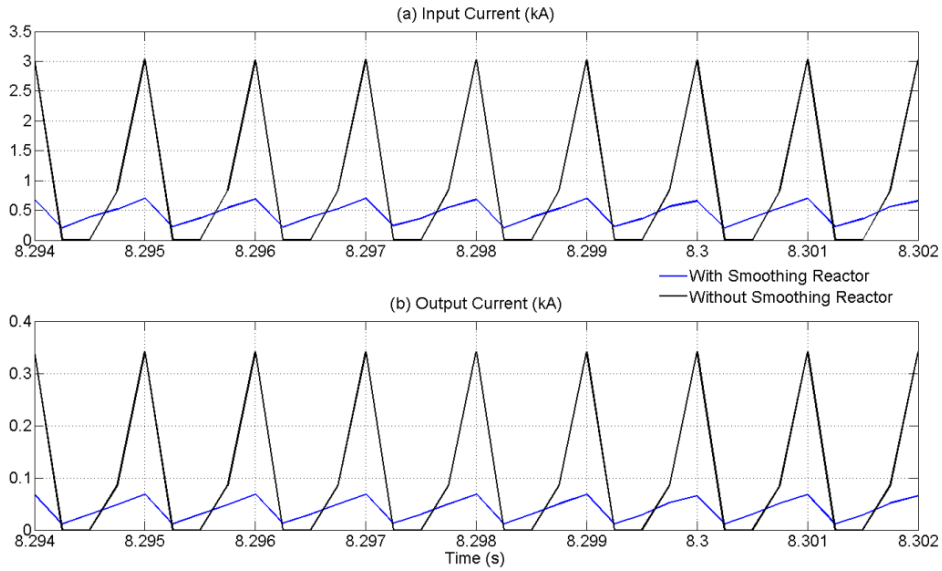

Fig. 3.15. Current waveforms of a WECS with SAB and HVDC system.

3.4.2. INPUT PARALLEL AND OUTPUT SERIES CONNECTION OF SAB CONVERTERS

Despite of their significantly lighter weight and smaller size, high frequency transformers are not manufactured in big capacities like normal frequency transformers. The main restrictions include high isolation requirements and winding losses, etc. [94]. Although the total core loss is reduced, skin and proximity effects increase the winding losses [83]. Moreover, the core loss density increases significantly with the increasing operation frequency, which makes the cooling more difficult. In [95], a dual active bridge converter with rated dc-link voltage of 5 kV and continuous power of 5 MW has been designed and constructed. However, the highest ratings of high frequency transformers designed in industry are around 20-30 kVA [96-97], with voltages up to 10 kV.

The capacity of the boost converter applied for massive offshore wind power is limited by the high frequency transformer rating. For this reason, several boost

converters need to be connected in certain patterns to match the wind power collection demand. Reference [84] connects DC/DC converters in parallel to reduce the current rating of each semiconductor device. The benefits of SAB paralleling are summarized as higher efficiency, better dynamic response, redundancy implementation and ease of maintenance [84, 98-99]. From the device manufacturing point of view, the parallel connection decreases the rated power, rated currents and transformer size of each converter. Furthermore, the reduced current ripples as a result of interleaved switching lower the requirement of capacitor values. However, the filter inductor is required to be bigger, which restricts the quantity of parallel connected converters.

In this research, the inputs and outputs of several SAB boost converters (SAB cluster) are connected in parallel and series respectively. On one hand, the input voltage of the connected cluster matches the WSC output voltage for the reason of the parallel connection. On the other, the output voltage of the SAB cluster can meet the HVDC transmission level since the boosted voltages after boost converters are added up. In the meantime, the high capacity wind power is collected and delivered. As mentioned earlier, the input and output currents of a SAB converter have big ripples. To deal with this problem, the IGBT switching signals among the SABs can be phase shifted evenly in the range of 0 to 360°. In this way, the added up input current ripples are greatly reduced. The ripples in the output current remain the same since all converter output terminals share the same current due to the series connection in the outputs. The Input Parallel Output Series (IPOS) connection structure is shown in Fig. 3.16, where the input currents of each boost converter are denoted by i_{l1}, i_{l2}, …, i_{ln} and the output voltages are represented by V_{dch1}, V_{dch2}, …, V_{dchn}.

A parallel wind power collection system with 2 units and 4 boost converters is studied. The boost converters are identical SAB converters with single-phase high frequency transformers. The SAB parameters are listed in Table 3.4. The same smoothing reactors are employed here as in the former subsection. The two cases of the SAB converters with and without phase shift are simulated in PSCAD and termed as case-1 and case-2 respectively. The simulation results are shown in Figs. 3.17 and 3.18.

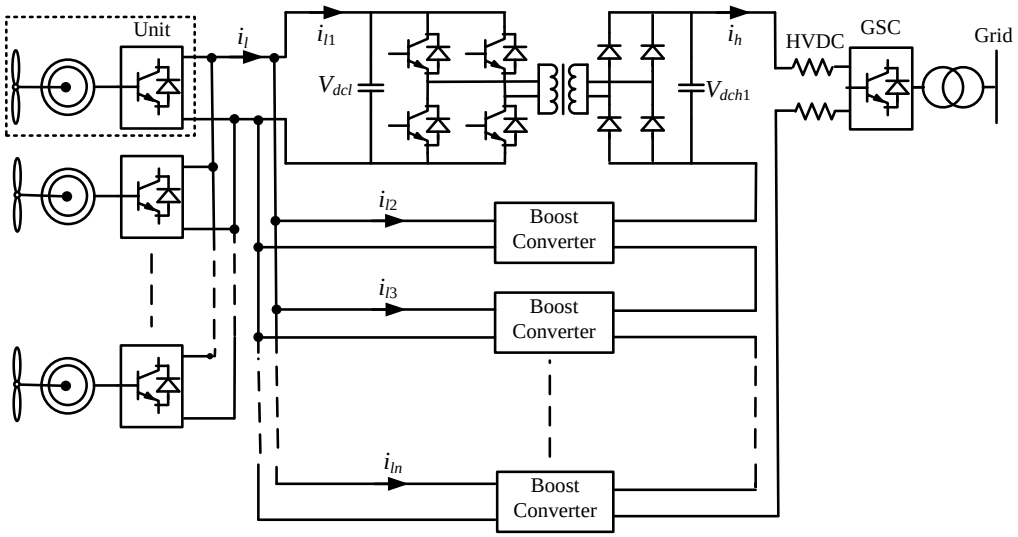

Fig. 3.16. WECSs with IPOS boost converters.

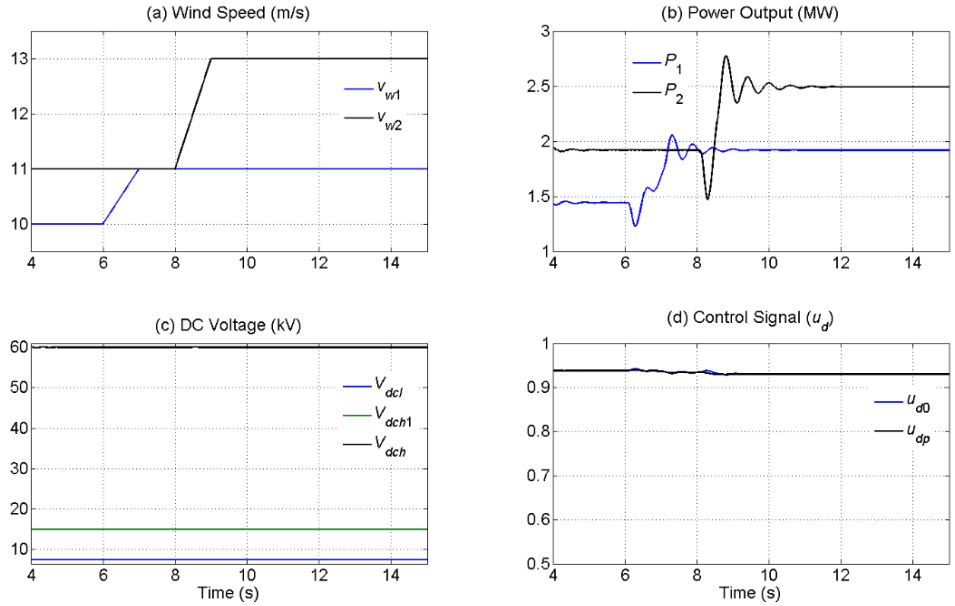

Fig. 3.17. Simulation results of WECSs with IPOS boost converters.

The wind speeds on both cases are set as in the same pattern, where v_{w1} ramps up from 10 m/s to 11 m/s between 6 s and 7s, while v_{w2} increases from 11 m/s at 8 s and reaches 13 m/s after 1 s (Fig. 3.17 (a)). The waveforms of the power outputs and DC voltages in the two cases have the same nature as the same control algorithm is applied to the WECS. It can be seen from Fig. 3.17 (b) that the power outputs of both power units follow their respective wind speed curves with fluctuations during ramping transients. Fig. 3.17 (c) shows the voltage before boosting (V_{dcl}), the voltage of each SAB after boosting (V_{dch1}) and the total boosted DC voltage (V_{dch}). It can be seen that V_{dcl} is boosted to V_{dch1} by each SAB and the DC output voltages of the four

SABs are added up to V_{dch} as a result of the series connection. It is obvious that all the three voltages are controlled at their individual reference values regardless of wind speed changes. The control signals plotted in Fig. 3.17 (d) shows slight difference between case-1 (u_{d0}) and case-2 (u_{dp}). This is the result of different switching delays among SABs for the two cases.

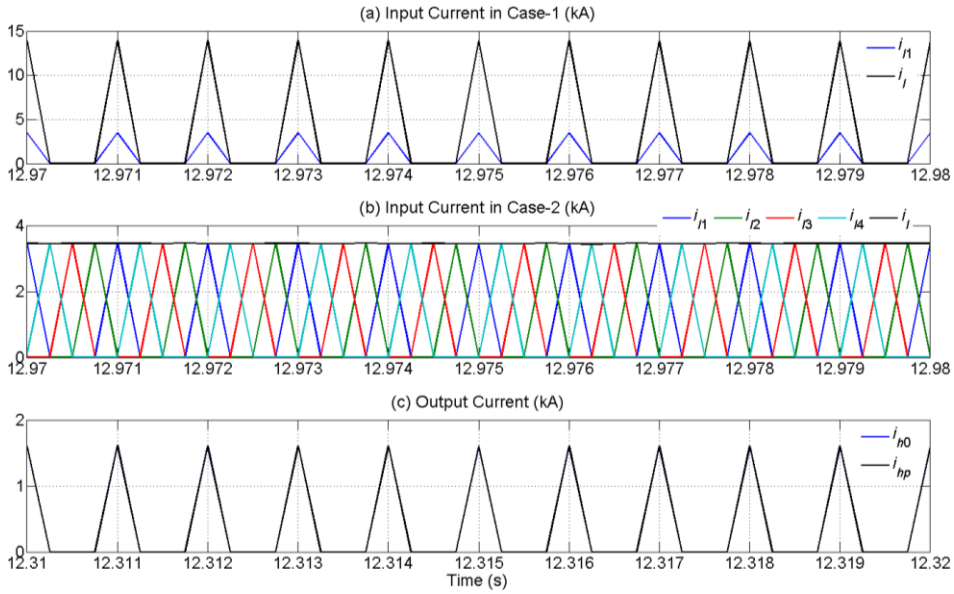

Fig. 3.18. Current comparison of WECSs with IPOS boost converters.

Table 3.4: Parameters of the SABs and switching control for the IPOS system.

Converter and Control	Parameters Names	Parameter Values
Boost Converter	Transformer capacity	6 MVA
	Transformer turns ratio	1:2.143
	Transformer leakage inductance	0.52 mH
	Transformer base frequency	6500 Hz
	Capacitor (C_1 and C_2)	12000 µF
	Rated voltage after boosting	15 kV
	Rated voltage before boosting	7.5 kV
Switch Controller	Proportional gain	0.01
	Integral time constant	1.0 s
	Upper/ lower limit	1.0/ 0
	Triangular frequency	6500 Hz
	Triangular mimimum/ maximum output level	0/ 1.0

Fig. 3.18 shows the input and output DC currents of the SAB converters. In case-1, plotted in Fig. 3.18 (a), the input currents (i_{l1}) of each SAB are the same,

which adds up a total input current with high ripples (i_l). It can be seen from Fig. 3.18 (b) that the input currents of the four SABs (i_{l1}, i_{l2}, i_{l3}, i_{l4}) are equally phased shifted in case-2. As a result, the waveform of the total input current (i_l) becomes flat with almost no ripples. Fig. 3.18 (c) shows the identical output currents for the two cases (i_{h0} for case-1 and i_{hp} for case-2) after the boosting stage. It is clear that output currents do not get influenced by the interleaved switching strategy of case-2. But their amplitudes are much smaller than that of the input currents. It is also noted that all the input and output currents of the SABs are in a discontinuous mode, indicating that the applied smoothing reactor value might need to be increased, if necessary.

3.5. WIND SIDE FAULT STUDIES

The parallel connection concept in this chapter refers to the wind side converters being connected in parallel on their DC sides. The three main parallel connected topologies described above include (a) the diode with non-isolated boost converter in parallel, (b) the parallel connected wind power units with a high rated SAB boost converter and (c) with input parallel output series interfaced SABs. These three topologies are simply termed as diode in parallel, VSC in parallel and VSC with IPOS respectively. Considering the large power capacities of offshore wind farms, the latter two wind power collection topologies are preferred. The fault studies of the VSC in parallel and VSC with IPOS systems are conducted in this section. In this, the fault does not indicate a line fault, but a failure of a wind turbine system and its removal from the power supply. No electrical fault has been considered, since protection is not the main aim of this study.

Theoretically speaking, when some wind turbines fail, their relevant wind power units can be disconnected directly. This is because the DC voltages of parallel connected wind power units are independent on each other. No fault transients of DC voltages should occur on the non-faulty units and the whole system should continue to operate steadily in this case. Simulations are conducted in PSCAD using the two models in Subsections 3.3.4 (single-phase) and 3.4.2 to verify the safe disconnection of faulty wind power units. The faults occur to unit-4 and unit-2 respectively for VSC in parallel and VSC with IPOS. The system responses of these two cases are shown in Figs. 3.19 and 3.20. It is noted that v_{w3} and v_{w4} are equal as they are not visible in Fig. 3.20 (a). In general, it can be seen from Figs. 3.19 and 3.20 that, with

different wind speeds, both of the two systems operate in steady states without causing disturbance due to the disconnection of faulty wind power units.

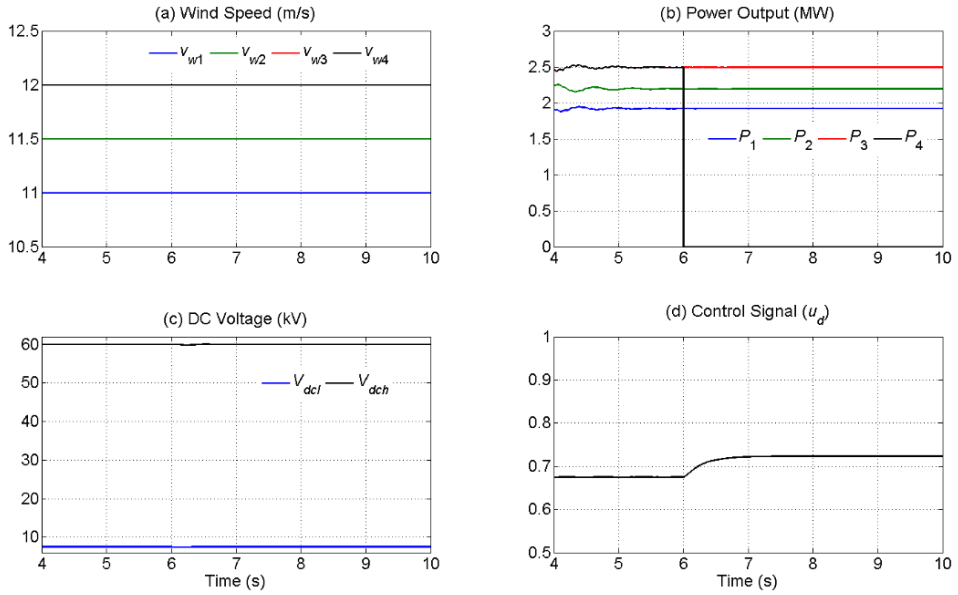

Fig. 3.19. System response of VSC in parallel.

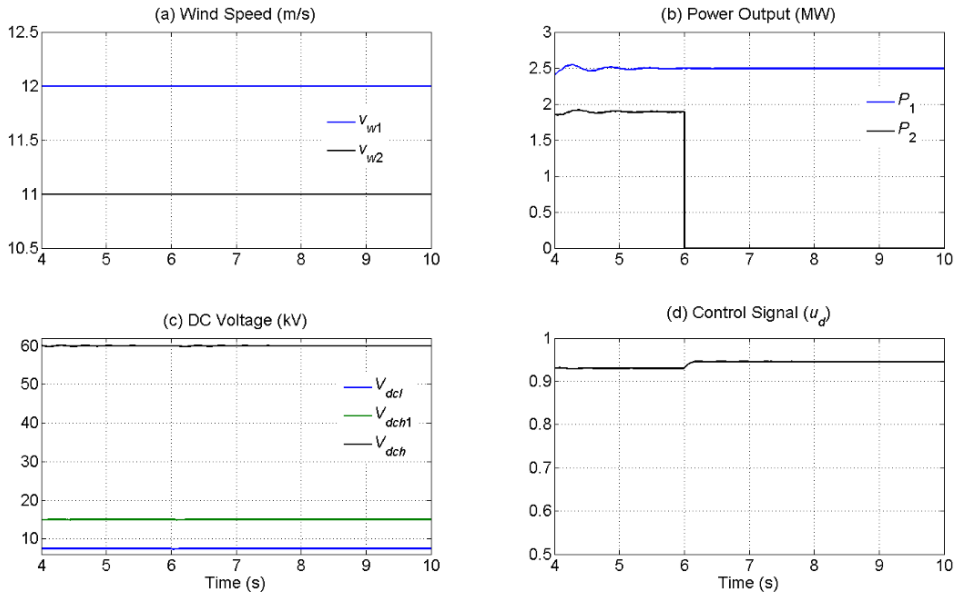

Fig. 3.20. System response of VSC with IPOS.

3.6. CONCLUSIONS

Offshore wind power DC collection systems based on parallel connection is discussed in this chapter. To boost the DC voltage of a WECS for HVDC power delivery, four different topologies are proposed.

First, several diode rectifiers with a non-isolated two-channel boost converter each are connected in parallel. The MPPT operation of each wind generator is controlled by its respective boost converter.

Second, the VSC WSC with a two-channel boost converter system is studied. However, this topology is not preferred because of its disadvantages compared to other WECSs and thus not connected in parallel.

Third, the parallel connected VSC WSCs with an isolated boost converter topology is discussed. The single active bridge converter is chosen for the voltage boosting of massive offshore wind power due to its advantages. The VSC WSC controls MPPT, while the SAB switches are under voltage control.

Fourth, the system of several VSC based wind power units connected in parallel with a number of IPOS interfaced SAB boost converters is proposed. The latter two collection topologies are favoured for offshore wind power integration. The fault condition of losing wind power units is simulated for these two topologies. The simulation results considering fault further verify the offshore wind power DC collection systems proposed in this chapter.

CHAPTER 4

NOMINAL OPERATION OF SERIES DC COLLECTION SYSTEMS

Series connection and parallel connection are the two basic connection types in wind power systems. For offshore wind power, parallel DC collection systems studied in Chapter 3, are widely discussed in research literature. In this chapter, first, various collection topologies are discussed. Specific attention is given to the voltage restrictions imposed due to wind power fluctuations. Thereafter, a new power collection system based on series DC connection is proposed for offshore wind farms. The series DC collection topology is advantageous mainly from the economical point of view and thus discussed in this chapter. The DC voltages of each wind power unit in this collection system are limited within the specified range by controlling their respective power outputs.

As HVDC is suitable for offshore wind power delivery, the voltage of a DC collection system must be staged up to accommodate high transmission voltages. As mentioned in Chapter 3, the use of boost converters is not ideal because of their high costs. In a series DC collection system, the DC sides of each wind side converter are connected in series [37]. The basis of applying series connection among wind turbines is the fact that at any given instant, the wind speed within an offshore wind farm (almost) does not change from one location to another. This is because offshore wind is not blocked by any hindrance and the wind speeds to each wind turbine are thus very similar. In addition, a wind farm in real projects usually employs the same type of wind turbines. Therefore, these uniform wind turbines within an offshore wind farm have similar power outputs and they can be stacked up on their DC side. In this way, the DC voltage at the collection point is added up and boost converters are no longer required. For example, given an offshore wind farm with 20 wind turbines and 7.5 kV DC voltage of each wind side converter, the series collected DC voltage would be 150 kV (7.5×20), which is high enough for HVDC transmission. Therefore, the obvious advantage of a series DC collection system over a parallel one is the greatly reduced investment costs. This advantage is particularly significant for offshore wind power projects, the investment of which could only be offset after years of operation [11].

However, the functioning of a series DC collection system is highly sensitive to wind turbine operation as the same DC current flows through all the wind side converters [37]. In this case, when the wind speeds to each wind turbine within an offshore wind farm vary too much, the wind side converters with bigger power flow would have relatively higher DC voltages and those with smaller power flow would have lower DC voltages. Therefore, undervoltage and overvoltage are potential issues related to series DC collection systems. Furthermore, if one or more wind turbines are out of operation, the high collected DC voltage would be imposed on the remaining turbines. In this way, the DC voltages of the connected wind side converters would rise and semiconductor devices might get damaged. For example, assume the collected transmission voltage of an offshore wind farm with 20 wind turbines is 150 kV, then the nominal DC voltage of each WSC would be 7.5 kV (150÷20). When two wind turbines fail and get disconnected, the rest of the wind side converters would have an average voltage of 8.33 kV (150÷18), which is probably out of the allowable voltage range. Therefore, in the condition of wind turbine failures, series overvoltage might occur.

To alleviate the problem of uneven wind speeds within the wind farm, two voltage balancing strategies are proposed for the series DC collection systems. Both strategies aim at achieving similar power outputs amongst all the wind power units. First, a small battery is connected to each unit for absorbing excess power or for compensating insufficient power. Second, the power references for some Wind Side Converters (WSCs) are reduced from their respective references obtained from MPPT control. The excess generator power is dissipated in chopping resistors. Alternatively, the pitch control system for each wind turbine is modified to capture less wind energy according to the new power references. The effectiveness of using each proposed strategy is demonstrated by simulation studies using PSCAD.

4.1. OFFSHORE WIND POWER COLLECTION SYSTEMS AND VOLTAGE RESTRICTIONS

The power generated by wind turbines within an offshore farm must be collected together for integration with a grid. Offshore wind power collection systems can have various topologies. In this section, different collection systems are described and compared mainly from investment and power loss considerations. The

collection systems also include a proposed series DC collection topology suitable for offshore wind farms. The DC voltage restrictions for wind power units are defined.

4.1.1. OFFSHORE WIND POWER COLLECTION TOPOLOGIES

The usual way to collect offshore wind power through an AC system is shown in Fig. 4.1 [38], where each WECS (wind turbine, generator and back-to-back power converters) is connected to a common collection bus through short submarine cables in parallel. Transformers (marked in yellow) are used to boost the bus voltage such that the collected power can be sent out by HVDC. In this topology, WECSs which are close by can form a wind generation cluster. The WECSs within one cluster are connected in parallel and the terminal voltage of the cluster can be stepped up by a transformer (marked in green). Then all the generation clusters are collected by an AC bus. Another transformer (marked in red) can be used to further boost the voltage, if necessary. Therefore, there are three potential locations for transformer installation (yellow, green and red areas). However all these may not be necessary. As the AC voltage, before the HVDC rectifier must be high enough to match the HVDC transmission level, at least one boosting stage is needed for the wind farm. The selection of transformers and their installation locations are based on the consideration of various factors. In general, how many WECSs should form a cluster and where transformers should be installed mainly depend on power losses and investment cost.

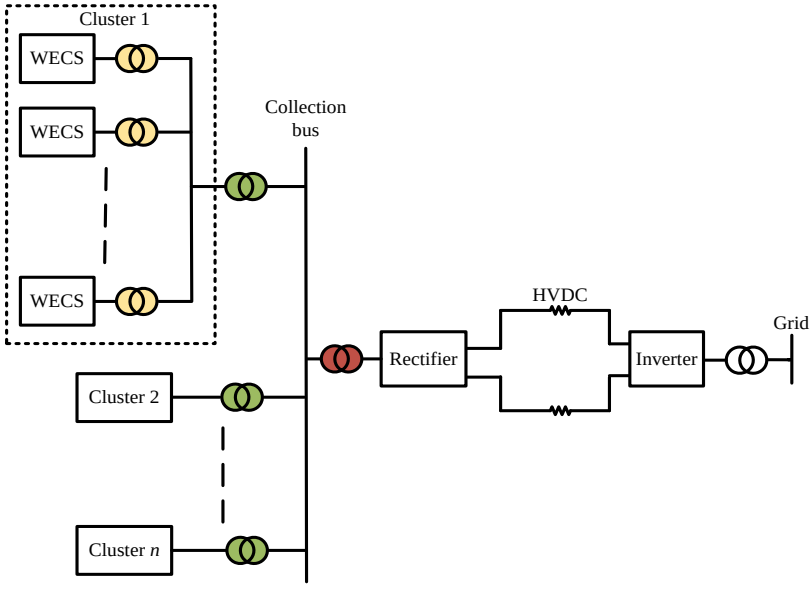

Fig. 4.1. AC collection system.

In a DC collection system, offshore wind power is collected through submarine DC cables. Apart from the parallel DC collection configuration (Fig. 3.9 of Chapter 3), the series-parallel topology has been shown to be amongst the promising structures for the power collection of a distant offshore wind farm [100]. This topology is displayed in Fig. 4.2, where each unit cluster formed by series connection is termed as a "wind power branch" or simplified as a "branch". Identical wind power units are included in each branch such that these units share the same DC current and the DC voltage distributes evenly amongst them. All the wind power branches are then connected in parallel to from a series-parallel DC collection system. The collected power is sent out through HVDC lines and then integrated into an AC grid. A common inverter (GSC) is used on the grid side to maintain the terminal voltage of the DC collection system. An obvious advantage of the series-parallel DC topology is that the voltage and current of the collection system is added up by series and parallel connection respectively so that voltage boosting stages can be omitted. Also, the number of converters required is greatly reduced, which significantly lowers the investment cost. However, due to the series interconnection of wind power units in each branch, the aggregated power in a series-parallel topology is highly sensitive to the operation of wind generators.

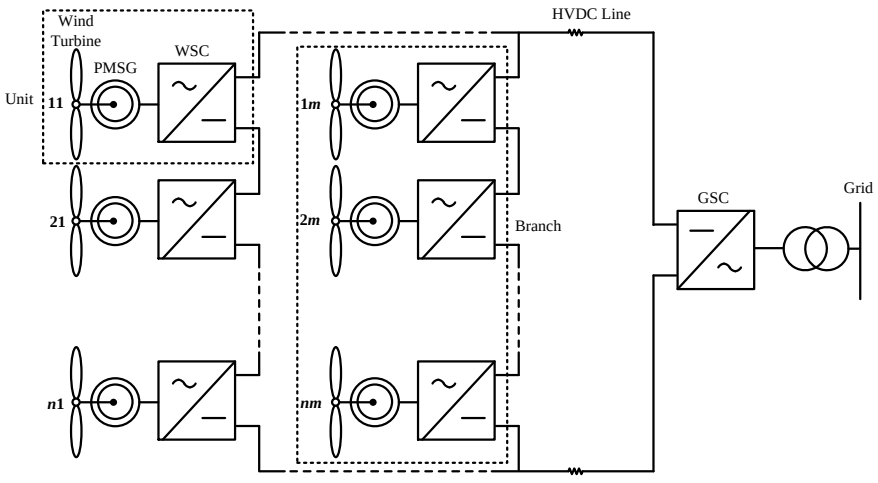

Fig. 4.2. Series-parallel DC collection system.

A review of the largest 35 offshore wind farms (25 operational and 10 under construction) reveals that almost all of them individually employ only one type of wind turbines. Therefore, this thesis assumes that identical wind turbines are installed within a wind farm.

A new wind power collection topology with only series DC connection is proposed in this thesis. This is shown in Fig. 4.3 and proposed below. The realization of collecting wind power in a purely series connected pattern is based on the special environment of offshore wind farms. Compared to onshore wind farms, wind within an offshore area is not hindered by buildings or trees. Wind speeds can thus be considered the same or slightly uneven (in the case of very large wind farms). Therefore, power outputs from identical turbines within an offshore wind farm do not vary much. According to [101], no obvious power magnitude difference from turbine to turbine can be discerned. The natural condition and construction feature facilitate offshore wind turbines being stacked up.

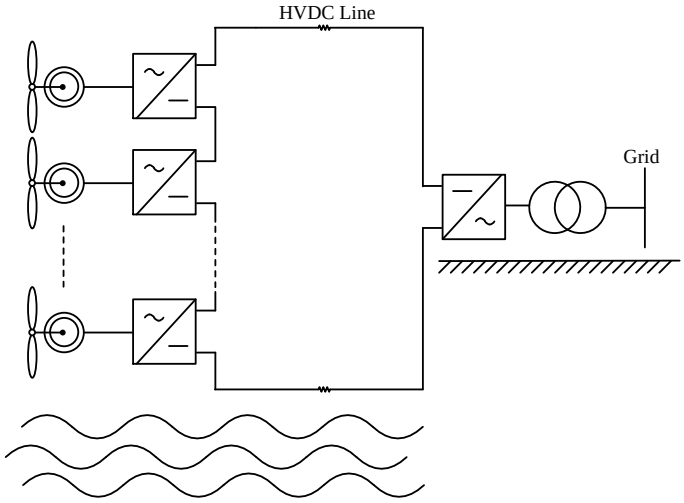

Fig. 4.3. Series DC collection system.

4.1.2. DISCUSSION OF OFFSHORE WIND POWER DC COLLECTION TOPOLOGIES

Compared to AC collection, the size of DC collection systems is reduced and transformer weights are decreased [39]. Therefore, the collection topology comparison in this subsection is on DC collection systems. As mentioned in the last subsection, the series-parallel DC collection topology adds up both the DC voltage and DC power through the connection structure itself instead of using boost converters. For the concern of investment cost, the series-parallel DC connection has greater advantages than the use of only parallel DC connection. However, the series-parallel topology might require extra devices to deal with fault conditions.

As to the comparison of DC collection systems with pure parallel connection and pure series connection, Figs. 4.3 and 4.4 illustrate their differences. It is noted that the parallel DC collection system shown in Fig. 4.4 is the employed topology in Section 3.3 of Chapter 3. In these two figures, wavy lines represent water, while horizontal straight lines with slashes stand for land surface. It can be seen from Fig. 4.4 that for the parallel DC collection, wind turbines, wind side converters and the boost converter (marked in a dashed frame) are all built offshore. In the case of the series DC collection system shown in Fig. 4.3, no boost converters are needed as the series connected structure adds up the DC voltages to an HVDC transmission level. Besides, only wind turbines with their wind side converters are in the offshore area. Without the installation of boost converters, the series DC collection topology is much simpler and cheaper.

The series-parallel topology is the same with the series topology as in offshore installation. An important difference between the two topologies is that overvoltage caused by fault in the series DC collection system can be prevented by modifying control strategies instead of using extra devices (discussed below). Due to the reasons above, the use of only series DC connection is preferred.

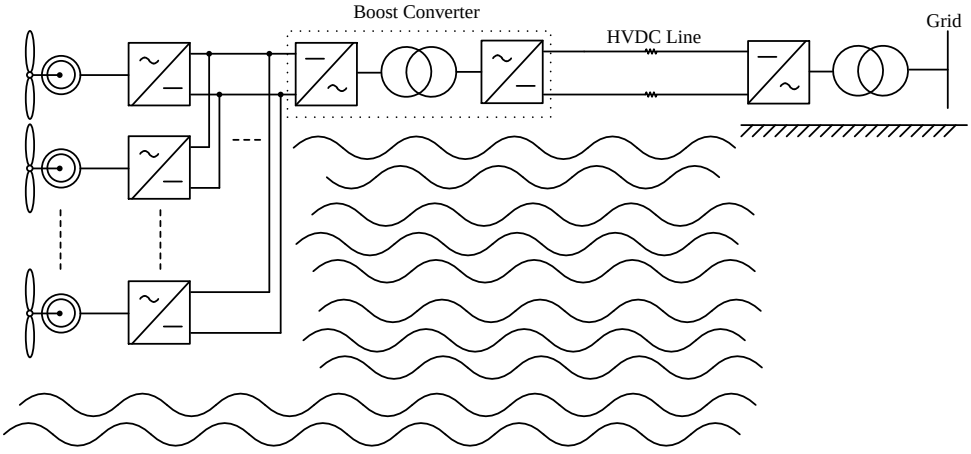

Fig. 4.4. Parallel DC collection system.

4.1.3. DETERMINATION OF VOLTAGE RESTRICTIONS

The series DC collection system for offshore wind farms will be discussed in details in this chapter and the next. For a series wind power collection system, the GSC can only maintain the total voltage at the collecting point constant. The DC

voltage of each wind power unit cannot be controlled independently. Neglecting HVDC line losses, the input voltage reference of the GSC is set as

$$V_{TN} = n \times V_N \tag{4.1}$$

where V_{TN} is the rated transmission voltage, V_N is the nominal DC voltage of each unit, and n is the number of series connected wind power units. Since series connection requires the same DC current to flow out of each unit in a branch, their DC voltages are proportional to their own power outputs. However, the transmission voltage, denoted by V_T, is kept constant at the rated value as per (4.1). This dependent voltage control method is termed as Voltage Distribution Principle (VDP) in this thesis.

With only series connection, if wind speeds in different areas vary significantly, the power outputs from the wind turbines will vary accordingly. According to VDP, units with relatively bigger power outputs will have higher DC voltages, which might damage their semiconductor switches. Similarly, units with smaller power outputs might encounter tracking failure for their low DC voltages, which is explained below.

For power converters under SPWM control, suppose the DC voltage and AC line-to-line RMS voltage of a power converter are denoted by V_d and V_{LL} respectively. The conversion equation between V_d and V_{LL} under the SPWM technique is [102]

$$V_{LL} = \frac{\sqrt{3}}{2\sqrt{2}} \times m_a \times V_d \tag{4.2}$$

where m_a is the modulation index ($0 \leq m_a \leq 1$). With a given AC voltage, the minimum DC voltage is obtained when $m_a = 1$. It means that the DC side voltage of a power converter must meet (4.3) to prevent signal tracking failure.

$$V_N \geq \frac{2\sqrt{2}}{\sqrt{3}} \times V_{LL} = 1.633 V_{LL} \tag{4.3}$$

Besides, overvoltage is likely to happen when some units are faulted, which will be discussed in Chapter 5. Considering the restriction in (4.3) and certain safety margin, the lower DC voltage limit for each converter is set at $V_{lw} = 0.9V_N$, while the upper limit is considered as $V_{up} = 1.1V_N$ in the steady state. So the acceptable DC

voltage range of power converters are ±10%V_N for steady operation. An overvoltage limit of 1.5V_N is allowed for each unit during fault transients [26].

As mentioned earlier, wind speeds within an offshore wind farm are almost equal. For a series DC collection system, small DC voltage deviations which are caused by slightly different wind speeds normally do not go out of the ±10%V_N range. Even if the DC voltages for some units exceed the specified range as a result of power output differences, the deviations will not be much. To limit the DC side voltages of series connected units, two control strategies are proposed in this thesis and discussed below.

4.2. SMALL SIZED BATTERY APPLICATION

Batteries are widely applied in power systems [103-105]. With the development in related technique and material areas, the prices of batteries are generally decreasing [106-107]. In this section, small-capacity batteries are applied to balance the power outputs of wind power units in a series DC collection system. The batteries do not need to have large capacities since the differences in the wind speed amongst the units within an offshore wind farm will be small. Also, smaller batteries mean lower costs. This voltage control strategy by exchanging power with batteries is termed as Small Sized Battery Application (SSBA) in this thesis.

4.2.1. TOPOLOGY AND CONTROL OF SMALL SIZED BATTERY APPLICATION

The schematic diagram of a series DC collection system with SSBA for offshore wind power is illustrated in Fig. 4.5. In this, a small sized battery is connected in parallel with the WSC through a DC/AC power converter on the AC side of each unit. The combination of a battery and its connected DC/AC converter is considered as a power sink. It is noted that the frequency of the converter in each power sink is synchronized with the variable generator frequency. The subscripts 1, 2, …, n of the parameters represent the numbering for unit-1, unit-2, …, unit-n respectively. In this way, P_{outi} (i = 1, 2, …, n) stands for the power output of a wind generator; P_i denotes the power output of a unit (or WSC); P_{bi} is the exchanged power with a power sink; V_i represents the DC voltages of a wind power unit.

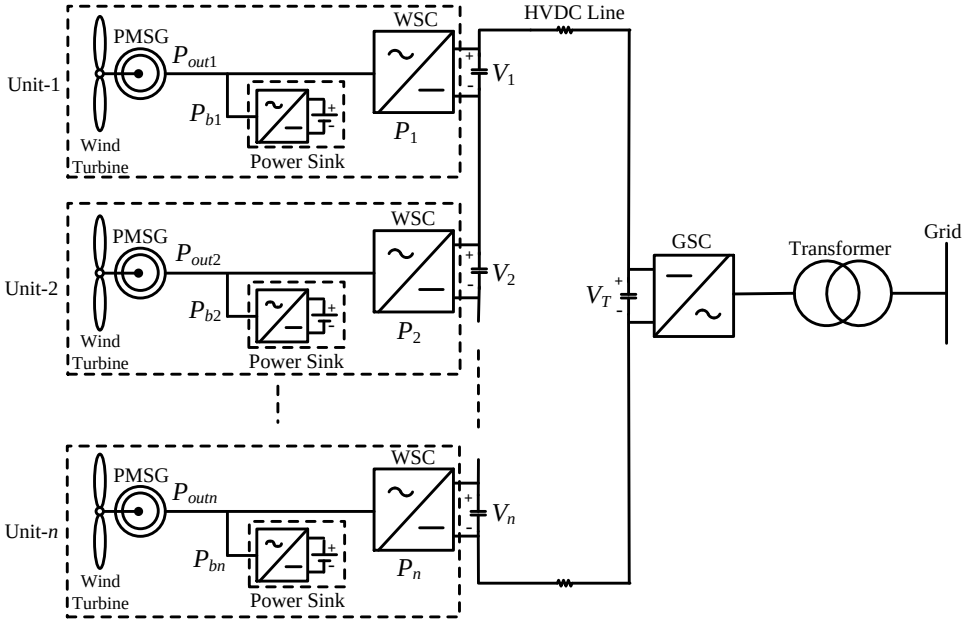

Fig. 4.5. Configuration of a series DC collection system with small sized batteries.

The DC voltage of each unit is expected to meet the specified restrictions by applying small sized batteries, which is

$$0.9V_N \le V_i \le 1.1V_N, \quad i = 1, \cdots, n \tag{4.4}$$

Suppose the DC current is I_d, the average DC voltage and average power output of WSCs are V_{av} and P_{av} respectively. Since

$$V_N = \frac{V_T}{n} = V_{av} \tag{4.5}$$

then

$$\begin{aligned} P_{av} &= \frac{P_1 + P_2 + \cdots + P_n}{n} = \frac{V_1 \cdot I_d + V_2 \cdot I_d + \cdots + V_n \cdot I_d}{n} = \frac{(V_1 + V_2 + \cdots + V_n)}{n} \cdot I_d \\ &= V_{av} \cdot I_d = V_N \cdot I_d \end{aligned} \tag{4.6}$$

With V_N being constant, a certain amount of I_d produces a certain amount of P_{av}. Therefore, P_{av} can be regarded as the suppositional variable rated power output of each unit as the wind speeds (unit power outputs) change. Based on VDP, to control the DC voltage of each unit to meet the requirement in (4.4), the unit power outputs must vary within the range of ±10% of their suppositional rated value. The control objective of the power outputs from the wind power units is thus

$$P_{\min} \le P_i \le P_{\max}, \quad i = 1, \cdots, n \tag{4.7}$$

where $P_{\min} = 0.9P_{av}$ and $P_{\max} = 1.1P_{av}$.

To achieve (4.7), the power references P_{1ref}, P_{2ref}, …, P_{nref} for angle control (2.8 in Chapter 2) are modified to P'_{1ref}, P'_{2ref}, …, P'_{nref} respectively according to the following equations.

$$P'_{iref} = \begin{cases} 0.9P_{av} & P_{iref} \le P_{\min} \\ P_{iref} & P_{\min} \le P_{iref} \le P_{\max}, \quad i = 1, \cdots, n \\ 1.1P_{av} & P_{iref} \ge P_{\max} \end{cases} \tag{4.8}$$

It is shown in (4.8) that the modified power references can be bigger or smaller than their previous values, which means power exchanges with power sinks in Fig. 4.5 are bidirectional. Suppose the power flow towards batteries is positive, then

$$P_{bi} = P_{outi} - P_i, \quad i = 1, \cdots, n \tag{4.9}$$

Accordingly, δ_w in (2.8) is modified for each WSC as (the subscript is omitted)

$$\delta_w = K_{Pw}(P'_{ref} - P) + K_{Iw}\int (P'_{ref} - P)dt \tag{4.10}$$

It can be seen from (4.10) that the power flow towards each WSC (i.e., the unit power output) is controlled to satisfy (4.7) by following their modified reference values. The batteries deal with the power differences between generators and WSCs by either providing or absorbing power. Since (4.7) is satisfied, the DC voltages for all units are limited within the specified range.

It should be noted that although small-capacity battery with power converter devices are much cheaper compared to large ones, SSBA still increases the total investment cost of an offshore wind farm. Therefore, before the installation of these batteries, a study of historical wind data is required. The batteries are installed only if the wind speeds have the potential to cause more than 10% power output differences according to the historical records.

4.2.2. SIMULATION STUDIES

To verify the control effectiveness of SSBA, simulation studies are conducted in PSCAD, where four wind power units are connected in series, with each facing different and variable wind speeds. The wind speed pattern for each turbine varies distinctly to show the robustness of the series DC collection topology. The grid is modelled as an ideal voltage source (infinite bus). The GSC output AC voltage reference is set at 16 kV (four times the rated line-to-line RMS voltage of the PMSG). Since the rated DC voltage for each unit is 7.5 kV, the GSC holds the DC line voltage of the system at 30 kV according to (4.1). As per (4.4), the two voltage limits of each power unit are therefore

$$\begin{cases} V_{lw} = 0.9 \times 7.5kV = 6.75kV \\ V_{up} = 1.1 \times 7.5kV = 8.25kV \end{cases} \tag{4.11}$$

Case 1*: Series DC collection system with varied wind speeds.*

The simulation results on normal condition without SSBA are illustrated in Fig. 4.6. The wind speed inputs of unit-1 to unit-4, denoted by v_{w1}, v_{w2}, v_{w3} and v_{w4} respectively, are illustrated in Fig. 4.6 (a), where their initial values are 10.5 m/s, 11.5 m/s, 11 m/s and 12 m/s individually. It can be seen that v_{w1}, v_{w2} and v_{w3} ramp up at 10 s, 11 s and 12 s respectively and settle at values bigger than the rated wind speed of 12 m/s, while v_{w4} decreases between 12 s and 13 s, settling at 11 m/s. Fig. 4.6 (b) shows that the waveforms of the wind power outputs follow their corresponding wind speeds with small fluctuations during the changes in wind speeds. Note that the power output in the simulation studies of this section all refers to the power from a WSC. V_1, V_2, V_3, V_4 depicted by Fig. 4.6 (c) are distributed among the four units based on VDP. It can also be seen in Fig. 4.6 (c) that V_1 is below V_{lw} before v_{w1} ramps up, while V_4 is out of the predefined range both before and after v_{w4} changes. The total DC voltage is maintained at 30 kV by the GSC, a scaled version of which is shown in Fig. 4.6 (c).

Case 2*: SSBA in the series DC collection system with varied wind speeds.*

Now SSBA is adopted in the same simulation model as in Case 1 to control the DC voltages of the four units within the specific range irrespective of wind speed differences and variations. The simulation results are shown in Fig. 4.7, where the power from each PMSG follows its respective wind speed with transient fluctuations

(Fig. 4.7 (a)). It can be seen from Fig. 4.7 (b) that the power outputs of all the four units are controlled between $P_{\min}$ and $P_{\max}$ at steady states. Therefore, the four DC voltages are all within the allowable range, which is illustrated in Fig. 4.7 (c). The transmission voltage is still kept constant and not shown here. Fig. 4.7 (d) shows the power exchange between the small sized batteries and WECSs. As per (4.9), negative exchange values indicate batteries supply power while positive values imply batteries absorb power. It is noted that the system needs longer time to stabilize in Case 2 than in Case 1 due to the employment of small sized batteries.

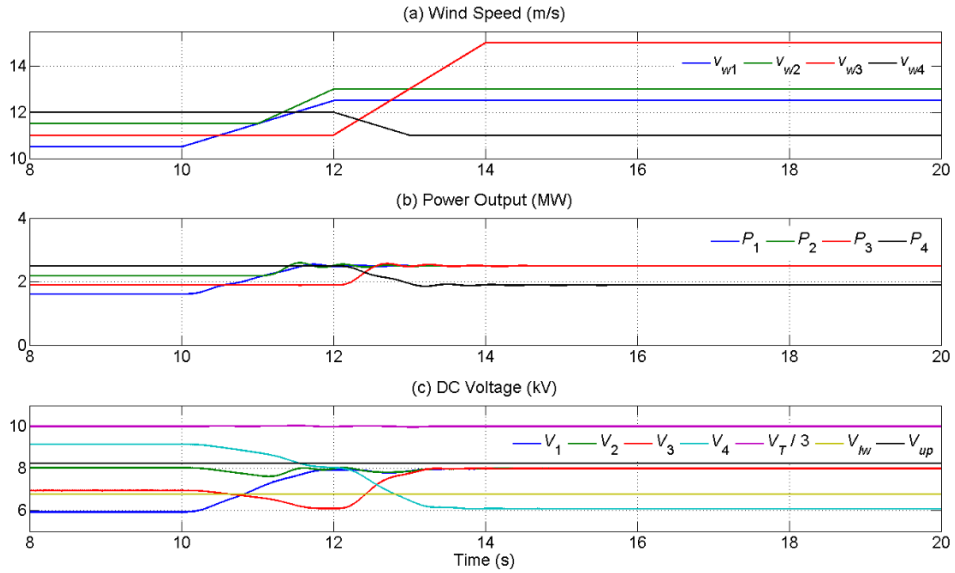

Fig. 4.6. Simulation results of a series DC collection system with four units.

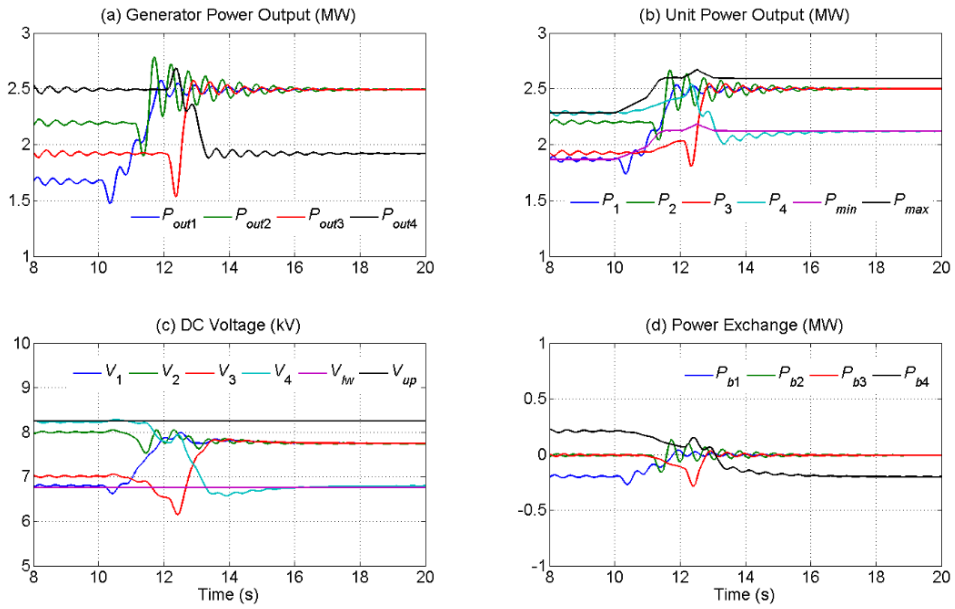

Fig. 4.7. Simulation results of a series DC collection system of four units with SSBA.

4.3. POWER REFERENCE MODIFICATION BASED ON MPPT

It has been mentioned in the last section that SSBA will incur additional costs to offshore wind farms. Besides, the power sinks only come into operation when wind speeds cause more than 10% power output differences. This implies that the batteries with their connected power converters are at standby mode for most of the time. Therefore, the decision of whether SSBA should be employed in a series DC collection system is based on the comparison between the investment on batteries and the economic loss in terms of power output without them. To reduce construction cost, in this section, the power reference of each wind power unit is modified to balance the unit voltages in a series DC collection system. This proposed strategy is termed as Power Reference Modification (PRM) in this thesis. With PRM, the output power of wind power units might not follow MPPT, but still will remain close to MPPT due to small wind speed differences within an offshore wind farm.

4.3.1. OPERATION PRINCIPLE OF POWER REFERENCE MODIFICATION

As mentioned in Subsection 4.2.1, the power references of a number of n wind power units under MPPT in a series DC collection system are denoted by P_{1ref}, P_{2ref}, …, P_{nref}. These are then arranged in the sequence from the lowest power output to the highest power output as per

$$P_{1re} \le P_{2re} \le \cdots \le P_{nre} \tag{4.12}$$

It is to be noted that $P_{ire} \neq P_{iref}$, $i = 1, \ldots, n$. For example, consider a wind farm with only 5 units. Then, at a particular instant, the MPPT references and their ordered sequence are listed in Table 4.1.

Table 4.1: MPPT power references and their ordered sequence.

	Unit-1	**Unit-2**	**Unit-3**	**Unit-4**	**Unit-5**
MPPT reference identifiers and their values in per unit	P_{1ref}	P_{2ref}	P_{3ref}	P_{4ref}	P_{5ref}
	0.98	0.93	1.02	1.0	1.02
Ordered sequence identifiers	P_{2re}	P_{1re}	P_{4re}	P_{3re}	P_{5re}

Three distinct modes are possible. These are discussed below.

A. Mode-1: Normal Mode:

In this mode, the wind speeds to each turbine in a wind farm vary within a small range such that (4.7) is satisfied. This means that the specified range of (4.4) is not violated. Therefore, the MPPT references need not be modified.

B. Mode-2: Undervoltage and Possible Overvoltage:

This mode is invoked when the MPPT references of some of the wind turbines are below 0.9 times the power average, while some of the wind turbines may have their MPPT references above 1.1 times the power average. Note that this is an undervoltage condition and the overvoltage is not a necessary condition to invoke this mode. The MPPT average value at the beginning of the process is computed as

$$P_{av} = (P_{1re} + P_{2re} + \cdots + P_{nre}) \Big/ n \tag{4.13}$$

The biggest MPPT reference values are systematically reduced till the smallest MPPT reference value reaches 0.9 times the resulting average value. Assume that the MPPT reference P_{1re} is below 0.9 times the MPPT average P_{av}. A new average value ($P^{(1)}_{av}$) is now formed, which is equal to P_{1re} divided by 0.9. The step-by-step process for undervoltage solution is given below.

Step-1: A reduction in the average value needs a reduction in the largest MPPT value. Hence

$$\begin{cases} P^{(1)}_{av} = P_{1re}/0.9 \\ P^{(1)}_{mx} = n \times P^{(1)}_{av} - (P_{1re} + P_{2re} + \cdots + P_{(n-1)re}) \end{cases} \tag{4.14}$$

where $P^{(1)}_{mx}$ is the new value of the biggest power reference P_{nre}. We now check the following

$$P^{(1)}_{mx} \geq P_{(n-1)re} \tag{4.15}$$

If this is correct, the process is terminated. Otherwise, go to step-2.

Step-2: Reduce the two biggest values of the MPPT references – P_{nre} and $P_{(n-1)re}$. The resulting equation is

$$2\times P_{mx}^{(2)} = n\times P_{av}^{(1)} - (P_{1re} + P_{2re} + \cdots + P_{(n-2)re}) \tag{4.16}$$

We now check the following

$$P_{mx}^{(2)} \geq P_{(n-2)re} \tag{4.17}$$

If this is correct, the process is terminated. Otherwise, the process is repeated where the three largest values of P_{nre}, $P_{(n\text{-}1)re}$ and $P_{(n\text{-}2)re}$ are reduced. In this manner, the largest MPPT values are reduced till all the MPPT references are equal to or above the lower limit of 0.9 times the total average value. This method ensures that the power curtailment is kept at a minimum for all the wind turbines. After the under voltage solution process, we now check

$$P_{mx\_new} \leq 1.1P_{av}^{(1)} \tag{4.18}$$

where P_{mx_new} is the resulting maximum power. If this is correct, the process is terminated. Otherwise, Mode-3 is evoked and the process is given below.

C. Mode-3: Overvoltage:

In this mode, some of the wind turbines produce significantly more power than the others. This will cause overvoltage in these turbines. It has been assumed that all the MPPT references are above or equal to $0.9P_{av}$, but some of them are bigger than $1.1P_{av}$. A sequence of average values are then computed, taking 2 of the smallest power outputs, then 3 of the smallest power outputs, and so on, till (n-1) of the smallest power outputs. This sequence is given by

$$\begin{cases} P_{av2} = (P_{1re} + P_{2re})/2 \\ P_{av3} = (P_{1re} + P_{2re} + P_{3re})/3 \\ \vdots \\ P_{av(n-1)} = (P_{1re} + P_{2re} + \cdots + P_{(n-1)re})/(n-1) \end{cases} \tag{4.19}$$

The step-by-step procedure of power reference modification is then given below.

Step-1: Reduce the biggest value of the MPPT reference P_{nre} such that this becomes equal to 1.1 times the new average value $P^{(1)}_{av}$. This average is then given by

$$P_{nre}^{(1)} = 1.1 \times P_{av}^{(1)}$$
$$\Rightarrow n \times P_{av}^{(1)} = 1.1 \times P_{av}^{(1)} + (P_{1re} + P_{2re} + \cdots + P_{(n-1)re}) \quad (4.20)$$

Note that $P^{(1)}_{av}$ will be smaller than P_{av} of (4.13). We now check the following

$$P_{av}^{(1)} \geq P_{av(n-1)} \quad (4.21)$$

If this is correct, the process is terminated. Otherwise, it is implied that $P_{(n\text{-}1)re}$ now has a value which is larger than $P^{(1)}_{nre}$. Then, go to step-2.

Step-2: Reduce the two biggest values of the MPPT references – P_{nre} and $P_{(n\text{-}1)re}$, such that they are now equal to 1.1 times the new average value $P^{(2)}_{av}$. This average is then given by

$$P_{nre}^{(2)} = P_{(n-1)re}^{(2)} = 1.1 \times P_{av}^{(2)}$$
$$\Rightarrow n \times P_{av}^{(2)} = 2 \times 1.1 \times P_{av}^{(2)} + (P_{1re} + P_{2re} + \cdots + P_{(n-2)re}) \quad (4.22)$$

We now check the following

$$P_{av}^{(2)} \geq P_{av(n-2)} \quad (4.23)$$

If this is correct, the process is terminated. Otherwise, the process is repeated where the three largest values of P_{nre}, $P_{(n\text{-}1)re}$ and $P_{(n\text{-}2)re}$ are reduced. In this manner, the largest MPPT values are reduced till all the MPPT references are within a small variation range of ±10% of the total average value. The resulting new power average is assumed to be P_{av_new}. Also note that through this method, the power curtailment is kept at a minimum for all the wind turbines.

Through the modifications mentioned above, the original MPPT references P_{1ref}, P_{2ref}, …, P_{nref} are modified to P_{1rm}, P_{2rm}, …, P_{nrm}, respectively. These are called PRM references, where PRM stands for power reference modification. Let the biggest PRM references of all the three modes be denoted by P_{md}. Then, for the three different modes, we have

- Mode-1: $P_{nre} = P_{md}$
- Mode-2: $P_{md} = P_{mx\_new}$
- Mode-3: $P_{md} = 1.1 P_{av\_new}$

The PRM references for all the wind power units can be determined using P_{md}. Taking unit-*i* as an example, its PRM reference is given as:

$$P_{irm} = \begin{cases} P_{iref} & P_{iref} \le P_{md} \\ P_{md} & P_{iref} > P_{md} \end{cases} \tag{4.24}$$

4.3.2. SIMULATION STUDIES

To verify the effectiveness of the proposed PRM strategy, simulation studies with a series DC collection system incorporating 6 wind power units are conducted in PSACD. Ideal power sources are employed to reduce the simulation burden with the large number of wind turbines. The equation of each unit equivalent model is given by

$$P_i = V_i \cdot I \tag{4.25}$$

where P_i and V_i are respectively the power output and DC voltage of the *i*th unit, and I is the DC current. The GSC input voltage reference is set as 45 kV as per (4.1), where the DC side voltage of each wind side converter is assumed to be 7.5 kV. The line-to-line RMS voltage at the grid side is chosen as 24 kV. With the voltage limits given in (4.11), there are three areas that the DC voltages of the wind power units might fall in, as shown in Fig. 4.8. In this, areas *A*, *B* and *C* of the axis represent DC voltages below the lower limit (6.75 kV), within the defined range and above the upper limit (8.25 kV) respectively.

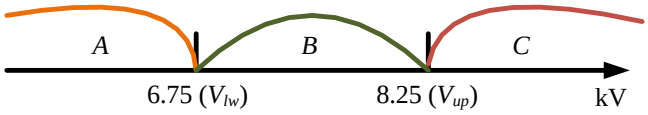

Fig. 4.8. Area division of voltage levels.

To include all the voltage distribution possibilities, four conditions are tested depending on the DC voltages of the six wind power units:

- *Case-AB*: the voltages are in areas *A* and *B*;
- *Case-ABC*: the voltages are in all three areas;
- *Case-B*: all the voltages are in area *B*;
- *Case-BC*: the voltages are in areas *B* and *C*.

It is noted that as the wind speed differences between adjacent turbines are very small, *Case-AC* is not possible and thus not considered here. The applied MPPT power references for each case are listed in Table 4.2. In this, the calculated voltages (MPPT voltages) based on VDP are also listed and the voltages out of range are marked in red. The simulation results in each case are shown in Figs. 4.9 to 4.12, where P_{minr} and P_{maxr} are the PRM limits. It has been assumed that the average value of the PRM references is denoted by P_{av_new}, then $P_{minr} = 0.9P_{av\_new}$ and $P_{maxr} = 1.1P_{av\_new}$.

Table 4.2: MPPT power references and DC voltages.

MPPT References		**Unit-1**	**Unit-2**	**Unit-3**	**Unit-4**	**Unit-5**	**Unit-6**
Case-AB	MW	2.0	2.5	2.6	2.65	2.45	2.55
	kV	6.10	7.63	7.93	8.08	7.47	7.78
Case-ABC	MW	2.45	2.8	2.0	2.55	2.6	2.5
	kV	7.40	8.46	6.04	7.70	7.85	7.55
Case-B	MW	2.55	2.45	2.6	2.7	2.5	2.65
	kV	7.43	7.14	7.57	7.86	7.28	7.72
Case-BC	MW	2.5	2.55	2.45	3.0	2.65	2.6
	kV	7.14	7.29	7.0	8.57	7.57	7.43

Case-AB: At the beginning, the MPPT references are sorted in an increasing manner, as shown in Fig. 4.9 (a). This shows that all the MPPT references except for P_{1re} are within the power limits ($P_{\min}$ and $P_{\max}$). This value of P_{1re} results in a low voltage that is below 6.75 kV (U_{lw}), as marked in Table 4.2. The power reference modification method is now applied, by which the power references of unit-2 to unit-6 are decreased to a same value of around 2.27 MW, as shown in Fig. 4.9 (b). Since P_{md} in this case is smaller than P_{maxr}, the value of P_{md} is calculated from

$$\begin{cases} P_{av\_new} = \dfrac{P_{1re}}{0.9} \\ 6 \times P_{av\_new} = 5 \times P_{md} + P_{1re} \end{cases} \tag{4.26}$$

Fig. 4.9 (b) also shows that all the PRM references are within their limits (P_{minr} and P_{maxr}), as a result of which, all the six unit DC voltages after PRM (PRM voltages) are limited between V_{lw} and V_{up} (Fig. 4.9 (c)). It is also to be noted from Fig. 4.9 (c) that the GSC input voltage V_T (HVDC transmission voltage) is kept constant at 45 kV. This value V_T is obtained for all the three other cases as well. Therefore, for a better visibility, the waveform of V_T is only plotted for this case.

Case-ABC: Just as the previous case, the MPPT references are sorted in an increasing manner, as shown in Fig. 4.10 (a), which shows that P_{6re} is over $P_{\max}$, while P_{1re} is below $P_{\min}$. This implies that the voltages of two units are outside the specified range (Table 4.2). The PRM method is applied now. It can be seen from Fig. 4.10 (b) that apart from unit-3, all the other 5 MPPT references become equal to the value of P_{md}. This case has the same PRM references as in *Case-AB*, which brings the same satisfactory PRM voltage values, shown in Fig. 4.10 (c). The calculation equation for P_{md} is thus the same as (4.26).

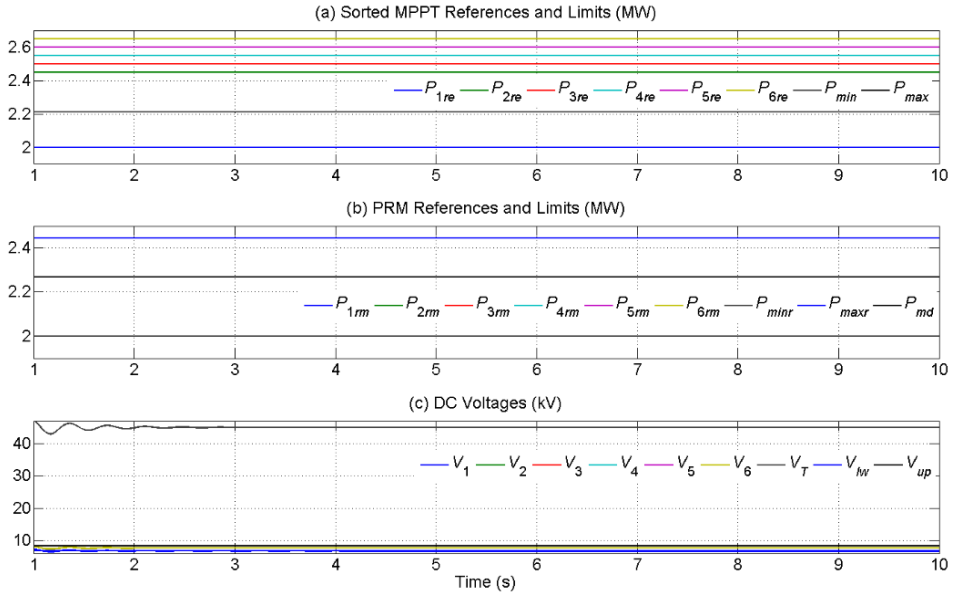

Fig. 4.9. Simulation results of *Case-AB*.

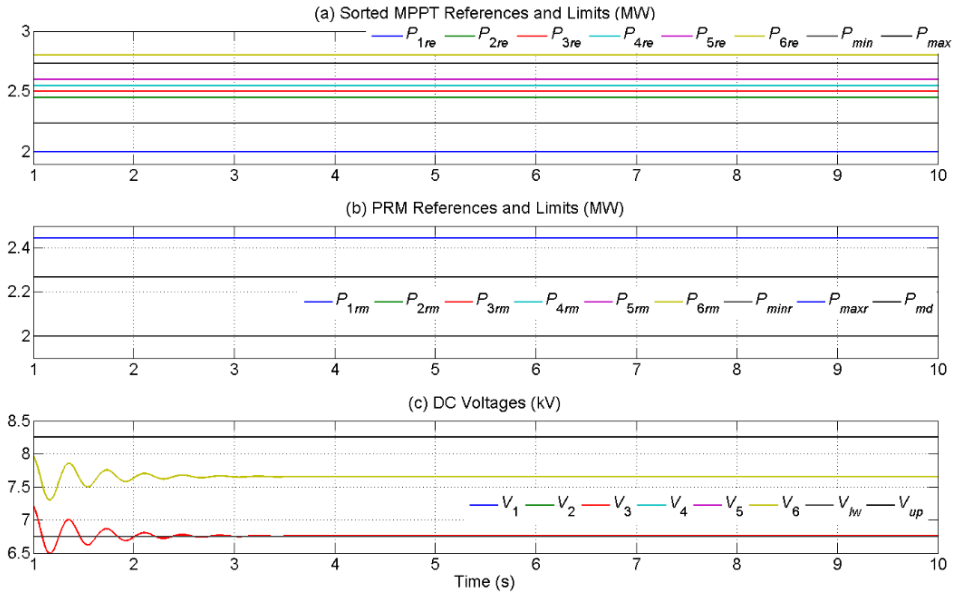

Fig. 4.10. Simulation results of *Case-ABC*.

Case-B: As shown in Fig. 4.11 (a), all the six sorted MPPT references are within the range of $P_{\min}$ to $P_{\max}$. Therefore, the PRM references (Fig. 4.11 (b)) do not change from their MPPT references (Table 4.2). It can be seen from Fig. 4.11 (b) that P_{md} is equal to the biggest power reference (P_{6re} or P_{4rm}) as per its definition. The DC voltages of each wind power unit plotted in Fig. 4.11 (c) are all within the safe area, which is in accordance to Table 4.2.

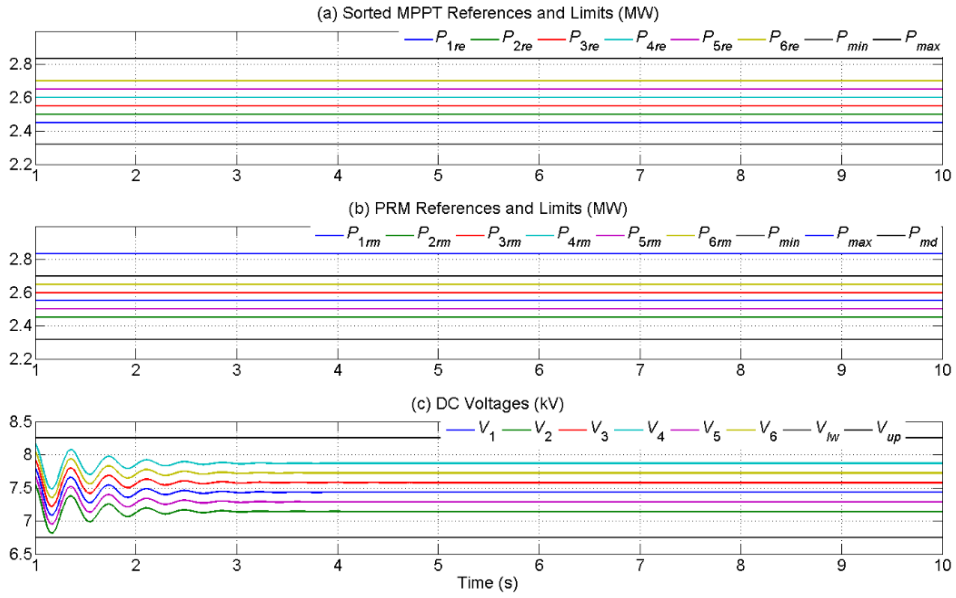

Fig. 4.11. Simulation results of *Case-B*.

Case-BC: Fig. 4.12 (a) illustrates the overvoltage mode, where the biggest MPPT reference (P_{6re}) is above the upper limit ($P_{\max}$). Table 4.2 shows the overvoltage occurs to unit-4. It can be seen from Fig. 4.12 (b) that P_{4ref} decreases to $P_{4rm} = P_{md}$ (approximately 2.86 MW), which is equal to the PRM upper limit (P_{maxr}), while other MPPT references remain the same. Therefore, the calculation equation to obtain P_{md} is

$$\begin{cases} 6\times P_{av\_new} = 1.1\times P_{av\_new} + (P_{1re} + P_{2re} + P_{3re} + P_{4re} + P_{5re}) \\ P_{md} = 1.1\times P_{av\_new} \end{cases} \tag{4.27}$$

It is clear from Fig. 4.12 (c) that the DC voltage of unit-4 is reduced to the upper limit (V_{up}) and all the other voltages are within the specified range. The four cases simulated above cover all the possible voltage deviation types and therefore validate the effectiveness of the proposed PRM strategy for series DC collection systems of offshore wind farms.

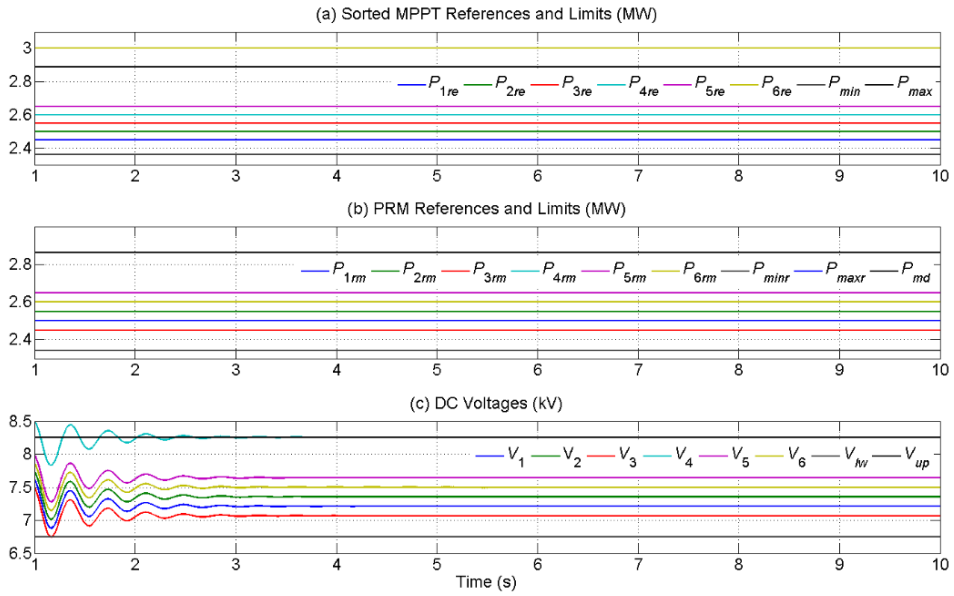

Fig. 4.12. Simulation results of *Case-BC*.

4.4. POWER REFERENCE MODIFICATION APPLICATION

In this section, the proposed power reference modification method is applied in a series DC collection system with detailed unit models and varied wind speeds. The most direct way to withdraw wind power according to PRM references (instead of MPPT references) is to modify the power references in the pitch control of each wind turbine. However, large wind turbines are normally designed to capture the maximum energy from wind by its pitch control mechanism. To keep the uniformity of the pitch control systems, chopping resistors [108-111] are employed to absorb the excess power from wind generators. The power dissipations of each chopping resistor for each unit are dependent on their respective PRM references. The employed method is termed as the strategy of PRM with chopping resistors (PRM-CR). An alternate strategy is also employed simply by modifying the pitch control mechanism. This is called PRM-PCM in this thesis.

4.4.1. PRM-CR STRATEGY

Based on the proposed PRM method, a number of wind power units in a series DC collection system might need to decrease their power outputs to limit the voltages on their DC sides. Therefore, the power from a WSC might be smaller than that from its connected wind generator. This power difference is balanced by dissipating excess power through a chopping resistor. The configuration of a series DC collection system

with chopping resistors is similar to Fig. 4.5 except that the power sink in each unit is replaced with a variable resistor.

Let the power dissipated on each resistor be denoted by P_{Ri} (i = 1, 2, …, n), then

$$P_{Ri} = P_{iref} - P_{irm} \tag{4.28}$$

Therefore, the value of each variable chopping resistor per phase is calculated as

$$R = \frac{(\frac{V_{LL}}{\sqrt{3}})^2}{\frac{P_R}{3}} = \frac{V_{LL}^2}{P_R} \tag{4.29}$$

where V_{LL} is the AC line-to-line RMS voltage at the wind generator terminal, R is the chopping resistor value (here the subscript i is omitted for convenience). It is obvious that the chopping resistor must be variable as wind power references are not constant with varied wind speeds. The MPPT control of a series DC collection system with PRM-CR is the same as when SSBA is employed. It is noted that the power references for the angle control of WSCs are modified to P_{irm}.

The series DC collection model without SSBA in Section 4.2 is applied in this subsection to validate the effectiveness of the proposed PRM-CR strategy. The simulation results without and with PRM-CR are shown in Figs. 4.13 and 4.14 respectively. Same patterns of wind speeds are applied on the two conditions, which are plotted in Fig. 4.13 (a). It can be seen that v_{w1}, v_{w2}, v_{w3} increase from 8 s, 9 s, 10 s and settle at 13 m/s ,13 m/s, 15 m/s after 2 s, 1 s, 2 s respectively, while v_{w4} drops from 12 m/s to 11 m/s between 10 s and 11 s. The MPPT references (Fig. 4.13 (b)) ramp up or down following their respective wind speeds except that they do not increase when their corresponding wind speeds exceed the rated speed of 12 m/s. It can be seen by comparing Figs. 4.13 (b) and 4.13 (c) that the power outputs of each unit coincide with their references barring fluctuations during the changes in wind speeds. It is clear that the steady-state DC voltage of unit-4 (V_4) is above the upper limit (V_{up}) before v_{w4} decreases and below the lower limit (V_{lw}) after the change in v_{w4}. The DC voltages of other units are within the two limits in all steady states and the total voltage is kept constant by the GSC with negligible fluctuations.

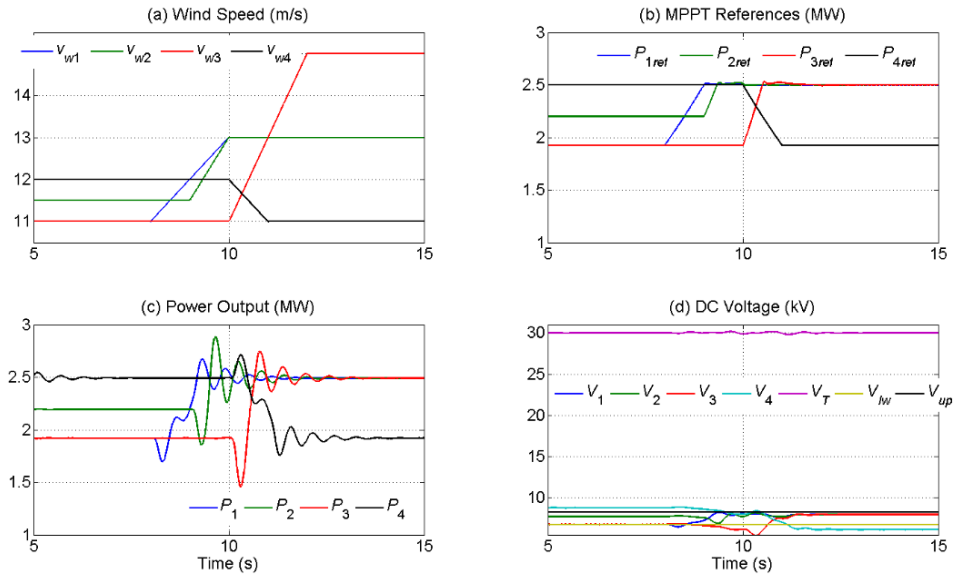

Fig. 4.13. Simulation results of a series DC collection system without voltage control strategy.

The modified power references by applying PRM are shown in Fig. 4.14 (a). It can be seen that P_{1rm} does not change from P_{1ref} before v_{w1} increases but becomes smaller than P_{1ref} after v_{w1} ramps up. P_{2rm} and P_{3rm} have similar changes with P_{1rm}, while P_{4rm} is smaller than P_{4ref} at the initial state and equal to P_{4ref} after the reducing of v_{w4}. The steady-state MPPT and PRM references before and after wind speed changes are listed in Table 4.3. It is indicated in Table 4.3 that, before any change in the four wind speeds, only unit-4 decreases its power output to control V_4 at V_{up}. When the wind speeds attain a new steady state, unit-1, unit-2 and unit-3 reduce their power outputs to bring V_4 back to V_{lw}.

Table 4.3: MPPT and PRM references (approximate values).

Units	**Unit-1**		**Unit-2**		**Unit-3**		**Unit-4**	
Wind Speed	Before change	After change	Before change	After change	Before change	After change	Before change	After change
MPPT References (MW)	1.93	2.50	2.20	2.50	1.93	2.50	2.50	1.93
PRM References (MW)	1.93	2.21	2.20	2.21	1.93	2.21	2.30	1.93

It can also be seen in Fig. 4.14 (a) that during wind speed variations, the PRM references change in opposite directions against each other to achieve small power output differences among the four units. Fig. 4.14 (b) shows the four power outputs, which are in accordance with their respective PRM references except for fluctuations

during the changes in wind speeds. As shown in Fig. 4.14 (c), it is obvious that all the DC voltages are within the specified range at steady states. V_4 is lowered at V_{up} before v_{w4} changes and is raised to V_{lw} after v_{w4} decreases. Same as in Fig. 4.13 (d), the transmission voltage here is kept at its reference value by the GSC. Fig. 4.14 (d) shows the power dissipated by the chopping resistors. By referring to Table 4.3, it can be seen that the steady-state power consumed by each resistor is equal to the difference between MPPT and PRM references all along. This conclusion applies to wind speed changing durations, which can be seen by comparing Figs. 4.13 (b) and 4.14 (a).

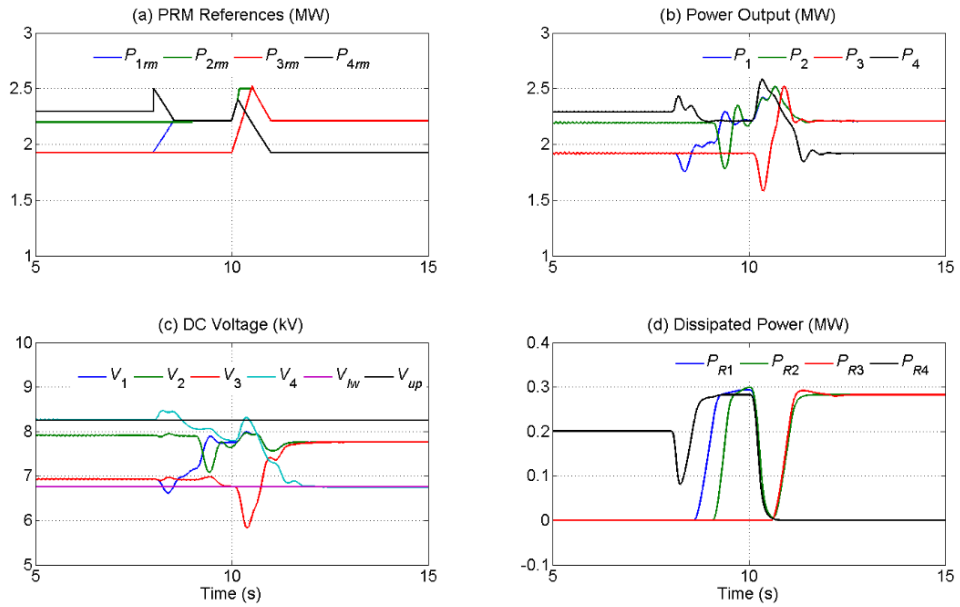

Fig. 4.14. Simulation results of a series DC collection system with PRM and chopping resistors.

4.4.2. PRM-PCM STRATEGY

The PRM method requires equal or less power to the WSCs than their respective MPPT references. Apart from dissipating the excess generator power, corresponding PMSGs can be controlled to generate less power by adjusting the pitch angles of the turbines blades. The pitch control system depicted in Fig. 2.1 of Chapter 2 uses the power difference between the reference and measured power as the input signal. To extract the maximum power from wind energy, the power reference is obtained from MPPT control. However, this reference value is modified to the PRM reference to reduce wind power extraction, when required. The new pitch control diagram is shown in Fig. 4.15, where P and P_{rm} respectively are the measured

power and PRM reference for a certain wind power unit. It is noted that the power loss from the wind turbine to the wind generator is assumed to be negligible.

In the PRM method, the PRM references are obtained based on their respective MPPT references. As opposed to the PRM-CR strategy, in which MPPT references can be measured, the MPPT control is not even used here. In fact, for a given wind turbine, the maximum power versus wind speed curve is provided by the manufacturer [20]. Therefore, in a real-life situation, the MPPT references are available according to the given MPPT profile [112]. As for the wind turbine employed in this thesis, the MPPT profile is drawn by simulating a WECS in PSCAD, where small steps of wind speed increment are used to approach a continuous wind speed curve from 0 to 15 m/s. The power profile of the wind turbine is shown in Fig. 4.16. It can be seen that the cut-in speed is approximately 2 m/s and the rated wind speed is 12 m/s as mentioned previously. Based on this curve, the MPPT reference at any given wind speed is obtained and the PRM method can thus be employed.

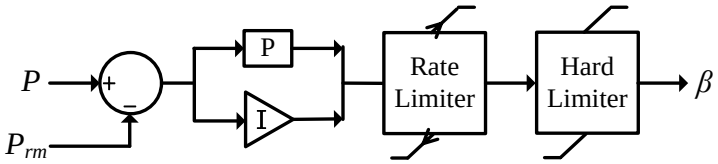

Fig. 4.15. Schematic diagram of the modified pitch control.

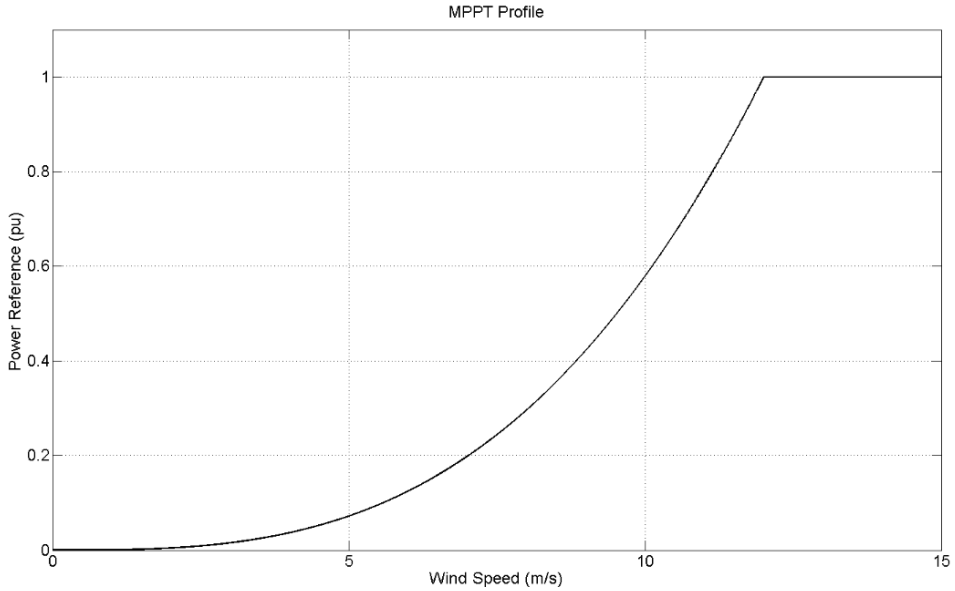

Fig. 4.16. MPPT profile of the wind turbine.

The simulation model of the series DC collection system used in the previous subsection is also employed here to study the effectiveness of PRM-PCM. The simulation results are shown in Fig. 4.17. Constant wind speeds of 11 m/s, 11.2 m/s and 11.8 m/s are given to the turbines of unit-1, unit-2 and unit-3 respectively, while v_{w4} decreases from the rated wind speed of 12 m/s to 11.5 m/s between 8 s and 9 s as plotted in Fig. 4.17 (a). The MPPT references and power outputs of the four units are shown in Fig. 4.17 (b). It can be seen that before v_{w4} changes, the power outputs of unit-3 and unit-4 are smaller than their MPPT references, while unit-1 and unit-2 have power outputs equal to their respective MPPT references. After the change in v_{w4}, only unit-3 has a power smaller than its MPPT reference (P_{3ref}) and the power outputs of other units are equal to their respective MPPT values. All these power values are summarized in Table 4.4.

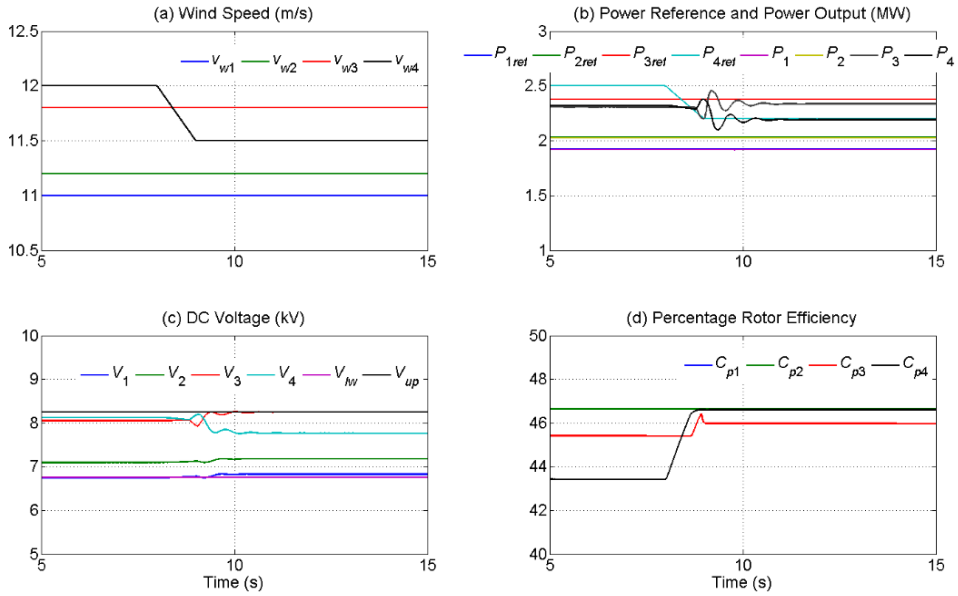

Fig. 4.17. Simulation results of a series DC collection system with PRM and pitch control modification.

Table 4.4: MPPT references and power outputs (approximate values).

Units	**Unit-1**		**Unit-2**		**Unit-3**		**Unit-4**	
Wind Speed	Before change	After change	Before change	After change	Before change	After change	Before change	After change
MPPT References (MW)	1.93	1.93	2.03	2.03	2.38	2.38	2.50	2.20
Power Output (MW)	1.93	1.93	2.03	2.03	2.30	2.33	2.30	2.20

The DC voltages of each wind power unit are shown in Fig. 4.17 (c), where it can be seen that before the change in v_{w4}, V_1 is controlled at the lower limit (V_{lw}) and the other voltages are within the specified range. This is achieved by the reduced power outputs of unit-3 and unit-4. Similarly, after the change in the wind speed, V_3 is controlled at the upper limit (V_{up}) resulting from the decreased power output of unit-3 and the other voltages are between V_{lw} and V_{up}. The rotor efficiencies of each wind turbine are shown in Fig. 4.17 (d). It can be seen that C_{p1} and C_{p2} are always at the rated value of 46.64% (mentioned in Subsection 2.2.4 of Chapter 2) since the power outputs of unit-1 and unit-2 are equal to their MPPT references. For the same reason, C_{p4} reaches to the rated efficiency after the change in v_{w4}. However, before v_{w4} ramps up, the turbines of unit-3 and unit-4 operate at lower rotor efficiencies (45.41% and 43.43% respectively) as their power outputs are smaller than the respective MPPT references. C_{p3} becomes higher after the change in v_{w4} but still remains below the rated value. It is also noted that for a specific wind turbine, the bigger the difference between the MPPT reference and real power output is, the lower the rotor efficiency is. Therefore, even though the PRM-PCM strategy for series DC collection systems does not require any additional device, it results in lower rotor efficiencies, which is expected.

For the DC voltage balancing among the wind power units in a series DC collection system, both SSBA and PRM can achieve the control target. SSBA is obviously more expensive than PRM, since this method requires small batteries and power converters. But PRM results in lower power output of a wind farm as some power is consumed by chopping resistors or the pitch angles of some wind turbines are adjusted to withdraw less wind energy than they actually can. Therefore, the selection of these two strategies should mainly consider the extra cost of SSBA against the power loss by employing PRM. Both factors are related to the wind speed distribution within an offshore wind farm.

4.5. CONCLUSIONS

This chapter focuses on the proposed series DC collection system for offshore wind farms. Different collection topologies are discussed and the advantages of the proposed system are presented. The DC voltage control of wind power units in a series DC collection system is based on the voltage distribution principle, which

transforms the voltage control problem to power control. First, a small sized battery is applied between each wind generator and its WSC. By balancing the power from each WSC through SSBA, the DC voltages of the wind power units are restricted within the predefined range. A second strategy is proposed for voltage limitation, where the power references for the angle control of some WSCs are reduced from the previous references obtained by MPPT. In this way, the average power output among units in a series DC collection system is decreased to a lower value but all unit power outputs are within a small range around this average power. The DC voltages are thus limited to the allowable range due to VDP. Chopping resistors are employed to dissipate the extra power that does not convert by WSCs. Alternatively, the pitch control system is modified to decrease the generator power according to the new references.

Simulation studies are conducted in PSCAD for series DC collection systems both with and without the proposed strategies. For the power reference modification method, all possible conditions of out-of-range voltages are considered with ideal power sources to show the robustness of this strategy. Detailed WECS models are used for all other simulation studies. The simulation results validate the proposed series DC collection system for offshore wind power and the effectiveness of the proposed voltage control strategies are demonstrated. It is noted that the SSBA strategy is not as economical as PRM, but a series DC collection system has lower power output with PRM. All the systems with control strategies discussed in this chapter are based on the sound operation of all wind power units. The control schemes with wind turbine failures in a series DC collection system will be studied in the next chapter.

CHAPTER 5

SERIES DC COLLECTION SYSTEMS UPON TURBINE FAILURES

The DC side voltages of wind power units in a series DC collection system are sensitive to the operation of wind turbines. It has been discussed in Chapter 4 that the uneven wind speed in an offshore wind farm, which results in power differences among units, might cause out-of-range voltages. According to the voltage distribution principle, if a number of wind power units are bypassed when they fail, overvoltage will probably occur whether the wind speed is even or not. The failure of wind turbines is regarded as the fault condition in this thesis and will be studied in this chapter to ensure the safe operation of series DC collection systems for offshore wind power.

Two voltage control strategies are proposed to prevent the occurrence of overvoltage when such a fault happens. Both strategies allow for a variable HVDC transmission voltage. First, the input DC voltage reference of the Grid-Side Converter (GSC) is modified upon fault. To accommodate the DC voltage range of the GSC, the output AC voltage on the grid side needs to be reset accordingly. For a series DC collection system, where the grid side voltage cannot be flexibly changed, an On Load Tap Changing (OLTC) transformer is employed at the output terminal of the GSC. Therefore, this strategy includes the DC side voltage modification and AC side voltage regulation of the GSC, which is called GSC Adaptation (GA) in this thesis. Second, the original series DC collection system is modified by replacing the single GSC with multiple small sized GSCs. A proper portion of the small GSCs are disconnected upon fault, according to the voltage requirement. This voltage control strategy with the modified series DC collection system is termed as GSC Reconfiguration (GR).

For fault conditions with unevenly varied wind speed in an offshore farm, simulation studies are conducted respectively using the combinations of GA with SSBA and GA with PRM. The effectiveness of GA and GR is validated through various simulation cases in PSCAD.

5.1. DC SIDE VOLTAGE MODIFICATION

For a series DC collection system, if one or more wind turbines get faulty, the usual way is to bypass the corresponding faulty units. However, unlike the undisturbed fault response in parallel DC collection systems discussed in Chapter 3, faulty unit bypass in a series DC collection system will result in the voltage rise of the non-faulty units [26]. This analysis is based on the Voltage Distribution Principle (VDP). Overvoltage might or might not occur depending on the characteristics of the specific series DC collection system. In this section, the influence of a fault on the DC voltages of wind power units in a series DC collection system is studied. As stated earlier, there are two control aspects of the proposed GSC Adaptation (GA) strategy. Out of these, the DC side voltage modification of the GSC, is discussed in this section.

5.1.1. VOLTAGE RESPONSE OF A SERIES DC COLLECTION SYSTEM UPON FAULT

As per Chapter 4, the DC voltage of the wind power unit-i in a series DC collection system are denoted by V_i (i = 1, 2, …, n). With similar power outputs of turbines within an offshore wind farm, a rough estimation can be made by assuming

$$V_1 = V_2 = \cdots = V_n = V_N = \frac{V_T}{n} \tag{5.1}$$

When one unit is bypassed, the DC voltage for the non-faulty units (denoted by V_i') will rise to

$$V_1' = V_2' = \cdots = V_n' = \frac{V_T}{n-1} \tag{5.2}$$

As the upper voltage limit is set as $1.1 \times V_N$, the following restriction must be satisfied if no extra voltage control strategy is applied.

$$\frac{V_T}{n-1} \le 1.1 \times V_N \tag{5.3}$$

Combining (5.1) with (5.3), we get

$$n \ge 11 \tag{5.4}$$

Equation (5.4) indicates that at least 11 wind turbines need to be included in a series DC collection system to avoid overvoltage in case 1 unit is bypassed. Similarly, suppose the maximum turbines being faulty simultaneously is *y*. Then we have

$$n \geq 11y \tag{5.5}$$

It is implied by (5.5) that the more units a series DC collection system contains, the stronger it is in fault tolerance. In some small wind farms, however, wind turbine quantities are not big enough to limit serious voltage rising. To deal with this situation, the GSC Input Voltage Reference Modification (IVRM) method is proposed and discussed in the next subsection.

5.1.2. GSC INPUT VOLTAGE REFERENCE MODIFICATION

To suit the non-ideal condition, where the DC voltages for each unit are not all the same, the DC side voltage of the GSC is modified upon fault. If turbines of unit-(n - y + 1) to unit-n are faulty at the same time, the operating unit number will be (n - y) after bypassing the faulty units. Suppose unit-k is found to have the biggest power output among the (n - y) non-faulty units, then it has the highest DC voltage after fault. The voltage relationships before and after fault are given in (5.6) and (5.7) respectively.

$$V_1 + V_2 + \cdots + V_k + \cdots + V_n = V_T \tag{5.6}$$

$$V_1' + V_2' + \cdots + V_k' + \cdots + V_{n-y}' = V_T \tag{5.7}$$

As indicated in the last subsection, V_1', V_2', …, V_k', …, $V_{n\text{-}y}'$ are the DC voltages of unit-1 to unit-(n - y) after fault. The VDP among units does not change after fault. Since V_k' is the biggest among V_1' to $V_{n\text{-}y}'$, as long as V_k' is controlled equal to or smaller than V_{up}, the DC voltages for other non-faulty units will be below V_{up}, which has been defined as 1.1 times the rated voltage V_N in Chapter 4. If V_k' is bigger than V_{up}, the transmission voltage reference is modified as described below.

Assume the DC voltage of unit-k is limited at V_{up} by modifying V_T to V_T''. Let the voltage values of the non-faulty units after the modification be denoted by V_1'', V_2'', …, V_k'', …, $V_{n\text{-}y}''$. Based on VDP, a quantity named DC Voltage Decrease Ratio (DVDR) is

defined as each voltage without modification divided by its corresponding voltage after modification. Suppose DVDR is denoted by r_d ($r_d > 1$), then

$$r_d = \frac{V_1'}{V_1''} = \frac{V_2'}{V_2''} = \cdots = \frac{V_k'}{V_k''} = \cdots = \frac{V_{n-y}'}{V_{n-y}''} = \frac{V_T}{V_T''} \tag{5.8}$$

As $V_k'' = V_{up} = 1.1V_N$, the modified transmission voltage reference is expressed in (5.9) according to (5.8).

$$V_T'' = \frac{1.1 \times V_N}{V_k'} \times V_T \tag{5.9}$$

Since V_k changes to V_k'' directly following IVRM, V_k' is just a suppositional value. Given that it does not exist in the real system, V_k' cannot be measured. However, V_k' can be calculated based on the measured power as the power outputs from the non-faulty units do not get affected because of the fault. Suppose V_T is not modified after the fault happens, then V_k' is obtained as in (5.10) according to VDP.

$$V_k' = \frac{P_k}{P_1 + P_2 + \cdots + P_k + \cdots + P_{n-y}} \times V_T \tag{5.10}$$

The modified reference value for the IVRM method is therefore obtained by combining (5.9) with (5.10), which is

$$V_T'' = \frac{P_1 + P_2 + \cdots + P_k + \cdots + P_{n-y}}{P_k} \times 1.1 \times V_N \tag{5.11}$$

By reducing the transmission voltage reference according to (5.11), serious overvoltage under fault conditions can be prevented.

5.2. AC SIDE VOLTAGE REGULATION

As discussed in Chapter 4, the DC side voltage of a VSC under SPWM control must be at least 1.633 times the AC side line-to-line RMS voltage to avoid signal tracking failure. To meet this requirement, with IVRM employed, the AC voltage at the receiving end needs to be regulated to a relatively lower value. In this section, two schemes are presented for the GSC output AC side voltage regulation – (1) through nominal AC voltage reset and (2) by employing an OLTC transformer.

5.2.1. AC SIDE VOLTAGE RESET

Suppose the rated voltage input of the WSC and output of the GSC are denoted by V_w and V_g respectively, which are both line-to-line RMS values. Following the same voltage reference determination pattern of the WSC, V_g is set as

$$V_g = V_w \times n \tag{5.12}$$

However, with the decrease of V_T when IVRM is applied, tracking failure of the GSC control might happen if V_g remains the same.

To suit the demand due to IVRM, the output voltage reference of the GSC is reset at a relatively low value and represented by V_g'' as

$$V_g'' = r_a \times V_g \tag{5.13}$$

where r_a ($0 < r_a < 1$) is termed as the AC Voltage Decrease Ratio (AVDR). In this way, the GSC operates at a smaller SPWM modulation index than WSCs operating under normal condition. In the case of IVRM being applied, it is obtained based on VDP that, the transmission voltage reference will be decreased most when all units' power outputs are equal. According to (5.11), it is calculated as

$$V_T'' = 1.1 \times (n - y) \times V_N \tag{5.14}$$

As per (4.2) of Chapter 4, the input and output voltages of the WSC and the GSC have the following relationships.

$$V_w = \frac{\sqrt{3}}{2\sqrt{2}} \times k_w \times V_N \tag{5.15}$$

$$V_g'' = \frac{\sqrt{3}}{2\sqrt{2}} \times k_g \times V_T'' \tag{5.16}$$

where k_w and k_g are the modulation indices of the WSC and the GSC respectively. Therefore, the AVDR is obtained by combing (5.12) to (5.16) as

$$r_a = \frac{1.1 \times (n - y)}{n} \times \frac{k_g}{k_w} \tag{5.17}$$

For a better utilization of the GSC, a relatively big value of V_g'' is preferred. Therefore, the biggest AVDR is selected with k_g = 1. The reset voltage reference of the GSC output is thus

$$V_g'' = \frac{1.1\times(n-y)}{n\times k_w}\times V_g = \frac{1.1\times(n-y)}{n}\times\frac{n\times V_w}{k_w} = 1.1\times(n-y)\times\frac{\sqrt{3}}{2\sqrt{2}}\times V_N \qquad (5.18)$$

It is to be noted that with k_g assumed to be 1, V_g'' calculated from (5.18) is not always smaller than V_g. If $V_g'' \geq V_g$, it implies that the overvoltage is not serious enough to cause tracking failure. In this case, the GSC output voltage reference obtained by (5.12) remains unchanged. Only when $V_g'' < V_g$, this reference is reset as V_g''.

5.2.2. EMPLOYING AN OLTC TRANSFORMER

An alternative strategy to prevent tracking failure that might result from IVRM is formulated by using an On Load Tap Changing (OLTC) transformer between the GSC and the gird. This is shown in Fig. 5.1, where the rated AC line-to-line RMS voltages before and after the OLTC transformer are represented by V_{g1} and V_{g2} respectively. The transformer windings on the GSC side and the grid side are respectively denoted by winding-1 and winding-2. Here the tap changer is assumed to be installed in winding-1 of the transformer. As the grid has its specific nominal voltage, the OLTC is set to alter the transformer turns-ratio in such a way that the GSC output voltage is lowered following IVRM, while the gird voltage is kept constant at V_{g2}.

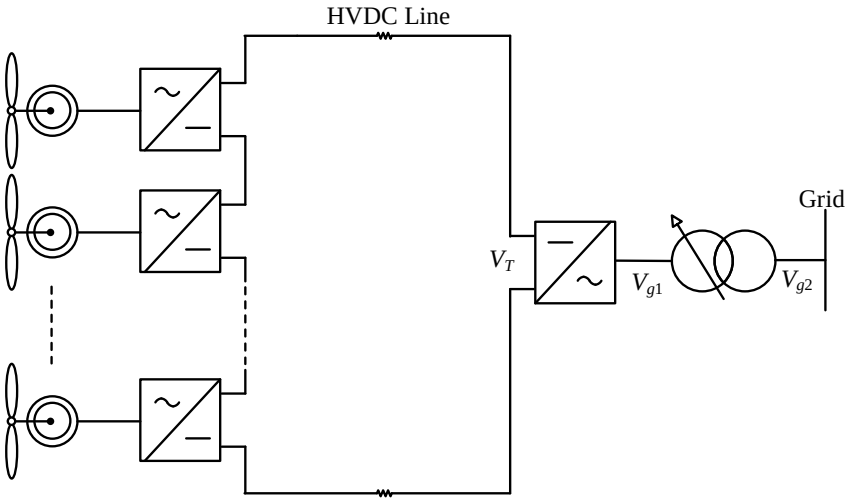

Fig. 5.1. Configuration of a series DC collection system with an OLTC transformer.

Standard tap changers offer the change of ±10% of the rated voltage [113]. Suppose the turns-ratio of the OLTC transformer without tap adjustment is $1:\eta$, then the adjustable range is $0.9:\eta$ to $1.1:\eta$. To make full use of this turns-ratio range, a tap ratio of 1.1 for winding-1 is chosen for the normal operating condition. This accommodates for the maximum possible drop in the winding-1 voltage due to removal of faulty wind turbines. Therefore, the relationship between the winding voltages under nominal condition is given by

$$\frac{V_{g1}}{V_{g2}} = \frac{1.1}{\eta} \tag{5.19}$$

To select an appropriate OLTC transformer, the physical parameters that need to be determined include the MVA rating, the rated voltage and adjustable range of the tap winding, the number of tap positions, etc [114-115]. The voltage information of the tap winding (winding-1) is obtained below.

When the tap in winding-1 is at the rated position, the primary side voltage of the transformer is

$$V_{tf1N} = \frac{V_{g1}}{1.1} = 0.909V_{g1} \tag{5.20}$$

where V_{tf1N} is the rated voltage of winding-1. As the lowest turns-ratio that can be reached through tap adjustment is $0.9:\eta$, the lowest voltage of winding-1 is thus

$$V_{tf1\min} = V_{tf1N} \cdot 0.9 = \frac{V_{g1}}{1.1} \cdot 0.9 = 0.818V_{g1} \tag{5.21}$$

where $V_{tf1\min}$ is the lower voltage limit of winding-1. According to reference [113], each step of the tap changer usually represents a change of ±1.25% in the low voltage side. Based on this, the voltage change of each step (V_{tp}) is given by

$$V_{tp} = 1.25\% \cdot V_{tf1N} = 1.25\% \cdot \frac{V_{g1}}{1.1} = 1.136\% \cdot V_{g1} \tag{5.22}$$

With the upper limit of V_{g1} and the lower limit of $V_{tf1\min}$, the adjustable range in the voltage of winding-1(V_{rg}) is obtained by

$$V_{rg} = V_{g1} - V_{tf1\min} = V_{g1} - \frac{V_{g1}}{1.1} \cdot 0.9 = 0.182 V_{g1} \tag{5.23}$$

Therefore, the number of tap positions (n_{tp}) can be calculated through (5.22) and (5.23), as given by

$$n_{tp} = \frac{V_{rg}}{V_{tp}} + 1 = \frac{10\% \cdot V_{tf1n} \cdot 2}{1.25\% \cdot V_{tf1n}} + 1 = 17 \tag{5.24}$$

In this case, it can be concluded from (5.20) to (5.24) that: (1) the rated voltage of winding-1 is $0.909V_{g1}$, (2) the adjustable range is between $0.818V_{g1}$ and V_{g1}, and (3) the number of tap positions is 17. Based on these values and some other required data, the OLTC transformer that accommodates IVRM can be selected.

With the selected OLTC transformer, the tap position upon a certain fault can be determined. Suppose for some instant, the required voltage of winding-1 following IVRM is denoted by $V_{g1}^{''}$ and the expected decrease step number is represented by x, then

$$\frac{V_{g1} - V_{g1}''}{V_{tp}} = x \tag{5.25}$$

$V_{g1}^{''}$ can be obtained based on (5.18) by replacing y with the actual number of faulty units. If the value of x calculated through (5.25) does not match a correct tap setting, the nearest lower voltage tap position will be selected to avoid tracking failure.

Different from the voltage reference reset method, the voltage decrease range by applying an OLTC transformer is limited by its tap positions [116-117]. Assume the lowest modified transmission voltage that the tap changer can match up with is denoted by $V_{T\min}^{''}$, then according to (5.16),

$$V_{tf1\min} = \frac{\sqrt{3}}{2\sqrt{2}} \cdot k_g \cdot V_{T\min}'' \tag{5.26}$$

where $k_g = 1$. Substituting (5.21) into (5.26), $V_{T\min}^{''}$ is calculated to be

$$V_{T\min}'' = 1.336 V_{g1} \tag{5.27}$$

It means that if $V_T^{''}$ in (5.14) is bigger than $V_{T\min}^{''}$ in (5.27), the OLTC transformer is capable of matching up with the IVRM method unconditionally. If $V_T^{''}$ is smaller than $V_{T\min}^{''}$, the effectiveness of employing the OLTC transformer is not guaranteed. To find the boundary condition, let us assume $V_T^{''} \geq V_{T\min}^{''}$. This restriction is converted to the following equation using (5.14) and (5.27),

$$1.1 \times V_N \times (n - y) \geq 1.336 \times V_{g1} \tag{5.28}$$

Solving (5.28), the following condition is obtained

$$y \leq n - 1.2145 \times \frac{V_{g1}}{V_N} \tag{5.29}$$

Therefore, to ensure the feasibility of OLTC transformer application, the maximum number of faulty turbines must satisfy (5.29). Otherwise, the GSC output voltage reference must be reset to suit IVRM. The IVRM method proposed in the last section and the AC voltage reset/ OLTC transformer application discussed in this section form the GA strategy for overvoltage prevention.

5.3. APPLICATION OF GA WITH SSBA AND PRM

Due to the dependency of the DC voltage control among wind power units in a series DC collection system, out-of-range voltages can result from the uneven wind speed within an offshore wind farm or the failure of wind turbines. In general, the voltage deviations caused by wind speed differences are relatively small, while turbine failures might result in serious overvoltage occurrence. In this section, the proposed voltage control strategies without faults (SSBA and PRM in Chapter 4) and with faults (GA) are combined to control DC voltages for various operating conditions.

5.3.1. COMPARISON OF THE THREE VOLTAGE CONTROL STRATEGIES

As stated in Chapter 4, SSBA ensures that all the generated offshore wind power is delivered to the onshore grid. First, the maximum power is extracted from wind energy through MPPT control. Second, with bidirectional power exchange with small batteries, excess power is stored temporarily at the wind side but sent out by HVDC eventually. However, SSBA apparently increases the construction investment

of an offshore wind project. Furthermore, additional maintenance work is required. Compared to SSBA, PRM adds almost no extra cost either with pitch control modification or chopping resistors. However, as less wind energy is extracted (PRM-PCM) or some generated wind power is converted to heat (PRM-CR), the power output of an offshore farm is lower than when SSBA is employed. Therefore, when the wind speed distributes almost evenly within an offshore farm, PRM is preferred as no DC voltage is out of range the majority of the time and little available wind energy is wasted. When the wind speed in an offshore wind farm causes relatively bigger power differences among PMSGs, the wasted energy, through the application of PRM, might be equivalently more valuable than the extra investment with SSBA being employed. In this case, SSBA is preferred. It is concluded that the characteristics of the wind speed determines the voltage control strategy selection (SSBA or PRM) on normal operation. If historical records show nearly equal wind speeds for each turbine in an offshore farm, no DC voltages of wind power units exceed the prescribed range and thus neither SSBA nor PRM is required.

It is proposed in this chapter that GA is used to limit the overvoltage resulting from fault. Actually, all types of overvoltage in series DC collection systems, whether it is caused by fault or uneven wind speeds, can be avoided by the GA strategy. Compared to SSBA, GA is cheaper (if OLTC is not employed) and simpler. The DC voltages of wind power units can be controlled below the upper limit with GA, by simply measuring the power outputs and adding some extra control. Besides, SSBA cannot fix serious overvoltage problems. This is because no matter how much power small sized batteries absorb from or provide to wind power units, the constant DC voltage at the collecting point is distributed among fewer numbers of units when fault happens.

However, the GA strategy has the disadvantage that the DC voltages of all units can only be adjusted in the same direction. For example, with the same DVDR according to (5.8), the DC voltages of each unit are increased under fault conditions. But if the overvoltage is due to uneven wind speeds instead of fault, the DC voltages of all wind power units are reduced as a result of VDP following the transmission voltage decrease. In this case, units with relatively smaller power outputs might confront control signal tracking failure. Apart from managing overvoltage situations, the transmission voltage reference can also be increased to prevent tracking problem.

Similarly, overvoltage might happen to units with relatively bigger power outputs in this situation. Therefore, compared to GA, SSBA has the advantage of adjusting DC voltages in both directions by either absorbing or providing power through power sinks.

As for PRM and GA, both are cost-effective as only control system modification is required. Similar to SSBA, PRM cannot be employed for voltage control on fault conditions. But same with GA, PRM can only adjust DC voltages among wind power units in one direction.

Considering the features of the three voltage control strategies discussed above, the best strategy is to take advantage of their merits while avoiding their defects. As GA might generate problems dealing with voltage fluctuation of normal operation, SSBA or PRM is used to restrict small voltage deviations resulting from uneven wind speeds. It has been mentioned that the selection between SSBA and PRM is based on economic consideration. As for overvoltage caused by fault, GA is employed. As a conclusion of the voltage control for series DC collection systems, SSBA and PRM are used to deal with small voltage deviations if necessary, while GA is applied when overvoltage happens due to fault. With the combination of SSBA (or PRM) and GA, the DC voltages of all wind power units can be controlled within the acceptable range. In this way, series DC collection systems for offshore wind farms can operate safely. It is to be noted that GA and SSBA (or PRM) are independent control strategies, which can be employed together or separately depending on the needs.

5.3.2. SIMULATION STUDIES

In this subsection, various operation conditions of a series DC collection system are studied for offshore wind power integration. As the effectiveness of the normal operation voltage control strategies (SSBA and PRM) has been verified in Chapter 4, the simulation studies here focus on fault conditions with varied wind speeds. The voltage control strategy combinations of SSBA with GA and PRM with GA are also included in the simulation work and the AC voltage reset method is employed as GA. The effectiveness of OLTC transformer application employed as GA is studied separately.

***Case 1**: Application of GA*

The series DC collection system applied in Chapter 4 is used for the fault study here. It has been assumed that neither SSBA nor PRM is required in this case. The fault condition is that unit-2 is removed from operation at 8 s. The simulation results without overvoltage control are shown in Fig. 5.2. The wind speeds for the four turbines are plotted in Fig. 5.2 (a), where v_{w1}, v_{w2}, and v_{w3} ramp up from their initial values of 11.5 m/s, 11.6 m/s and 11.8 m/s to 13.5 m/s, 13.1 m/s and 12.8 m/s respectively during the time intervals of 8 s to 10 s, 9 s to 10 s and 10 s to 12 s. The wind speed for unit-4 (v_{w4}) decreases from the rated speed of 12 m/s to 11.5 m/s between 10 s and 11 s. Fig. 5.2 (b) shows that the power outputs of the four units follow their respective wind speeds except that P_2 drops to 0 at 8 s because of fault. The power outputs from the three non-faulty units experience fluctuations during the changes in their respective wind speeds. It can be seen from Fig. 5.2 (c) that before fault happens, all the four DC voltages of wind power units are between the two limits (V_{lw} and V_{up}). At 8 s, the DC voltage of unit-2 (V_2) becomes 0 following P_2. The DC voltages of all the three non-faulty units are above the upper limit (V_{up}). The transmission voltage (V_T) is kept constant at its reference value of 30 kV barring acceptable fluctuations during fault transient.

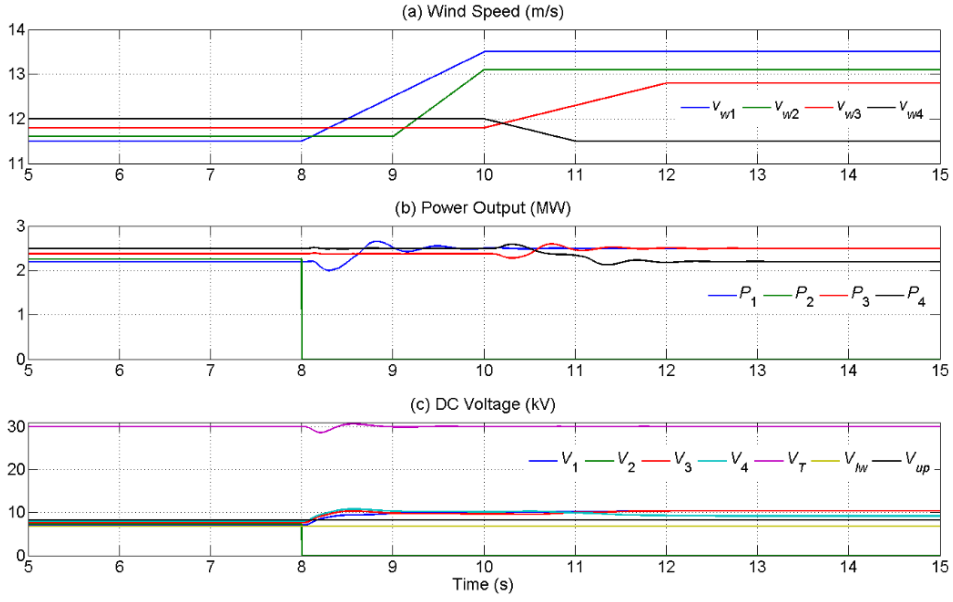

Fig. 5.2. Fault condition of four units connected in series without GA.

To prevent the overvoltage occurrence in Fig. 5.2 (c), the proposed GA strategy is applied and the simulation results are shown in Fig. 5.3. In this case, the

GSC output voltage reference is reset as 15.156 kV calculated from (5.18). The wind speeds to each turbine are given in the same patterns with Fig. 5.2 (a). It can be seen by comparing Figs. 5.2 (b) and 5.3 (a) that the power outputs of the four units with GA are the same as those without GA, indicating that the AC side of the wind power units do not get influenced by their DC side control modification. It is shown in Fig. 5.3 (b) that the DC voltages of the three non-faulty units are limited equal to or below the upper limit (V_{up}) and no voltage falls below the lower limit (V_{lw}). Fig. 5.3 (c) illustrates the waveforms of the measured transmission voltage and its reference under IVRM control. It can be seen that the GSC input voltage reference (V_T'') is reduced after fault happens at 8 s, with the actual transmission voltage (V_T) following V_T'' closely. The voltage oscillations here are due to the power output fluctuation.

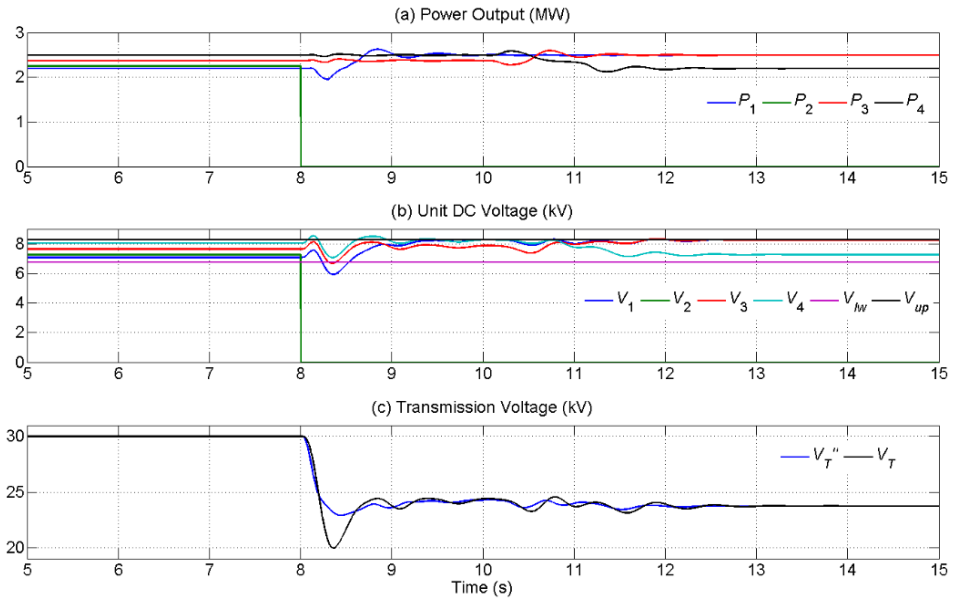

Fig. 5.3. Fault condition of four units connected in series with GA.

***Case 2**: Application of GA and SSBA*

The same simulation model as in Case 1 is employed to verify the effectiveness of the GA and SSBA combination, where the GSC output voltage reference is reset as 15.156 kV as well. A fault occurs to unit-2 at 18 s. The simulation results are shown in Fig. 5.4, where the four wind speeds are shown in Fig. 5.4 (a). In this, v_{w1}, v_{w2}, and v_{w3} ramp up from 10.5 m/s, 11.5 m/s and 11 m/s to 12.5 m/s, 13 m/s and 15 m/s respectively from 10 s to 12 s, 11 s to 12 s and 12 s to 14 s, while v_{w4} drops from 12 m/s to 11 m/s between 12 s and 13 s. The generator power output curves in Fig. 5.4 (b) follow their respective wind speeds except that P_{out2} drops to 0 at 18 s. It can

be seen by comparing Figs. 5.4 (b) and 5.4 (c) that the power outputs from the WSCs are limited to a smaller range with P_2 becoming 0 following P_{out2}. Fig. 5.4 (d) shows the power exchanges between each unit and its connected battery, where the power flows toward a battery is represented by a positive value as in Chapter 4. The combination of Figs. 5.4 (b) to 5.4 (d) demonstrates that the power differences between each PMSG and WSC are balanced by their respective small sized batteries.

The DC voltages of each unit are shown in Fig. 5.4 (e). After the fault at 18 s, V_2 drops to 0, while V_1 and V_3 are limited at the upper limit (V_{up}). V_4 settles after fault at a value bigger than the lower limit (V_{lw}). It is clear in Fig. 5.4 (f) that the transmission voltage reference (V_T'') drops to a lower value after fault due to the application of IVRM. The actual transmission voltage (V_T) follows V_T'' closely as in Case 1. It is noted that all power and voltage waveforms experience acceptable fluctuations during fault transient.

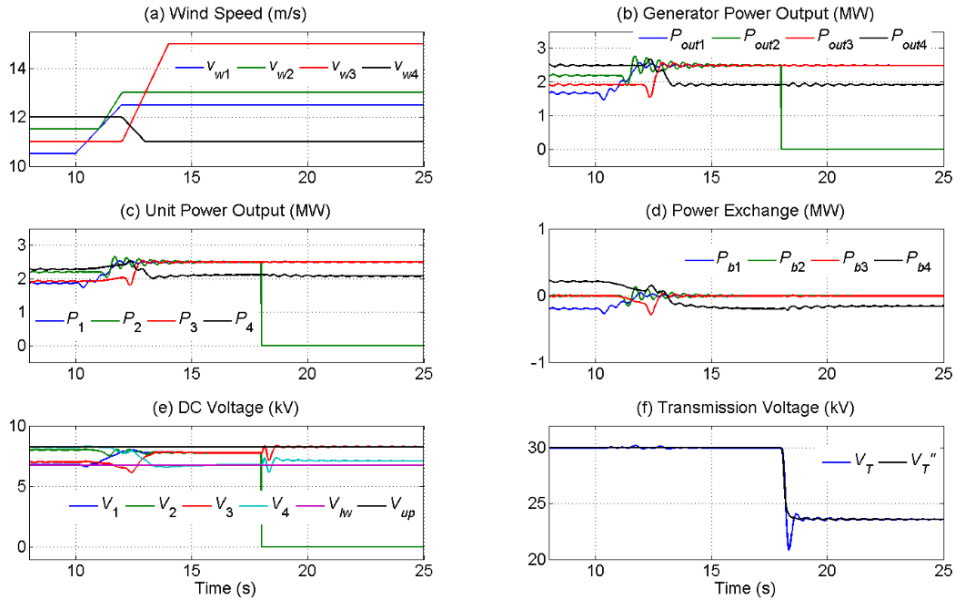

Fig. 5.4. Fault condition of four units connected in series with GA and SSBA.

***Case 3**: Application of GA and PRM*

The same simulation model in Cases 1 and 2 is applied here to validate the combined application of GA and PRM (taking PRM-CR as an example). Here a fault happens to unit-2 at 16 s. The simulation results are shown in Fig. 5.5. Fig. 5.5 (a) illustrates the four wind speeds, where v_{w1}, v_{w2}, and v_{w3} ramp up from 11 m/s, 11.5 m/s and 11 m/s to 13 m/s, 13 m/s and 15 m/s respectively from 8 s to 10 s, 9 s to 10 s

and 10 s to 12 s, while v_{w4} drops from 12 m/s to 11 m/s between 10 s and 11 s. The power outputs of each PMSG plotted in Fig. 5.5 (b) follow their respective wind speeds due to MPPT control, with P_{out2} dropping to 0 at 16 s. Fig. 5.5 (c) shows the WSC power outputs, where the power of unit-2 becomes 0 upon fault.

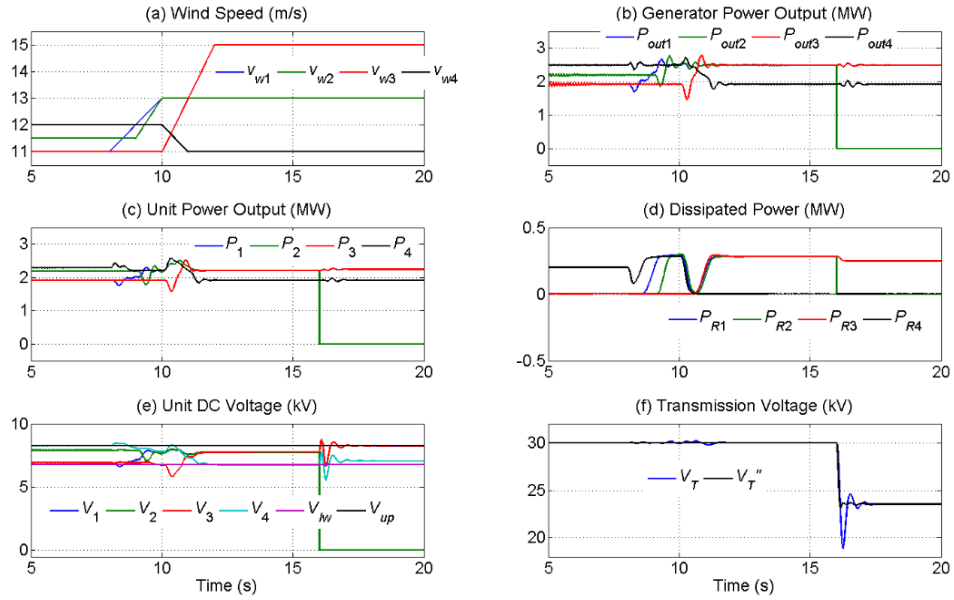

Fig. 5.5. Fault condition of four units connected in series with GA and PRM-CR.

It can be seen by comparing Figs. 5.5 (b) and 5.4 (c) that the power outputs from some WSCs are reduced from their respective generator power outputs to narrow down the range of the non-faulty unit power. The trimmed power from each generator to its connected WSC is consumed by chopping resistors as shown in Fig. 5.5 (d). Therefore, each generator power is the sum of their respective unit power outputs plus the dissipated power. These power waveforms indicate the effectiveness of PRM-CR. Fig. 5.5 (e) shows the DC voltage waveforms. After the fault, V_2 becomes 0 and the other three voltages (V_1, V_3 and V_4) are limited within the specified range of V_{lw} to V_{up}. Fig. 5.5 (f) shows that the transmission voltage (V_T) drops following V_T'' and settles at a new stable value after the fault due to its reference modification through IVRM. It is noted in Fig. 5.5 that acceptable fluctuations occur to all the discussed parameters during the changes in the wind speeds and upon fault.

***Case 4**: Application of an OLTC Transformer*

In this case, a series DC collection system with 6 wind power units is studied. Therefore, the transmission voltage reference for normal operation is V_T = 45 kV (7.5

kV × 6) and the GSC output voltage reference is V_{g1} = 24 kV (4 kV × 6). Suppose the line-to-line RMS voltage of the grid is 220 kV (V_{g2}), then from (5.19), we get η = 10.083. It is obtained respectively from (5.21) and (5.27) that the lowest available voltage of winding-1 and the transmission voltage that an OLTC transformer can accommodate are $V_{tf1\min}$ = 19.63 kV (0.818 × 24 kV) and $V''_{T\min}$ = 32.07 kV (1.336 × 24 kV). It is assumed that each unit operates at the rated power output.

Three fault conditions are considered. For condition-1, one wind turbine gets faulty. Using (5.11), the modified transmission voltage reference upon fault is calculated as

$$V''_T = 5 \times 1.1 \times V_N = 41.25kV \tag{5.30}$$

Since $V''_T \geq V''_{T\min}$, the application of the OLTC transformer will be effective for this fault condition. Based on the restriction in (4.3) of Chapter 4, the DC voltage of a SPWM controlled VSC must be at least 1.633 times the AC line-to-line RMS voltage. If no transformer tap setting is used (i.e., indicates V_{g1} remains 24 kV), then the minimum DC voltage of the GSC (denoted by $V_{T\min}$) is 39.19 kV (1.633 × 24 kV). As V''_T under this condition is bigger than 39.19 kV, no tap position adjustment is required here. Condition-2 and condition-3 respectively consider 2 turbines and 3 turbines get faulty simultaneously. Similar calculations can be conducted as those for condition-1. The calculation results are summarized below:

- Condition-2: Using (5.11), the transmission voltage is modified to be 33 kV (7.5 kV × 1.1 × 4). As this modified value is smaller than $V_{T\min}$ in condition-1, the tap position must be changed. From (5.18), V''_{g1} is calculated to be 20.21 kV. Subsequently, from (5.25), x is calculated to be 12.63. Therefore, a decrease of 13 voltage steps is needed and the resulting AC voltage is 20.1 kV (24 kV – 24 kV × 13 × 1.25%), which is bigger than $V_{tf1\min}$. Therefore, V''_{g1} is reset at 20.1 kV through tap position change. The effectiveness of employing the OLTC transformer can also be validated through substituting the given values into (5.29).
- Condition-3: The transmission voltage is modified to be 24.75 kV (7.5 kV × 1.1 × 3). As for condition-2, the tap position must be changed. From (5.18), V''_{g1} is calculated to be 15.16 kV, which is smaller than $V_{tf1\min}$. Therefore, the

required voltage cannot be achieved through the tap position adjustment of the OLTC transformer. The incapability of the OLTC transformer application for this condition can also be verified through the fact that (5.29) is not satisfied.

The simulation results of the three fault conditions are shown in Fig. 5.6. For condition-3, $V_{tf1\min}$ = 19.63 kV has been assigned as the GSC AC voltage reference ($V_{g1}^{''}$). It can be seen from Fig. 5.6 (a) that the transmission voltages under all three conditions drop to the new reference values upon faults and operate stably all the time. The reference and actual voltages of phase-*a* are shown in Figs. 5.6 (b) to 5.6 (d). Even though proper voltage tracking is achieved for conditions 1 and 2 (Fig. 5.6 (b) and Fig 5.6 (c)), voltage distortion can be observed for condition-3 in Fig. 5.6 (d). Note that further loss in wind turbine will result in complete voltage collapse. The simulation results are in accordance with the theory analysis and demonstrate the limitation in the effectiveness of OLTC transformer application.

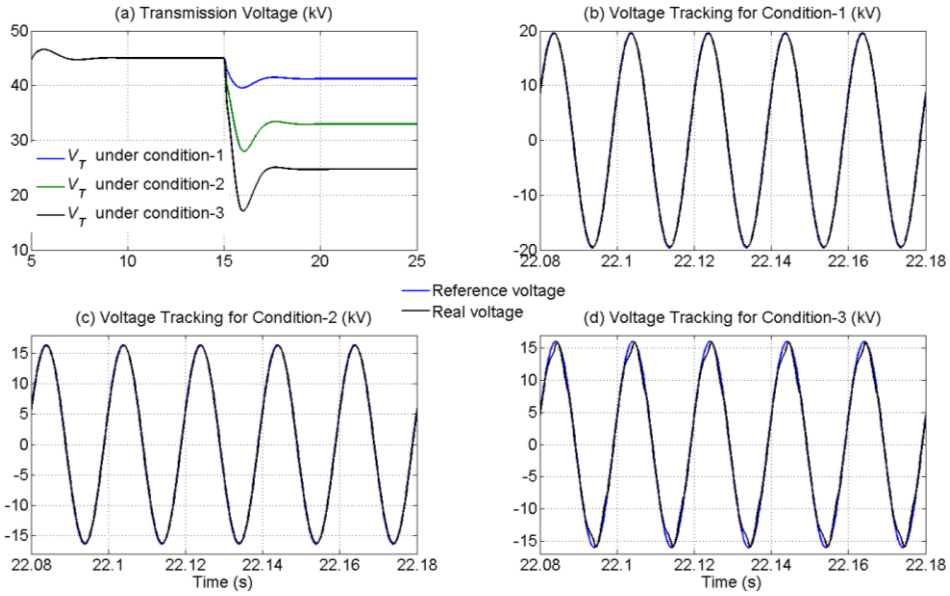

Fig. 5.6. 3 fault conditions of six units connected in series with an OLTC transformer.

***Case 5**: Fault Condition for Large Number of Series Connected Wind Power Units*

The simulation studies from Case 1 to Case 4 are all for the conditions that GA is required when fault happens. However, with the improvement of wind turbine reliability and the increasing scales of offshore wind farms, it is most likely that no

extra fault control strategy is needed for the DC voltage restriction of wind power units. It has been concluded previously that the more turbines a wind farm contains, the less likely that overvoltage will occur in the series DC collection system. In this case, the fault condition without the requirement for GA is studied. As mentioned in Section 5.1, if the number of the series connected units is equal to or bigger than 11*y*, the collection system can tolerate fault conditions without any additional control strategy. Based on the restriction in (5.5), a series DC collection system containing 50 wind power units with 2 units getting faulty is used for this simulation study case. As the focus here is fault study, it has been assumed that all wind power units operate at the rated power of 2.5 MW. Besides, voltage fluctuations caused by different wind speeds are much smaller than when fault happens. Therefore, if no overvoltage happens even with fault, wind speed variation within an offshore wind farm cannot cause out-of-range voltages.

For this case, simplified wind turbine models have been used, while a detailed model of the GSC is considered. The GSC input and output reference voltages are set as 375 kV DC (7.5 kV × 50) and line-to-line AC RMS 200 kV (4 kV × 50) respectively. It has been assumed that unit-49 and unit-50 are disconnected at 15 s and 20 s respectively. The simulation results are shown in Fig. 5.7, where V_1 represents the voltage of unit-1, which is a non-faulty unit. Note that all the other non-faulty units (2 to 48) are assumed to have the same voltage as V_1.

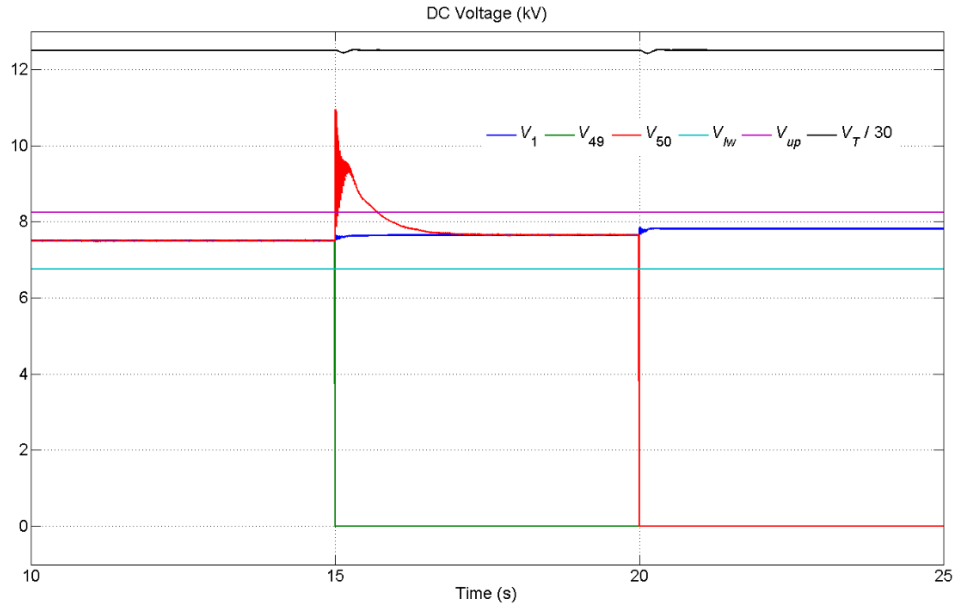

Fig. 5.7. Fault condition of 50 units connected in series.

It can be seen from Fig. 5.7 that the DC voltage of each unit is stable at 7.5 kV before any fault. When the first fault happens at 15 s, the DC voltage of unit-49 (V_{49}) drops to 0, and as a consequence, the voltage of the nearest unit-50 (V_{50}) sees a large transient. However, both V_{50} and V_1 eventually settle at around 7.65 kV, which is between the upper and the lower limits. When unit-50 is bypassed at 20 s, V_{50} becomes 0 and the DC voltages of the non-faulty units 1 to 48 increase to approximately 7.81 kV. A scaled version of the GSC input voltage (V_T) is also shown in this figure. It can be seen that this is kept constant at the reference value ($12.5 \times 30 = 375$ kV). Although all the DC voltages experience small fluctuations during the faults, no voltage of the non-faulty units exceeds the upper limit (V_{up}) at steady states. This simulation study case indicates that additional voltage control strategies upon fault might be unnecessary for some offshore wind farms. It is also to be noted from the 5 simulations cases that all the DC voltages during fault transient are below the transient overvoltage limit of $1.5V_N$ defined in Subsection 4.1.3 of Chapter 4.

5.4. MULTIPLE INVERTER APPLICATION

The GA strategy proposed above is based on the series DC collection topology as in Fig. 4.3, where only one large sized inverter is employed at the grid side. In this section, the large GSC is replaced with several small inverters to prevent DC overvoltage when wind turbines get faulty. The topology and control of this new GSC configuration are discussed below.

5.4.1. GSC WITH MULTIPLE INVERTERS

The topology of a series DC collection system with multiple grid side converters is shown in Fig. 5.8, where the wind side configuration remains unchanged from Fig. 4.3. It has been assumed previously that the maximum number of faulty units in a series DC collection system can be up to y for reliable operation. Then in this topology of multiple GSCs, it has been assumed that there are y number of small converters (termed from GSC-1 to GSC-y) and a larger converter. The larger converter is denoted by GSC-(y + 1). Each of the smaller GSCs has the same rating as a WSC. All these GSCs are connected in series on their DC side and in parallel on their AC side. Also note from Fig. 5.8 that two transformers are employed here – one

connecting the smaller GSCs to the grid, while the other connecting the bigger GSC to the grid.

Suppose the nominal DC voltage for each small GSC is denoted by V_{ST1N}, which is equal to V_N, then the reference DC voltage of GSC-(y + 1) denoted by V_{ST2N} is given as

$$V_{ST2N} = n \times V_N - y \times V_{ST1N} = (n - y) \times V_N \tag{5.31}$$

It is obvious that

$$V_{TN} = y \times V_{ST1N} + V_{ST2N} \tag{5.32}$$

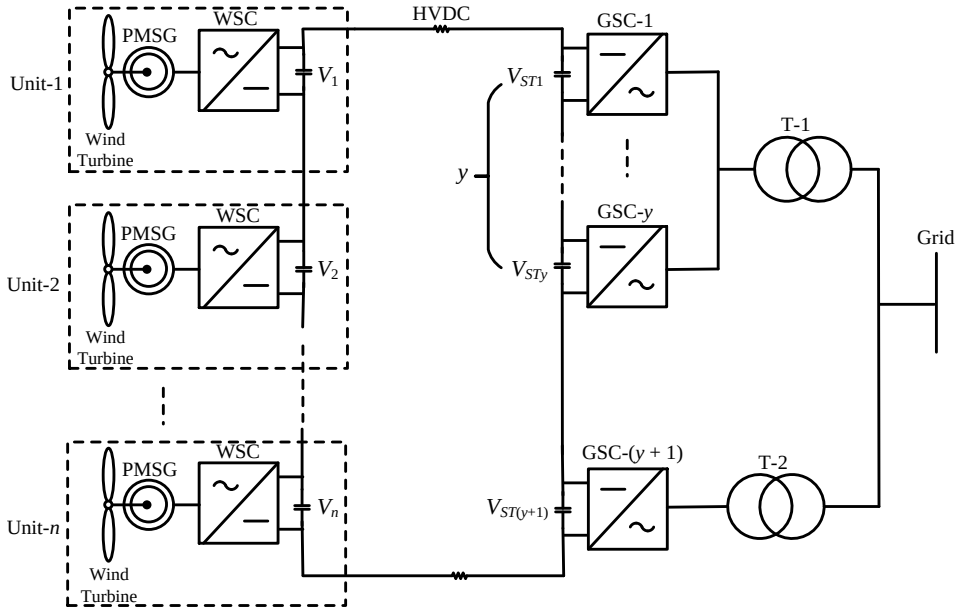

Fig. 5.8. Configuration of a series DC collection system with multiple inverters.

In Fig. 5.8, the measured DC voltages of each small GSC and the big GSC are denoted by V_{ST1} to V_{STy} and $V_{ST(y+1)}$ respectively. With two types of GSC sizing, two transformers are required accordingly, which are represented by T-1 and T-2 as shown in Fig. 5.8. The input line-to-line RMS voltage references for T-1 and T-2 are obtained based on (5.12), which are

$$\begin{cases} V_{gs} = V_w \\ V_{gb} = (n - y) \times V_w \end{cases} \tag{5.33}$$

where V_{gs} and V_{gb} are the rated output voltages for GSC-1 (to GSC-y) and GSC-(y + 1) respectively.

When a number of wind turbines get faulty in a series DC collection system with multiple inverters, the voltage control strategy is to bypass (or disconnect) the same number of small GSCs. This fault voltage control strategy with the modified series DC collection system is termed as GSC Reconfiguration (GR) in this thesis. It is equivalent to changing the size of an offshore wind farm.

With GR, the total DC voltage is reduced to such a level that the non-faulty units operate exactly around their rated voltage (V_N) instead of bearing the extra voltage resulting from fault. This means better control efficiency. Furthermore, the control system by employing GR is simpler than using GA. However, the employment of more inverters in the GR strategy obviously increases the total investment cost of an offshore project. Given that small inverters are not as expensive as big ones, the cost difference between multiple inverters and a big inverter in some cases might be balanced by the simpler control system and better control efficiency of GR.

5.4.2. SIMULATION STUDIES

Two simulation cases are discussed for the fault condition of the series DC collection with multiple GSCs. First, the detailed models of each WECS component are applied. Second, wind power units are replaced by ideal power sources. No normal operation voltage control strategies are considered in this subsection given that the effectiveness of SSBA and PRM has been validated repeatedly. Besides, the control target of GR is to prevent overvoltage upon fault.

For the studies performed in this subsection, a *y* of 2 has been assumed, i.e., at most 2 wind turbines can go offline at any time. A total number of 6 wind turbines are assumed to be connected in series. Therefore, there are 2 smaller GSCs and a larger GSC. It has also been assumed that all the wind turbines are operating at their rated power. The DC and AC voltage references of each GSC are listed in Table 5.1. Note that since GSC-1 and GSC-2, both with output AC voltages of 4 kV, are connected in parallel, only one ordinary transformer T-1 is sufficient. For these studies, it has been assumed that unit-2 goes offline at 15 s, followed by unit-3 going offline at 20 s.

Table 5.1: Voltage references of multiple inverters.

Quantities	**Rated Voltages**
GSC input DC voltages	GSC-1 and GSC-2: 7.5 kV GSC-3: 30 kV
GSC output AC voltages (RMS, line-to-line)	GSC-1 and GSC-2: 4 kV GSC-3: 16 kV
Transfomer winding voltages (RMS, line-to-line)	T-1: 4 kV:220 kV T-2: 16 kV:220 kV

The simulation results with the GR strategy are shown in Fig. 5.9. Fig. 5.9 (a) illustrates the DC voltages of unit-1 to unit-3, where the voltages for the non-faulty units (unit-4 to unit-6) are the same with V_1 and thus not plotted here. It is obvious that V_1 is kept at the rated value of 7.5 kV regardless of the two faults. The voltages V_2 and V_3 are equal to V_1 before fault and become 0 upon their respective fault occurrences. It can be seen from Fig. 5.9 (b) that V_{T1} and V_{T2} drop from 7.5 kV to 0 at 15 s and 20 s respectively with the disconnections of GSC-1 and GSC-2 upon each fault. With V_{T3} remaining constant at 30 kV, the transmission voltage (V_T) is 45 kV before any fault, 37.5 kV after unit-2 gets offline and 30 kV after unit-3 is also disconnected.

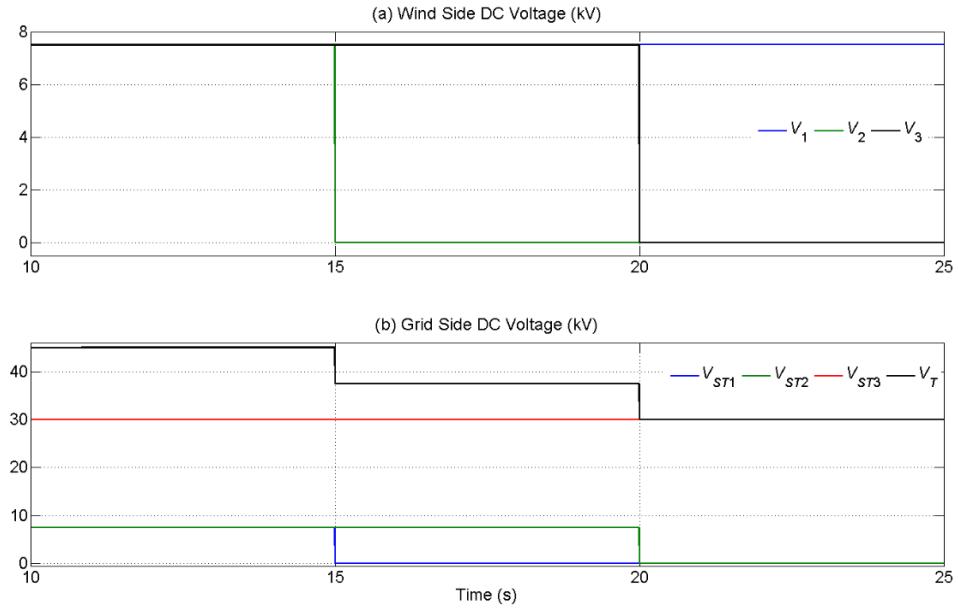

Fig. 5.9. Simulation results of two turbines getting faulty in a series DC collection system with multiple inverters.

5.5. CONCLUSIONS

In this chapter, the fault condition resulting from wind turbine failures is studied for the series DC collection system. The overvoltage problem of the offshore series DC collection system is analysed and the demand for fault voltage control strategies is demonstrated. To prevent overvoltage occurrence upon fault, two voltage control strategies are proposed. First, the transmission voltage reference is reduced when fault happens by modifying the input voltage reference of the GSC. The AC side voltage of the GSC is reset accordingly or adjusted by an OLTC transformer. To avoid setting the grid side AC voltage at a too low level and conquer the limitation of OLTC transformer application, it is worth considering the combining of the two AC voltage regulation methods. Second, the GSC is replaced by several inverters with smaller capacities. One small GSC with the same capacity and voltage level of a WSC is bypassed upon each fault. The scale of the series DC collection system for an offshore wind farm is essentially decreased using this strategy when fault happens.

Compared to altering the GSC voltage references, the application of multiple inverters will probably increase the investment cost for an offshore wind power project. However, the voltage control strategy with multiple inverters has simpler control logic and better control efficiencies. Furthermore, the employment of multiple GSCs improves the safe operation of the grid side power conversion. This is because the small GSCs can be the backup of each other. In case one small operating GSC is faulty, a non-faulty GSC which is bypassed can be put back into operation to replace the faulty GSC. Simulation studies are conducted with both detailed WECSs and ideal power sources replacing large numbers of wind power units. The control effectiveness of GSC adaptation and GSC reconfiguration for fault conditions are validated individually through the simulation results in PSACD. It is noted that GA and GR can be combined to prevent overvoltage upon fault in series DC collection systems.

CHAPTER 6

SERIES-PARALLEL DC COLLECTION SYSTEMS

In this chapter, the DC collection system with series-parallel connected wind power units for an offshore farm is discussed. The terminology of series-parallel refers to the combination of series and parallel connections, where several wind power units are connected in series as a branch and several such branches are connected in parallel. The DC terminal voltage of the collection system is still maintained by a common grid side converter (GSC) that is connected at the end of an HVDC line. The series-parallel DC collection system is suitable for offshore wind farms with wind turbines distributed in a matrix pattern.

The wind turbines within an offshore wind farm are sometimes installed in several lines due to construction factors. In this case, although the wind speed of an entire offshore wind farm is usually evenly distributed, downstream wind turbines might get reduced wind speed from upstream wind turbines. As the series DC collection system proposed in Chapter 4 requires similar wind speeds to each wind turbine, it is not applicable in this situation. The series-parallel DC collection system is proposed for the condition when wind turbines in different rows are subjected to different wind speeds. It is obvious that for wind turbines positioned in a matrix pattern, the parallel DC collection system could be employed as well. However, the high costs of boost converters are again the downside of using parallel DC collection.

In series-parallel DC collection, the DC outputs of wind side converters in the same line are connected in series and several such series connected branches are connected in parallel [42]. Therefore, the collected DC voltage of a series-parallel collection system is still added up due to the series connection. An advantage of this collection topology over the series collection is that the total DC current is distributed in different branches and therefore the convert ratings can be lower. In other words, the series-parallel DC collection system is more cost-effective as the series DC collection system as boost converters could be omitted in both systems. However, the problems with the series DC collection system are also associated with the series-parallel DC collection system. Undervoltage and overvoltage could still appear when the wind speeds to each wind turbine in the same branch are different.

On the other hand, although wind turbine failures in one branch do not affect the safe operation of wind turbines in other branches, overvoltage would probably happen to the non-faulty wind turbines in the faulty branch. Therefore, same as the series DC collection system, the series-parallel DC collection system has similar disadvantages due to the dependence of series connected wind turbines.

For the voltage control on normal (non-fault) operation, the previously proposed strategies (SSBA and PRM) can be applied to the series-parallel DC collection topology. However, to prevent overvoltage occurrence upon fault, the control strategies proposed in Chapter 5 (GA and GR) are only conditionally effective. This is because these strategies are based on the variable transmission voltage operation. In this chapter, a branch containing one or more faulty units will be termed as a faulty branch, while in a non-faulty branch, all the units are assumed to be operational. If the transmission voltage is reduced due to a faulty branch, the DC voltages of the units in the non-faulty branches will also decrease and this may result in tracking failures. Therefore, extra devices need to be employed for a series-parallel DC collection system to cater to fault conditions.

First, power switches are used between adjacent branches for collection topology reconfiguration when fault happens. Second, an auto-transformer is applied to control the total voltage of a faulty-branch such that the total voltage of the non-faulty branches remains unchanged. It is to be noted that not all fault conditions require extra voltage control strategies. This is dependent on the turbine reliability and the turbine number of an offshore wind farm.

6.1. NORMAL OPERATION OF SERIES-PARALLEL DC COLLECTION SYSTEMS

Although the voltage control strategies proposed for normal (non-fault) operation are based on the series DC collection system of an offshore wind farm, they also apply to series-parallel DC collection systems. In this section, the control effects by employing SSBA and PRM in series-parallel DC systems are studied.

6.1.1. SIMULATION STUDIES

A 2×2 series-parallel DC collection system is simulated in PSCAD, where PMSG based WECSs are modelled in detail. It is assumed that unit-1 and unit-2 are connected in series as branch-1, while unit-3 and unit-4 form branch-2. The GSC input and output voltage references are set as 15 kV and 8 kV (RMS, line-to-line) respectively by referring to Table 2.1. The simulation results with SSBA and PRM are shown in Figs. 6.1 and 6.2 respectively.

To show the robustness of the voltage control strategies, distinctively different wind speeds are given to the four wind power units. These are shown in Figs. 6.1 (a) and 6.2 (a). With SSBA, the wind speeds are

- v_{w1}: ramps up from 10.5 m/s to 12.5 m/s between 12 s and 14 s;
- v_{w2}: ramps up from 11.5 m/s to 13 m/s between 13 s and 14 s;
- v_{w3}: ramps up from 11 m/s to 15 m/s between 14 s and 16 s;
- v_{w4}: ramps down from 12 m/s to 11 m/s between 14 s and 15 s,

while with PRM, these are

- v_{w1}: ramps up from 11 m/s to 13 m/s between 8 s and 10 s;
- v_{w2}: ramps up from 11.5 m/s to 13 m/s between 9 s and 10 s;
- v_{w3}: ramps up from 11 m/s to 15 m/s between 10 s and 12 s;
- v_{w4}: ramps down from 12 m/s to 11 m/s between 10 s and 11 s.

It can be seen from Figs. 6.1 (b) and 6.2 (b) that the generator power outputs of each unit follow their respective wind speed curves with both SSBA and PRM due to the MPPT control. Fig. 6.1 (c) shows the power from each unit with SSBA. Compared to Fig. 6.1 (b), the unit power outputs of branch-1 and branch-2 are both in a smaller range due to the bi-directional power exchange with small batteries. Similarly, it can be seen by comparing Fig. 6.2 (c) and Fig. 6.2 (b) that the unit power outputs of branch-1 and branch-2 with PRM are also in a smaller range. This is the result of excess power dissipating on chopping resistors. It can be seen from Figs. 6.1 (d) and 6.2 (d) that the four unit DC voltages are all limited between V_{lw} of 6.75 kV and V_{up} of 8.25 kV with SSBA and PRM individually. The transmission voltage with each strategy is kept at the reference value of 15 kV. It is noted that the power and voltage waveforms experience short-term fluctuations during the changes in the wind speeds.

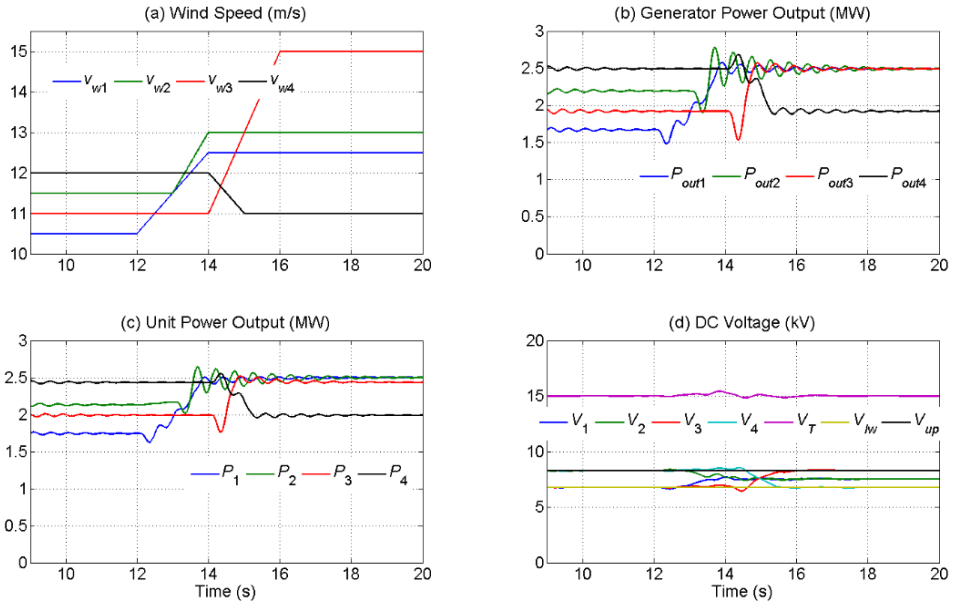

Fig. 6.1. Simulation results of a 2×2 series-parallel DC collection system with SSBA.

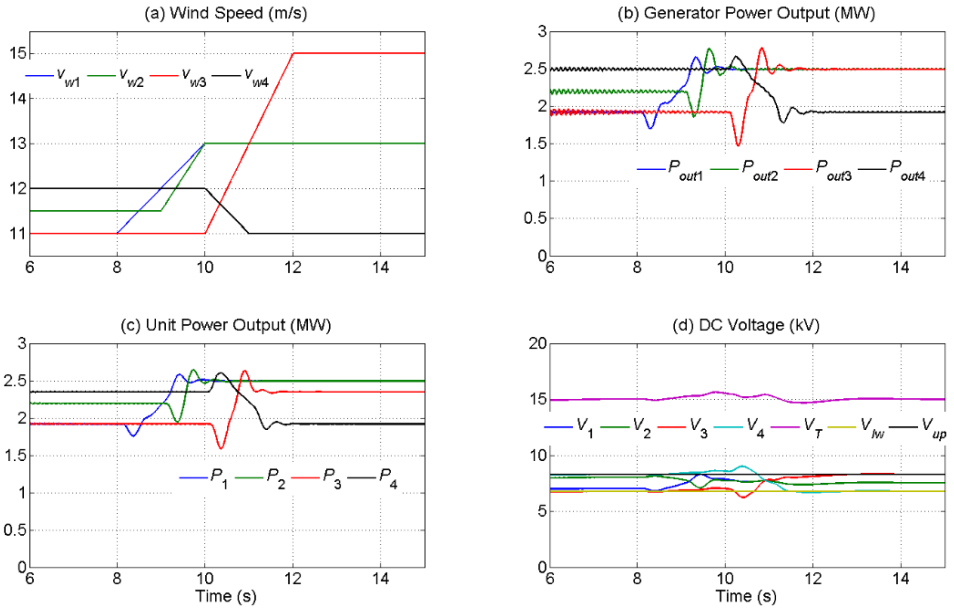

Fig. 6.2. Simulation results of a 2×2 series-parallel DC collection system with PRM.

The simulation studies with the detailed models of each WECS component demonstrate the safe operation of series-parallel DC collection systems for offshore wind farms. With the satisfactory control effects through either SSBA or PRM on normal operation, the power differences among units within each branch are restricted. The DC voltage control on fault conditions are discussed in the rest of this chapter.

6.2. CONDITIONAL APPLICATION OF IVRM FOR SERIES-PARALLEL DC COLLECTION SYSTEMS

When wind turbine failure happens, the voltage control strategies for a series DC collection system – GA and GR, are not always applicable to a series-parallel DC collection system. This is because both GA and GR require a decrease in the transmission voltage and a substantial decrease might result in VSC tracking failure of turbine units in the non-faulty branches. Note that, for a same fault, the transmission voltage decrease using GA is bigger than when GR is employed. This implies that compared to GR, GA has a better control effect for a series-parallel DC collection system. Therefore in this section, the application of IVRM (main part of GA) is discussed for the series-parallel topology.

6.2.1. RESTRICTION OF IVRM APPLICATION FOR SERIES-PARALLEL DC COLLECTION

Although it is naturally variable, wind energy is not unreliable. According to [118], none of the thousands of modern wind turbines in the U.S. have experienced a catastrophic failure, blade throw or a collapse. Given that the possibility of wind turbine failure is so small, chances of more than 2 turbines getting faulty at the same time is almost negligible. Although the fault control strategies for a series DC collection system (GA and GR) apply to any number of faulty units, the worst fault condition considered for a series-parallel system is when 2 wind turbines have to be simultaneously bypassed.

Let us denote the series connected unit number for each branch is n. For simplicity, it has been assumed that each unit has the same DC voltage V_N. Then, according to (5.5), no additional voltage control strategy will be required with 2 faulty turbines when

$$n \geq 22 \tag{6.1}$$

Equation (6.1) implies that no overvoltage will occur upon fault if $n \geq 22$. However, if n is smaller than 22, IVRM is to be applied and the voltage control effectiveness is not guaranteed. This is due to the possibility of tracking failure in the non-faulty branches when the transmission voltage is reduced.

When n is smaller than 22, according to (5.11), the modified transmission voltage reference upon fault is calculated as

$$V_T'' = 1.1 \times (n-2) \times V_N \tag{6.2}$$

Then the DC voltage of units in the non-faulty branches is

$$V_N'' = \frac{V_T''}{n} = \frac{1.1 \times (n-2) \times V_N}{n} \tag{6.3}$$

where V_N'' is the DC voltage of each non-faulty unit after fault with the application of IVRM. As per Chapter 4, the lower limit for the DC voltage of each unit is $0.9V_N$. Therefore, V_N'' must meet the following requirement

$$V_N'' \geq 0.9V_N \tag{6.4}$$

Combining (6.3) and (6.4), we have

$$n \geq 11 \tag{6.5}$$

Equation (6.5) indicates that to ensure the safe operation of a series-parallel DC collection system, each branch must contain at least 11 units if IVRM is to be applied effectively. For series-parallel systems that do not satisfy (6.5), extra devices can be used to prevent overvoltage upon fault. For this, power switches and auto-transformers are employed in the following sections.

6.2.2. SIMULATION STUDIES

Based on the previous discussion, three cases of $n \geq 22$, $11 \leq n < 22$ and $n < 11$ are simulated in PSCAD. Ideal power sources are used to model the large numbers of wind power units with each operating at the rated power level. The fault conditions are all set as unit-1 and unit-2 in branch-1 successively get faulty at 18 s and 24 s respectively. The simulation models of each case are described as below.

Case 1 ($n \geq 22$): The simulation model is a 25×4 series-parallel DC collection system. The input and output voltage references of the GSC are calculated to be 187.5 kV and 100 kV (RMS, line-to-line) respectively.

Case 2 ($11 \leq n < 22$): The simulation model is a 15×4 series-parallel DC collection system. The input and output voltage references of the GSC are calculated to be 112.5 kV and 60 kV (RMS, line-to-line) respectively. It is noted that the GSC output voltage reference calculated by (5.18) is bigger than 60 kV, indicating that this reference is not required to be reset.

Case 3 ($n < 11$): The simulation model in this case is a 6×4 series-parallel DC collection system. The input and output voltage references of the GSC are calculated to be 45 kV and 20.21 kV (RMS, line-to-line, obtained by (5.18)) respectively.

The simulation results of the three cases are shown in Fig. 6.3, where

$V_{nf\text{-}1}$: the DC voltage of the non-faulty units in branch-1,
$V_{nf\text{-}o}$: the DC voltage of the non-faulty units in the non-faulty branches,
V_{f1}: the DC voltages of unit-1 in branch-1, and
V_{f2}: the DC voltage of unit-2 in branch-1.

Note that the scaled versions of the transmission voltages to make them compatible with the unit voltages are plotted for each case. It can be seen from Fig. 6.3 (a) that all the unit voltages are kept constant at the reference value of 7.5 kV initially. The DC voltages of unit-1 and unit-2 in branch-1 become 0 at 18 s and 24 s respectively as a result of the faults. The voltage of the non-faulty units in branch-1 increases after each fault, but remains below the upper limit (V_{up}) all along. The transmission voltage (V_T) and the unit voltage in the non-faulty branches remain at their reference values regardless of fault. The DC voltages in Case 2 are shown in Fig. 6.3 (b), where the transmission voltage is reduced from the initial 112.5 kV to around 107.25 kV due to the application of IVRM. The steady-state voltage of the non-faulty units in branch-1 are limited at 8.25 kV (V_{up}) after the first fault. The unit voltage of the non-faulty branches is decreased to another steady value but above the lower limit (V_{lw}). It is seen from Fig. 6.3 (c) that the transmission voltage decreases twice in Case 3. After the first fault at 18 s, V_T reduces from 45 kV to around 41.25 kV and further decreases to approximately 33 kV after the second fault at 24 s. The voltage of the non-faulty units in branch-1 is limited at the upper limit (V_{up}) after the first fault happens. Although the unit voltage in the non-faulty branches decreases, it still remains above the lower limit (V_{lw}) after the first fault. However, the unit voltage drops below V_{lw} after the second fault.

As a conclusion of the fault simulation study for the three cases, no extra voltage strategy is needed in Case 1, expected control effectiveness is achieved in Case 2 through IVRM (GA), and extra control strategies other than GA is required in Case 3. These simulation results verify the fault analysis for a series-parallel DC collection system in Subsection 6.2.1.

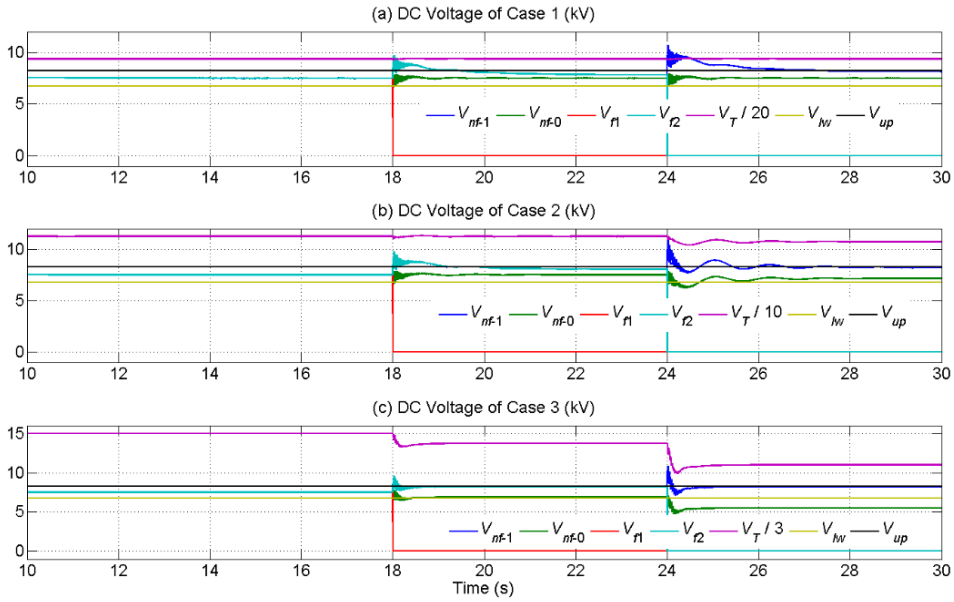

Fig. 6.3. DC Voltages of wind power units in 3 series-parallel DC collection systems with faults.

6.3. SERIES-PARALLEL DC COLLECTION SYSTEMS WITH POWER SWITCHES WHEN ARRAY EFFICIENCY IS 1

As GA cannot be applied unconditionally to a series-parallel DC collection system, extra devices are required when turbine failure occurs. Switches between adjacent branches to change the collection topology upon fault are applied in [26]. But it only considers faulty units in the same branch with the ideal operating condition. In practical situations, however, all types of fault scenarios can happen. It has been assumed in this chapter that each unit within a wind power branch has the same power output as the main focus is to study the fault condition.

A general structure of the series-parallel DC collection system is illustrated in Fig. 6.4. Here, each wind power unit is represented by a square box and numbered in a matrix pattern. A wind power branch is equivalent to a matrix column, while the rows contain the units. It can be seen that this topology represents an $n \times m$ series-parallel system with m branches and n units in each branch. There are $(n - 1)$ power

switches that connect each adjacent branch pair. These are normally open and denoted after the branch numbers to which they are connected. The switching strategies upon fault discussed in this section and the next are based on this topology.

When some of its energy is extracted by a rotor, the wind speed goes down. However at a distance downwind, the wind speed recovers. Array efficiency is defined as the predicted output divided by the power that would result if there were no interference [14, 119-120]. Therefore, there are no power differences from branch to branch when array efficiency is equal to 1. In this section, the ideal situation of unit array efficiency is studied to facilitate the fault condition analysis. Four fault scenarios are considered; these are discussed below.

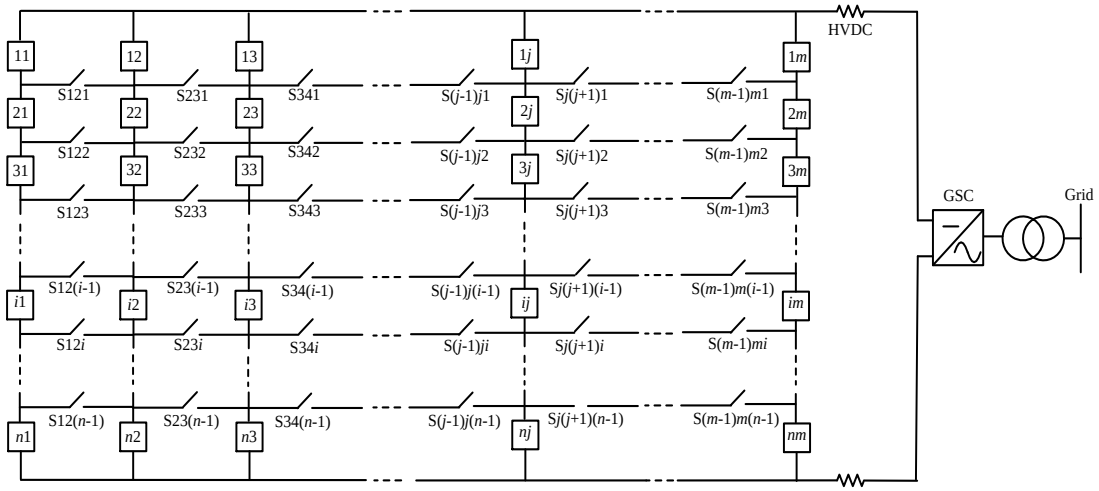

Fig. 6.4. Series-parallel DC collection with power switches.

6.3.1. SCENARIO-1: ONE UNIT GETS FAULTY

Fig. 6.4 is redrawn in Fig. 6.5, in which alphabetical characters instead of numerals are used to illustrate a most general configuration. In scenario-1, suppose unit-*fb* is faulty. If no switches are closed, the DC voltage of the non-faulty units in branch-*b* will rise to

$$V_{b0} = \frac{n}{n-1} \times V_N \tag{6.6}$$

where V_{b0} is the voltage of the other units in branch-*b* and V_N is the rated unit voltage as before. From the restriction of $V_{b0} \leq 1.1V_N$, it is obtained that $n \geq 11$. Therefore, power switches are required to operate when $n < 11$, such that a new current path is

generated for the non-faulty units in the faulty branch. To avoid bypassing any non-faulty unit, it is obvious that the adjacent switches of the faulty unit are desired to be closed for topology reconfiguration. Furthermore, the number of operating switches should be minimized considering switching losses.

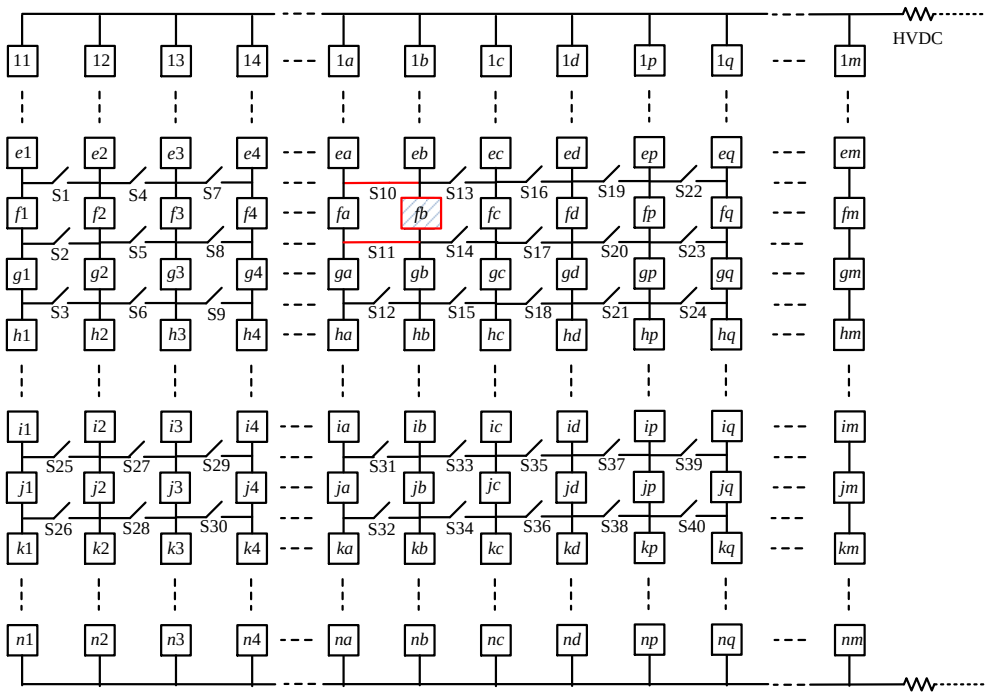

Fig. 6.5. Renumbered series-parallel DC collection with power switches for Scenario-1.

For unit-*fb*, the adjacent power switches on the left and right are respectively {S10, S11} and {S13, S14}, of which either Switch Combination (SC) can be closed to provide a current path. Suppose {S10, S11} are closed upon the fault, then branch-*a* and branch-*b* form an enhanced branch named as branch-*ab*. Apart from unit-*fa*, voltages of all other units in branch-*ab* are equal. Therefore, according to VDP, we get the following two voltage values

$$\begin{cases} V_{p1} + (n-1) \times V_{p2} = n \times V_N \\ V_{p2} = 2 \times V_{p1} \end{cases} \tag{6.7}$$

where V_{p1} is the DC voltage of unit-*fa* and V_{p2} is the DC voltage of all other units. From (6.7), we get

$$\begin{cases} V_{p1} = \dfrac{n}{2n-1} \times V_N \\ V_{p2} = \dfrac{2n}{2n-1} \times V_N \end{cases} \tag{6.8}$$

As $V_{p2} > V_{p1}$, with the predefined range of $0.9V_N$ to $1.1V_N$, the voltage constraints are given as

$$V_{p1} \geq 0.9 \times V_N \tag{6.9}$$

$$V_{p2} \leq 1.1 \times V_N \tag{6.10}$$

Constraint (6.9) cannot be satisfied. Therefore, to achieve a safe operation after fault, the rated DC voltage of WSCs (V_N) must be set as a relatively higher value such that no tracking failure is caused by the operation of power switches. In this way, the lower voltage limit will be less than $0.9V_N$. It is assumed that when power switches are employed, all the voltages are above the lower limit by setting the DC voltage reference (V_N) properly. Therefore, overvoltage prevention is considered as the control target upon fault. It is calculated from (6.10) that

$$n \geq 5.5 \tag{6.11}$$

As n is an integer, (6.11) implies that if each wind power branch has at least 6 units, overvoltage can be prevented by closing one adjacent SC of the faulty unit. Otherwise, more switches need to be closed as discussed below.

If the unit number in each wind power branch is smaller than 6, it is assumed that both adjacent SCs ({S10, S11} and {S13, S14}) are closed. The enhanced branch is thus branch-*abc* and two types of unit voltages are generated. Suppose unit-*fa* and unit-*fc* are in type-1 and the other non-faulty units of branch-*abc* are in type-2. Similar to (6.7), the following equations are obtained

$$\begin{cases} \dfrac{V_{p1}}{V_{p2}} = \dfrac{2}{3} \\ V_{p1} + (n-1) \times V_{p2} = n \times V_N \end{cases} \tag{6.12}$$

It can be seen from the first equation of (6.12) that V_{p2} is bigger than V_{p1}. Therefore, V_{p2} must meet

$$V_{p2} \leq 1.1 V_N \tag{6.13}$$

By combining (6.12) and (6.13), the restriction for n is calculated to be

$$n \geq 3.67 \tag{6.14}$$

It is expected that (6.14) will be satisfied for almost all offshore wind farms.

In conclusion, overvoltage can be prevented by employing power switches for scenario-1. The switching schemes are summarised as:

- if the number of the wind power units in each branch is greater than or equal to 11, no switching operation is required;
- if the number of the wind power units in each branch is greater than or equal to 6, but less than 11, one adjacent SC need to be closed;
- if the number of the wind power units in each branch is smaller than 6, two adjacent SCs need to be closed.

It is to be noted that if not specified, the switching strategies stated above and below are all based on the assumption that each faulty unit has two adjacent switch pairs. If a faulty unit is in the first/ last row/ column, then less switches are required to be closed.

6.3.2. SCENARIO-2: TWO UNITS IN THE SAME ROW GET FAULTY

In scenario-2, assume unit-*fc* and unit-*fd* get faulty (shown in Fig. 6.6). Without switching operation, the DC voltage of the non-faulty units in branch-*c* and branch-*d* will increase to the same level as in (6.8). The restriction for n is thus $n \geq 11$ as well. If n is smaller than 11, then at least two adjacent SCs (one for each fault) are need to be closed. The first possibility is

SC-1: {S13, S14, S16, S17} or {S16, S17, S19, S20}

Taking {S13, S14, S16, S17} being closed as an example, the enhanced branch is then termed as branch-*bcd*. Two unit voltage types are formed in branch-*bcd* – unit-*fb* is in type-1 and all the other non-faulty units are in type-2. Thus

$$\begin{cases} V_{p2} = 3 \times V_{p1} \\ V_{p1} + (n-1) \times V_{p2} = n \times V_N \end{cases} \tag{6.15}$$

With the voltage restriction of $V_{p2} \leq 1.1 V_N$, it is calculated that

$$n \geq 7.33 \tag{6.16}$$

There is also an alternate possible switch combination, given by

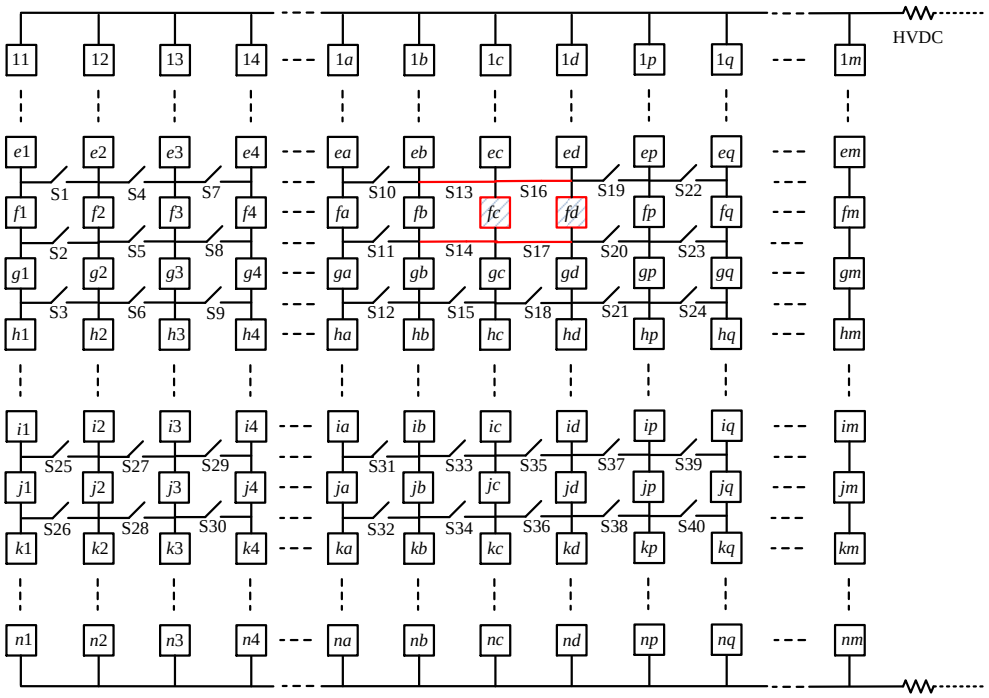

Fig. 6.6. Renumbered series-parallel DC collection with power switches for Scenario-2.

SC-2: {S13, S14, S19, S20}

Two enhanced branches of branch-*bc* and branch-*dp* are formed by closing {S13, S14, S19, S20}. These two branches are in the same situation as branch-*ab* in scenario-1. Therefore, the restriction for n here is the same as in (6.11). As the restriction in (6.16) is stricter than that in (6.11), SC-2 rather than SC-1 is preferred to be closed upon fault. This indicates that faulty branches should be avoided existing in a common enhanced branch. Overall, if $n \geq 6$, overvoltage can be prevented by closing SC-2.

However, if the number of units in a branch is less than 6, the following switch combination can be used.

SC-3: {S10, S11, S13, S14, S19, S20, S22, S23}

Apart from {S13, S14, S19, S20}, more switches are required to operate if $n <$ 6. As the two faulty units (unit-*fc* and unit-*fd*) have been bypassed, so are the switches between them ({S16, S17}). Therefore, closing {S16, S17} cannot generate any control effect. In this situation, the adjacent SCs of the two enhanced branches *bc* and *dp*, which are {S10, S11} on the left and {S22, S23} on the right, need to be chosen to operate. As a result, the SC becomes {S10, S11, S13, S14, S19, S20, S22, S23} and the new enhanced branches are branch-*abc* and branch-*dpq*. These two enhanced branches are in the same situation as branch-*abc* in scenario-1. Therefore, the restriction for *n* in (6.14) applies here.

In conclusion, overvoltage can be prevented by employing power switches in scenario-2. The switching schemes are summarized as:

- if the number of the wind power units in each branch is greater than or equal to 11, no switching operation is required;
- if the number of the wind power units in each branch is greater than or equal to 6, but less than 11, two adjacent SCs need to be closed on the condition that faulty branches should be included into different enhanced branches;
- if the number of the wind power units in each branch is smaller than 6, then two pairs of adjacent switches are required be closed for each fault on the condition that faulty branches should be included into different enhanced branches.

By incorporating the faulty branches into different enhanced branches, the switching conclusions in scenario-2 are essentially the same as those in scenario-1. It means that the optimum switching strategy for scenario-2 is to treat the two faulty units as a single faulty unit.

6.3.3. SCENARIO-3: TWO UNITS IN THE SAME BRANCH GET FAULTY

For this scenario, the minimum series connected units per branch is calculated to be 22 if power switches are not applied. When $n < 22$, the potential adjacent switches that need to be closed can be on same sides (left or right) of the faulty

branch or on different sides. These two potential switching strategies are discussed below by taking unit-*fc* and unit-*jc* getting faulty as an example (shown in Fig. 6.7).

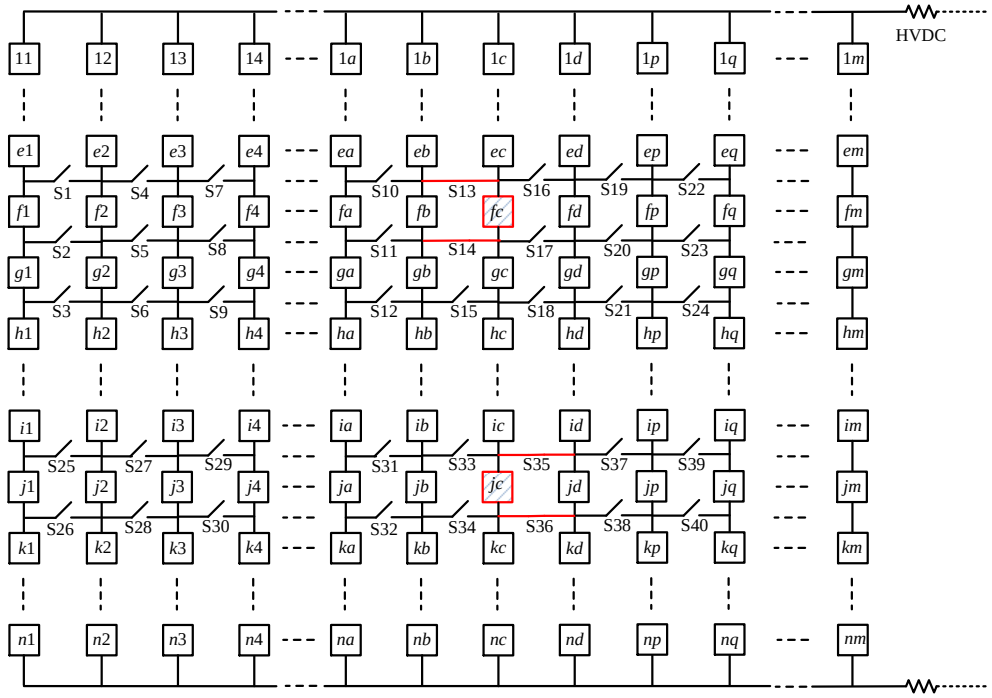

Fig. 6.7. Renumbered series-parallel DC collection with power switches for Scenario-3.

SC-1: switches on different sides

If {S13, S14, S35, S36} are selected to be closed, the enhanced branch is branch-*bcd*. It can be seen from Fig. 6.7 that unit-*gc* to unit-*ic* in branch-*c* have direct connections to both branch-*a* and branch-*b*, like a "bridge". An enhanced branch with a bridging connection is a bridging branch termed in this thesis. In fact, a bridging branch can be formed in various fault scenarios by closing certain groups of switches. The influence of bridging branches on the overvoltage control effect of series-parallel DC collection systems is discussed below.

A simple example is given in Fig. 6.8 (a), which shows a 3×3 series-parallel DC topology with power switches of S121, S122, S231 and S232. In accordance with fault scenario-3, suppose unit-12 and unit-32 are disconnected due to fault and the switches S121 and S232 are closed simultaneously. The new collection topology is shown in Fig. 6.8 (b), where the closed switches are shorted and the open switches are removed.

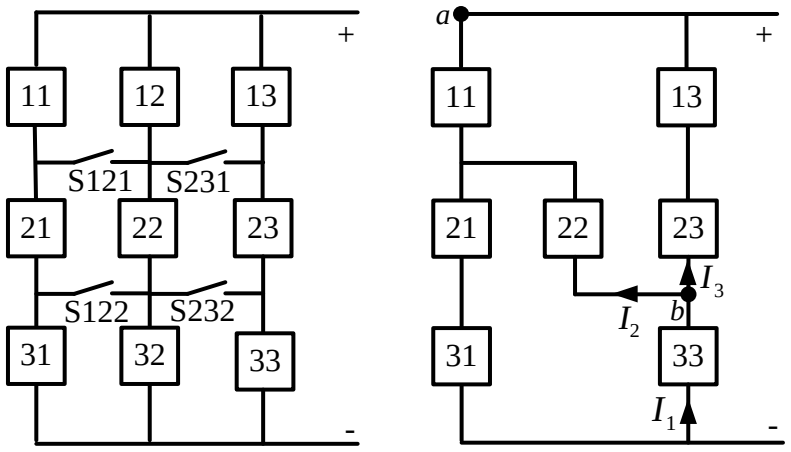

(a) (b)

Fig. 6.8. 3×3 series-parallel DC collection topology with power switches for scenario-3: (a) normal operation and (b) fault operation.

It can be seen from Fig. 6.8 (b) that three unit voltage types are formed in the fault operation mode. Let us assign that unit-11 and unit-31 are in type-1 with the voltage of V_{p1}, unit-22 is in type-2 with the voltage of V_{p2}, and the rest of the non-faulty units are in type-3 with the voltage of V_{p3}. Assume the DC currents through unit-33, unit-22 and unit-23 are I_1, I_2, and I_3 respectively, as shown in Fig. 6.8 (b), then using KCL, we get $I_1 = I_2 + I_3$, and hence $I_1 > I_2$. For equal power from all units, it can be obtained that

$$V_{p1} \times I_1 = V_{p2} \times I_2 \tag{6.17}$$

This indicates that $V_{p2} > V_{p1}$. From node *a* to node *b* marked in Fig. 6.8 (b), we get

$$2 \times V_{p3} = V_{p1} + V_{p2} \tag{6.18}$$

Therefore, $V_{p2} > V_{p3}$. This implies that the highest DC voltage amongst all the units will be impressed upon unit-22.

It can be seen from this example that a bridging branch introduces a higher voltage to units on the bridge and is better to be avoided. Therefore, the SC of {S13, S14, S35, S36} in Fig. 6.7 and any other switching operations resulting in bridging branches are not preferred.

SC-2: switches on same sides

Similar to the definitions of faulty and non-faulty branch, rows with and without faulty units are termed as faulty row and non-faulty row respectively. Here,

switches on same sides refers that the adjacent switches of the two faulty rows that are closed to bypass the two faulty units must be symmetrical. For example, with the faulty units *fc* and *jc*, if {S10, S11, S13, S14} in Fig. 6.7 are closed, then the switches on the symmetrical positions adjacent to the other faulty row {S31, S32, S33, S34} must be closed. Similarly, if {S13, S14, S16, S17} are closed, then {S33, S34, S35, S36} need to be closed. Only in this way can the bridging branches be avoided.

When adjacent switches on same sides of the two faulty units are selected, it is assumed that the non-faulty units in the faulty rows are in type-1 and the units in the non-faulty rows are in type-2. Suppose the number of non-faulty branches incorporated in the enhanced branch is *s*, then based on VDP, we get

$$\begin{cases} \dfrac{V_{p1}}{V_{p2}} = \dfrac{s}{s+1} \\ 2 \times V_{p1} + (n-2) \times V_{p2} = n \times V_N \end{cases} \tag{6.19}$$

Given that V_{p2} is larger than V_{p1}, V_{p2} is calculated from (6.19). With the restriction of $V_{p2} \leq 1.1 V_N$, it is obtained that

$$s \geq \frac{22}{n} - 1 \tag{6.20}$$

Therefore, the conclusion for scenario-3 is that overvoltage can be prevented by employing power switches. The switching strategy is that the corresponding switches are to be closed based on the included non-faulty branch number selected by (6.20).

6.3.4. SCENARIO-4: TWO UNITS IN DIFFERENT BRANCHES AND DIFFERENT ROWS GET FAULTY

It is obvious that a two-unit fault is more serious than a one-unit fault. Therefore, the best switching strategy for this scenario is to treat the two faulty units independently. This favoured strategy is the same as in scenario-2, where the two faulty units should be included in different enhanced branches.

However, for either scenario-2 or scenario-4, there are not always enough non-faulty branches to form one enhanced branch with each faulty one. The reason might

be the small number of wind power branches in a collection system or the faulty units are in the side branches (in/close to branch-1 or branch-*m*). For example, in Fig. 6.9, if unit-*f*1 and unit-*j*2 get faulty, {S1, S2} need to be closed to provide a current path for the non-faulty units in branch-1. This switching operation results in an enhanced branch containing two faulty branches. In this situation, the switching strategy should follow the same rule as for scenario-3, where switches on same sides must be closed. Therefore, {S25, S26} need to be closed together with {S1, S2} such that no bridging branch is generated. The reason for avoiding the bridging branch here for scenario-4 is discussed below.

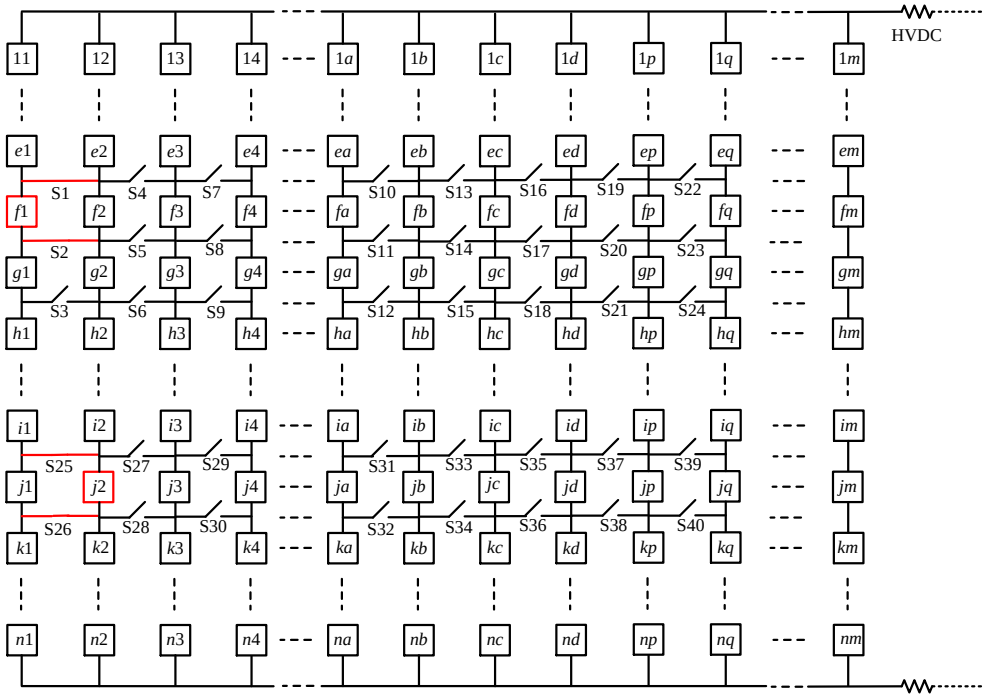

Fig. 6.9. Renumbered series-parallel DC collection with power switches for Scenario-4.

Using the 3×3 series-parallel topology in Fig. 6.8 (a) as an example, suppose switches S121 and S232 are closed when unit-11 and unit-33 are disconnected due to fault. The collection topologies before and after fault are illustrated in Fig. 6.10, where the DC currents through unit-32, unit-22 and unit-23 after switching operation are I_1, I_2 and I_3 respectively. Let us assume unit-32 and unit-12 are in type-1, unit-22 is in type-2 and the other non-faulty units are in type-3. Similar to the analysis in scenario-3, the following equations can be obtained.

$$\begin{cases} I_1 = I_2 + I_3 \Rightarrow I_1 > I_2 \\ V_{p1} \times I_1 = V_{p2} \times I_2 \\ 2 \times V_{p3} = V_{p1} + V_{p2} \end{cases} \tag{6.21}$$

It can be seen from (6.21) that the DC voltage of the bridging unit (V_{p2}) is the biggest among the three types of voltages. This result is the same as concluded in scenario-3, which indicates that bridging branches tend to cause higher unit voltages. In fact, with the ideal condition of equal unit power, the post-fault topology in Fig. 6.10 (b) is the same as in Fig. 6.8 (b). A further analysis demonstrating the high voltage of the bridging branch using Fig. 6.10 (b) is presented below.

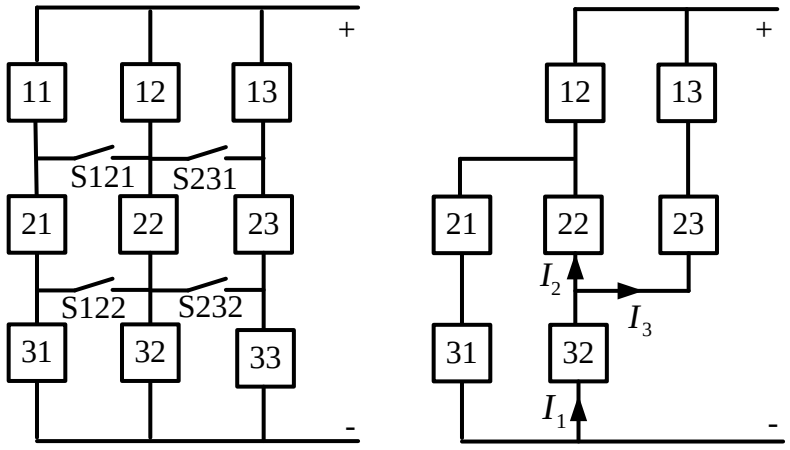

(a) (b)

Fig. 6.10. 3×3 series-parallel DC collection topology with power switches for scenario-4: (a) normal operation and (b) fault operation.

It can be seen from the first equation of (6.21) that

$$\begin{cases} I_1 > I_2 \\ I_1 > I_3 \end{cases} \tag{6.22}$$

With equal unit power outputs, it is obtained according to (6.22) that

$$\begin{cases} V_{p1} < V_{p2} \\ V_{p1} < V_{p3} \end{cases} \tag{6.23}$$

Since $V_{p3} < V_{p2}$, the voltage relationship among the three voltage types is

$$V_{p1} < V_{p3} < V_{p2} \tag{6.24}$$

The voltage relation in (6.24) is transformed into current relationship as

$$I_1 > I_3 > I_2 \tag{6.25}$$

Suppose $I_{av} = (I_2 + I_3) / 2$, then $I_1 = 2I_{av}$, $I_2 < I_{av}$. Based on the second equation of (6.21), it is obtained that

$$\frac{V_{p2}}{V_{p1}} = \frac{I_1}{I_2} > \frac{2I_{av}}{I_{av}} = 2 \tag{6.26}$$

Equation (6.26) indicates that the highest voltage is more than twice big as the lowest voltage in the post-fault topology. Therefore, to eliminate the bridging branch in Fig. 6.10 (b), the power switches {S122, S231} are closed apart from {S121, S232} to ensure switches on same sides are closed following scenario-3. This switching strategy (closing {S121, S122, S231, S232}) results only 2 unit voltage types and the ratio of the high voltage to the low voltage is only 1.5. This smaller voltage ratio implies a narrower voltage deviation range and thus better voltage limitation effect than when a bridging branch exists.

It is to be noted that bridging branches are only possible when faulty units are in different rows – scenario-3 and scenario-4. For these two scenarios, the maximum ratio of the high voltage to the low voltage is 2 without bridging branches. This happens when an enhanced branch is combined by 1 faulty and 1 non-faulty branches. However, the voltage ratio for topologies with bridging branches is always bigger than 2 as in (6.26). Therefore, bridging branches should be avoided on any fault scenario.

Overall, the conclusion for scenario-4 is that overvoltage can be prevented by employing power switches. The switching strategy is that the two faulty units are preferred to be treated independently as two one-fault units. When the two faulty units are included in one enhanced branch inevitably, switches on same sides should be closed to avoid bridging connection.

6.3.5. SIMULATION STUDIES

A 10×8 (m = 8, n = 10) series-parallel DC collection system is studied in PSCAD for all the fault scenarios discussed above. Ideal power sources are

employed to model the large number (80) of wind power units. The transmission voltage is set to be controlled at 75 kV by the GSC. It is noted that although the rated DC voltage and power of each unit remain unchanged from before, the AC side voltage of each WSC should be decreased to avoid tracking failure as mentioned previously. This cannot be simulated with ideal power sources but it has been assumed that all unit DC voltages are above the reduced lower limit when power switches are employed. It has been assumed that all the faults occur at 10 s and the faulty units for each scenario are set as:

- scenario-1: unit-23,
- scenario-2: {unit-23, unit-24},
- scenario-3: {unit-16, unit-36},
- scenario-4: {unit-26, unit-38} and {unit-17, unit-38}.

Based on switching conclusions from Subsections 6.3.1 to 6.3.4, the switches that to be closed for each fault scenario are listed as:

- scenario-1: the adjacent switch pair between unit-22 and unit-23,
- scenario-2: the adjacent switch pair between unit-22 and unit-23, plus the adjacent switch pair between unit-24 and unit-25,
- scenario-3: the two adjacent switch pairs between unit-16 and unit-18, plus the two adjacent switch pairs between unit-36 and unit-38,
- scenario-4: the adjacent switch pair between unit-25 and unit-26, plus the adjacent switch pair between unit-37 and unit-38 for the first fault condition {unit-26, unit-38}, and same switching strategy with scenario-3 for the second fault condition.

The simulation results are shown in Fig. 6.11, where V_{p0} represent the voltages of units which are not in the enhanced branches. V_{p1}, V_{p2}, V_{up} and V_T have the same meanings as before. With the switching strategies above, the faulty units in both scenario-2 and the first condition of scenario-4 are treated independently. Therefore, the resulting DC voltages in the two scenarios are the same with those in scenario-1, which are shown in Fig. 6.11 (a). The DC voltages in scenario-3 and the second condition in scenario-4 are shown in Figs. 6.11 (b) and 6.11 (c) respectively. It is clear from Fig. 6.11 that only two voltage types are formed in each scenario through

the proper switching operations. A scaled version of the transmission voltage (V_T) is shown in each figure, which is kept constant at its reference value (9.375 kV × 8 = 75 kV) irrespective of different fault scenarios. All unit voltages (V_{p0}, V_{p1}, V_{p2}) are below the upper limit (V_{up}) at steady states. It is noted that each DC voltage contain small fluctuations during fault transients.

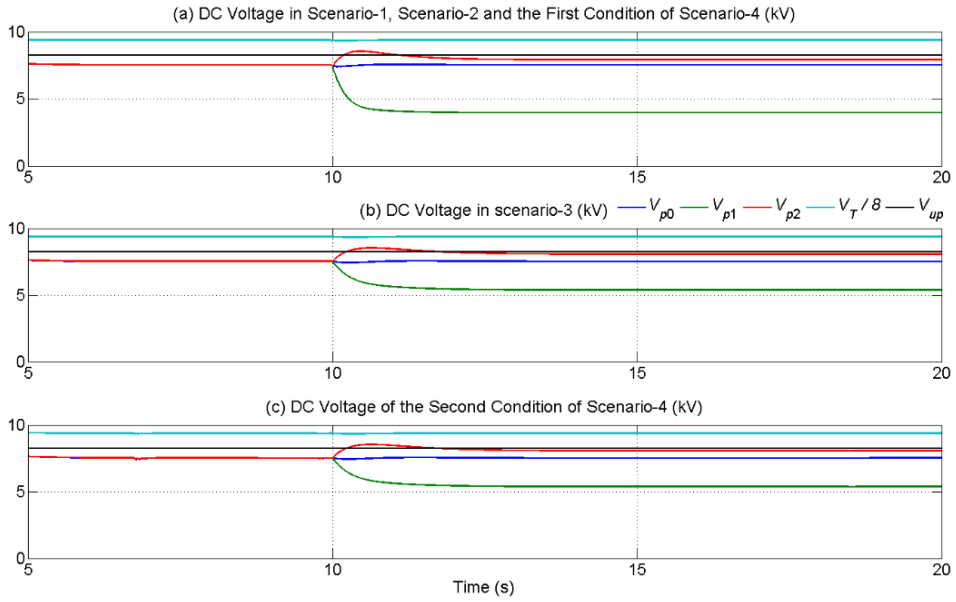

Fig. 6.11. Simulation results of 10×8 series-parallel DC collection topology with power switches for each scenario.

6.4. SERIES-PARALLEL DC COLLECTION SYSTEMS WITH POWER SWITCHES WHEN ARRAY EFFICIENCY < 1

On most conditions in real wind power projects, array efficiencies are smaller than 1. This is because downstream turbines are in a more turbulent flow environment than the upstream ones [121-122]. In this situation, closing the power switches on one side of the faulty unit generates different effects from closing the switches on the other side. In this section, the array efficiency is considered to be lower than 1 for further fault studies.

Derived from array efficiency, branch efficiency is defined as the power output of a downstream branch divided by that of its adjacent upstream branch and is denoted by K_{BE}. As the array efficiency is smaller than 1, K_{BE} is assumed to be between 0 and 1. Suppose the wind blows from the left side of the topology in Fig.

6.4, the power outputs of each unit in branch-1, branch-2, …, branch-*m* are thus respectively 1 (pu), K_{BE}, …, K^{m-1}_{BE}.

6.4.1. SWITCH SELECTION WITH ONE FAULTY UNIT

For a single fault scenario, taking unit-*f*2 getting faulty as an example (shown in Fig. 6.12), the adjacent upstream and downstream SCs are {S1, S2} and {S4, S5} respectively. It has been assumed that in an enhanced branch, a non-faulty unit in a faulty row is in type-1 and a unit in a non-faulty row is in type-2. According to VDP, we get

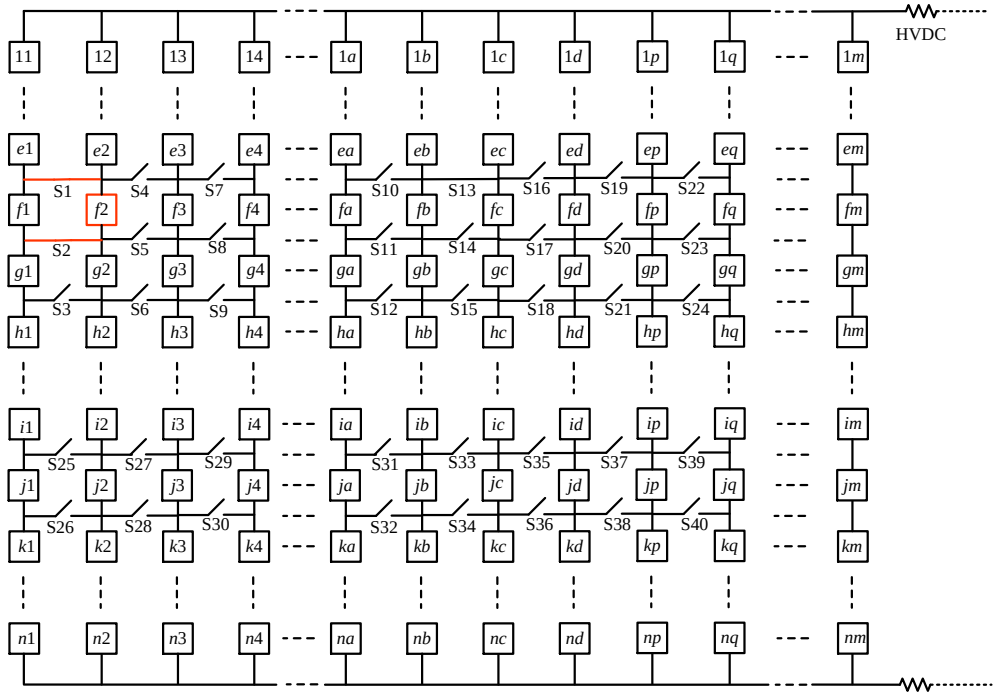

Fig. 6.12. Renumbered series-parallel DC collection with power switches for one faulty unit.

$$\begin{cases} \dfrac{V_{p1u}}{V_{p2u}} = \dfrac{1}{1+K_{BE}} \\ V_{p1u} + (n-1)\times V_{p2u} = n\times V_N \end{cases} \tag{6.27}$$

and

$$\begin{cases} \dfrac{V_{p1d}}{V_{p2d}} = \dfrac{K_{BE}^2}{K_{BE}^2 + K_{BE}} \\ V_{p1d} + (n-1)\times V_{p2d} = n\times V_N \end{cases} \tag{6.28}$$

where V_{p1u} and V_{p2u} represent the type-1 and type-2 voltages respectively by closing the adjacent upstream SC, while V_{p1d} and V_{p2d} denote the counterparts by closing the adjacent downstream SC. It is calculated from (6.27) and (6.28) that

$$\begin{cases} V_{p1u} = \dfrac{n}{n + K_{BE} \times (n-1)} \times V_N \\ V_{p2u} = \dfrac{(1 + K_{BE}) \times n}{n + K_{BE} \times (n-1)} \times V_N \end{cases} \tag{6.29}$$

and

$$\begin{cases} V_{p1d} = \dfrac{K_{BE} \times n}{n + K_{BE} \times n - 1} \times V_N \\ V_{p2d} = \dfrac{(1 + K_{BE}) \times n}{n + K_{BE} \times n - 1} \times V_N \end{cases} \tag{6.30}$$

It can be seen from (6.29) and (6.30) that the two type-2 voltages are bigger than their corresponding type-1 voltages. Furthermore, V_{p2u} is smaller than V_{p2d}. This indicates that closing the adjacent upstream switches of the faulty unit results in better fault voltage limitation than closing the adjacent downstream ones. It is obvious that this conclusion applies to other faulty units in the series-parallel system as well. Therefore, the adjacent upstream switches are preferred to be closed upon fault if both adjacent branches of the faulty branch are non-faulty. This switch selection method is termed as the Upstream Switch Preference Rule (USPR) in this thesis.

6.4.2. SWITCH SELECTION WITH TWO FAULTY UNITS

As per Section 6.3, for fault scenarios with two faulty units, each is preferred to be treated independently as two one-unit faults. This conclusion is termed as the Unit Independence Rule (UIR) for convenience. UIR has been proved for array efficiency of 1, but it needs to be reassessed when it is smaller than 1. For each faulty unit, if overvoltage can be prevented by incorporating certain upstream non-faulty branches in an enhanced branch, UIR is accordance with USPR. However, when a faulty branch exists among the to-be-incorporated upstream branches, UIR conflicts with USPR. To study this situation, suppose units-*fc* and unit-*fd* are the faulty units (shown in Fig. 6.13). According to UIR, the SC of {S13, S14, S19, S20} should be

closed upon fault (option-1), while the SC of {S13, S14, S16, S17} is to be closed following USPR (option-2).

For switching option-1, there will be two enhanced branches *bc* and *dp*, while the enhanced branch with option-2 is branch-*bcd*. It has been assumed that the per unit power outputs of units in branches *b*, *c*, *d*, *p* are K_{BE}^{b-1}, K_{BE}^{b}, K_{BE}^{b+1}, K_{BE}^{b+2} respectively. It is known from USPR that the type-2 voltage of the enhanced branch-*dp* is bigger than that of branch-*bc* when option-1 is applied. Therefore, the highest voltage with option-1 ($V^{(1)}_{p2}$) is calculated applying VDP to branch-*dp*, which is equal to V_{p2d} in (6.30). The type-2 voltage for switching option-2 ($V^{(2)}_{p2}$) is also calculated based on VDP as

$$V_{p2}^{(2)} = \frac{(1+K_{BE}+K_{BE}^2)\times n}{n+K_{BE}\times n+K_{BE}^2\times n-K_{BE}-K_{BE}^2}\times V_N \tag{6.31}$$

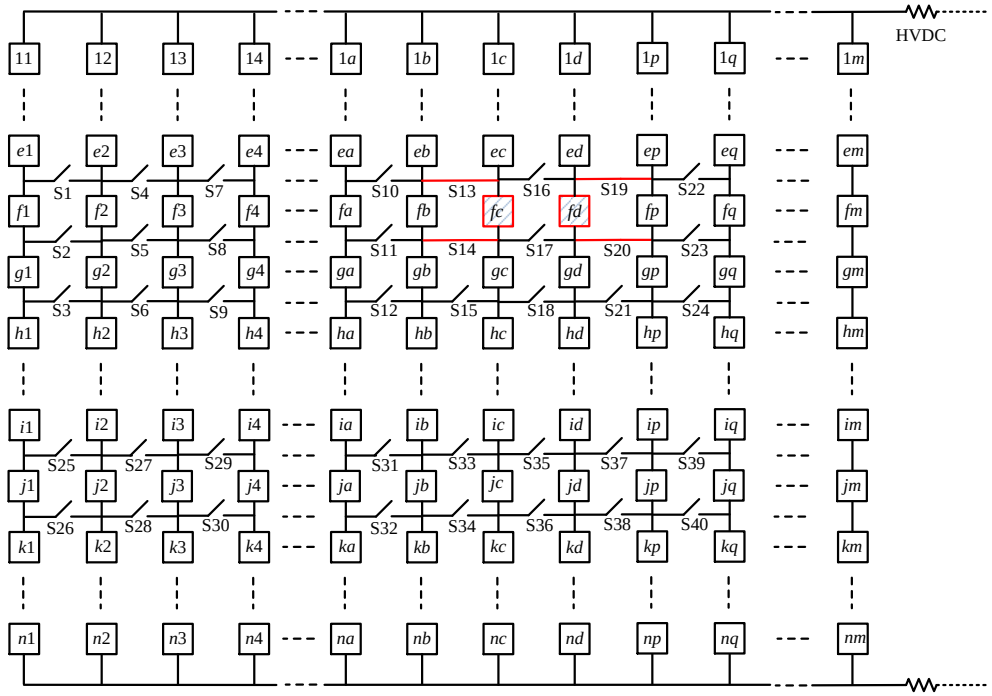

Fig. 6.13. Renumbered series-parallel DC collection with power switches for two faulty units.

To compare the voltage limitation effect of the two switching options, the difference between $V^{(1)}_{p2}$ and $V^{(2)}_{p2}$, denoted by V_{df}, is given by

$$V_{df} = V_{p2}^{(2)} - V_{p2}^{(1)} = \frac{(K_{BE}^3+K_{BE}^2-1)\times n\times V_N}{(n+K_{BE}\times n+K_{BE}^2\times n-K_{BE}-K_{BE}^2)\times(n+K_{BE}\times n-1)} \tag{6.32}$$

It is noticed that the denominator of (6.32) is bigger than 0. By assuming $V_{df} > 0$, we get that

$$K_{BE}^3 + K_{BE}^2 - 1 > 0 \tag{6.33}$$

With K_{BE} in the range of 0 to 1, it is calculated from (6.33) that

$$K_{BE} > 0.7549 \tag{6.34}$$

Equation (6.34) indicates that when $K_{BE} > 0.7549$, the assumption of $V_{df} > 0$ is correct and switching option-1 results in better voltage limitation effect. Similarly, when $K_{BE} < 0.7549$, switching option-2 is preferred and either option can be selected when $K_{BE} = 0.7549$. For offshore wind farms, the value of the branch efficiency (K_{BE}) is estimated below.

6.4.3. ESTIMATION OF BRANCH EFFICIENCY

Array efficiency is a concept based on the power output from an entire wind farm. In practical situations, neither wind speed nor wind direction is fixed or stable. So upstream branches can become downstream and wind turbines in a same branch may generate different amounts of power as well. Therefore, the previous calculations based on equal branch efficiency are simplistic. However, according to the data collected by WindPower Program, there is no obvious effect of branch position [101]. This is demonstrated by taking the Kentish Flats Project as an example.

The Kentish Flats wind farm in the Thames estuary started operating in 2006. It uses thirty Vestas V90 3 MW offshore wind turbines. The grid layout of the thirty turbines approximately follow the pattern of a 5×6 matrix. It is noted that the turbine layout here does not stand for the connection topology. In this project, turbines on the sixth line of the layout grid are more often downstream. The biggest power difference among wind turbines can be estimated by comparing the mean powers of the most upstream and most downstream turbines. The power ratio is defined as the mean power of the first line (line-1) turbines divided by that of the sixth line (line-6) turbines. Fig. 6.14 shows the power ratios based on data in 2006, where the mean values (power or wind speed) are monthly based.

It can be seen from Fig. 6.14 that the power ratios are scattered between approximately 0.95 and 1.09. A large power ratio indicates a large decrease in power from the upstream to the downstream, and thus, a low array efficiency. Therefore, the array efficiency is the lowest when the ratio is 1.09. It has been assumed that wind power between adjacent lines decreases at an equal branch efficiency from upstream to downstream. For the worst case, the smallest branch efficiency is calculated by using the biggest power ratio of 1.09. Suppose the mean power of line-1 is 1.09, then the mean power of line-6 is 1.0. From this, we get

$$1.09 \times K_{BE}^{5} = 1 \tag{6.35}$$

It is calculated from (6.35) that K_{BE} = 0.9829, which is far bigger than the boundary value of 0.7549 in (6.36). Therefore, V_{df} in (6.32) is bigger than 0 and switching option-1 in Subsection 6.4.2 is to be selected.

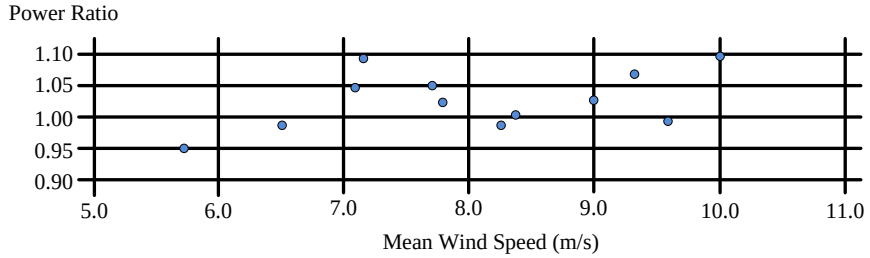

Fig. 6.14. Power comparison between the most upstream and downstream turbines of the Kentish Flats Project [101].

Typically, wind speed decreases when some of its energy is extracted by rotor blades. This indicates that the mean power tend to reduce from upstream to downstream as assumed in the example using the Kentish Flats wind farm. However, for some cases, the wind speed recovers at some distance downwind and so is the power. The wind speed recovery brings up the array efficiency of an offshore wind farm, which implies a bigger average branch efficiency. All in all, even with the array efficiency being non-ideal in an offshore wind farm, it is still preferred to treat faulty units independently.

In practice, the array efficiency cannot reach 1. The generic switching strategies when power switches are employed for a series-parallel DC collection system are concluded based on the discussions in Sections 6.3 and 6.4 as:

- deal with each fault independently if possible;
- if two faulty units have to be included in one enhanced branch, bridging branches should be avoided;
- if the two adjacent branches of the faulty unit are both non-faulty, close the adjacent switches upstream;
- no unnecessary switches are closed to maintain lowest switching power losses.

6.4.4. SIMULATION STUDIES

Simulation studies are conducted in PSCAD using the same series-parallel model as in Section 6.3. Suppose the wind blows from branch-1 to branch-8, the power outputs of branches 1 to 8 are given as 1 pu to 0.93 pu with a decrease of 0.01 pu between branches from upstream to downstream. To validate USPR and the small influence from array efficiency stated in this section, two fault conditions are considered. The faulty units for each condition are set as

- condition-1: {unit-16, unit-36}, and
- condition-2: {unit-23, unit-24}.

For condition-1, two adjacent branches need to be connected with the faulty branch (branch-6) as an enhanced branch according to (6.22). To demonstrate USPR, the voltage limitation effect with enhanced-456 is compared to that with enhanced branch-678. Fault condition-2 is to show UIR overruling USPR, of which two switching options are considered as in Subsection 6.4.2. According to UIR, the switch pair between unit-22 and unit-23 plus the pair between unit-24 and unit-25 are closed upon fault (option-1). Following USPR, two adjacent switch pairs between unit-22 and unit-24 are closed upon fault (option-2). Fault occurring time is still set as 10 s.

The simulation results are shown in Fig. 6.15, where all the denotations represent the same voltages as before. It can be seen that for both fault conditions, the DC voltages of all wind power units are limited below the upper limit (V_{up}) and settle at new steady states. The type-2 voltages (V_{p2}) in Figs. 6.15 (a) and 6.15 (b) are approximately 8.056 kV and 8.068 kV, which validates USPR. In Figs. 6.15 (c), the two type-2 voltages have the relationship of V_{p2d} (approximately 7.924 kV) bigger

than V_{p2u} (approximately 7.918 kV). This is in accordance with UIR. The type-2 voltage in Fig. 6.15 (d) is around 8.058 kV, which is much bigger than V_{p2d} (around 7.924 kV). Therefore, the switching option-1 results in better fault voltage control effect. This demonstrates the significance of keeping the independencies of the faulty units. A scaled version of the transmission voltage (V_T) is shown in each figure, which is always controlled constant (9.375 kV × 8 = 75 kV), barring small fluctuations when fault happens.

With the demonstrated control effectiveness for series-parallel DC collection systems using power switches, this strategy is not completely ideal. First, switching operations can not only prevent overvoltage but also cause decreases in the DC voltages of some wind power units. It is mentioned previously that to prevent tacking failure, a transformer might be needed to lower the input AC voltage of a WSC. An alternative way is to increase the rated DC voltage of each unit. With either way of voltage reference determination, a WSC will operate with a small modulation index, indicating a low utilization of a converter. Furthermore, the power switches add extra construction investment and complicate the control system of an offshore wind farm. Therefore, the employment of power switches should be based on the consideration of both control effect and economic matters.

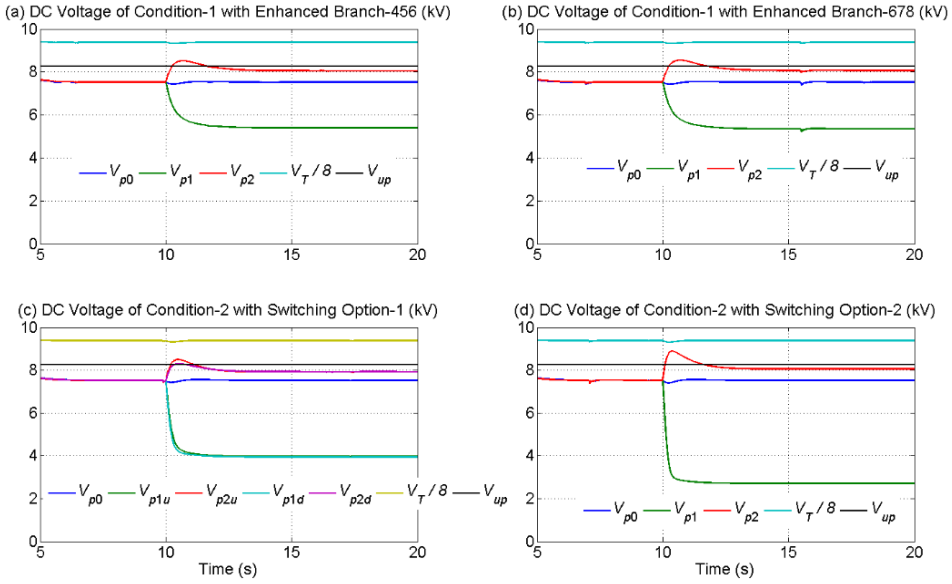

Fig. 6.15. Simulation results of 10×8 series-parallel DC collection topology with power switches considering array efficiency.

6.5. AUTO-TRANSFORMER APPLICATION

It has been proved that the employment of power switches is effective for overvoltage prevention of series-parallel DC collection systems. However, the disadvantages of this scheme are also discussed in the previous section. In this section, auto-transformers are employed such that the total added voltages of each wind power branch do not have to follow the transmission voltage reference on fault conditions.

6.5.1. EMPLOYMENT OF AUTO-TRANSFORMER BASED DC/DC CONVERTERS

According to VDP, the reason of voltage rising upon fault lies on a reduced number of wind power units sharing the unchanged transmission voltage. To deal with this problem, a DC/DC converter is employed for each wind power branch. The previously discussed single active bridge converter is adopted as the DC/DC converter here. Considering the high prices of high frequency transformers, an auto-transformer is used instead as the AC connection of each DC/DC converter. Considering that a three-phase autotransformer has the limitations of not suppressing harmonic currents and acting as another source of ground fault currents [123-124], only the single-phase type is applied in this thesis.

As part of the same winding acts as both the primary and secondary sides, an autotransformer is generally smaller, lighter, and cheaper than a typical dual-winding transformer. However, if the voltage turns-ratio is beyond 3:1 (high voltage winding to low voltage winding), a two-winding transformer is usually more economical [125]. In this section, the DC/DC converter is used to accommodate the voltage difference between a faulty branch and a normal one. Therefore, auto-transformers are expected to operate with small turns-ratios (approaching 1). Auto-transformers also have the advantages of lower leakage reactance, lower losses, lower excitation current, and increased VA rating for a given size and mass [126].

The schematic diagram of a series-parallel DC collection system with DC/DC converters is shown in Fig. 6.16, where a DC/DC converter is connected in parallel with each wind power branch. Suppose the series-parallel topology remains $n \times m$, it can be seen that the active bridge of each DC/DC converter is connected to the wind side, while the passive bridge is connected to the HVDC transmission lines. The

parallel connection of wind power branches is at the outputs of the DC/DC converters. The auto-transformer operates at a high frequency and has such a turns-ratio that the DC/DC converter operates as a boost converter. While the input DC voltages are variable, the output DC voltage of each DC/DC converter is the constant transmission voltage that is achieved by adjusting the duty cycle of each DC/DC converter.

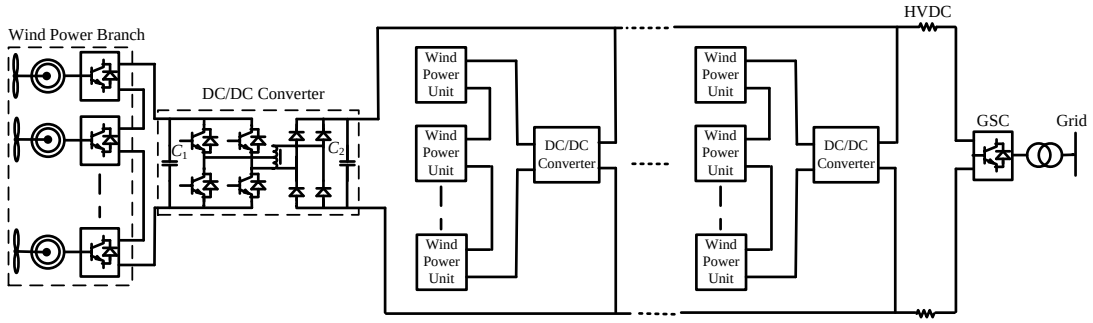

Fig. 6.16. An $n \times m$ series-parallel DC collection system with DC/DC converters.

It is assumed that the input DC voltages for branch-1, branch-2, …, branch-m are denoted by V_{l1}, V_{l2}, …, V_{lm} with references of V_{l1}^*, V_{l2}^*, …, V_{lm}^* respectively. The control scheme of the DC/DC converter is shown in Fig. 6.17, where V_{lx} and V_{lx}^* respectively represent the actual and reference input DC voltages of the DC/DC converter connected to branch-x (x = 1, 2, …, m). The error between V_{lx}^* and V_{lx} is sent to a PI controller and then a hard limiter. A triangular wave carrier is applied in the PWM control to get the control signal (u_{dx}) for switching control. It is noted that the triangular waveforms for each leg are phased shifted by 180° in this single-phase condition.

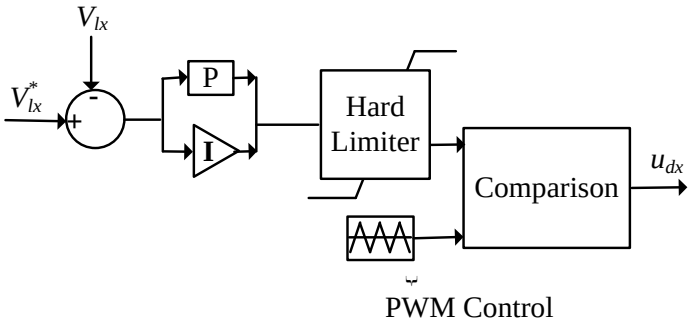

Fig. 6.17. Switching control of DC/DC converters in series-parallel DC collection systems.

During normal operation, $V_{l1}^* = V_{l2}^* = \ldots = V_{lm}^* = n \times V_N$. Suppose a unit in branch-k gets faulty, then the respective DC/DC converter will adjust V_{lk} to a lower

value by changing V_{lk}^{*} to $(n-1) \times V_N$. In this way, overvoltage is prevented as the non-faulty units in the faulty branch-k share a smaller voltage and each still operates around the DC voltage reference (V_N). Accordingly, when two faulty-units exist in a branch, the respective voltage reference will be adjusted to a further lower value by changing the input voltage reference of the connected DC/DC converter to $(n-2) \times V_N$. It is noted that the turns-ratio of the auto-transformers must meet the following equation

$$\frac{w_l}{w_h} < \frac{(n-2)\times V_N}{n \times V_N} = \frac{n-2}{n} \tag{6.36}$$

where w_l and w_h are the low voltage and high voltage windings respectively. Otherwise, the SAB cannot operate properly with a 2-unit fault in its corresponding branch.

The fault voltage control strategy with DC/DC converters proposed above is termed as Independent Branch Control (IBC) in this thesis. It can be seen from the control scheme of IBC that each DC/DC converter operates at a conversion ratio close to 1 with or without fault. This is in accordance with the expectation from the economical point of view. In conclusion, the DC voltage at the collection terminal reaches HVDC transmission level through the series connection structure, while IBC is only responsible for small voltage regulation on fault conditions.

6.5.2. SIMULATION STUDIES

Simulation studies of IBC applied in series-parallel DC collection systems are conducted in this subsection. First, a 2×2 simulation model with detailed representation of wind power units (detailed model) is employed, where unit-1 and unit-2 are in branch-1 and unit-3 and unit-4 are in branch-2. Second, a 4×2 series-parallel model with ideal power sources (simplified model) is simulated and the units are numbered in the matrix pattern. The previously developed WECS models are applied and related collection system parameters are listed in Table 6.1. As the control effectiveness of normal operation strategies (SSBA and PRM) on series-parallel systems has been validated in Section 6.1, it is assumed here that wind speed differences within a branch are ignored. Simulation results of using the detailed model and the simplified model are shown in Figs. 6.18 and 6.19 respectively.

Table 6.1: Related system parameters for the series-parallel simulation examples.

Simulation Model	System Quantities	Values
2×2 series-parallel simulation model	Rated input voltage of DC/DC converters	15 kV
	Nominal transmission voltage/ GSC input voltage	15 kV
	GSC output voltage	8 kV (RMS, line-to-line)
	Transformer turns ratio (w_l / w_h)	1: 2.14
	PI parameters for switching control	0.01 and 10 s
4×2 series-parallel simulation model	Rated input voltage of DC/DC converters	30 kV
	Nominal transmission voltage/ GSC input voltage	30 kV
	GSC output voltage	16 kV (RMS, line-to-line)
	Transformer turns ratio (w_l / w_h)	1: 1.43
	PI parameters for switching control	0.01 and 100 s

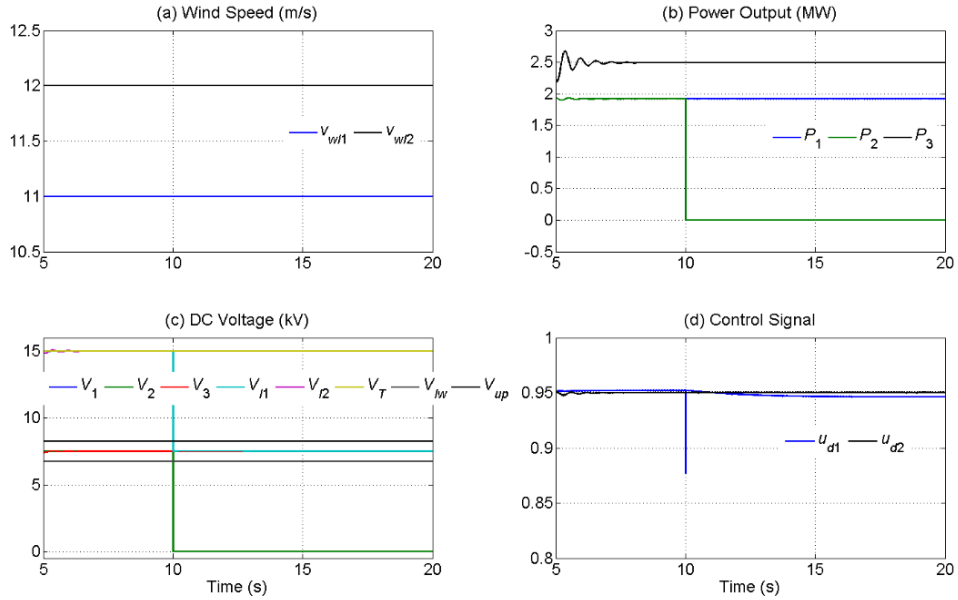

Fig. 6.18. Simulation results with the 2×2 detailed model.

In the 2×2 system, unit-2 is assumed to get faulty at 10 s. The wind speeds for turbines in branch-1 and branch-2 are represented by v_{wl1} and v_{wl2} with their respective values of 11 m/s and 12 m/s. These are plotted in Fig. 6.18 (a). The wind power outputs and DC voltages are illustrated in Figs. 6.18 (b) and 6.18 (c) respectively, where P_4 and U_4 are not shown as the simulation results for unit-3 and unit-4 are same. It can be seen from Fig. 6.18 (b) that P_3 is bigger than P_1 and P_2 due to the bigger wind speed for branch-2 (v_{wl2}) and P_2 drops to 0 upon fault. Fig. 6.18 (c) shows that all the non-faulty units operate at the rated DC voltage irrespective of fault. It can also be seen that the input voltage of the DC/DC converter for branch-1

(V_{l1}) decreases to 7.5 kV after fault, while its counterpart for branch-2 (V_{l2}) and the transmission voltage (V_T) stay unchanged. It can be seen from Fig. 6.18 (d) that the switch control signal for branch-2 (u_{d1}) is reduced after fault, which is to achieve the new input voltage reference (7.5 kV) of the DC/DC converter for branch-1. Despite the change in u_{d1}, u_{d2} is constant as no fault occurs in branch-2.

For the 2×4 series-parallel DC collection system, the power output of each unit is 2.5 MW for branch-1 and 2.0 MW for branch-2. The fault condition is set as unit-41 becomes faulty at 20 s. The DC voltages are shown in Fig. 6.19 (a), where V_{11} and V_{12} represent the voltages of the non-faulty units in branch-1 and branch-2 respectively. It can be seen that the input voltage of the DC/DC converter for branch-1 (V_{l1}) drops to the new reference value of 22.5 kV after fault transient. The transmission voltage (V_T), and the unit voltage in branch-1 (V_{11}) are kept constant at their respective rated values barring acceptable fluctuations upon fault. It is also noticed through the waveforms of V_{l2} and V_{12} that the fault occurrence in branch-1 has negligible influences on branch-2. Fig. 6.19 (b) shows the PWM control signals of the two DC/DC converters (u_{d1} for branch-1 and u_{d2} for branch-2). It can be seen that u_{d1} decreases after fault to coordinate the new input voltage reference and the constant output voltage reference of the DC/DC converter connected to branch-1. In accordance with the voltage transients in Fig. 6.19 (a), u_{d1} experiences fluctuations and u_{d2} has almost no transients upon fault.

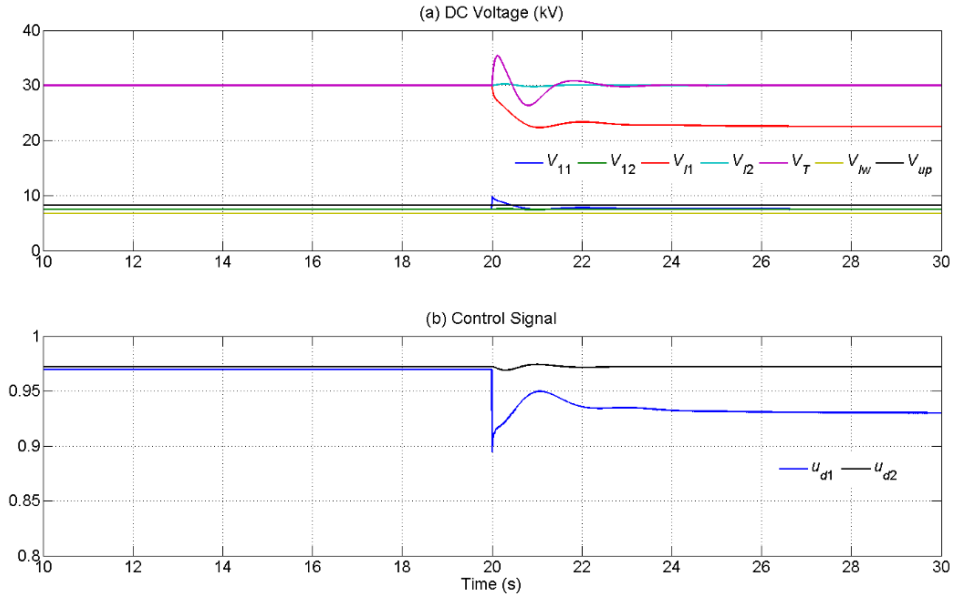

Fig. 6.19. Simulation results with the 4×2 simplified model.

6.6. CONCLUSIONS

The series-parallel DC collection topology for offshore wind farms is discussed in this chapter. It has been analysed and demonstrated that the strategies of SSBA and PRM designed for the series DC collection system in Chapter 4 apply to the series-parallel DC collection system effectively. For fault conditions, the IVRM (Input Voltage Reference Modification) proposed in Chapter 5 can only ensure the safe operation of series-parallel DC collection systems with at least 11 units in each branch.

To suit series-parallel DC collection systems of all scales, power switches are employed to prevent overvoltage upon fault. First, the array efficiency of an offshore wind farm is assumed to be 1. Failure of wind turbines in different locations are analysed and corresponding switching strategies of power switches are determined. Second, the array efficiency is considered as smaller than 1. Based on calculations for different switch selection with different fault locations, the array efficiency shows no significant influence on switching strategies of power switches. The general fault voltage control rule of using power switches in series-parallel DC collection systems are summarised as avoiding fault interconnection and operating upstream switches when both adjacent branches are non-faulty. Proper switches need be closed to prevent bridging connection if faults cannot be treated independently. To maintain low power losses, all the switching strategies should ensure that no unnecessary switches are involved.

Despite of its satisfactory control effect, the employment of power switches adds extra cost and power losses. As a competitive strategy for series-parallel DC collection systems, a DC/DC converter is connected at the terminal of each wind power branch to realize independent voltage control among branches. The outputs of the DC/DC converters are then connected in parallel. The DC/DC converter applied in the IBC (Independent Branch Control) strategy is a single-phase SAB (Single Active Bridge) with an auto-transformer. The DC voltage of each unit can be controlled around the rated value with IBC. Compared to power switch application, IBC features a simpler control system, more efficient control effect, possibly less cost and lower power losses.

Extensive simulation studies of the two fault voltage control strategies applied for series-parallel DC collection systems are conducted in PSCAD. Various simulation conditions are considered including the selection of wind power unit models (detailed or simplified) and array efficiencies (unit or non-unit). The simulation results validate the safe operation of series-parallel DC collection systems for offshore wind farms with the proposed strategies.

CHAPTER 7

MULTI-TERMINAL OPERATION OF OFFSHORE WIND FARMS

Two or more offshore wind farms form a multi-terminal HVDC transmission system with an onshore grid. To maintain the reference terminal voltage of each collection system, the DC side voltage of the grid is manipulated according to the instantaneous power outputs and terminal voltages of each wind farm. In the previous chapters, the HVDC transmission losses have not been discussed explicitly. The resistances of HVDC cable systems will affect the power flow and can result in loop flows in a multi-terminal HVDC system, while this is not important for a point-to-point HVDC system. However, careful consideration needs to be given for the power flow control in a multi-terminal DC grid.

Three different DC collection topologies for offshore wind farms and their control methods are discussed in details in Chapters 3 to 6. The discussion in these chapters assume that these are used for point-to-point HVDC transmission, where the offshore wind power is transmitted to an onshore AC grid. This chapter studies multi-terminal HVDC transmission, where two DC collection systems are connected in parallel with the DC side of a grid through HVDC lines, as shown in Fig. 7.1, where l_1, l_2 and l_3 are the three DC lines. Three different combinations of DC collection topologies for two wind farms are considered for the studies in this chapter: (a) two parallel DC collection systems, (b) one parallel plus one series DC collection system and (c) two series DC collection systems. The series-parallel DC collection system is not discussed here since its operation is similar to that of the series DC collection system.

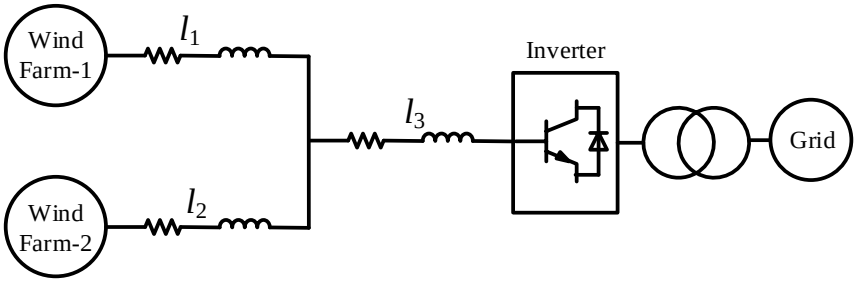

Fig. 7.1. A simple 3-terminal HVDC system.

This chapter focuses on a 3-terminal HVDC system, in which two offshore wind farms are connected together and then to an onshore grid through 3 DC lines, as shown in Fig. 7.1. For a specific system, first the Integration Point (I-point) of the two offshore wind farms with the grid is located. Second, different types of wind power collection topologies are applied to the 3-terminal HVDC system. If one or both offshore wind farms employ the parallel DC collection system, the voltages at the parallel connection point in each wind farm can be maintained at their respective references through the employed DC/DC converters. When wind powers from both wind farms are collected through the series DC collection system, the resistances of transmission cables need to be changed. In this case, variable resistors are applied to facilitate wind power flow to the grid. Finally, simulation studies under various operation conditions are conducted in PSCAD to validate the proposed voltage control strategies.

7.1. INTEGRATION POINT LOCATION FOR OFFSHORE WIND FARMS

In a multi-terminal HVDC system, offshore wind farms are connected in parallel with the grid. The terminal voltages of each wind farm should be equally constant during normal operation, which is essentially the transmission voltage (V_T) used in the previous chapters. Depending on the geographical locations of each terminal, voltage drops on the HVDC lines vary when different integration points are selected. Furthermore, the fluctuating power outputs and turbine failures of wind farms influence the voltage drops as well. In this section, the I-point of a 3-terminal HVDC system is located for voltage control studies.

7.1.1. INTEGRATION RULE OF OFFSHORE WIND FARMS

In Chapter 4, it has been shown how the PRM method can be employed to reduce the entire output of an offshore wind farm to maintain the voltages in a series DC collection system. In Doubly Fed Induction Generator (DFIG) based WECSs, crowbars are widely employed to dissipate excess wind power [127-130]. Besides, DC cable transmission has power losses as low as around 0.3% to 0.4% per 100 km [131]. However, while planning a multi-terminal HVDC system, careful consideration must be given to the cost of HVDC cables. Longer cables will incur higher costs. Therefore, the I-point selection of a multi-terminal HVDC system

generally aims at the shortest cable length rather than the lowest power loss. Also, the shorter the cables are, the lower the power losses are.

Both submarine and land cables can be of various types [132]. Therefore, it is imperative that the cable resistances are normalized to a uniform standard. Suppose the reference cable has a resistance of per unit length denoted by R_B, then the physical lengths of each cable can be converted to new values taking R_B as the base resistance. A converted cable length is termed as a Relative Cable Length (RCL) in this chapter. The conversion equation is given by

$$l_i = \frac{R_i}{R_B} \tag{7.1}$$

where R_i (i = 1, 2, 3) is the per unit length resistance of cable-i and l_i is the RCL of cable-i. It is to be noted that all the cable lengths used in this chapter are represented in their RCLs.

A 3-terminal HVDC system (2 offshore wind farms and 1 grid) is studied for the I-point location. Let us denote the cables connected to Wind Farm-1 (WF-1), Wind Farm-2 (WF-2) and the grid respectively as cable-1 (with length of l_1), cable-2 (with length of l_2) and cable-3 (with length of l_3). Fig. 7.2 shows the DC voltage distribution against RCL under different circumstances. In this, the vertical axes V_{l1}, V_{l2} and V_{l3} denote the distributed voltages on cable-1, cable-2 and cable-3 respectively and the horizontal axis l is the RCL. The voltage drops in V_{l1}, V_{l2} and V_{l3} are respectively shown in green, red and blue. It has been assumed that l = 0 at the beginning of cable-1. The rest of the parameters shown in Fig. 7.2 are defined as:

V_T – Terminal DC voltage of the two offshore wind farms;
V_I – DC voltage at the I-point;
V_G – DC voltage at the grid terminal;
l_d – RCL difference of the two cables (cable-1 and cable-2);
l_I / l_G – RCL to the I-point / grid;
l_{G1} / l_{G2}– RCL between WF-1 / WF-2 and the grid.

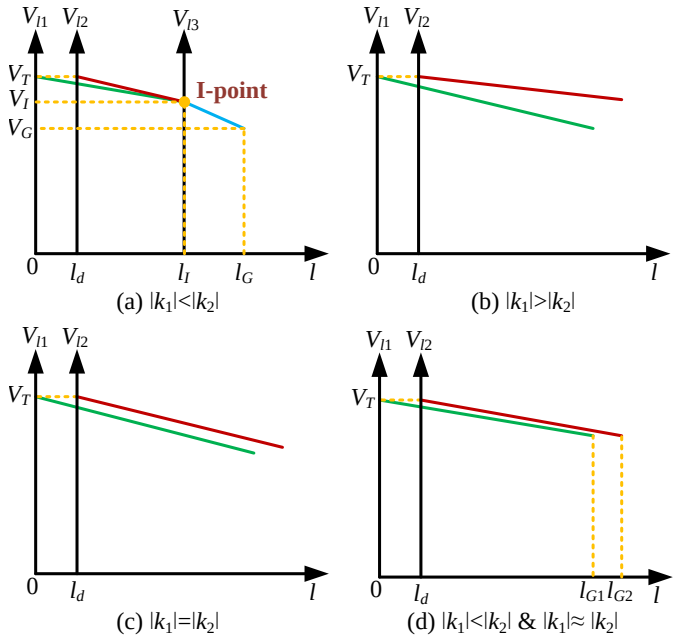

Fig. 7.2. Voltage characteristics of a 3-terminal HVDC system.

It can be seen from Fig. 7.2 that as RCL gets bigger, both V_{l1} and V_{l2} drop from the DC terminal voltage V_T with fixed slopes. Note that these slopes are shallow due to high transmission voltage level. A proper cable selection, in which an I-point can be reached, is shown in Fig. 7.2 (a). In this, V_{l1} and V_{l2} intersect at a distance of l_I, which is the predefined I-point. After cable-1 and cable-2 are connected, the power from the two offshore wind farms is delivered to the grid by cable-3. The voltage on cable-3 drops from V_I as RCL increases and the dropping rate is slightly bigger. V_{l3} decreases to V_G when cable-3 reaches the grid at the RCL of l_G.

The decreasing rate of a DC terminal voltage is dependent on the power output of the offshore wind farm. For a 3-terminal system, assume the power output from a wind farm is P_{wi} (i = 1, 2), then

$$I_i = \frac{P_{wi}}{V_T} \tag{7.2}$$

where I_i is the current flowing through cable-i. The slope of the voltage drop (k_i) is given by

$$-k_i = \frac{\Delta V_{li}}{\Delta l} = \frac{\Delta V_{li}}{\frac{\Delta R_i}{R_B}} = I_i \times R_B \tag{7.3}$$

Equation (7.2) indicates that the current flowing through (say) cable-1, is the power output from WF-1, divided by its terminal voltage. Then (7.3) indicates that the slope of the voltage drop is fixed at an instant and is proportional to the current only.

It can be seen in the case of Fig 7.2 (a) that $|k_1|$ is smaller than $|k_2|$. According to (7.2), this implies that P_{w1} is smaller than P_{w2}. Figs. 7.2 (b) to 7.2 (d) show the situations when an I-point cannot be located. In Fig. 7.2 (b), V_{l1} and V_{l2} drift away with the increasing of l as $|k_1| > |k_2|$. In Fig. 7.2 (c), where $|k_1| = |k_2|$, V_{l1} and V_{l2} are in parallel and do not cross either. In the case of Fig. 7.2 (d), although $|k_1| < |k_2|$, V_{l1} and V_{l2} drop at similar rates and cannot cross before cable-1 and cable-2 reach the grid. The three latter cases result in no I-point, which indicates no power flow can occur. Therefore, the integration rule of offshore wind farms in a multi-terminal HVDC system is that the I-point must have a certain longer RCL to the wind farm with the lowest power output than to the other wind farms. Consider the situation illustrated by Fig. 7.2 (c), where $P_{w1} = P_{w2}$, l_d must be equal to 0.

7.1.2. DETERMINATION OF I-POINT LOCATION

The locations of a 3-terminal HVDC system are set in a coordinate system as shown in Fig. 7.3. In this, the green dots, red dot and yellow dot represent the offshore wind farms, the grid and the assumed I-point respectively. Suppose the coordinate values (based on RCLs) of WF-1, WF-2, the grid and the I-point are (x_1, y_1), (x_2, y_2), (x_0, y_0) and (x_I, y_I) respectively, then the shortest cable length is achieved when L_T, which is given by the following equation, is minimised.

$$L_T = \sqrt{(x_1 - x_I)^2 + (y_1 - y_I)^2} + \sqrt{(x_2 - x_I)^2 + (y_2 - y_I)^2} + \sqrt{(x_0 - x_I)^2 + (y_0 - y_I)^2} \tag{7.4}$$

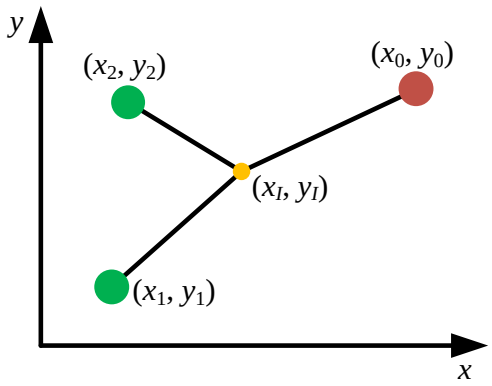

Fig. 7.3. Coordinate location of a 3-terminal HVDC system.

It has been analysed in the previous subsection that the I-point location is related to the power outputs of the two wind farms. In accordance with the nominal operation of a 3-terminal HVDC system, the I-point is located based on the rated capacities of the wind farms. As per Fig. 7.2 (a), it has been assumed that WF-1 and WF-2 have the rated capacities of P_{r1} and P_{r2} respectively and $P_{r1} < P_{r2}$.

The equations for V_{l1}, V_{l2} and V_{l3} in Fig. 7.2 (a) can be obtained through the starting points (0, V_T), (l_d, V_T), (l_G, V_G) and the I-point (l_I, V_I). These are given as

$$\begin{cases} V_{l1} = \dfrac{V_I - V_T}{l_I} \times l + V_T \ \text{(shown in green)} \\ V_{l2} = \dfrac{V_I - V_T}{l_I - l_d} \times l + \dfrac{V_T \times l_I - V_I \times l_d}{l_I - l_d} \ \text{(shown in red)} \\ V_{l3} = \dfrac{V_G - V_I}{l_G - l_I} \times l + \dfrac{V_I \times l_G - V_G \times l_I}{l_G - l_I} \ \text{(shown in blue)} \end{cases} \tag{7.5}$$

Using (7.3), the following equations are obtained

$$-k_1 = -\frac{V_I - V_T}{l_I} = \frac{P_{r1}}{V_T} \times R_B \tag{7.6}$$

$$-k_2 = -\frac{V_I - V_T}{l_I - l_d} = \frac{P_{r2}}{V_T} \times R_B \tag{7.7}$$

$$-k_3 = -\frac{V_G - V_I}{l_G - l_I} = \frac{P_I}{V_I} \times R_B \tag{7.8}$$

where k_3 is the slope of V_{l3} and P_I is the power at the I-point, which is calculated by deducting the power losses on cable-1 and cable-2 from the total wind power generation by the two wind farms. This is given by

$$P_I = [P_{r1} - (\frac{P_{r1}}{V_T})^2 \times l_I \times R_B] + [P_{r2} - (\frac{P_{r2}}{V_T})^2 \times (l_I - l_d) \times R_B] \tag{7.9}$$

From (7.6) and (7.7), we get

$$l_I = \frac{(V_T - V_I) \times V_T}{P_{r1} \times R_B} \tag{7.10}$$

$$l_I - l_d = \frac{(V_T - V_I) \times V_T}{P_{r2} \times R_B} \tag{7.11}$$

Hence the power at the I-point is obtained by substituting (7.10) and (7.11) into (7.9) as

$$P_I = (P_{r1} + P_{r2}) \times (\frac{V_I}{V_T}) \tag{7.12}$$

Furthermore, the RCL from the I-point to the grid is calculated by substituting (7.12) into (7.8) and is written as

$$l_G - l_I = \frac{(V_I - V_G) \times V_T}{(P_{r1} + P_{r2}) \times R_B} \tag{7.13}$$

Based on Fig. 7.3 and (7.10) to (7.13), we get

$$\sqrt{(x_1 - x_I)^2 + (y_1 - y_I)^2} = l_I = \frac{(V_T - V_I) \times V_T}{P_{r1} \times R_B} \tag{7.14}$$

$$\sqrt{(x_2 - x_I)^2 + (y_2 - y_I)^2} = l_I - l_d = \frac{(V_T - V_I) \times V_T}{P_{r2} \times R_B} \tag{7.15}$$

$$\sqrt{(x_0 - x_I)^2 + (y_0 - y_I)^2} = l_G - l_I = \frac{(V_I - V_G) \times V_T}{(P_{r2} + P_{r2}) \times R_B} \tag{7.16}$$

Combining (7.14) and (7.15), the coordinate values of the I-point (x_I, y_I) can be written as two functions of V_I, which are given by

$$\begin{cases} x_I = f(V_I) \\ y_I = g(V_I) \end{cases} \tag{7.17}$$

Substituting (7.17) into (7.16), we get the relationship between V_I and V_G. Therefore, V_G can also be written as a function regarding V_I, which is given by

$$V_G = h(V_I) \tag{7.18}$$

The shortest cable length L_T in (7.4) can be rewritten using known values and V_I by combining (7.14), (7.15), (7.16) and (7.18). This is given by

$$L_T = \frac{(V_T - V_I) \times V_T}{P_{r1} \times R_B} + \frac{(V_T - V_I) \times V_T}{P_{r2} \times R_B} + \frac{(V_I - h(V_I)) \times V_T}{(P_{r2} + P_{r2}) \times R_B} \tag{7.19}$$

Therefore, the I-point location problem is converted into a problem of determining V_I such that L_T is minimized. It is obvious from Fig. 7.2 (a) that V_I can vary between 0 and V_T. However, not all the values within this wide range can be used as a potential V_I. The boundary values for V_I are obtained below.

First, V_{l1} and V_{l2} must drop to an equal value at some point before or when cable-1 and cable-2 reach the grid. Therefore, a boundary condition is when the I-point is at the grid terminal and the boundary value of l_d (denoted by l_{dB}) is given by

$$l_{dB} = \sqrt{(x_1 - x_0)^2 + (y_1 - y_0)^2} - \sqrt{(x_2 - x_0)^2 + (y_2 - y_0)^2} \tag{7.20}$$

To determine the meaning of l_{dB}, Fig. 7.2 (a) is modified as shown in Fig. 7.4. In this, the voltage and cable lengths denoted with the superscript (′) represent the corresponding values with the I-point closer to the grid. It can be seen that with an equal V_T, a smaller l_d results in a smaller l_I. Therefore, the boundary value l_{dB} is the upper limit of l_d, which implies

$$l_d \leq l_{dB} \tag{7.21}$$

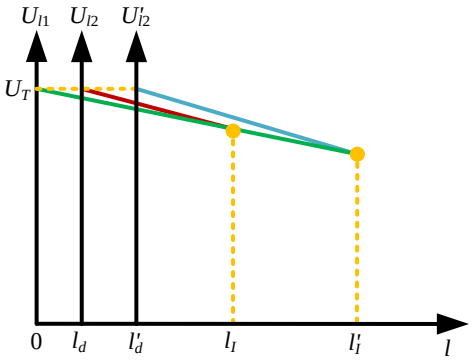

Fig. 7.4. Voltage characteristics with different l_d.

From (7.10) and (7.11), we get

$$l_d = l_I - (l_I - l_d) = \frac{(V_T - V_I) \times V_T}{R_B} \times (\frac{1}{P_{r1}} - \frac{1}{P_{r2}}) \tag{7.22}$$

Using (7.20) and (7.22), (7.21) is converted to

$$\frac{(V_T - V_I) \times V_T}{R_B} \times (\frac{1}{P_{r1}} - \frac{1}{P_{r2}}) \leq \sqrt{(x_1 - x_0)^2 + (y_1 - y_0)^2} - \sqrt{(x_2 - x_0)^2 + (y_2 - y_0)^2} \tag{7.23}$$

The first restriction for V_I is obtained by solving (7.23) as

$$V_I \geq V_T - \frac{R_B \times P_{r2} \times P_{r1} \times [\sqrt{(x_1 - x_0)^2 + (y_1 - y_0)^2} - \sqrt{(x_2 - x_0)^2 + (y_2 - y_0)^2}]}{V_T \times (P_{r2} - P_{r1})} \tag{7.24}$$

The second restriction for V_I is based on the triangle rule that the addition of any two sides of a triangle is bigger than the third side. By referring Fig. 7.3, we get that the added length of cable-1 and cable-2 must be no shorter than the distance between the two offshore wind farms. This is represented by

$$l_I + (l_I - l_d) \geq \sqrt{(x_1 - x_2)^2 + (y_1 - y_2)^2} \tag{7.25}$$

Similarly, by using (7.10) and (7.11), (7.25) is transformed into

$$\frac{(V_T - V_I) \times V_T}{R_B} \times (\frac{1}{P_{r1}} + \frac{1}{P_{r2}}) \geq \sqrt{(x_1 - x_2)^2 + (y_1 - y_2)^2} \tag{7.26}$$

The second restriction for V_I is thus obtained by solving (7.26) and given by

$$V_I \le V_T - \frac{R_B \times P_{r2} \times P_{r1} \times \sqrt{(x_1 - x_2)^2 + (y_1 - y_2)^2}}{V_T \times (P_{r2} + P_{r1})} \tag{7.27}$$

Therefore, with the restrictions in (7.24) and (7.27), a V_I can be determined to gain the minimum L_T in (7.19) within the safe operation range. The coordinate values of the I-point are then obtained through (7.17), which indicates that the I-point of the 3-terminal HVDC system has been located. It is to be noted that extra control strategies are required to maintain the voltage stability at the I-point as wind power outputs fluctuate with wind speeds. Besides, the terminal voltage of a series DC collection system might be reduced on fault conditions. The I-point voltage stability of a 3-terminal HVDC system is discussed in the next section.

7.2. I-POINT VOLTAGE STABILITY WITH DIFFERENT COLLECTION SYSTEMS

As the I-point of a 3-terminal HVDC system has been located based on nominal operation, the voltage stability at the I-point cannot be guaranteed by manipulating the grid voltage under all circumstances. In this section, different collection topologies for offshore wind farms are discussed for 3-terminal HVDC systems. Corresponding voltage control strategies are put forward considering various conditions of operation.

A schematic diagram of a 3-terminal HVDC system is illustrated in Fig. 7.5, where the two offshore DC collection systems and the DC side of the grid are simplified as voltage sources. As per the last section, the terminal voltages of the two wind farms and the grid are denoted by V_{T1}, V_{T2} and V_G respectively with the I-point voltage represented by V_I. The currents (I_1, I_2 and $I = I_1 + I_2$) are marked in the circuit as well. The line resistances between WF-1 and the I-point, between WF-2 and the I-point, between the I-point and the grid are assumed to be R_1, R_2 and R_0 respectively.

The circuit equations for the 3-terminal HVDC system are given by

$$V_{T1} - I_1 \times R_1 = V_{T2} - I_2 \times R_2 = V_G + (I_1 + I_2) \times R_0 = V_I \tag{7.28}$$

As the currents of the 3-terminal HVDC system are not under control, it can be concluded from (7.28) that either the terminal voltages or line resistances need to be

adjusted for the I-point voltage equalization. All the discussions in the rest of the chapter are based on Fig. 7.5. The voltage and power levels are generally selected according to the WECS applied in the previous chapters. It is to be noted that V_{T1} and V_{T2} might or might not be equal to V_T in the last section – this depends on the operation conditions.

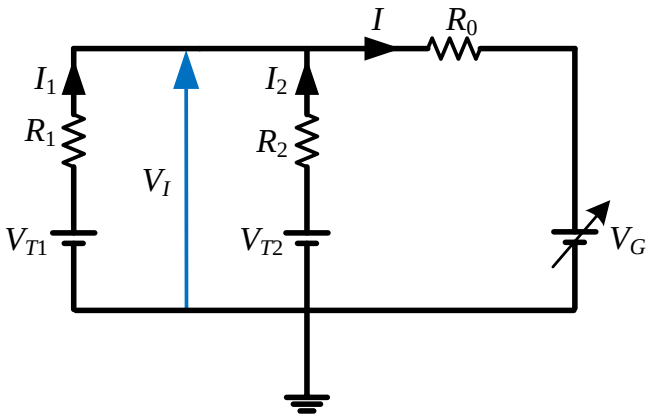

Fig. 7.5. Schematic diagram of a 3-terminal HVDC system.

7.3. THREE-TERMINAL HVDC TRANSMISSION WITH PARALLEL DC COLLECTION SYSTEM(S)

Parallel DC collection systems are discussed in Chapter 3, where DC/DC boost converters are employed for power delivery through HVDC. Therefore, for a 3-terminal HVDC transmission with at least one parallel DC collection system, the I-point voltage equalization can be achieved by terminal voltage adjustment. This is due to the fact that a DC/DC converter can accommodate the DC voltage fluctuations on one side and keep the DC voltage constant on the other side. There are two possible combinations of DC collection systems – (1) two parallel and (2) one parallel and one series. These are discussed below.

7.3.1. THREE-TERMINAL HVDC TRANSMISSION WITH 2 PARALLEL DC COLLECTION SYSTEMS

In this case, the parallel DC collection system is assumed to be applied for both wind farms. Therefore, all the three DC voltage sources are variable as shown in Fig. 7.6 (a). As both V_{T1} and V_{T2} are adjustable, the I-point voltage can be equalized by changing either of them. Since nominal operation is preferred, the terminal voltage of

the wind farm with a power output closer to its rated power is maintained at the reference voltage (V_T) and that of the other wind farm is adjusted accordingly.

For example, if

$$\frac{P_{w1}}{P_{r1}} \le \frac{P_{w2}}{P_{r2}} \tag{7.29}$$

then U_{T2} is controlled at U_T. It can be obtained by combining (7.2) and (7.28) that

$$V_{T1} = V_T - I_2 \times R_2 + I_1 \times R_1 = V_T - \frac{P_{w2}}{V_T} \times R_2 + \frac{P_{w1}}{V_{T1}} \times R_1 \tag{7.30}$$

$$\begin{aligned} V_G &= V_I - (I_1 + I_2) \times R_0 = V_T - I_2 \times R_2 - (I_1 + I_2) \times R_0 \\ &= V_T - \frac{P_{w2}}{V_T} \times R_2 - (\frac{P_{w2}}{V_T} + \frac{P_{w1}}{V_{T1}}) \times R_0 \end{aligned} \tag{7.31}$$

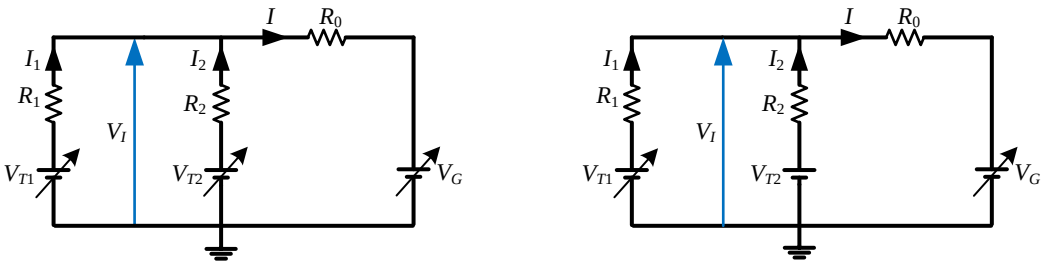

(a) 2 parallel DC collection systems

(b) 1 series and 1 parallel DC collection systems

Fig. 7.6. Schematic diagram of 3-terminal HVDC transmission with parallel wind power collection system(s).

With the measured power outputs (P_{w1} and P_{w2}) and the values of the resistances R_1, R_2 and R_0, V_{T1} can be calculated out from (7.30). Subsequently, V_G is calculated through (7.31). The reference voltage of the DC/DC converter for WF-1 is thus modified to the new V_{T1} to maintain the voltage stability at the I-point. It is to be noted that to equalize the I-point voltage, the terminal voltage adjustment pattern of the two wind farms can be numerous as the DC/DC converters can adjust either of the two DC side output voltages.

7.3.2. THREE-TERMINAL HVDC TRANSMISSION WITH SERIES PLUS PARALLEL DC COLLECTION SYSTEMS

In this case, it has been assumed that WF-1 employs the parallel DC collection system. The power of WF-2 is collected by the series DC collection system, which has been studied in Chapters 4 and 5. Those studies show that the safe operation of a series DC collection system is sensitive to its terminal voltage, which might decrease when one or more of the wind turbines fail and go out of service. Therefore, V_{T1} is adjustable, while V_{T2} must be kept constant at its reference value (original or decreased). Fig. 7.6 (b) shows the modified circuit of the 3-terminal HVDC system, where V_{T1} is modified as a variable DC voltage source. From (7.28), we get

$$V_{T1} = V_{T2} - I_2 \times R_2 + I_1 \times R_1 = V_{T2} - \frac{P_{w2}}{V_{T2}} \times R_2 + \frac{P_{w1}}{V_{T1}} \times R_1 \tag{7.32}$$

$$V_G = V_{T2} - I_2 \times R_2 - (I_1 + I_2) \times R_0 = V_{T2} - \frac{P_{w2}}{V_{T2}} \times R_2 - (\frac{P_{w2}}{V_{T2}} + \frac{P_{w1}}{V_{T1}}) \times R_0 \tag{7.33}$$

Similar to Case 1, V_{T1} can be calculated from (7.32) and, consequently, V_G is calculated from (7.33). The reference voltage of the corresponding DC/DC converter is modified to the new V_{T1} such that the I-point voltage is equalized.

7.4. THREE-TERMINAL HVDC TRANSMISSION WITH SERIES DC COLLECTION SYSTEMS

Since the terminal voltage of a series DC collection system must be strictly maintained at the reference value, V_{T1} and V_{T2} in a 3-terminal HVDC system are not under control in this case. When only series DC collection systems are applied, the only option for I-point voltage equalization is to adjust line resistances. In this section, variable resistors are employed to regulate the wind farm terminal voltages such that the I-point voltage stability can be guaranteed with various levels of power outputs.

7.4.1. EFFECTIVENESS OF VARIABLE RESISTOR APPLICATION

As stated previously, the I-point has been located based on the rated capacities of the offshore wind farms. Note that the rated output from a wind farm cannot be

maintained, especially when the wind speeds are low. This poses a serious challenge to the voltage equality at the I-point.

For a multi-terminal HVDC system with only series DC collection systems, a variable resistor is connected in series with the cables from each wind farm (l_1 and l_2). When wind power outputs vary, the RCLs of l_1 and l_2 are equivalent to be adjusted by changing their respective series connected resistors. An increased resistance indicates an extending in the value of RCL, while a reduced resistance signifies a shortened RCL. However, it is not practical to reduce the RCL of a cable as this may incur the connection of a resistor in parallel with the entire cable. Therefore, an algorithm is formed through which the resistance of a cable is increased from its nominal value in a controlled manner.

The effectiveness of employing variable resistors is illustrated by considering the case of Fig. 7.2 (d). This is modified to Fig. 7.7 (a), in which, the vertical axis of V_{l2} is moved to $V_{l2}^{'}$ by changing l_d to $l_d^{'}$. It can be seen that an I-point is obtained by changing the RCL, which can be realized by varying line resistances. Similarly, when the terminal voltage reference of a wind farm is reduced, the I-point voltage equalization can also be achieved through variable resistors as shown in Fig. 7.7 (b). It can be seen that after the terminal voltage of WF-1 is reduced from V_T to $V_T^{'}$, the I-point voltage cannot be equalized as the blue line and the red line do not cross at the CRL of l_I. By changing l_d to $l_d^{'}$, the red line is moved to the purple line and this intersects the blue line at the I-point. In conclusion, the I-point voltage equalization can be achieved by applying variable resistors irrespective of collection system operation modes (normal or faulty).

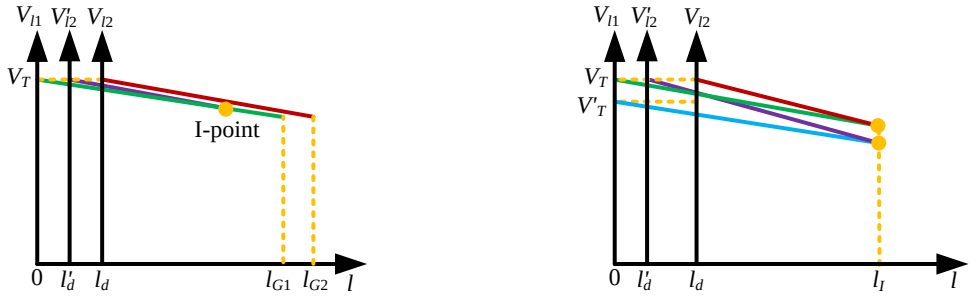

(a) Voltage characteristics by changing RCL with constant V_T

(b) Voltage characteristics by changing RCL with decreased V_T

Fig. 7.7. Influences of RCL on voltage stability of a 3-terminal HVDC system.

7.4.2. APPLICATION PRINCIPLE OF VARIABLE RESISTORS

The variability in the series connected resistors is achieved by using IGBT switches. The equivalent circuit of a 3-terminal HVDC system with variable resistors is shown in Fig. 7.8. In this, each variable resistor (incorporated in a dashed frame) contains a fixed resistor denoted by R_{vi} (i = 1, 2), and an IGBT-i with gate signals represented by g_i [133].

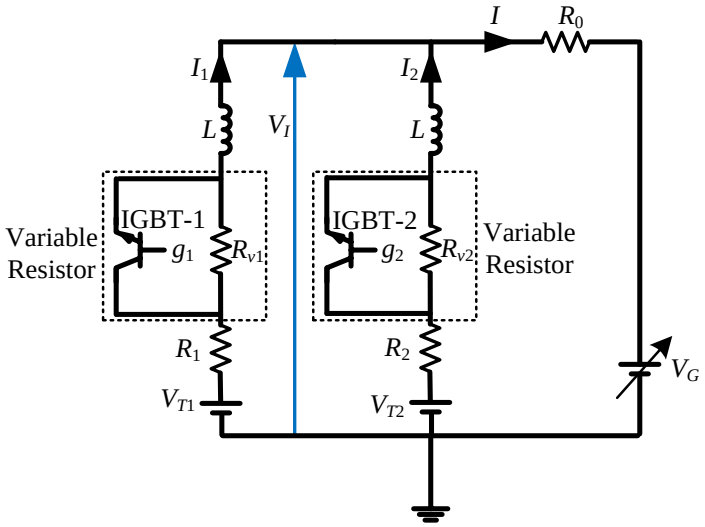

Fig. 7.8. Schematic diagram of 3-terminal HVDC transmission with variable resistors.

The average resistance of each variable resistor is denoted by R_{avi}. It can be seen that when the IGBT is conducting, the corresponding fixed resistor is bypassed and R_{avi} = 0. Similarly, when the IGBT is off, R_{avi} = R_{vi}. Therefore, with the switching of each IGBT, we get

$$R_{avi} = D_i \times 0 + (1 - D_i) \times R_{vi} = (1 - D_i) \times R_{vi} \tag{7.34}$$

where D_i is the conducting duty ratio of IGBT-i. A small inductor is connected in series with each variable resistor to smooth the DC currents. The modified line resistance for each cable is assumed to be R_{mi} and given by

$$R_{mi} = R_i + R_{avi} = R_i + (1 - D_i) \times R_{vi} \tag{7.35}$$

It is implied from the integration rule (stated in Subsection 7.1.1) that with the I-point located based on the rated values, a decreased power output from a wind farm requires a longer connected RCL. If both wind farms in a 3-terminal HVDC system have reduced power outputs from their respective ratings, only one of the line

resistances is increased through the corresponding controlled variable resistor. The resistance of the other variable resistor is controlled to be 0. This control principle applies to the situation when the terminal voltage references of the two wind power collection systems are unequal due to fault. In this way, unnecessarily increasing the line resistance, which results in increased power loss, is avoided. Irrespective of the power levels and the terminal voltage references of the two offshore wind farms, the line resistance changing strategy is determined as described below.

At the beginning it has been assumed that no variable resistors are applied to the 3-terminal HVDC system. Then the voltages at the I-point for the two wind farms are calculated based on their supplied powers as

$$\begin{cases} V_{I1} = V_{T1} - \dfrac{P_{w1}}{V_{T1}} \times R_1 \\ V_{I2} = V_{T2} - \dfrac{P_{w2}}{V_{T2}} \times R_2 \end{cases} \tag{7.36}$$

where V_{I1} and V_{I2} are the dropped terminal voltages after cable-1 and cable-2 respectively. If V_{I1} and V_{I2} are unequal, the voltage equalization must be achieved by increasing the line resistance of the cable which produces higher I-point voltage in (7.36). In this way, this higher voltage can be decreased to the same value with the lower I-point voltage.

It is obvious that the line resistance of a cable can only be increased by using a variable resistor but cannot be decreased from its original resistance (R_1 and R_2). The lowest terminal voltage drop by a cable will be when the corresponding power output of a wind farm is the least. Subsequently, the biggest difference of V_{I1} and V_{I2} will occur when the other wind farm has its rated power level. The sizing of the resistors R_{v1} and R_{v2} is determined based on this consideration. Using these boundary conditions, the values of the two fixed resistors in the 3-terminal HVDC system are determined by

$$\begin{cases} \dfrac{P_{r1}}{V_T} \times R_1 = \dfrac{P_{\min 2}}{V_T} \times (R_2 + R_{v2}) & V_{I1} < V_{I2} \\ \dfrac{P_{r2}}{V_T} \times R_2 = \dfrac{P_{\min 1}}{V_T} \times (R_1 + R_{v1}) & V_{I1} > V_{I2} \end{cases} \tag{7.37}$$

where P_{min1} and P_{min2} are the minimum power outputs at the cut-in wind speeds of WF-1 and WF-2 respectively. Equation (7.37) provides the same voltage drops on the two cables and thus equalizes the I-point voltage. It is to be noted that when the terminal voltage reference of a wind farm is modified upon fault, the power output decrease rate will be bigger than the terminal voltage decrease rate. This implies that the DC current from the wind farm will be smaller than the current that generated by the rated power and original terminal voltage. The cable voltage drop will thus be smaller consequently. Therefore, the boundary condition considers when $V_{T1} = V_{T2} = V_T$.

7.4.3. CONTROL BLOCK FOR 3-TERMINAL HVDC TRANSMISSION WITH VARIABLE RESISTORS

Taking $V_{I1} > V_{I2}$ as an example, the control block of a variable resistor in 3-terminal HVDC system is shown in Fig. 7.9. Based on the designed control strategy, the line resistance of cable-1 needs to be increased given that $V_{I1} > V_{I2}$. Therefore, the current from wind farm-2 (I_2) is calculated by the measured power (P_{w2}) divided by the terminal voltage (V_{T2}), as in the control diagram. Then I_2 is sent into two control loops, where the upper loop is to determine the manipulated grid DC voltage U_G and the lower loop is used to regulate the variable resistor connected in cable-1.

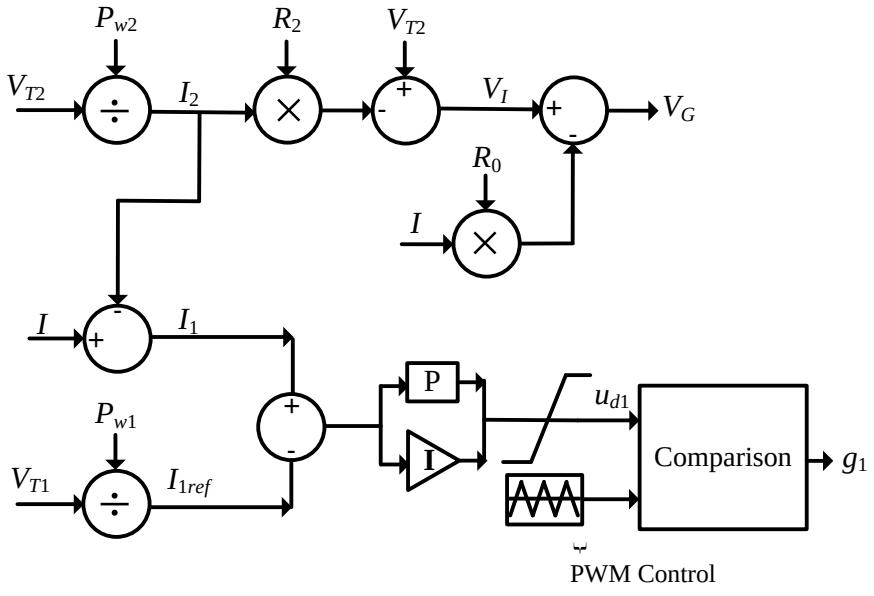

Fig. 7.9. Control block of 3-terminal HVDC transmission with variable resistors.

In the upper control loop, the voltage drop on cable-2 is calculated by its current (I_2) times the line resistance (R_2). Then the I-point voltage (V_I) is obtained using the terminal voltage (V_{T2}) subtracting the voltage drop. The current on cable-3 (I) is measured and multiplied by the resistance (R_0) and V_G is obtained using V_I deducting this voltage drop.

In the lower control loop, the real current of cable-1 is obtained by using the measured total current (I) subtracting the current of cable-2 (I_2). The current reference of cable-1 (I_{1ref}) is calculated by the measured power (P_{w1}) divided by the terminal voltage (V_{T1}). The difference of the two currents is sent to a PI controller and then the PWM control signal for IGBT-1 (u_{d1}) is obtained after an amplitude limiter. It is to be noted that the PWM control signal is related but not equal to the duty ratio of the IGBT. This is due to the existence of semiconductor resistances. The gate signal IGBT-1 (g_1) is obtained by the PWM control. The line resistance of cable-1 is thus adjusted through the IGBT control following (7.35).

7.5. SIMULATION STUDIES

Simulation studies are conducted in PSCAD for 3-terminal HVDC systems with different wind power collection systems. It is assumed that the I-point has been located with the line resistances R_1 = 0.8 Ω, R_2 = 1.0 Ω and R_0 = 5.0 Ω for all the cases.

***Case 1**: 2 Parallel DC Collection Systems*.

In this case, the power outputs from WF-1 and WF-2 are respectively assumed to be 150 MW and 250 MW at a certain instant. The terminal rated DC voltage of each wind farm is set as 600 kV. Besides, V_{T2} is assigned to be kept at V_T. Substituting the given values in (7.30), we get

$$V_{T1} = 600 - \frac{250}{600} \times 1.0 + \frac{150}{V_{T1}} \times 0.8 \tag{7.38}$$

From (7.38), V_{T1} is calculated to be 599.78 kV and V_I is 599.58 kV. Therefore, V_G can be obtained by (7.31) as

$$V_G = 600 - \frac{250}{600} \times 1.0 - (\frac{250}{600} + \frac{150}{599.78}) \times 5.0 = 596.25kV \tag{7.39}$$

By setting the two controlled voltages V_{T1} and V_G at the calculated values above, the simulation results of the DC currents through cable-1 to cable-3 are shown in Fig. 7.10. It can be seen that the three currents are at their respectively stable values with I_1 = 0.25 kA, I_2 = 0.42 kA and I = 0.67 kA. It is also noted that $I = I_1 + I_2$. This indicates that there is no circulating current in the 3-terminal HVDC system and the I-point voltage is equalized.

***Case 2**: 1 Parallel and 1 Series DC Collection Systems*

In this case, it is assumed that WF-1 has a parallel DC collection system and WF-2 is operated in series DC collection system. WF-2 has 80 turbines each rated 2.5 MW at 7.5 kV. Therefore, the rated capacity of the series DC collection system is 200 MW at 600 kV. The parallel DC collection system also has a rated DC terminal voltage of 600 kV, as in Case 1.

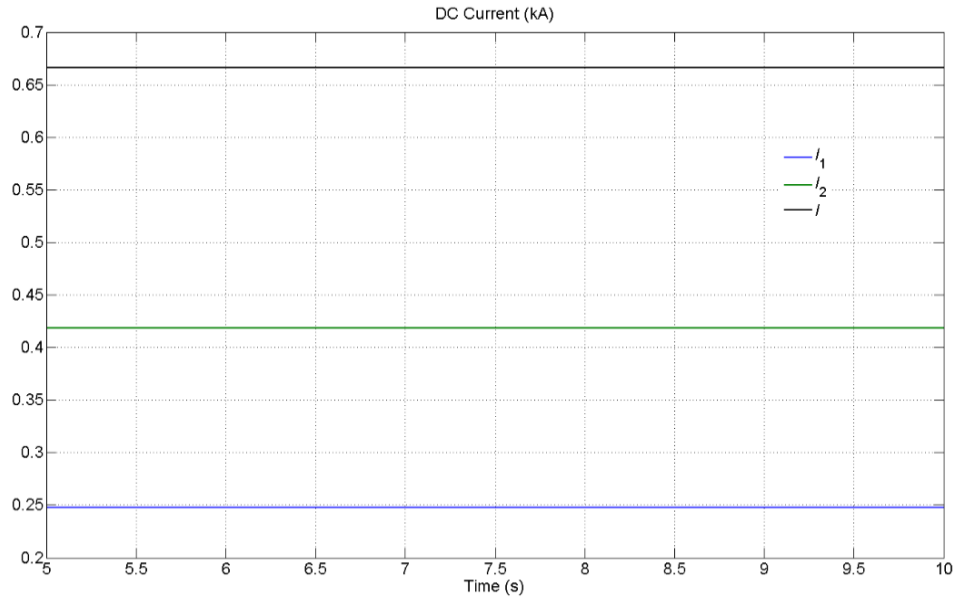

Fig. 7.10. DC currents of the 3-terminal HVDC transmission with 2 parallel DC collection systems.

For this simulation, it has been assumed that the power outputs of WF-1 and WF-2 are respectively 200 MW and 180 MW initially. At 10 s, the wind speed in WF-2 increases to the rated speed, but two turbines of WF-2 get faulty. Therefore, the output of WF-2 changes to 195 MW (2.5 MW × 78 turbines) at 10 s. Irrespective of normal or fault operation modes, V_{T2} must be maintained at V_T = 600 kV. Similar to Case-1, substituting the given values to (7.32) and (7.33), we get

$$V_{T1} = 600 - \frac{P_{w2}}{600} \times 1.0 + \frac{200}{V_{T1}} \times 0.8 \tag{7.40}$$

$$V_G = 600 - \frac{P_{w2}}{600} \times 1.0 - (\frac{P_{w2}}{600} + \frac{200}{V_{T1}}) \times 5.0 \tag{7.41}$$

where P_{w2} increases from 180 MW to 195 MW at 10 s, despite two faulted turbines.

It is calculated based on (7.40) and (7.41) that before 10 s, V_{T1} = 599.97 kV, V_I = 599.7 kV, V_G = 596.53 kV and after 10 s, V_{T1} = 599.94 kV, V_I = 599.675 kV, V_G = 596.38 kV. Using these calculated values to control the voltage sources, the simulation results are shown in Fig. 7.11, where Fig. 7.11 (a) illustrates the DC voltages. The DC currents are plotted in Fig. 7.11 (b). It can be seen that the 3-terminal HVDC system operates stably irrespective of wind turbine failures. The relationship that $I = I_1 + I_2$ is always met, indicating the non-existence of circulating currents and the stability of the I-point voltage.

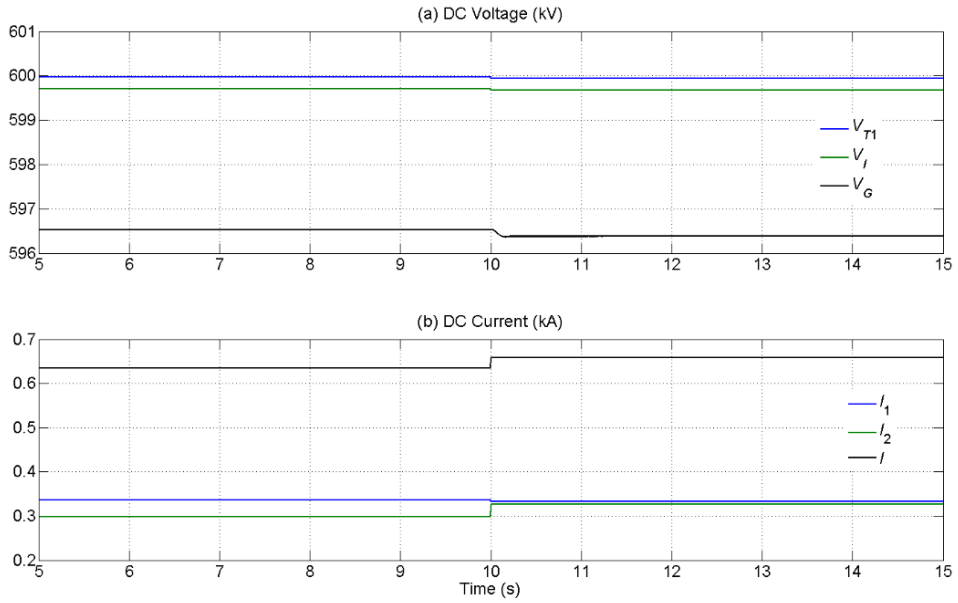

Fig. 7.11. Simulation results of the 3-terminal HVDC with parallel + series collection systems.

***Case 3**: 2 Series DC Collection Systems*

In this case, two series DC collection systems are considered. Wind farm WF-1 has a total number of 20 turbines each rated 2.5 MW at 7.5 kV, while WF-2 has a total number of 125 turbines each rated 2 MW at 2 kV. Therefore, the output

voltages of both the wind farms are 150 kV. However, the maximum power output from WF-1 is 50 MW, while that for WF-2 is 250 MW.

The minimum power outputs of the two wind farms are presumed to be 8% of their respective ratings. According to (7.37), we get

$$\begin{cases} P_{r1} \times R_1 = 0.08 \times P_{r2} \times (R_2 + R_{v2}) \\ P_{r2} \times R_2 = 0.08 \times P_{r1} \times (R_1 + R_{v1}) \end{cases} \tag{7.42}$$

It is calculated from (7.42) that R_{v1} = 61.7 Ω, R_{v2} = 1.0 Ω.

Suppose P_{w1} is at its rated value of 50 MW initially and drops to 40 MW at 10 s due to two turbines going offline. As a consequence, the terminal voltage of WF-1 gets modified to 148.5 kV (as per equation 5.11 in Chapter 5). The output power of WF-2 (P_{w2}) is 150 MW before 20 s and rises to 200 MW afterwards due to an increase in the wind speed. Therefore, there are three time durations that need to be considered. The I-point voltages during these time durations are calculated based on (7.36) and listed in Table 7.1. The bigger I-point voltages are marked in red and their corresponding line resistances need to be increased through variable resistors. The other line resistances are kept unchanged by setting the PWM control signal for their respective IGBTs to be 1 according to (7.35).

The simulation results of the 3-terminal HVDC system with two small offshore wind farms are shown in Fig 7.12. The DC voltages of the three terminals and the I-point are plotted in Fig. 7.12 (a), where V_{T1}, V_{T2} and V_I are in accordance with the values in Table 7.1. It can be seen that V_G drops slightly with the decrease of P_{w1} and V_{T1} at 10 s and reduces to a further lower level after P_{w2} increases at 20 s. These changes result from the upper control loop in Fig. 7.9. Fig. 7.12 (b) shows the DC currents, where I_1 is generally smaller than I_2 due to the lower power outputs of WF-1 and $I = I_1 + I_2$ is satisfied all the time.

Table 7.1: The I-point voltages at different time durations.

System Quantities	0-10 s	10-20 s	20-30 s
V_{T1} (kV)	150	148.5	148.5
V_{T2} (kV)	150	150	150
P_{w1} (MW)	50	40	40
P_{w2} (MW)	150	150	200
V_{I1} (kV)	149.73	148.28	148.28
V_{I2} (kV)	149	149	148.67
V_I (kV)	149	148.28	148.28

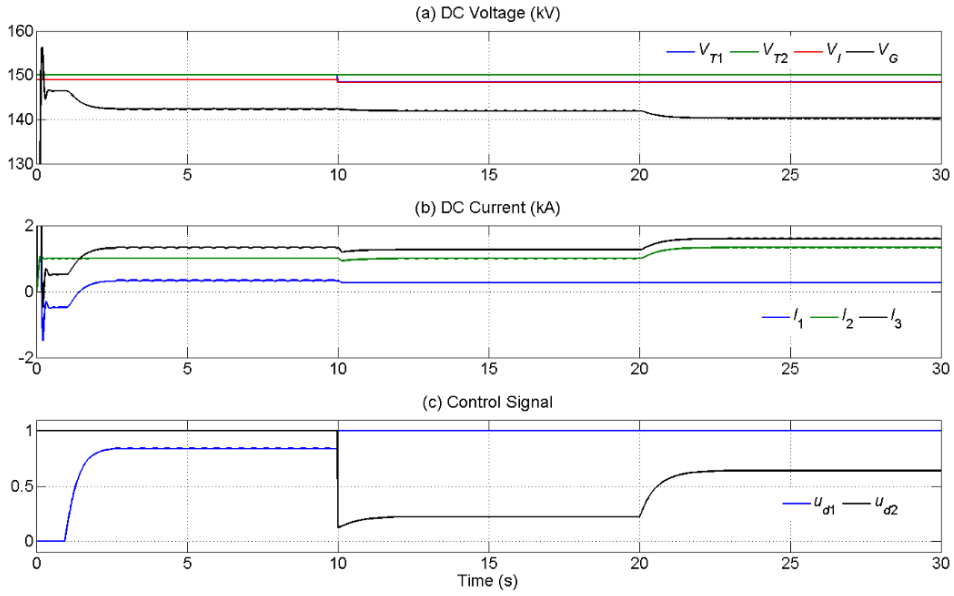

Fig. 7.12. Simulation results of the 3-terminal HVDC transmission with 2 series DC collection systems.

The PWM control signals for the two IGBTs are illustrated in Fig. 7.12 (c). It can be seen that u_{d1} settles at around 0.84 before 10 s, indicating an increased line resistance for cable-1. After 10 s, u_{d2} is smaller than 1 due to the line resistance increasing requirements of cable-2. It can be seen that u_{d2} rises from approximately 0.22 to 0.64 at 20 s. As a PWM control signal is related to its corresponding duty ratio, the increase of u_{d2} implies that the resistance of the variable resistor R_{av2} is reduced. This change can be analysed from Table 7.1, where the I-point voltage difference during 20 s – 30 s is smaller than that between 10 s and 20 s. Besides, I_2 gets bigger with the increase of P_{w2} at 20 s. These two factors together result in a reduced line resistance at 20 s. It is to be noted that during the simulation, the variable resistor connected to the cable that does not need to increase resistance is

bypassed and the corresponding duty ratio is set as 1. This is also shown in Fig. 7.12 (c), where u_{d2} is 1 before 10 s, while after 10 s, u_{d1} is set at 1. It should also be noted that the required line resistances at different time durations can be sorted out based on Table 7.1.

7.6. CONCLUSIONS

The multi-terminal operation of offshore wind farms with a grid is discussed in this chapter for a 3-terminal HVDC system. An integration method aiming at the least cable use is proposed based on the nominal operation of the two wind farms. When the power outputs of the wind farms are smaller than their respective ratings, the voltage at the integration point must be stabilized by either changing the wind farm terminal voltages or line resistances. The operation of 3-terminal HVDC transmission with different wind power collection systems are discussed and corresponding strategies for integration point voltage equalization are proposed.

When one or both wind farms are in the parallel DC collection topology, the integration point voltage can be stabilized by changing the terminal voltages through DC/DC converters in the parallel collection systems. If the series DC collection system is employed by both wind farms, their connected line resistances must be adjusted. This is achieved by variable resistor application, where PWM controlled semiconductors are employed for the line resistance variations. It is to be noted that a communication medium will be required when two series DC collection systems are used. A central controller needs to determine the resistance that need to be added in order to match the I-point voltage of the two wind farms. This controller will require inputs of the voltages and power outputs of the wind farms. The output of the controller will send command to manipulate the variable resistors and the DC voltage of the grid terminal.

The effectiveness of all the proposed voltage control strategies is verified through simulation studies using PSCAD. The discussions in this chapter are based on 3-terminal HVDC systems. For multi-terminal HVDC wind power delivery with more than 3 terminals, 2 or more integration points might exist. This complicates the integration point location and voltage stabilization, which will not be considered here.

CHAPTER 8

CONCLUSIONS AND SCOPE OF FUTHER RESEARCH

In this chapter, the general conclusions of the thesis and the scopes of further research are presented.

8.1. GENERAL CONCLUSIONS

These are listed below.

1. The Permanent Magnet Synchronous Generator (PMSG) based Wind Energy Conversion System (WECS) is the most promising choice for offshore wind power generation. This however requires a back-to-back converter system. Depending on the power level, various possible converter topologies are available. However, for the power range of 2-4 MW, a three-leg Voltage Source Converter (VSC) is favored as it has simpler control configurations.

2. The High Voltage Direct Current (HVDC) technique is advantageous for offshore wind power delivery systems. In such systems, the voltage of a wind farm has to be boosted to around 100 kV for efficient power transmission. The wind farm power can be collected through either AC or DC collection systems. In this thesis, only DC collection systems have been considered. Furthermore, there are three possible configurations for a DC collection system – series, parallel and series-parallel.

3. In a parallel DC collection system, the DC sides of all the wind side converters are connected in parallel, at a much lower voltage level. Therefore, voltage boosting is required for HVDC transmission. The Single Active Bridge (SAB) converter is shown more suitable for boosting the DC voltage compared to other converter topologies. In this configuration, the VSC WSC controls MPPT, while the SAB switches are under voltage control. Alternatively, parallel connected VSC WSCs with a number of Input Parallel Output Series (IPOS) interfaced SAB converters can also be used. This scheme is advantageous as high frequency transformers that are required in SAB usually have smaller ratings. Therefore, a number of them is preferable compared to a single large

one. Furthermore, the current ripples in this scheme are shown to be much smaller.

4. A series DC collection system is proposed for offshore wind farms. This collection system has several advantages. The voltage control in a series DC collection system is realized through the proper control on wind power. When the wind speed within an offshore wind farm is uneven, the DC voltages of each WSC must be restricted within the predefined range. To achieve this, two power balancing strategies among WSCs are proposed. In one of them, a small sized battery is installed between each wind generator and the connected WSC to provide smoothening effect by controlled charging or dis-charging. Alternatively, the power references of some of the WSCs can be lowered by employing chopping resistors or modifying the pitch control. Even if the first method is more expensive to install and more complicated to control, it generally requires no wind power curtailment.

5. When some wind turbines in a series DC collection system fail, overvoltage might occur. To deal with this problem, the transmission voltage reference is reduced upon fault by modifying the voltage references of the Grid Side Converter (GSC), as and when necessary. Another overvoltage prevention strategy is proposed based on a modified version of the original series DC collection system. In this, the large capacity GSC is replaced by several converters with smaller capacities such that each of them has the same rating as a WSC. Depending on the number of the faulted wind turbines, some of the smaller GSCs are bypassed.

6. For a series-parallel DC collection system on normal operation, the proposed power balancing strategies are effective in voltage limiting. When wind turbine failure occurs, power switches are applied to prevent overvoltage. This is achieved through the system topology reconfiguration by closing certain switches. Fault interconnection should be avoided for a better voltage control effect. Another overvoltage prevention strategy employs a DC/DC converter at the terminal of each wind power branch. Using this strategy, the DC voltage of each WSC can be controlled around the rated value.

7. For multi-terminal connection of offshore wind farms with a grid using HVDC, an integration method aiming at the least cable length to use is proposed. Once an integration point is selected by the proposed method, the voltage at the integration point must be stabilized by either changing the wind farm terminal voltages or line resistances for varied wind power outputs. The terminal voltage of a parallel DC collection system is adjustable, while that of a series DC collection system must follow its reference value. For a 3-terminal HVDC system interconnecting two offshore wind farms and one grid, the line resistances need to be changed using variable resistors if only series DC collection is employed. Otherwise, the voltage stabilization at the integration point can be achieved through the DC/DC converter in the parallel DC collection system.

8.2. SCOPE OF FURTHER RESEARCH

Some scopes of future work are identified as below.

1. The discussions on offshore wind power integration in the thesis are based on wind turbines in operation. However, the starting of an offshore wind farm using the proposed collection systems should be studied. Besides, specific operation strategies at cut-in and cut-out wind speeds need to be identified.

2. For a series-parallel DC collection system employing power switches, the switching strategies discussed in the thesis require the information of fault positions. Therefore, a communication system is needed, which may introduce time delays. An intelligent switching determination algorithm without communication is worth to be studied.

3. For both normal and fault operations of different collection topologies, several voltage control strategies are proposed in the thesis. To utilize the advantages of these strategies and eliminate the disadvantages, the resultant voltage control effects using different combined strategies are worth to be investigated.

4. For multi-terminal HVDC wind power delivery, this thesis focuses on a 3-terminal system, which has one integration point. However, with more than 3 terminals, 2 or more integration points might exist. This complicates the integration point location and voltage stabilization, which need to be studied.

5. This thesis focuses on the fault condition of wind turbine failures. Other fault scenarios such as AC or DC line short-circuit, ground fault and disconnection of the grid are worth to be studied.

REFERENCES

[1] Wise Power Systems, "Wind energy – another gift from the sun?" available at: http://wisepowersystems.com/learn-more/wind-energy-another-gift-from-the-sun/

[2] P. R. Crowe, "The trade wind circulation of the world," *Transactions and Papers (Institute of British Geographers)*, no. 15, pp. 39-56, 1949.

[3] From TES website "Trade winds lessons," available at: https://www.tes.com/lessons/b61DhvZnXxYtNA/trade-winds

[4] Office of Energy Efficiency & Renewable Energy: "History of wind energy," available at: http://energy.gov/eere/wind/history-wind-energy

[5] Wind Energy Foundation, "History of wind energy," available at http://windenergyfoundation.org/about-wind-energy/history/

[6] Third Plant Windpower, "History," available at http://www.thirdplanetwind.com/energy/history.aspx

[7] J. K. Kaldellis, and D. Zafirakis, "The wind energy (r)evolution: a short review of a long history," *Renewable Energy*, vol. 36, no. 7, pp. 1887–1901, 2011.

[8] From CBC website "Timeline: a history of wind power," available at http://www.cbc.ca/doczone/features/timeline1

[9] The Gardian, "Timeline: the history of wind power," available at https://www.theguardian.com/environment/2008/oct/17/wind-power-renewable-energy

[10] AltEnergyMag, "Wind energy timeline – from persian windmills crushing grains to vesta's wind turbines churning out 8 MW of output," available at http://www.altenergymag.com/article/2015/04/wind-energy-timeline-%E2%80%93-from-persian-windmills-crushing-grains-to-vesta%E2%80%99s-wind-turbines-churning-out-8-mw-of-output/19496

[11] Global Wind Energy Council, "Global wind report," available at http://www.gwec.net/wp-content/uploads/vip/GWEC-Global-Wind-2015-Report_April-2016_22_04.pdf

[12] Global Wind Energy Council, "Offshore wind," available at http://www.gwec.net/wp-content/uploads/2016/05/Global-offshore-1.pdf

[13] Global Wind Energy Council, "Offshore wind power," available at http://www.gwec.net/global-figures/global-offshore/#

[14] G. M. Masters, *Renewable and Efficient Electric Power Systems*, pp. 307-377, 2004.

[15] P. J. Schubel, and R. J. Crossley, "Wind turbine blade design," *Energies*, vol. 5, pp. 3425-3449, 2012.

[16] IEEE PES Wind Plant Collector System Design Working Group, "Characteristics of wind turbine generators for wind power plants," *2009 IEEE Power & Energy Society General Meeting*, pp.1-5, 2009.

[17] M. Singh, and S. Santoso, "Dynamic models for wind turbines and wind power plants," 2011.

[18] Australian Energy Market Operator, "Wind turbine plant capabilities report-2013 Wind Integration Studies," 2013.

[19] H. Li, and Z. Chen, "Overview of different wind generator systems and their comparisons," *IET Renew. Power Gener.*, vol. 2, no. 2, pp. 123–138, 2008.

[20] B. Wu, Y. Lang, N. Zargari and S. Kouro, Proc. *Power Conversion and Control of Wind Energy Systems*, 2011.

[21] M.A. Abdullah, A.H.M. Yatim, C.W. Tan, R. Saidur, "A review of maximum power point tracking algorithms for wind energy systems," *Renewable and Sustainable Energy Reviews*, vol. 16, no. 5, pp. 3220– 3227, 2012.

[22] B. Meghni, A. Saadoun, D. Dib, and Y. Amirat, "Effective MPPT technique and robust power control of the PMSG wind turbine," *IEEJ Transactions on Electrical and Electronic Engineering IEEJ Trans*; vol. 10, no. 6: 619–627, 2015.

[23] H. G. Jeong, R. H. Seung, and K. B. Lee, "An improved maximum power point tracking method for wind power systems," *Energies*, vol. 5, no. 5, pp. 1339-1354, 2012.

[24] K. Padmanabham, K. B. N. K. Reddy, and M. Tech, "A new MPPT control algorithm for wind energy conversion system," *International Journal of Engineering Research & Technology* (*IJERT*), vol. 4, no. 3, 2015.

[25] D. Kumar, and K. Chatterjee, "A review of conventional and advanced MPPT algorithms for wind energy systems," *Renewable and Sustainable Energy Reviews*, vol. 55, pp. 957–970, 2016.

[26] S. Chuangpishit, A. Tabesh, and M. Saeedifard, etc., "Topology design for collector systems of offshore wind farms with pure DC power systems," *IEEE Trans. Ind. Electron*, vol. 61, no.1, pp. 320 - 328, 2014.

[27] H. J. Bahirat, B. A. Mork, and H. K. Høidalen, "Comparison of wind farm topologies for offshore applications," *2012 IEEE Power and Energy Society General Meeting*, San Diego, CA, pp. 1-8, Jul., 2012.

[28] S. Lundberg, "Evaluation of wind farm layouts," *EPE Journal: European Power Electronics and Drives*, vol. 16, no. 1, pp. 14-21, 2006.

[29] A. Madariaga, J. L. Martin, and I. Zamora, etc., "Technological trends in electric topologies for offshore wind power plants," *Renewable and Sustainable Energy Reviews*, vol. 24, pp. 32-44, 2013.

[30] S. J. Shao, and V. G. Agelidis, "Review of DC system technologies for large scale integration of wind energy systems with electricity grids," *Energies*, vol. 3, pp. 1303-1319; 2010.

[31] J. Lin, "Integrating the first HVDC-based offshore wind power into PJM system—a real project case study," *IEEE Trans. on Ind. Appl*., vol. 52, no. 3, pp. 1970-1978, 2016.

[32] O. Gomis-Bellmunt, A. Junyent-Ferre, and A. Sumper, etc., "Control of a wind farm based on synchronous generators with a central HVDC-VSC converter," *IEEE Trans. on Power Syst*., vol. 26, no. 3, pp. 1632-1640, 2010.

[33] M. Gil, O. Gomis-Bellmunt, and A. Sumper, etc., "Power generation efficiency analysis of offshore wind farms connected to a SLPC (single large power converter) operated with variable frequencies considering wake effects," *Energy*, vol. 37, no. 1, pp. 455-468, 2012.

[34] M. Prada, L. Igualada, and C. Corchero, etc., "Hybrid AC-DC offshore wind power plant topology: optimal design," *IEEE Trans. on Power Syst*., vol. 30, no. 4, pp. 1868-1876, 2015.

[35] P. Lakshmanan, J. Liang, and N. Jenkins, "Assessment of collection systems for HVDC connected offshore wind farms," *Electric Power Systems Research*, vol. 129, pp. 75-82, 2015.

[36] M. A. Parker, and O. Anaya-Lara, "Cost and losses associated with offshore wind farm collection networks which centralise the turbine power electronic converters," *IET Renewable Power Generation*, vol. 7, no. 4, pp. 390-400, 2013.

[37] N. Holtsmark, H. J. Bahirat; and M. Molinas; etc., "An all-DC offshore wind farm with series-connected turbines: an alternative to the classical parallel AC model?" *IEEE Trans. on Ind. Electron*., vol. 60, no. 6, pp. 2420-2428, 2012.

[38] N. R. Chaudhuri, and A. Yazdani, "An aggregation scheme for offshore wind farms with VSC-based HVDC collection system," *IEEE Power and Energy Society General Meeting*, San Diego, July 2013.

[39] C. Meyer, M. Höing, A. Peterson, and R. W. De Doncker, "Control and design of DC grids for offshore wind farms," *IEEE Trans. Ind. Appl*, vol. 43, no. 6, pp. 1475 - 1482, 2007.

[40] Z. Wang, L. Yao, and J. Wu, etc., "Large offshore wind power collection using DC grid technology," International Conference on Renewable Power Generation (RPG 2015), pp. 1-6, Beijing, Oct., 2015.

[41] Y. Lian, G. P. Adam, and D. Holliday, "Medium-voltage DC/DC converter for offshore wind collection grid," *IET Renewable Power Generation*, vol. 10, no. 5, pp. 651-660, 2016.

[42] Y. Li, Z. Xu and H. W. Ngan, etc., "A novel topology design for integration of offshore wind farm via high-voltage DC transmission", *Electric Power Components and Systems*, vol. 43, no. 8-10, pp. 1100-1112, 2015.

[43] A. Mogstad, and M. Molinas, "Power collection and integration on the electric grid from offshore wind parks," *NORPIE/2008, Nordic Workshop on Power and Industrial Electronics*, June, 2008.

[44] N. Negra, J. Todoravic, and T. Ackermann, "Loss evaluation of HVAC and HVDC transmission solutions for large offshore wind farms," *Electric Power Systems Research*, vol. 76, no. 11, pp. 916-927, 2006.

[45] P. Bresesti, W. L. Kling, and R. L. Hendriks, etc., "HVDC connection of offshore wind farms to the transmission System," *IEEE Trans. Energy Convers*., vol. 22, no. 1, pp. 37-43, 2007.

[46] O. Gomis-Bellmunt, J. Liang, and J. Ekanayake, etc., "Topologies of multiterminal HVDC-VSC transmission for large offshore wind farms," *Electric Power Systems Research*, vol. 81, no. 2, pp. 271-281, 2011.

[47] S. Liu, Z. Xu, W. Hua, G. Tang, and Y. Xue, "Electromechanical transient modelling of modular multilevel converter based multi-terminal HVDC systems," *IEEE Trans. Power Syst*., vol.29, no. 1, pp. 72-83, 2014.

[48] R. E. Torres-Olguin, M. Molinas, and T. Undeland, "Offshore wind farm grid integration by VSC technology with LCC-based HVDC transmission," *IEEE Trans. Sustain. Energy*, vol. 3, no. 4, pp. 899-907, 2012.

[49] L. Xu, L. Yao, and M. Bazargan, "DC grid management of a multi-terminal HVDC transmission system for large offshore wind farms," In *Proc. International Conference on in Sustainable Power Generation and Supply (SUPERGEN)*, pp. 1-7, 2009.

[50] Z. Lidong, L. Harnefors, and H. P. Nee, "Interconnection of two very weak AC systems by VSC-HVDC links using power-synchronization control," *IEEE Trans. Power Syst.*, vol. 26, no. 1, pp. 344-355, 2011.

[51] Z. Lidong, L. Harnefors, and H. P. Nee, "Power-synchronization control of grid-connected voltage-source converters," *IEEE Trans. Power Syst*., vol. 25, no. 2, pp. 809-820, 2010.

[52] J. Arrillaga, Y. H. Liu, and N. R. Watson. *Flexible power transmission: The HVDC options*, 2007.

[53] R. T. Pinto, P. Bauer, and S. F. Rodrigues, etc., "A novel distributed direct-voltage control strategy for grid integration of offshore wind energy systems through MTDC network," *IEEE Trans. Ind. Electron*., vol. 60, no. 6, pp. 2429-2441, 2013.

[54] Y. Ye, M. Kazerani, and V. H. Quintana, "Current-source based STATCOM modelling and control," *IEEE Trans. Power Deliv*. vol. 20, no. 2, pp. 795–800, 2005.

[55] D. Jovcic, "Offshore wind farm with a series multiterminal CSI HVDC," *Electric Power Systems Research*, vol. 78, no. 4, pp. 747-755, 2008.

[56] J. Liang, O. Gomis-Bellmunt, and J. Ekanayake, etc., "Control of multi-terminal VSC-HVDC transmission for offshore wind power," *2009 13th European Conference on Power Electronics and Applications*, pp. 1-10, 2009.

[57] A. Egea-Alvarez, J. Beerten, D. Van Hertem, and O. Gomis-Bellmunt, "Primary and secondary power control of multiterminal HVDC grids," *AC and DC Power Transmission (ACDC 2012), 10th IET International Conference on*, pp. 1-6, Dec., 2012.

[58] F. D. Bianchi, J. L. Domínguez-García, O. Gomis-Bellmunt, “Control of multi-terminal HVDC networks towards wind power integration: a review,” *Renewable and sustainable energy reviews*, vol. 55, pp. 1055-1068, 2016.

[59] R. T. Pinto, S. F. Rodrigues, and P. Bauer, etc., “Comparison of direct voltage control methods of multi-terminal DC (MTDC) networks through modular dynamic models,” in *Proc. 2011 14th Eur. Conf. Power Electronics and Applications (EPE 2011)*, pp. 1-10, 2011.

[60] T. Nakajima, and S. Irokawa. “A control system for HVDC transmission by voltage sourced converters,” *Power Engineering Society Summer Meeting*, vol.2; pp.1113–1119, Jul, 1999.

[61] J. Zhu, and C. Booth, “Future multi-terminal HVDC transmission systems using voltage source converters,” *Universities Power Engineering Conference (UPEC), 2010 45th International*, pp. 1-6, 2010.

[62] V. Mier, P. G. Casielles, and T. Coto, etc., “Voltage margin control for offshore multi-use platform integration,” *Proceedings of the European Association for the development of Renewable Energies, Environ Power Qual (EA4EPQ)*; pp. 1-6, Mar., 2012.

[63] C. Dierckxsens, K. Srivastava, and M. Reza, “A distributed DC voltage control method for VSC MTDC systems,” *Electric Power Systems Research*, vol. 82, no. 1, pp. 54–58, 2012.

[64] J. Beerten, S. Cole, and R. Belmans, “Modeling of multi-terminal VSC HVDC systems with distributed DC voltage control,” *IEEE Trans. On Power Syst.*, vol. 29, no. 1, pp. 34-42, 2014.

[65] L. Xu, L. Yao, and M. Bazargan, “DC grid management of a multi-terminal HVDC transmission system for large offshore wind farms,” *2009 Proceedings of the international conference on sustainable power generation and supply*; pp. 1-7, Apr., 2009.

[66] D. Chen, and L. Xu, “Autonomous DC voltage control of a DC microgrid with multiple slack terminals,” *IEEE Trans. On Power Syst.*, vol. 27, no. 4, pp. 1897-1905, 2012.

[67] T. K. Vranaa, J. Beerten, and R. Belmans, “A classification of DC node voltage control methods for HVDC grids,” *Electric Power Systems Research*, vol. 103, pp. 137–144, 2013.

[68] S. Chondrogiannis, and M. P. Blanco, "Market integration scheme of a multi-terminal HVDC grid in the North Seas," *IEEE Trans. On Power Syst*., vol. 31, no. 3, pp. 2415-2422, 2016.

[69] X. Zhao, Q. Song, and H. Rao, etc., "Control of multi-terminal VSC-HVDC system to integrate large offshore wind farms," *International Journal of Computer and Electrical Engineering*, vol. 5, no. 2, pp. 201-206, 2013.

[70] X. Ran, S. Miao, and Y. Wu, "Improved adaptive droop control design for optimal power sharing in VSC-MTDC integrating wind farms," *Energies*, vol., no. 7, pp. 7100–7121, 2015.

[71] A. A. Jadallah, D. Y. Mahmood, and Z. A. Abdulqader, "Optimal performance of horizontal axis wind turbine for low wind speed regime," *International Journal of Multidisciplinary and Current Research*, vol. 2, pp. 159-164, 2014.

[72] K. Kurohane, T. Senjyu, A. Yona, N. Urasaki, T. Goya, and T. Funabashi, "A hybrid smart AC/DC power system," *IEEE Trans. Smart Grid*, vol. 1, no. 2, pp. 199-204, 2010.

[73] Y. Zhao, C. Wei, Z. Zhang, and W. Qiao, "A review on position/speed sensorless control for permanent-magnet synchronous machine-based wind energy conversion systems," *IEEE Journal of Emerging and Slected Topics in Power Electronics*, vol. 1, no. 4, pp: 203-216, 2013.

[74] S. Musunuri and H. L. Ginn, "Comprehensive review of wind energy maximum power extraction algorithms," *in Proc. IEEE Power Energy Soc. General Meeting*, Jul., pp. 1–8, 2011.

[75] Y. Fan, M. Goyal, A. Ghosh, and F. Shahnia, "Integration of wind energy conversion system with microgrid and utility," *Australasian Universities Power Engineering Conference, AUPEC 2014*, pp. 1-6, 2014.

[76] M. Goyal, Y. Fan, and A. Ghosh, etc., "Techniques for a wind energy system integration with an islanded microgrid," *International Journal of Emerging Electric Power Systems*, vol. 17, no. 2, pp.191-203, 2016.

[77] A. Ghosh, G. Ledwich, and F. Zare, etc., "Stability analysis for multiple voltage source converters connected at a bus," *Energy 2011*, pp. 185-194.

[78] A. Ghosh, "Performance study of two different compensating devices in a custom power park," *IEE Proceedings - Generation, Transmission and Distribution*, vol. 152, no. 4, pp. 521-528, 2005.

[79] A. Ghosh, and G. Ledwich, "High bandwidth voltage and current control design for voltage source converters," *Australian Universities Power Engineering Conference (AUPEC 2010)*, Christchurch, Dec, 2010.

[80] N. Mohan, T. M. Undeland and W. P. Robbins, 3rd Ed., *Power Electronics: Converters, Applications and Design*, John Wiley, New York, 2003.

[81] Manitoba HVDC Research Center, *PSCAD/EMTDC Manual*, Apr. 2005.

[82] Y. Fan, and A. Ghosh, "Voltage control strategies for offshore wind power collection systems upon faults," *2016 Power Energy Society General Meeting (PESGM)*, Boston, USA, Jul., 2016.

[83] N. Soltau, R. U. Lenke, and R. W. De Doncker, *E.ON Energy Research Center Series: High-power DC-DC converter*, vol. 5, no. 5, 2013.

[84] K. Park, and Z. Chen, "Analysis and design of a parallel-connected single active bridge DC-DC converter for high-power wind farm applications," *Power Electronics and Applications (EPE), 2013 15th European Conference on*, pp. 1-10, Sept., 2013.

[85] F. Deng, and Z. Chen, "An offshore wind farm with dc grid connection and its performance under power system transients," in *Proc. IEEE Power and Energy Society Genernal Meeting*, pp. 1-8, Jul., 2011.

[86] J. Xue, *Single-phase vs Three-phase High Power High Frequency Transformers*, Mater thesis, Virginia Polytechnic Institute and State University, 2010.

[87] C. P. Dick, A. Konig, and R. W. De Doncker, "Comparison of Three-Phase DC-DC Converters vs. Single-Phase DC-DC Converters," *2007 7th International Conference on Power Electronics and Drive Systems*, pp. 217-224, Nov. 2007.

[88] J. Jacobs, M. Thommes, and R. De Doncker, "A transformer comparison for three-phase single active bridges," *Power Electronics and Applications, 2005 European Conference on*, pp. 1-10, Sept., 2005.

[89] J. Robinson, D. Jovcic, and G. Joós, "Analysis and design of an offshore wind farm using a MV DC grid," IEEE Trans. on Power Del., vol. 25, no. 4, pp. 2164-2173, 2010.

[90] R. W. De Doncker, D. M. Divan, and M. H. Kheraluwala, "A three-phase soft-switched high-power-density DC/DC converter for high-power applications," *IEEE Trans. on Ind. Appl.*, vol. 27, no. 1, pp. 63-73, 1991.

[91] Y. Ting, and Sjoerd. Haan, and J. A. Ferreira, "The partial-resonant single active bridge DC-DC converter for conduction losses reduction in the single active bridge," *ECCE Asia Downunder (ECCE Asia), 2013 IEEE*, pp. 987-993, Jun., 2013.

[92] A. Averberg, and A. Mertens, "Analysis of a voltage-fed full bridge DC-DC converter in fuel cell systems," *PESC Record - IEEE Annual Power Electronics Specialists Conference*, Jul., 2007.

[93] A. Averberg, and A. Mertens, "Characteristics of the single active bridge converter with voltage doubler," *Power Electronics and Motion Control Conference (13th EPE-PEMC)*, pp. 213-220, Sept., 2008.

[94] M. Bahmani, *Design and Optimization of HF Transformers for High Power DC-DC Applications*, PhD thesis, Chalmers University of Technology, Sweden, 2014.

[95] L. Max, and T. Thiringer, "Control method and snubber selection for a 5 MW wind turbine single active bridge DC/DC converter," *Power Electronics and Applications, 2007 European Conference on*, pp. 1-10, Sept., 2007.

[96] SuennLiang, "High voltage/ high frequency transformers," available at: http://www.suenn.com/products/high-voltage-frequency.html

[97] Marque Magnetics, "High frequency transformers," available at http://marquemagnetics.com/high-frequency-transformers/

[98] B.T. Irving and M.M. Jovanovic, "Analysis, design, and performance evaluation of droop current-sharing method" in *Proc. 15th Annu. IEEE Appl. Power Electon. Conf.*, pp. 235-241, 2000.

[99] K. Sano, and M. Takasaki, "A boost conversion system consisting of multiple DC-DC converter modules for interfacing wind farms and HVDC transmission," *2013 IEEE Energy Conversion Congress and Exposition*, pp. 2613-2618, Sept. 2013.

[100] S. Lundberg, *Wind Farm Configuration and Energy Efficiency Studies-Series DC versus AC Layouts*, Ph.D. dissertation, Chalmers Univ. Technol., Sweden, 2006.

[101] WindPower Program, available online: http://www.wind-power-program.com/large_turbines.htm

[102] J. D. Irwin, *Power Electronics Handbook*, pp. 225-267, 2001.

[103] H. Chen, T. N. Cong, and W. Yang etc., "Progress in electrical energy storage system: a critical review," *Progress in Natural Science*, vol. 19, no. 3, pp. 291-321, 2009.

[104] K.C. Divya, and J. Østergaard, "Battery energy storage technology for power systems—an overview," *Electric Power Systems Research*, vol. 79, no. 4, pp. 511-520, 2009.

[105] A. Malhotra, B. Battke, and M. Beuse etc., "Use cases for stationary battery technologies: A review of the literature and existing projects," *Renewable and Sustainable Energy Reviews*, vol. 56, pp. 705-721, 2016.

[106] M. Bragard, N. Soltau, and S. Thomas, etc., "The balance of renewable sources and user demands in grids: power electronics for modular battery energy storage systems," *IEEE Trans. on Power Electron*, vol. 25, no. 12, pp. 3049-3056, 2010.

[107] R. E. Ciez, and J. F. Whitacre, "Comparative techno-economic analysis of hybrid micro-grid systems utilizing different battery types," *Energy Conversion and Management*, vol. 112, pp. 435-444, 2016.

[108] W. Sun, *Investigation on Fault-ride Through Methods for VSC-HVDC Connected Offshore Wind Farms*, Mater thesis, Delft University of Technology, Norwegian University of Science and Technology, 2015.

[109] M. Kesraoui, O. Bencherouda, and Z. Mesbahi, "Power control of a PMSG based wind turbine system above rated wind speed," *International Renewable Energy Congress*, pp. 133-140, 2010.

[110] M. B. C. Salles, K. Hameyer, and J. R. Cardoso, "Crowbar system in doubly fed induction wind generators," *Energies 2010*, vol. 3, pp. 738-753, 2010.

[111] S. Divya, and T. Krishnakumari, "Review of control strategies for DFIG wind turbine to enhance LVRT*," IJISET - International Journal of Innovative Science, Engineering & Technology*, vol. 2, no. 4, pp. 339-342, 2015.

[112] V. Yaramasu, and B. Wu, "Three-level boost converter based medium voltage megawatt PMSG wind energy conversion systems," *2011 IEEE Energy Conversion Congress and Exposition*, pp. 561-567, 2011.

[113] S. W. Lee, S. B. Byun, and W. S. Kim, etc., "Design of a single phase 33 MVA HTS transformer with OLTC," *IEEE Trans. on Appl. Supercond*., vol. 17, no. 2, pp. 1939-1942, 2007.

[114] D. Dohnal, "On-load tap-changers for power transformers," *Mr Knowledge Base*, pp. 1-24, 2013.

[115] Y. Chistyakov, A. Minin, and E. Kholodova, etc. "Modeling of electric power transformer with on-load tap changer voltage control using complex-valued neural networks," *Proceedings of the 13th IASME/WSEAS International Conference on Mathematical Methods and Computational Techniques in Electrical Engineering Conference on Applied Computing*, pp. 128-133, 2011.

[116] N. Daratha, B. Das, and J. Sharma, "Coordination between OLTC and SVC for voltage regulation in unbalanced distribution system distributed generation," *IEEE Trans. On Power Syst.*, vol. 29, no. 1, pp. 289-299, 2014.

[117] Y. Wang, P. Gao, and E. Dong, etc., "Intelligent control of on-load tap changer of transformer," *2011 1st International Conference on Electric Power Equipment*, pp. 178-181, Xi'an, China, 2011.

[118] American Wind Energy Association, "Wind power myths vs facts," available online: http://www.pawindenergynow.org/wind/MythsvsFacts-FactSheet.pdf

[119] C. L. Archer, S. Mirzaeisefat, and S. Lee, "Quantifying the sensitivity of wind farm performance to array layout options using large-eddy simulation," *Geophysical Research Letters*, vol. 40, pp. 4963 – 4970, 2013.

[120] K. E. Johnson, and N. Thomas, "Wind farm control: addressing the aerodynamic interaction among wind turbines," *2009 American Control Conference*, St. Louis, USA, pp. 2104-2109, Jun., 2009.

[121] P. McKay, R. Carriveau, and D. S-K. Ting, "Wake impacts on downstream wind turbine performance and yaw alignment," *Wind Energy*, vol. 16, pp. 221–234, 2013.

[122] L. Vollmer, G. Steinfeld, and D. Heinemann, "Estimating the wake deflection downstream of a wind turbine in different atmospheric stabilities: an LES study," *Wind Energ. Sci. Discuss.*, pp. 1-23, 2016.

[123] A. Hoteit, and G. Hamidovich, "18 – pulse converter using 3/9 auto-transformer," *IJCSI International Journal of Computer Science Issues*, vol. 9, no. 3, pp. 387-392, 2012.

[124] M. Electronics, "Three phase auto transformer," available online: http://www.melectronics-jo.com/index.php?option=com_content&view=article&id=31&lang=en&Itemid=7

[125] GS Transformers, "Difference between isolation transformers and autotransformers," available online: https://www.gstransformers.com/technical/difference-between-isolation-transformers-and-autotransformers.html

[126] Nosmut, "Autotransformer," available at: http://www.nosmut.com/Autotransformer.html

[127] S. Seman, J. Niiranen, and A. Arkkio, "Ride-through analysis of doubly fed induction wind-power generator under unsymmetrical network disturbance," *IEEE Trans. Power Syst*., vol. 21, pp. 1782-1789, 2006.

[128] I. Erlich, J. Kretschmann, and J. Fortmann, etc., "Modeling of wind turbines based on doubly-fed induction generators for power system stability studies," *IEEE Trans. Power Syst*., vol. 22, pp. 909-919, 2007.

[129] A. H. Kasem, E. F. El-Saadany, and H. H. El-Tamaly, etc., "An improved fault ride-through strategy for doubly fed induction generator-based wind turbines," *IET Renewable Power Generation*, vol. 2, pp. 201-214, 2008.

[130] J. Lopez, E. Gubia, and E. Olea, etc., "Ride through of wind turbines with doubly fed induction generator under symmetrical voltage dips," *IEEE Trans. Ind. Electron*., vol. 56, pp. 4246-4254, 2009.

[131] ABB, "HVDC cable transmissions," available online: https://library.e.abb.com/public/d4863a9b0f77b74ec1257b0c00552758/HVDC%20Cable%20Transmission.pdf

[132] PRYSMIAN, "Extruded cables for HVDC power transmission," available online: http://www.prysmiangroup.com/en/business_markets/markets/hv-and-submarine/downloads/datasheets/Extruded_Cables_for_HVDC_Power_Transmission.pdf

[133] Q. Mu, J. Liang, and Y. Li, etc., "Power flow control devices in DC grids," *2012 IEEE Power and Energy Society General Meeting*, San Diego, CA, pp. 1-7, 22-26 July, 2012.

Every reasonable effort has been made to acknowledge the owners of copyright material. I would be pleased to hear from any copyright owner who has been omitted or incorrectly acknowledged.